LUND UNIVERSITY

Study of Two-Photon processes at low Q^2 using the VSAT calorimeter in the DELPHI experiment

Tyapkin, Pavel

2004

Organization LUND UNIVERSITY Department of Physics Professorsgatan 1, Box 118 SE-221 00, LUND	Document name **DOCTORAL DISSERTATION**
	Date of issue 17th of September 2004
	CODEN: LUNFD6/(NFFL-7221) 2004
Author(s) Pavel Tyapkin	**Sponsoring organization**

Title and subtitle
Study of Two-Photon processes at low Q^2 using the VSAT calorimeter in the DELPHI experiment.

Abstract

The study presented in this work is based on data collected at the LEP II accelerator
during the second period of the Large Electron-Positron collider operations (1996-2000).
During that time the DELPHI (DEtector with Lepton, Photon and Hadron
Identification) experiment collected about 90 Gb of data on tape corresponding to
687-691 pb^{-1} of luminosity. The data obtained by the VSAT (Very Small Angle Tagger)
electromagnetic calorimeter was stored separately by the VSAT team
and was used for luminosity measurements and for gamma-gamma physics analysis.
The analysis was concentrated on single and double tag events.
Three Monte Carlo sets were generated for years 1998-2000 using
three different generators (PYTHIA, PHOJET and TWOGAM).
Gamma-gamma physics at such high energies (from 189 up to 206 GeV
in the c.m. system) and small polar angles (3-12 milliradians) is quite unique.
Background and beam conditions influenced the analysis and were studied
in order to obtain a "clean" signal with as little background as possible.
The upgrade of the VSAT data-taking software and some hardware problems
due to aging are also discussed in this work.

Key words:

gamma-gamma, two-photon, virtual photons, hadronic cross-section,
photon structure function, single tag, double tag, antitag, LEP, DELPHI,
VSAT, STIC, QCD, VDM, GSP, PYTHIA, PHOJET, TWOGAM

Classification system and/or index terms (if any):	
Supplementary bibliographical information:	**Language** English
ISSN and key title:	**ISBN** 91-628-6168-9
Recipient's notes	**Number of pages** 188	**Price**
	Security classification	

Distribution by (name and address)
Pavel Tyapkin, Div. of Experimental High Energy Physics, Lund University,
Professorsgatan 1, Box 118, SE-221 00, LUND

I, the undersigned, being the copyright owner of the abstract of the above-mentioned dissertation, hereby grant to all reference sources the permission to publish and disseminate the abstract of the above-mentioned dissertation.

Signature _____ **Date** _____

Study of Two-Photon processes at low Q^2 using the VSAT calorimeter in the DELPHI experiment

Thesis submitted for the degree of
Doctor of Philosophy in Physics
by

Pavel Tyapkin

Contents

This thesis is based on the following papers, included as Appendices A to E:

A. G. Jarlskog, U. Mjoernmark, A. Nygren, P. Tyapkin, N. Zimin
1998 running review workshop, the VSAT project.
DELPHI internal note: 99-49 LEDI 11 **25 February 1999**

B. S. Ask, V. Hedberg, P. Niezurawski, A. Nygren, P. Tiapkine,
N. Zimin
LEP machine background and noise in the DELPHI calorimeters.
DELPHI internal note: 99-157 LEDI 12 **14 October 1999**

C. P. Tiapkine
Radiation damage and background monitoring by VSAT.
DELPHI internal note: 2000-153 CAL 144 **20 July 2000**

D. A. Nygren, P. Tyapkin, N. Zimin, G. Jarlskog
Exact position of VSAT modules and LEP beam
parameters measurements in 1998-2000.
DELPHI internal note: 2001-005 CAL 145 **06 February 2001**

E. S. Almehed, V. Hedberg, G. Jarlskog, P. Tyapkin, N. Zimin
A measurements of the Total Hadronic Cross-Section
in $\gamma\gamma$ collisions at very low Q^2 at LEP2.
DELPHI internal note: 2004-013-CONF-689 **and contributed paper**
for International Conference of High Energy Physics 2004 (Beijing)
16-22 August 2004.

To my farther

and his passion for physics

Chapter 1

Introduction

A short history of the photon

Before we knew anything about fundamental particles we had light as our primary sense.

This kind of emission is very important to human life since we get around 90% of all information about the environment around us from our eyes. Our sense of vision affects every aspect of our life, our decisions and our mentality to such an extent that we cannot even fully understand it. But it took a long time before the scientists realized the true nature of light! About 200 years ago a wave theory of light, and light interference, was invented by Thomas Young and others. James Maxwell published the idea of light propagation in vacuum in a paper in 1873. By this time, ideas about electrons also appeared (George Stoney 1874). The real experimental progress of understanding the nature of electromagnetic phenomena (involving light and electrons) came with the discovery of x-rays by Röntgen in 1895 and by the measurements of electrons by Joseph Thompson in 1898. Shortly afterwards, in 1900, Max Planck proposed idea about quantized radiation of light, i.e., the rule that radiation comes in discrete amounts (Blackbody radiation). Albert Einstein quickly realized the importance of Plank's discovery and deduced in 1905 that this implies that there should be a quantum of light, the photon. The photoelectric effect was described by him using this assumption of light as a particle.

The particle nature of the photon was experimentally confirmed by Arthur Compton in his experiments using x-rays in 1923. The controversy about the wave versus particle description of the photon was finally solved by Louis de Broglie in 1924 when he showed that all matter has wave properties. This, so-called wave-particle dualism, became a corner stone of modern physics. Interference (and diffraction as a special case of interference) proves the wave-like properties of light. In the same way the photoelectric effect proves the particle-like (quantized) behavior of light. With the creation of the Standard Model the photon took its place among other particles.

Today we know that the photon is a vector boson (spin 1) which mediates the electromagnetic force. It is massless and couples to the electric charge. When a photon is exchanged between charges (e.g. electrons) we observe an electromagnetic interaction. In the 1970-ies a Standard Model of particle physics was formulated which also included the weak and strong forces. Within the framework of this model the photon is intimately related with one of the mediators of the weak force, the neutral heavy vector boson Z. The Model requires, however, that there is a spin 0 Higgs field which can give the 91 GeV mass to the Z while preserving

the zero mass of the photon. The existence of such a field, which should be manifested by the existence of a neutral relatively heavy Higgs particle, still remains to be proved.

In principle the photon cannot interact with other photons since it does not carry charge. The quantum theory allows, however, for virtual particle states, i.e., a photon can for a very short time fluctuate to a pair of charged particles (e.g. electron-positron) which after a very short time reunite. This is allowed according to the Heisenberg uncertainty relation. The virtual state can also include light quark-antiquarks pairs and with less probability heavier pairs of leptons or quarks. If such a virtual state collides with another photon, electromagnetic interaction can take place and we call this two-photon collisions.

Such interactions have been observed by the DELPHI experiment at the Large Electron-Positron Collider (LEP) and this phenomena is what this thesis is about. We want to disentangle the probabilities of various virtual states of the photon and see how this depends on the photon collision energy.

My work in the DELPHI experiment started during the spring of 1999 and I worked as a VSAT expert until the end of the data-taking period (November 2000). All the problems and upgrades of the VSAT hardware and software made during this period are familiar to me. I also have a profound knowledge of the DELPHI Slow Control and Data Acquisition tasks and routines. Most of them are discussed in this thesis as well as the VSAT based Luminosity calculation, the determinations of the Beam Parameters, the Two-Photon double and single tag analysis together with Monte-Carlo simulations with different generators.

The articles in the Appendices are all connected with VSAT data-taking and two photon physics analysis that are based on data from VSAT.

Appendix A, entitled "1998 running review workshop", is a DELPHI internal note prepared in the beginning of 1999 for the DELPHI experimental workshop which usually took place before new data-taking started (i.e. in March-April). The situation with the VSAT detector hardware as well as software upgrade and changes in data storage routine are explained in the article. A large part of this note is devoted to the previous years (1998) detector performance.

Appendix B, entitled "LEP machine background and noise in the DELPHI calorimeters", was written during the summer of 1999. The main subject of the article is the background condition in VSAT, STIC and other calorimeters, the types of background and the problems connected with it. Some effective methods of removing background are proposed for each of the DELPHI calorimeters.

Appendix C, entitled "Radiation damage and background monitoring by VSAT", was written during June-July 2000. This article describes problems of the long-time radiation damage and the short periods of high background which caused an increase of the bias currents in the VSAT modules. The consequences of this, such as a change of energy calibration coefficients, were discussed and the total particle flux through the VSAT modules was calculated.

Appendix D, entitled "Exact position of VSAT modules and LEP beam parameters measurement in 1998-2000", summarizes all beam parameters changes, position shifts of the VSAT modules observed by geometrical surveys and consequences of that during a given period of time (nearly the whole LEP II period).

Appendix E, is devoted to the two-photons physics analysis of the DELPHI - VSAT data. The final analysis of two-photon events in double and single tag modes is presented here and compared with results obtained by using three Monte Carlo generators called TWOGAM, PYTHIA and PHOJET.

Chapter 2

Two Photon Physics

2.1 Two-Photon Interaction.

Classical electromagnetic theory only allows for the superposition of two crossing electromagnetic waves, but no interaction between them. In quantum field theory the situation is a little bit different and a real photon has a much more complicated nature. To first approximation, the photon is a point-like particle. According to quantum mechanics, it may, however, fluctuate into a (charged) fermion-antifermion pair which means that the photon is not truly point-like but has a structure.

This is the reason why photon-photon interactions are allowed in the quantum electrodynamic theory (QED). The probability of these interactions is extremely small at low energies and this prevents two-photon interactions to be observed with even the strongest of photon beams, such as lasers. These interactions have instead been studied at higher energies using colliding electron and positron beams since high intensity electron beams make the interactions more common.

Radiative quantum effects in QED allows the electrons and positrons to be surrounded by clouds of virtual photons. Photons from the clouds around the leptons can be described as a superposition of a number of virtual states. Each state represents the probability of the photon to fluctuate into a quark-antiquark or lepton-antilepton pair and can be represented by a wave-function. Due to theoretical difficulties, the quark-antiquark pairs are subdivided into high and low virtuality fluctuations, with a cutoff-limit (p_t) in the transverse momenta of the quarks. The high virtuality part can be calculated by perturbative QCD, whereas the low-virtuality part is described in a non-perturbative phenomenological model involving the summation over vector meson states.

In mathematical form the photon therefore is described as the bare photon plus three summation terms [9]:

$$| \gamma > = c_{bare} \mid \gamma_{bare} + \sum_{V=\rho^0,\omega,\phi,J/\psi} v_V > + \sum_{q=u,d,s,c,b,t} C_q|qq > + \sum_{l=e,\mu,\tau} c_l \mid l^+l^- > \quad (2.1)$$

The last term describes the fluctuation into a lepton-antilepton pair and is calculable to high precision by QED. In our case it is of less interest and will be discarded in the analysis by the requirement in the event selection of some hadronic activity in the other parts of the DELPHI detector than the VSAT. The two other terms describe the hadronic part of

the photon wave-function and studies of photon-photon collisions will help to improve the general understanding of the QCD photon structure.

The photon structure function term was created and adopted as a description of the photon contents in a similar way as the hadron is usually described as a state of parton constituents. The photon structure function is strongly related to the Parton Density Function (PDF) which describes the parton density as a function of x and Q^2 values (for definition of these variables see Fig. 2.1 and section 2.2).

The circulating e^+e^- beams of a collider like LEP can therefore be seen as the sources of strong but virtual photon beams. These photon beams have some special properties. The resulting photon luminosities are normally quite high and only about an order of magnitude smaller than the e^+e^- luminosities. As the cross-section for two-photon scattering increases with beam energy $E(\sim log^2(E/m_e))$, high-energy colliders are ideal machines for two-photon studies. The photons are radiated with a Bremsstrahlung-like spectrum (probability $\sim 1/E_\gamma$), and mainly at small angles ($\sim m_e/E$) relative to the beams. The two radiated photons have normally different energies and most two-photon event axes are strongly boosted along the e^+ or e^- beam directions. Here particles are more difficult to detect, making the visible (i.e. detected) cross-section appreciably smaller than the true (i.e. total) cross-section. Note that the energy spectra of the photons allows for different values of W (the invariant mass of the $\gamma\gamma$ system) to be measured, while the e^+e^- kinematics is fixed by the e^+e^- beam energy.

Two-photon studies have been performed by many e^+e^- experiments, e.g. at DESY by PLUTO [12], at SLAC by TPC/2γ [13] and at KEK by AMY [14]. Two-photon results have also been presented by all the four LEP experiments (ALEPH [15], DELPHI [53, 54, 58, 59], L3 [21] and OPAL [28]).

2.2   Kinematics

The typical two-photon or $\gamma\gamma$ interaction which is going to be discussed in the thesis can be described by the symbolic Feynman diagram in Fig. 2.1. If the energy of the incoming leptons e^+ and e^- is high enough and they are close to each other, the probability of an interaction becomes high. The interaction itself is carried out by two mediators, i.e., virtual photons radiated from the leptons. The invariant mass of the $\gamma\gamma$ system, $W_{inv}^{\gamma\gamma}$, can be estimated by measuring the outgoing lepton parameters as described in Fig. 2.1, i.e. θ angles and the momenta, p ,together with the initial energy of the leptons (i.e. the energy of the beams). This is the task which the VSAT calorimeter was designed for, i.e. to measure both such leptons (so-called double tag) or to measure one of them (single tag). The barrel part of the DELPHI experiment measures in addition the hadrons and other particles created in the interaction.
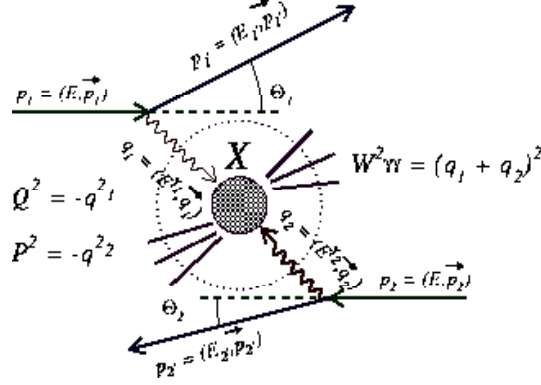
Figure 2.1: A Feynman diagram of a $\gamma\gamma$ interaction with hadronic production.

The momentum transfer Q_i^2 (see Fig. 2.1) at each lepton-photon vertex i in a two-photon reaction is important in the following analysis and it can be calculated as:

$$-Q_i^2 = q_i^2 = (p_i - p_i')^2 = 2m_e^2 - 2EE_i'(1 - \sqrt{1 - (m_e/E)^2}\sqrt{1 - (m_e/E_i')^2 \cdot cos\theta_i}) \quad (2.2)$$

which, for $\theta \gg m_e/E$, can be approximated by

$$-Q_i^2 = q_i^2 \approx -4EE_i'sin^2(\theta_i/2) \quad (2.3)$$

At LEP, $m_e/E \approx 10^{-5}$ and this is indeed much smaller than the polar angles, θ_i, at which it is possible to detect the scattered leptons with DELPHI and (2.2) is therefore applicable. With $E_i^\gamma = E - E_i'$ the invariant mass W of the produced particle system X is given by

$$W^2 = (q_1 + q_2)^2 = 4E_1^\gamma E_2^\gamma - 2E_1'E_2'(1 - cos\theta_1 cos\theta_2 - sin\theta_1 sin\theta_2 cos\Phi) \quad (2.4)$$

where Φ is the angle between the two planes defined by the two scattered leptons and the beam axis. Since we will here only treat the case with very small angle scattering $((1 - cos\theta_1 cos\theta_2) \to 0$ and $sin\theta_1 sin\theta_2 \to 0)$, equation (2.4) can be simplified to

$$W^2 \approx 4E_1^\gamma E_2^\gamma \quad (2.5)$$

In some cases the relative Bjorken variable x is used instead of W:

$$x = \frac{Q^2}{(Q^2 + W^2 + P^2)} \quad (2.6)$$

where P^2 is the transverse momentum squared of the leptons lost in the beampipe (i.e. it's close to zero).

2.3   Tagging

Experimentally one can measure the energy and angles of both, one or none of the leptons scattered in the two-photon reaction. This is called "tagging" the interacting photons. One differentiates between the three cases of double-tagging, single-tagging and no-tagging. Tagging is normally done by detectors placed in the very forward regions, typically covering $4 - 100$ mrad.

2.4   Double-tagging

Double-tagging means that both final state leptons are measured. Since both photon four-vectors are known, the full reaction kinematics is available for precise studies of the cross-section, structure functions F_2 etc. Double-tagging also ensures a complete dominance of the two-photon diagram over any competing diagrams but only after a tedious background rejection procedure. Experimental limits in the W resolution, limits the obtainable accuracy in these measurements. Due to the strong forward peaking of the angular distribution of the scattered leptons, the tagging needs to be done at very small angles. Here high-rate background sources, such as off-momentum electrons lost from the beam and small angle Bhabha scattering, can be difficult to reject since the experimentally visible cross-section for double-tagged two-photon events is very small.

2.5   Single-tagging

Detection of either the scattered electron or the scattered positron is necessary for studies of the Q^2 dependence of the photon structure function F_2^γ. The Q^2 of the virtual photon, which probes the target photon structure, is given by the measurement of the tagged lepton. An unfolding procedure is often required to link the visible W to the true W. Large Q^2-values are required to enter into the deep inelastic scattering range, implying rather large scattering angles ($\theta_{tag} > 100$ mrad). Here the cross-section is comparatively small due to the forward peaking of the angular distribution of the leptons. Moving to the low-Q^2 range ($\theta_{tag} < 30$ mrad) the event rate goes up, and one can, by analyzing relatively high-$W_{\gamma\gamma}$ events, study the production and properties of jets with high transverse momenta. The measured energy spectrum of the leptons can be useful in this analysis. Resonance formation studies can also be carried out with single-tagged two-photon events. Detecting a scattered lepton is furthermore useful for reducing different background sources, such as e^+e^- annihilation processes. One has, however, to make sure that the non-detected electron is not scattered into large angles (i.e. large Q^2), as the virtual Bremsstrahlung process with e^+e^- scattering will then dominate. Experimentally visible cross-sections for single-tagged two-photon events are typically about 50 times larger than for the double-tagged case.

2.6   No-tagging

If none of the scattered leptons are detected, the only information available is that of the produced hadronic system. Two-photon reactions generally involve small momentum transfers Q^2, at comparatively low W. The no-tagged events can be used for studying low-p_t jets, resonances etc. Not requiring any tagging greatly increases the visible cross-section, this being at least a factor 1000 larger than for the double-tagged case. It was mentioned earlier that in order to ensure the dominance of the two-photon process, it is necessary for the single-tagged and no-tagged analysis to require the untagged leptons to have small scattering angles. This can be done by an anti-tagging requirement, where an event is rejected if leptons are detected. Having a detector in the very forward direction thus assures very low Q^2 for the untagged leptons, i.e. they do not exit the beam pipe.

2.7 Models

The photon is a complicated object to describe since it has several different characteristics. In some respects it is similar to the proton since some photoproduction experiments show the characteristics of soft hadron interactions. Other experiments (e.g. high energy electron scattering) show a direct coupling to pointlike quarks inside the hadrons. The photon interaction is therefore described by both the VDM (Vector meson Dominance Model) and by the QPM (Quark Parton Model). A composite VDM+QPM model was able to explain all two-photon data before the KEK and LEP experiments started. Several experiments ([44]-[46]) have, however, reported an excess of high-p_t event which cannot be explained by this model. A third model, the QCD-based hard scattering model, has therefore been added to better describe the data. The latter model requires specific parton density functions in order to calculate the parton momenta fractions. It is called the QCD-RPC (Resolved Photon Contribution) model and mainly works with two types of parton density function parameterizations: GSP (Gordon-Storrow Parameterization) and GRV (Gluck-Reya-Vogt).

Below, a very brief overview is given of these models, each of which has some modes and variants. The combination of the different models for Monte-Carlo purposes appeared only during the last couple of years.

2.8 The VDM Model

The non-perturbative, phenomenological Vector meson Dominance Model (VDM) is well-known from hadron-hadron interaction physics. The model was developed more than 30 years ago. In order to describe the interaction between a photon and hadrons, VDM assumes that the photon converts into vector mesons such as ρ, ω and Φ. These then interact with hadrons through the strong force as is shown in Fig. 2.2.
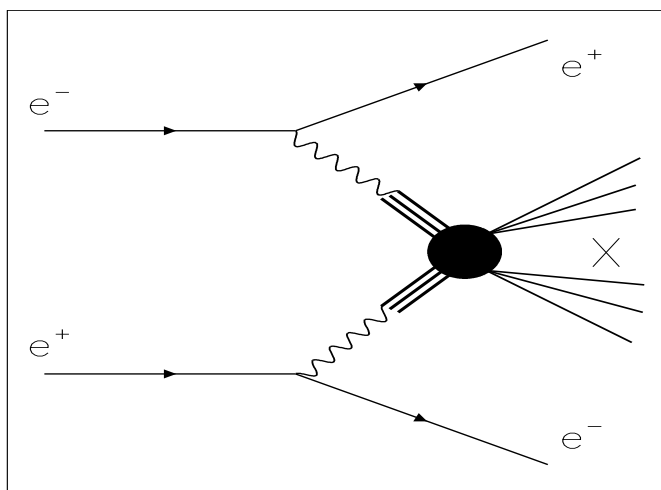
Figure 2.2: Feynman diagram of the VDM process.

The VDM model assumes virtual fluctuation of a photon into quark-antiquark pairs with lifetimes long enough to form a bound vector meson state. This is possible when the transverse momenta (p_t) of the branching $\gamma \rightarrow q\bar{q}$ is small. The model is therefore only describing the low p_t part of a $\gamma\gamma$ collision.

VDM thus predicts photon-photon scattering to have the characteristics observed in hadron-hadron scattering. The main contribution to the total two-photon cross-section comes from VDM processes.

The VDM cross-section is given by [47]:

$$\sigma_{\gamma\gamma}^{VDM}(Q_1^2, Q_2^2, W^2) = F_{VDM}(Q_1^2)F_{VDM}(Q_2^2)[A + \frac{B}{W}]) \tag{2.7}$$

where A and B are constants to be defined by experiments. The last term, in brackets, describes the W-dependence of $\sigma_{\gamma\gamma}$. The underlying theory here is the Regge model, resulting in a W-behavior of $W^{2\alpha-2}$ [48]. Treating only the terms with α=l/2, 1 and 2 as significant to $\sigma_{\gamma\gamma}$, a comparison with measured cross-sections results in A = 275 nb and B = 300 nb GeV [49]. These values were used for this work and they have been measured by previous experiments [12–14].

The first two terms describe how the cross-section $\sigma_{\gamma\gamma}$ varies with the momentum transfers Q_i^2. The quantity F_{VDM} is the VDM form factor. F_{VDM} is here taken from the Generalized VDM model (GVDM) since this model also takes into account effects from any higher mass resonances and the continuum. It is given by [50]:

$$F_{VDM}(Q^2) = \sum_{V=\rho,\omega,\phi} r_V \frac{1 + Q^2/4m_V^2}{(1 + Q^2/m_V^2)^2} + \frac{0.22}{1 + Q^2/m_0^2} \tag{2.8}$$

Here m_o =1.4 GeV and m_V denotes the mass of a vector meson V. The factors r_V are related to the coupling between the vector meson V and the photon. The following r_V-values were used [42]: r_ρ=0.65, r_ω=0.08 and r_ϕ=0.05. $\sigma_{\gamma\gamma}^{VDM}$ varies with P_t^2 as

$$\frac{d\sigma_{\gamma\gamma}^{VDM}}{dP_t^2} \approx \frac{1}{e^{\alpha P_t}} \tag{2.9}$$

This exponential behavior leads to a suppression of high-p_t VDM events.

2.9   The QPM Model

Previous experiments [95, 97, 98] have shown that photons can exhibit pointlike couplings directly to a quark-antiquark pair ($e^+e^- \rightarrow e^+e^- + q\bar{q}$), which subsequently fragments into hadrons (see Fig. 2.3). The resulting events show typical two-jet topologies. The lowest
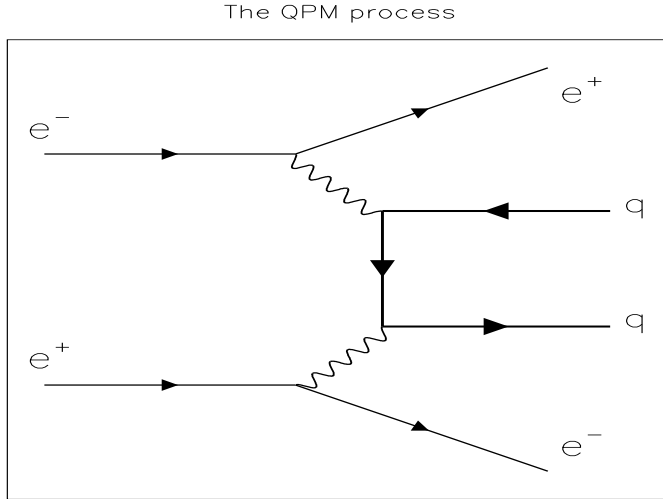
The QPM process

Figure 2.3: Feynman diagram of QPM process.

order Born approximation is modeled by the perturbative Quark Parton Model (QPM). Contrary to VDM, QPM is only applicable at large Q^2 or high quark P_t. In these regions the interaction times are too short for the formation of bound states. The dominant scale for the QPM model is p_t^2, meaning that $p_t^2 \rightarrow Q^2$ in the QPM case.

The QPM contribution to the total cross-section $\sigma_{\gamma\gamma}^{QPM}$ is comparatively small at the low Q^2 of most two-photon events. At large Q^2, however, the influence of the QPM process becomes significant. A full calculation of $\sigma_{\gamma\gamma}^{QPM}$ for hadron production is rather complicated and involves the sum of several terms [42].

The QPM model is similar to the QED case i.e. the cross-section $\sigma_{\mu\mu}$ for $e^+e^- \rightarrow e^+e^-\mu^+\mu^-$ is a manageable and instructive case [43]. The $\mu^+\mu^-$ production is given by the QED-diagram, where $q\bar{q}$ in Fig. 2.3 is replaced by $\mu^+\mu^-$. This diagram can be divided into two parts, the first one describing $e^+e^- \rightarrow \gamma\gamma$ and the second one describing the process $\gamma\gamma \rightarrow X \rightarrow \mu^+\mu^-$. Only the no-tag case is described here.

The Bremsstrahlung spectrum of the beam-radiated photons can be approximated by the Weizsacker-Williams formula, with $\omega = E_\gamma/E_{beam}$ and $\alpha \approx 1/137$:

$$\frac{dN}{d\omega} = \frac{\alpha}{2\pi} \frac{1 + (1-\omega)^2}{\omega} ln(\frac{E^2}{m_e^2}) \qquad (2.10)$$

The convoluted photon spectra at some W define a two-photon luminosity function $L_{\gamma\gamma}$. Its dependence on the energy fraction $s = W/\sqrt{s} = W/2E$ is given by

$$\frac{dL_{\gamma\gamma}}{ds} = (\frac{\alpha}{\pi})^2 \frac{f(s)}{s} \cdot ln^2(E^2 - m_e^2) \qquad (2.11)$$

with

$$f(s) = (2 + s^2)^2 ln(\frac{1}{s} - (1 - s^2)(3 + s^2)) \qquad (2.12)$$

This approximation describes the shape of $L_{\gamma\gamma}$ well but overestimates its value by around 10% for $s < 0.8$.

By finally convoluting $L_{\gamma\gamma}$ with the approximated cross-section $\sigma_{\gamma\gamma} = 4\pi\alpha^2/W^2$ for $\gamma\gamma \to X \to \mu^+\mu^-$, the total cross-section $\sigma_{\mu\mu}$ becomes

$$\sigma_{\mu\mu} = \int L_{\gamma\gamma}\sigma_{\gamma\gamma}ds = \frac{8\alpha^4}{\pi}\frac{1}{m_\mu^2}ln^2(\frac{E}{m_e})ln(\frac{E}{m_\mu}) \qquad (2.13)$$

Notice the lnE dependence of $\sigma_{\mu\mu}$, showing the increasing two-photon cross-section with energy.

The QPM W dependence to lowest order is found to follow

$$\sigma_{\gamma\gamma}^{QPM} = \frac{1}{W^2} \qquad (2.14)$$

while the p_t^2 dependence is given by

$$\frac{d\sigma_{\gamma\gamma}^{QPM}}{dp_t^2} \sim \frac{1}{p_t^4} \qquad (2.15)$$

By comparing formula (2.9) and (2.15), it is clear that the QPM hard scattering processes become dominant above a p_t of about 1 GeV. This p_t limit and the energies involved are quite small compared to other reactions. Two-photon events thus allow clean, low-energetic studies of hard scattering processes.

2.10   The QCD-RPC Model

In addition to the QPM model which generates two-jet events, other hard scattering multi-jet diagrams are also possible. In the case of $p_t^2 \to Q^2$, i.e. when Q^2 is very small, these diagrams start to dominate. Their contributions are described by the QCD Resolved Photon Contribution (QCD-RPC) model. Two cases are possible with single resolved or double resolved diagrams. By resolved is meant here that one or both of the photons are resolved into its (their) hadronic constituents. The resulting particles produce (in addition to the normal two jets) so-called remnant jets. The QCD-RPC model thus generates three-jet and four-jet events. The remnant jets are, however, mainly produced at very small angles relative to the beams, making them difficult to detect. The bulk of the visible QCD-RPC events will therefore be seen to have a similar high-p_t two-jet topology as the QPM events.

The single resolved QCD-RPC contribution contains two sub-processes, $\gamma g \to q\bar{q}$ and $\gamma g \to gq$, while the double resolved one contains eight $(q, \bar{q}, g)$ sub-processes. Here g means a gluon, while $q(\bar{q})$ is a quark (antiquark). These sub-processes allow experimental tests of the theoretical predictions of the photon quark and gluon densities.

Parton Density Functions (PDF) are important ingredients in cross-section calculations involving the incoming particle hadronic structures, such as the QCD-RPC model. The PDFs give for each parton the parton density for a given (x, Q^2)-value, where Q^2 is the momentum transfer. The variable x is here defined as the fraction of the total hadron longitudinal momentum carried by a given parton $(q, \bar{q}$ or $g)$. This is needed in perturbative QCD calculations as the PDF's are used in the Altarelli-Parisi equations which describe the Q^2 dependence of the parton densities.

There are several different PDF sets available, though some of them are not applicable to two-photon studies since they are derived from deep inelastic $e\gamma$ experiments at high Q^2.

Experimental results are needed to differentiate between the PDFs. A free parameter in each PDF is its p_t^{min} - value, i.e. the minimum transverse momentum required for the associated QCD-RPC process to take place. Since these processes are perturbative, such a p_t-cut is required to stay above the non-perturbative VDM region to avoid event double-counting. The p_t^{min} - values are constrained by the visible cross-sections. Normal values vary between 1.5 and 3.0 GeV, depending on the PDF set. The PDFs are finally compared by studying key physical distributions (*e.g.W*, $p_t^{jet}etc$).

The cross-section calculations of the single and double resolved QCD-RPC processes are as mentioned above dependent on the PDF. The resulting calculations are outside the scope of this work. An overview of the calculations for some different PDF sets is given in [42]. Asymptotically, the QCD-RPC cross-section is found to have a similar p_t^{-4}-behavior as in the QPM case (2.15).

2.11 Photon Structure Functions

A hadron can be described by its parton content. As photons fluctuate into partonic states a similar description can be adopted for the photon. The partonic content of a photon is described by the photon structure functions, which are closely related to the PDFs described previously. If one of the photons in a $\gamma\gamma$-collision is almost on-shell with a $Q^2 \sim 0$ (the single tag case), the whole process can be viewed as a deep inelastic scattering of the tagged electron on the quasi-real target photon. In this case the cross-section $d\sigma_{ee \to eX}$ can be changed into $d\sigma_{e\gamma \to eX}$ by: $d\sigma_{ee \to eX} = d\sigma_{e\gamma \to eX} \cdot f_{\gamma/e}$ where $f_{\gamma/e}$ means the flux of the target photons of the incoming electron. $f_{\gamma/e}$ can be calculated using the equivalent photon approximation (EPA). The cross-section can then be expressed as:

$$\frac{d\sigma_{e\gamma \to eX}}{dxdQ^2} = \frac{2\pi\alpha^2}{xQ^4}[(1 + (1-y)^2 F_2^\gamma(x, Q^2) - y^2 F_L^\gamma(x, Q^2)] \tag{2.16}$$

where the two variables x and y are given by:

$$x = \frac{Q^2}{2q_2 \cdot q_1} \approx \frac{Q^2}{Q^2 + W^2} \tag{2.17}$$

,

$$y = \frac{q_2 \cdot q_1}{kq_2} \approx 1 - \frac{E_{tag}}{E_{beam}cos^2(\frac{\theta_{tag}}{2})} \tag{2.18}$$

If the photon is almost real $P^2 \approx 0$ (once y is very small in the region studied) so it is only possible to measure F_2^γ. In the case of double tagged events $P^2 \neq 0$ and additional cross-section terms have to be taken into account. In the simple parton model F_2^γ is taken as a sum over the quark and antiquark density functions. The Q^2 evolution of these PDFs are described by the Altarelli-Parisi equations. In the case of the photon, there is an extra term corresponding to a gamma going into a $q\bar{q}$ pair. This renders the equations inhomogeneous and a linear rise of F_2^γ with $ln(Q^2)$ is expected. This has been observed by the LEP experiments.

The H1 and ZEUS experiments at HERA have provided one of the most important results in recent gamma-gamma physics. They observed a rise of the proton structure function (F_2^p) at low x-values. A similar rise is also expected for the F_2^γ structure function at very low x. Evidence for this is now emerging from the LEP experiments [42].

2.12   Total Cross section

The $\gamma\gamma$-collision processes at LEP II energies have cross-sections that are usually two to three orders of magnitude larger than the e^+e^- annihilation processes [43]. The cross-section for the process $\gamma\gamma \rightarrow hadrons$ is calculated from the measurement of $e^+e^- \rightarrow e^+e^- + hadrons$ [56]:

$$\frac{d\sigma_{ee}}{dW^2_{\gamma\gamma}/s} = \int \frac{dQ_1^2}{Q_1^2}\frac{dQ_2^2}{Q_2^2} \sum_{a,b=T,S} L_{ab}\sigma_{ab}^{\gamma\gamma}(W^2_{\gamma\gamma},Q_1^2,Q_2^2) \qquad (2.19)$$

Here $d\sigma_{ee}$ is the measured cross-section for the process $e^+e^- \rightarrow e^+e^- + hadrons$ in a certain dW interval. $\sqrt{s}$ is the center of mass energy and L_{ab} is the two photon luminosity function, which describes the photon flux. Q_i^2 are the virtualities (momentum transfer in the $e\gamma$ vertices) of the radiated photons. The hadronic cross-sections σ_{ab} correspond to specific helicity states (T=transverse and S=Scalar) of the interacting photons. If $W^2 > Q_i^2$ it is possible, to a very good approximation, to assume a factorization of the dependence of σ_{ab} in Q and W [45]:

$$d\sigma_{ab}(dW^2_{\gamma\gamma},Q_1^2,Q_2^2) = h_a(Q_1^2)h_b(Q_2^2)\sigma_{\gamma\gamma}(W^2_{\gamma\gamma}) \qquad (2.20)$$

The functions $h_{a,b}$ are model dependent and describe the Q^2 behavior of the hadronic cross-section. It is possible to extrapolate $\sigma_{ab}(W^2_{\gamma\gamma},Q_1^2,Q_2^2)$ to $Q^2 = 0$ if these functions are known. This factorisation procedure works better for small values of Q_i, which usually are dominating the notag data. At low Q^2, most of the hadronic system is, however, lost in the beampipe and the W measurement of notag data needs to be unfolded with different Monte Carlo simulations.

Double tag data, on the other hand, do provide an excellent W measurement from the tagged electrons and no model dependent unfolding is needed. The extrapolation to $Q^2 = 0$ from large Q^2 values is strongly model dependent and this can result in large uncertainties in the $\sigma_{\gamma\gamma}(W^2)$ measurement. The VSAT detector therefore has a big advantage, as it can measure double tag events at low Q^2 values due to the very small angular acceptance (4-7 milliradians).

Chapter 3

The LEP collider

3.1 LEP scientific goals

The main purpose of the LEP (Large Electron Positron) collider was the study of e^+e^- collisions in a new energy range, producing the mediators of the weak force, W^{+-} and Z^0. The Z^0 and its charged partners the W^{+-} were both discovered at CERN in 1983 [80]. In order to study the production and decays of the weak mediators in detail one needs not only a first class collider but also a good experimental setup (detectors like DELPHI). Four of them were constructed in four Interaction Points (IPs) distributed symmetrically along the collider circumference: ALEPH (Apparatus for LEp PHysics) [87], DELPHI (DEtector with Lepton, Photon and Hadron Identification) [92, 93], L3 (LEP underground area No. 3) [94, 95], OPAL (Omni Purpose Apparatus for Lep) [97, 98]. The LEP collider's initial energy was chosen to be around 91 GeV so that Z^0 particles could be produced (the LEP I phase). In order to produce pairs of W^{+-}s the energy required was about 163 GeV (the LEP II phase). Later in order to search for new particles like the Higgs boson the collision energy was increased up to 208 GeV.

Other primary experimental goals of LEP were to provide tests of the Standard Model, precise QCD studies and the possibility to investigate the problem of the Higgs boson [88, 90, 91, 96, 99], a hypothetical particle associated with the electroweak symmetry breaking mechanism, which is required to make the W^{+-} and Z^0 bosons massive.

An extensive search for supersymmetrical (SUSY) signals took a large part of the data analysis effort [89]. Many groups tried searching for the signals of the proposed supersymmetrical particles such as the chargino, the gravitino and the neutralino. These searches have a significant impact in the development of theoretical ideas such as the Higgs theory, new gauge bosons and Grand Unified Theories (GUT). No clear signals have been observed but the exclusion mass limits were pushed up significantly by LEP [76].

3.2 The history and overview of the LEP collider

The early development of the Large Electron-Positron storage ring (LEP) project is well described by John Adams in his Annual Reports to the CERN Council in 1979 and 1980.

Studies of the design of the LEP accelerator started at CERN in 1976 and the first practical design was published in 1978. This machine design had a cost-optimized energy of

70 GeV per beam and measured 22 km in circumference. After extensive discussions during the autumn of 1978 it was decided to embark on the design of a somewhat larger machine, 30 km in circumference, with a cost-optimized energy of about 90 GeV per beam. The energy of both these machines could be extended by using super-conducting RF cavities, when these become available, to 100 and 130 GeV respectively. One finally settled for a 27 km circumference which limited the energy to around 105 GeV per beam. This energy was obtained for a short time in the autumn of year 2000.

The construction took about 8 years. LEP is the biggest accelerator ever built, having a 26.67 km long tunnel. The tunnel itself represented less than half of the 1.4 million of cubic meters of material which had to be excavated for the project. The remainder of the underground work consisted of the four experimental caverns (the homes of the DELPHI, OPAL, ALEPH and the L3 experimental setups), 18 pits, 3 km of secondary tunnel, and some 60 chambers and alcoves. After an extensive campaign of test drilling in and around the area proposed for the LEP tunnel it was decided to incline the plane of the tunnel by 1.4%. This decision was made to ensure that all underground caverns and the main part of the tunnel would be located in solid rock while at the same time limiting the maximum depth of the shafts to less than 150 m and to avoid going too far into the Jura mountain ridge. The solid rock provided a stable base for the magnets and the vacuum beampipe. The deep position of LEP collider provided in addition good radiation shielding and minimized the environmental damage [77]. Too deep shafts might, however, be dangerous in case of an emergency underground (fire, explosion, flooding).

The main ring is actually not an ideal circle. It is formed by eight arcs and eight straight sections (500 meters long each). The reason for such a design was both a simplification of the magnet system and a reduction of the off-momentum electron and synchrotron radiation background around the interaction points [78]. A system of collimators close to and far away from the experimental setups also served the same purpose.

In addition to the underground civil-engineering work, the construction of LEP necessitated the construction of 71 surface buildings with a total area of some 51000 square meters, situated over eight sites.

The bending field of the dipole magnets was made unusually low (about 0.225 T for 100 GeV beams) so as to increase the bending radius and thereby reduce the amount of synchrotron radiation. The current in the main dipoles was 4200 A at 94.5 GeV and the current in the main quadruples was 400 A at 94.5 GeV.

The strength of all the magnets in the LEP ring were very accurately adjusted by controlling the current flowing in their coils. This was accomplished by the use of more than 750 precisely stabilized DC power supplies ranging from less than 1 kW to a maximum of 7 MW. The specifications for these power supplies were extremely tight, both individually and during energy ramping in their synchronization. For the main dipole and quadruple supplies, absolute accuracies down to 2 parts per 10^5 have been achieved with a resolution typically three times better.

Each magnet had of course its own cooling circuit. For the majority, the cooling was provided by unmineralized water circuits which were connected to 10 cooling towers with a capacity of 10 MW each. Some of the small corrector magnets were air-cooled, whilst the super-conducting quadruples and the super-conducting experimental solenoids were cooled by liquid helium at 4.2 K.

LEP was upgraded to LEP II during 1996 by using super-conducting RF cavities covered with niobium with a field gradient of up to 7 MV/m. As of 1998, the super-conducting system

consisted of 272 cavities. 4 cavities made one module and 1 klystron drove 2 modules and could deliver 1 MW of RF (Radio Frequency) power. The modules were made by the well-known companies Circa (France), Ansaldo (Italy) and Siemens (Germany).

LEP II reached 206-208 GeV in collision energy by the end of the operation (November 2000) in spite of the initial plans where the limit of the LEP energy was thought to be around 91 GeV. This was archived by improving the quality of the surface in the cavities and due to an upgraded cooling system. With even more superconducting RF cavities LEP could reach higher energies. At 94.5 GeV a particle would loose 2.33 GeV per turn to synchrotron radiation. If this was not replaced the particle would rapidly spiral into the beam pipe. At 94.5 GeV a total accelerating voltage of 2700 MV was provided by the RF (Radio Frequency) system.

The injection of the particles into the LEP main ring was complex and the accelerator chain consisted of four smaller accelerators and storage rings. First there were two linacs (LIL) for electrons and positrons. They accelerated the particles to energies of 200 and 600 MeV. Then particles were stored in the electron-positron accumulator called EPA. The Proton Synchrotron (PS) then accelerated them to 3.5 GeV. The SPS (Super Proton Synchrotron) delivered beams of the 22 GeV to the LEP main ring.

LEP took electrons and positrons from the SPS and in 1998, accelerated them up to 94.5 GeV. At the end of year 2000, 101.0 to 104.5 GeV were typical energies but the adjustment periods were longer and more difficult in comparison with energies below 101 GeV. The mini-ramp system (i.e. increasing energy in small 0.5 GeV steps as the beams intensity decreases) was proposed and used. Beams at high energy were quite unstable and the intensity was low.

The special feature of any high energy lepton accelerator is a fast rise of velocity to close to the speed of light and after that just an energy increase. At an energy of 94.5 GeV: $\gamma = 184932$ and v/c $= 0.999999999985380$, i.e., $c - v = 0.004386$ m/s, which can be compared to $c - v = 0.080926$ m/s at 22 GeV. Even through this is called acceleration, the beams do not actually pick up much speed, it's just the energy that continues to increase.

The duration of a typical run with particles for a physics fill was 12 hours at 45 GeV energy per beam. During this time each of the 10^{12} particles in the beams traversed the complete 26.67 km of the LEP vacuum chamber about 500 million times. In order to minimize particle losses due to collisions with residual gas molecules, the whole vacuum chamber must be pumped down to very low pressures. The achieved static pressure at LEP was between 10^{-10} to 10^{-9} Pa whereas in the presence of a beam the pressure rose to about 10^{-7} Pa. This pressure rise was due to gas evaporation from the inner vacuum-chamber wall, provoked by the synchrotron radiation of the circulating beam and it had a profound influence on the design of the LEP vacuum system. A lot of efforts were made to suppress the effects of synchrotron radiation induced evaporation.

The two main components of the vacuum system were the vacuum chamber itself and the pumping system. The LEP beampipe had a total volume of 270000 liters and to achieve the vacuum pressure needed, a number of different pumping methods had to be applied. First the LEP ring was heated up to about 150-300° C, this was called the bake-out and remove all the water vapor. An initial vacuum of about 10^{-7} Pa was then created by 60 pumping stations. About 2200 stationary ion pumps then took the pressure down to 10^{-8} Pa and finally 20 km long strips of getter ribbon and titanium sublimation pumps usually pushed the pressure down to 10^{-10} Pa.

Of the 27 km of the LEP vacuum chamber, a distance of about 22 km passed through the

dipole and quadruple magnets and the beampipe chamber itself and the machinery around it were subjected to heating due to synchrotron radiation. Although this heating represented a mere 100 W/m during LEP I phase, it rose to more than 2000 W/m during the LEP II period (1997-2000). The chambers therefore needed water-cooling channels and were constructed from aluminum because of its good thermal conductivity. Only about half the radiated power would however be absorbed by the aluminum. The remainder would normally escape into the tunnel and produce such a high radiation dose that organic materials such as gaskets, cables, electronic components, etc., would be destroyed. Severe damage could in addition result from the formation of ozone and nitric oxides which produced highly corrosive nitric acid in the presence of humid air. For these reasons, the aluminum chamber was covered with a lead cladding of a thickness varying between 3 and 8 mm, which greatly reduced the radiation that escaped into the tunnel during operation.

For reasons of reliability, the 26.7 km of the LEP vacuum beampipe was subdivided into smaller 'vacuum sectors' with a maximum length of 474 m. During shutdown periods, when there was no circulating beam and work was often going on in the tunnel, these vacuum sectors were isolated from each other by full-aperture gate vacuum 'sector valves'. So if an accident occurred or if the vacuum chamber had to be explored for services, only 474 m of vacuum would be affected and not the full 26.7 km.

The operation of the LEP collider started in August 1989. The 14 CERN member states contributed more than 1.3 billion Swiss francs to the construction of LEP. Two important dates can be mentioned: the first injection into the LEP collider took place on 14 July 1989 (one day earlier than scheduled) and the first collisions of electrons and positrons happened almost exactly one month later on the 13th of August 1989.

3.3 The LEP beam parameters and performance

The particles traveled in the main ring in four bunches. An eightfold minibunch scheme was also used later but was abandoned as it complicated the triggering of the experiments and did not improve the luminosity as expected.

The beam size depended on where in the ring the beam was. At the interaction points where the beams collided, the vertical beam size was between 3 and 4 microns and the horizontal beam size was 190 microns (0.19 mm). In other places, the beam size was 4 mm horizontally and less than 1 mm vertically. VSAT could provide some information about the beam size, the tilt and the acollinearity of the beams (Appendix D) at the DELPHI Interaction Point (Table 3.1) but one can note that the information from the VD (Vertex Detector) was more precise since the VD was closer to the IP and had a better angular resolution and geometrical acceptance. Typical values of ϵ and β (i.e. the transverse emittance and the betatron function) provided by LEP and σ_x, σ_y (i.e. the distance from the beam centre to the point where the intensity of the beam had decreased a factor e) provided by VSAT are presented in the Table 3.1 below.

Table 3.1: Beam dimensions at the DELPHI IP measured by VSAT (σ) and VD (ϵ and β)

period	typical values:	ϵ(nm)	β(mm)	VSAT $\sigma(\mu m)$	
LEP1:	x	35	2.5	296	
	y	0.7	0.05	5.9	

The beams were not allowed to collide during injection, accumulation, acceleration and energy ramping. Therefore they had to be well separated in the eight possible collision points (four of them occupied by experimental setups). All the eight places were equipped with four electrostatical separators providing a 2.5 MV/m strong electric field by 4 meters long plates separated by 11 cm. These separators were strong enough to make sure that the beams were clearly separated (more than 40 standard deviations of the beam size) in the vertical plane. At the same time the separation should not bend the beams too much to limit the production of synchrotron radiation and other backgrounds [78]. The separators were switched off after LEP reached the desired beam energies to allow for collisions and the physics data taking.

The bunch length at 94.5 GeV was about 2 cm with the ends of the bunch defined as a place with a 2σ drop of electron density compared to the maximum. A 6 mA total beam current consisted of about $3 \cdot 10^{12}$ particles and 14 MW RF power was taken by the beam. The RF system ran at 352 MHz (wavelength 85 cm). At high energy the total energy needed was about 130 MW with an approximate cost of $\sim$ 5500 CHF/hour.

The energy consumption for each subsystems was: Super-conducting RF: 39 MW, Copper RF: 20 MW, Cryogenics: 8 MW, Magnets: 22 MW, Water cooling: 5 MW, L3's solenoid: 4.5 MW, Other: 30 MW.

For the whole of CERN, when all accelerators were running (PS, SPS and LEP), the energy consumption was about 250 MW and the approximate cost was 12000 CHF/hour.

During the 10 years of running, the LEP luminosity was increased each year (Fig. 3.1). Luminosity at lower energies like 45 GeV per beam was, however, always higher than at higher energies no matter which kind of upgrades were made. In spite of careful checks and precise guidance of the beams, the four LEP experiments (ALEPH, DELPHI, OPAL, L3) nearly always received a different luminosity - a fact which made some of the collaborations happy and some not.
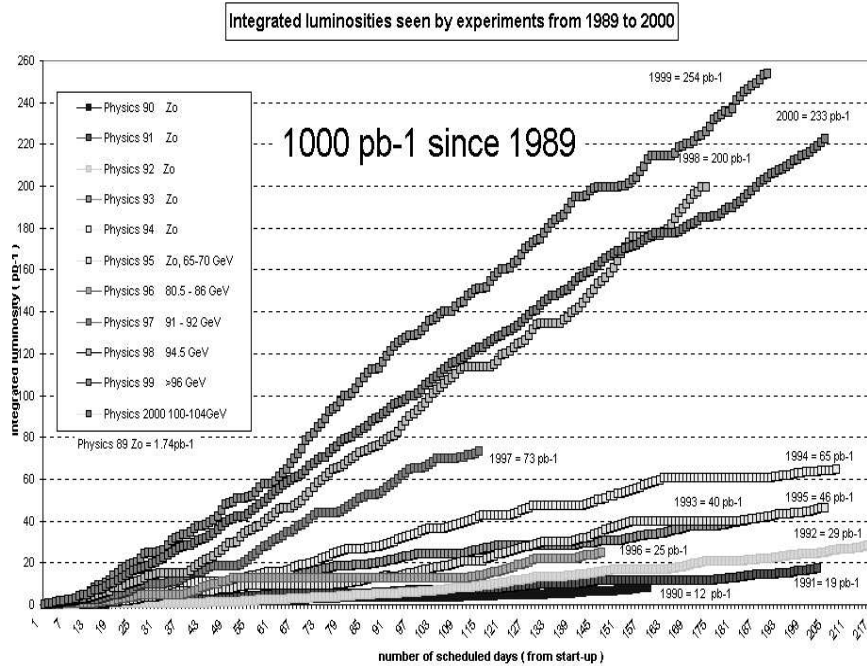
Figure 3.1: The integrated luminosity seen by the experiments at LEP

LEP provided 8984 physics fills during its lifetime. One fill meant one cycle of collider operation which consisted of injection, acceleration, adjustment and beams collision until beams were lost or got dumped because of too low intensity.

DELPHI and the other three LEP experiments have produced a vast amount of physics results (e.g. around 400 publications and more than 800 internal papers by the DELPHI collaboration to date). Many meetings and conferences have been committed to the discussion of LEP results and the talks were contributed both to the experimental and physics sessions [79]. One subject sparked especially deep interest, lively discussions and some regrets. It was the closure of LEP during year 2000 without taking into account the possibility of increasing the RF power (and the beam energy) by using more superconducting RF cavities, due to the very tight schedule of the LHC construction.

Chapter 4

The DELPHI experiment

4.1   The DELPHI experimental setup.

The DELPHI detector [92, 93] came into operation in 1989 and collected experimental data until the end of year 2000. The last physics data run by DELPHI was on November 2, 2000. Electron-positron annihilation has been studied at various centre-of-mass energies as is shown in Table 4.1:

Table 4.1: Luminosity recorded by DELPHI

E in c.m.s.	time period	Luminosity taken	Remarks
91.2 GeV	1989-1995	197 pb^{-1}	Z^0 peak
130-136 GeV	November 1995	11 pb^{-1}	
161 GeV	July/August 1996	10 pb^{-1}	
172 GeV	October/Nov 1996	15 pb^{-1}	
183 GeV	1997	73 pb^{-1}	
189 GeV	1998	200 pb^{-1}	
196 GeV - 200 GeV	1999	254 pb^{-1}	
200 GeV - 208 GeV	2000	233 pb^{-1}	miniramps

DELPHI (DEtector with Lepton, Photon and Hadron Identification) was designed as a general purpose detector for e^+e^- physics at LEP on and above the Z^0, offering three-dimensional information on the track curvature and measurement of the energy deposition with a fine spatial granularity as well as the identification of leptons and hadrons over most of the solid angle.

The detector was installed in a cavern 100 meters below ground. It was situated at the lowest point of the LEP tunnel and the cavern was well below the level of the Geneva lake. Data from the experiment was usually sent to the control room situated on the surface by means of an optical link. There a computer cluster based on VAX (Dell) machines recorded the data, wrote it to tapes and simultaneously sent it via fast broadband link to the CERN IT reprocessing centre where all raw data files were written to tapes. This procedure was adopted to minimize the accidental loss of data during reboot/blackout or network problems.

The coordinate system of DELPHI is LEP oriented and has a z axis along the beam pipe. The horizontal x-axis pointed toward the centre of the LEP circle and the y-axis pointed upward, perpendicular to the slightly tilted LEP horizontal plane. The polar angle θ is given with respect to z and the azimuthal angle ϕ counted from the horizontal plane.
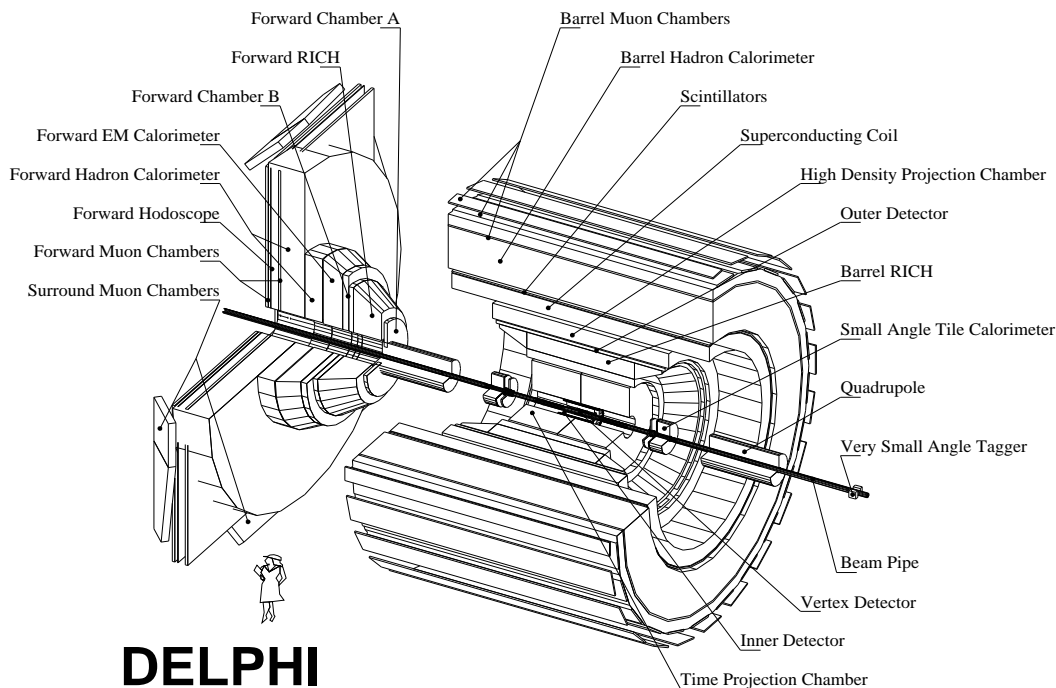

Figure 4.1: View of the DELPHI barrel and one end-cap (which is shown as separated from the barrel) with a set of VSAT modules around the beampipe on the right

4.2 The main structure

The DELPHI detector consisted of a cylindrical section (the barrel) with a length of about 10 meters and a radius of more than 5 meters. At each end of the barrel was an end-cap. Between the end-caps and the barrel was a gap (polar angles 43° and 137°) occupied by numerous cables and connectors. The barrel and end-caps were supported by a rail system which made it possible to move the endcaps perpendicular to the beam. The three main parts were surrounded by barracks with electronics, the gas system and the cryogenic plant which supplied nitrogen and helium to the superconducting coil.

The super-conducting solenoid provided a 1.23 T solenoidal field of high uniformity parallel to the beam axis in the volume containing the barrel tracking detectors. A current of 5000 A flowed through the coils of this 5.2 meters diameter solenoid.

4.3 Tracking devices

The tracking system consisted of the silicon Vertex Detector, the drift chambers in the Inner Detector, the Time Projection Chamber, the Outer Detector and the forward drift chambers. The location of the detectors are given in Fig. 4.1.

Tracking relied first on the Vertex Detector (VD) which consisted initially of two concentric silicon-strip shells surrounding the beam pipe. They had a radii of 9 and 11 cm and a lengths of 24 cm, covering a θ-range of 37° to 143°. Each shell was made up of 24 ϕ modules with each module put in space having four z segments. A third silicon-strip shell was later added (1994) when the beam-pipe at the DELPHI interaction point was changed to a tube of smaller diameter. Three $R\phi$-points per track could then be measured. The intrinsic $R\phi$ resolution was 6 μm. The Very Forward Tracker (VFT) was a part of the upgraded VD and was also added during 1994, to cover the θ angles 10°-25° and $155^o - 170^o$.

The second important subdetector of the tracking system, the Inner Detector (ID), consisted of two concentric parts. The inner part was a jet chamber having an inner radius of 12 cm, an outer radius of 22 cm and a length of 2x80 cm. This resulted in a θ-coverage of 17° to 163°. The jet chamber provided 24 $R\phi$-points per track through its 24 ϕ sectors, each having 24 sense wires. A coordinate resolution of 90 μm in the $R\phi$-plane was obtained. The outer part of the ID was a multi-wire proportional chamber (MWPC). Its radial location was between 23 and 28 cm, the length was 50 cm along the z coordinate and the θ-coverage was from 30° to 150°. The MWPC space contained five concentric layers, each having 192 wires and circular cathode strips. The wires provide fast trigger information (95% single track trigger efficiency) while the strips measured z with a resolution of < 1 mm.

The main tracking device was the Time Projection Chamber (TPC). It consisted of two cylindrical parts placed one after the other along the beam pipe. Each part had an active z-length of 134 cm, with inner and outer radii of 35 and 111 cm respectively. The θ angle was measured between 20° and 160°. The two cylindrical parts were each divided into six sectors in ϕ, each sector having 16 radial pad rows and 192 sense wires. The pads gave 16 points per track in the $R\phi$-plane, resulting in a space resolution of 230 μm. A z-resolution of 900 μm was obtained through the 192 track points provided by the wires.

The outermost tracking device was called the Outer Detector (OD). It consisted of 24 modules in ϕ. Each module was 4.7 m along z, had an inner radius of 198 cm and an outer radius of 206 cm. This lead to a θ-coverage between 43° and 137°. There were five radial layers of drift tubes in each module. All the layers measured the $R\phi$-coordinate with a

resolution of 110 μm. Three of them also contributed to a z-measurement with a resolution of 4.4 cm.

Each end-cap was equipped with two forward drift chambers: Forward Chambers A and B (FCA, FCB) for tracking in the forward and backward regions, i.e., between 11° to 35° and 145° to 169°. FCA was the inner detector, having a radial coverage of 30 to 103 cm and a z coverage of 155 to 165 cm. Each FCA-side contained three double layered half-disk chambers, rotated 120° in ϕ with respect to each other. The layers consisted of square cells (15 mm wide) with an anode wire in the centre. Six track points were measured by the FCA with a total resolution of 150 μm in the Rϕ-plane. The FCB covered a radius between 53 and 195 cm and a z between 267 and 283 cm. It also consisted of double layered half-disk chambers, but each half-disk was in the FCB divided into six ϕ segments. Each segment consisted of 12 pair-wise rotated sense wire planes, having a wire spacing of 2 cm. The 12 track points resulted in an FCB Rϕ-resolution of 120 μm.

4.4   The Electromagnetic Calorimeters

Electromagnetic showers were measured in the barrel with a high granularity by the High density Projection Chamber (HPC) using lead absorbers. It covered the polar angle from 43° to 137° and had an inner radius of 208 cm and an outer radius of 260 cm (i.e. the thickness was only 52 cm which corresponded to 18 radiation lengths).

The lead glass Forward Electromagnetic Calorimeter (FEMC) was used in the endcaps. It consisted of two modules, one in each endcap, situated between z-values 284 and 340 cm. Each module was made in the form of a disk having a radial coverage from 46 to 240 cm from the beam line. The θ-acceptance was from 10° to 36.5^o for the forward calorimeter and from 143.5^o to 170° for the one in the backward direction. A calorimeter was built up of 4532 lead glass blocks with the shape of truncated pyramids. They were arranged in such a way as to point toward the interaction point. Each pyramid was 20 radiation lengths deep and had a granularity of one degree in both θ and ϕ. Read-out was done with vacuum photo-triodes. FEMC had a 4% energy resolution at a beam energy of 45.6 GeV.

The smaller polar angles, essential for detecting electrons and positrons from two-photon processes and for luminosity measurements, were covered until 1994 by the Small Angle Tagger (SAT) and the Very Small Angle Tagger (VSAT).

The Small Angle Tagger (SAT) [13] also consisted of two end-cap calorimeters. They were placed between z=233 and 285 cm and radially between 10 and 36 cm. The SAT calorimeters were used to cover a θ-range between 2.5^o to 7.7^o (172.3^o to 17.5^o) in the forward (backward) direction. Each calorimeter was built by alternating lead sheets and plastic scintillating fibers, which were aligned parallel with the beam-pipe. Read-out was done by light-guides and photodiodes, segmented in the Rϕ-plane to have a granularity in ϕ of 7.5^o (15°) for the inner (outer) four radial rings, while θ-granularity was 0.7^o. The 28 radiation lengths deep modules had an energy resolutions of 1.6% at a beam energy of 45.6 GeV. Before the 1994 LEP run the SAT was replaced by the Small angle TIle Calorimeter (STIC).

The STIC was made of lead-scintillator towers arranged in a so called "shashlik" shape with 47 layers longitudinally and logically divided up into 160 towers for each of the two calorimeters (forward and backward). The signal was taken out from each tower to the photodiodes by means of optic fibers which were going through holes in the towers. STIC had in addition layers of silicon strips detectors with 3840 silicon strips that were used in

the reconstruction of the shower direction. The radial resolution of the silicon strips (1.7 mm pitch) was 400 μm. 64 scintillator wedges in front of STIC (the veto counters) were used to separate charged from neutral showers. The spatial resolution of the calorimeter alone was 1.5 degrees in ϕ and from 300 μ to 1 mm in radius. A 3% energy resolution at 45 GeV beam energy and a spatial uniformity better than 2% were measured on a test beam at the CERN SPS. The precise mechanical construction allowed to measure luminosity at the 2 per-mil level (systematic error).

In addition, scintillator systems called HOF (Horizontal Flight Tagger) in both end-caps and TOF (Time Of Flight counter) around the barrel were implemented for triggering purposes and in order to achieve complete hermeticity for high energy photon detection.

4.5 The Hadronic calorimeter

The HAdron Calorimeter (HAC) was the most massive subdetector of the DELPHI experiment. It consisted mainly of iron since the iron return yoke of the magnet was instrumented with limited streamer mode detectors to create the Hadron Calorimeter. The return yoke also served as a filter for muons which were identified by two drift chamber layers.

The muon reconstruction was provided by the system of MUon Chambers (MUC). These drift chambers were organized in the groups MUon Barrel and MUon Forward (MUB and MUF) with polar angle coverages $53^o - 88.5^o$ $(91.5^o - 127^o)$ and $20^o - 42^o$ $(138^o - 160^o)$.

In 1994 a layer of streamer tubes called the Surrounding Muon Chambers (SMC) was installed outside the end-caps to fill the gap between the barrel and forward regions.

4.6 Particle Identification

Charged particle identification was provided both in the barrel and the forward regions by mainly liquid and gas Ring Imaging Cherenkov Counters (RICH). Some information about the particle type was also obtained from the dE/dx measurements in the TPC. The RICH was the most unique subdetector of DELPHI and the one that really made the DELPHI experiment different from other LEP experiments. The polar angle region covered by the RICH detectors was large: from 15° to 165° but with a hole between 35° and 42° (138° - 145° on the other side).

There were two radiators which were used in two different kind of layers in the RICH: the C_6F_{14} liquid (with n=1.28) between quartz windows and C_5F_{12} or C_4F_{10} gas (with n=1.0018). The liquid layer was only 1 cm thick and the gas layer was up to 50 cm thick. Both radiators produced Cherenkov rings on the same photodetector but the light from the liquid radiator came directly and the gas radiator light needed to be reflected by spherical mirrors. The photodetector itself was a multiwire proportional chamber with drift tubes (with an applied voltage up to 54 kV). The whole RICH detector needed to be heated and maintained at a constant temperature of 40 ± 0.3^o C in order to avoid evaporation/condensation in the radiators. 280 temperature sensors, 40 heating circuits and 2 independent computers were needed to accomplish this task. The construction of the RICHes and their maintenance were challenging. The barrel RICH came into operation in 1992 and the forward RICH in 1994.

Chapter 5

The VSAT calorimeter

5.1 The geometrical location of the VSAT

The VSAT (Very Small Angle Tagger) detector [119] was one of the three DELPHI sub-detectors which were able to provide beam related information. The other two were the VD (Vertex Detector) around the interaction point and the STIC (Scintillator TIle Calorimeter) in each end of the barrel. VSAT was the most sensitive to the beam conditions since its position was very close to the beams and the measurements were therefore strongly affected by the background and any beam distortions.

The VSAT modules were quite far away from the interaction point (IP) and were mainly counting Bhabhas with a θ angle between 4 and 7 milliradians (ϕ angle within $\pm 50^o$ or $\pm 135^o$ at θ=6 milliradians).

VSAT consisted of four identical modules, each with a 3x5 cm sensitive area. They were placed as two pairs of modules 7.7 meters from the interaction point (IP) behind two superconducting quadruple magnets that were providing the low β (i.e. small beam size) at the IP see (Fig. 5.1). The field of the quadrupoles tended to focus particles in the vertical plane and defocus them in the horizontal plane.

The name of the four modules were: B1 and B2 for the backward modules (or modules 2 and 1) and modules F1 and F2 (4 and 3) for the forward ones in the direction of the electron beam (Fig. 5.1). Note that the modules situated on the outer side of the LEP ring were 1 and 3 or B2 and F2. These usually had more background than the modules on the inside of the LEP ring.
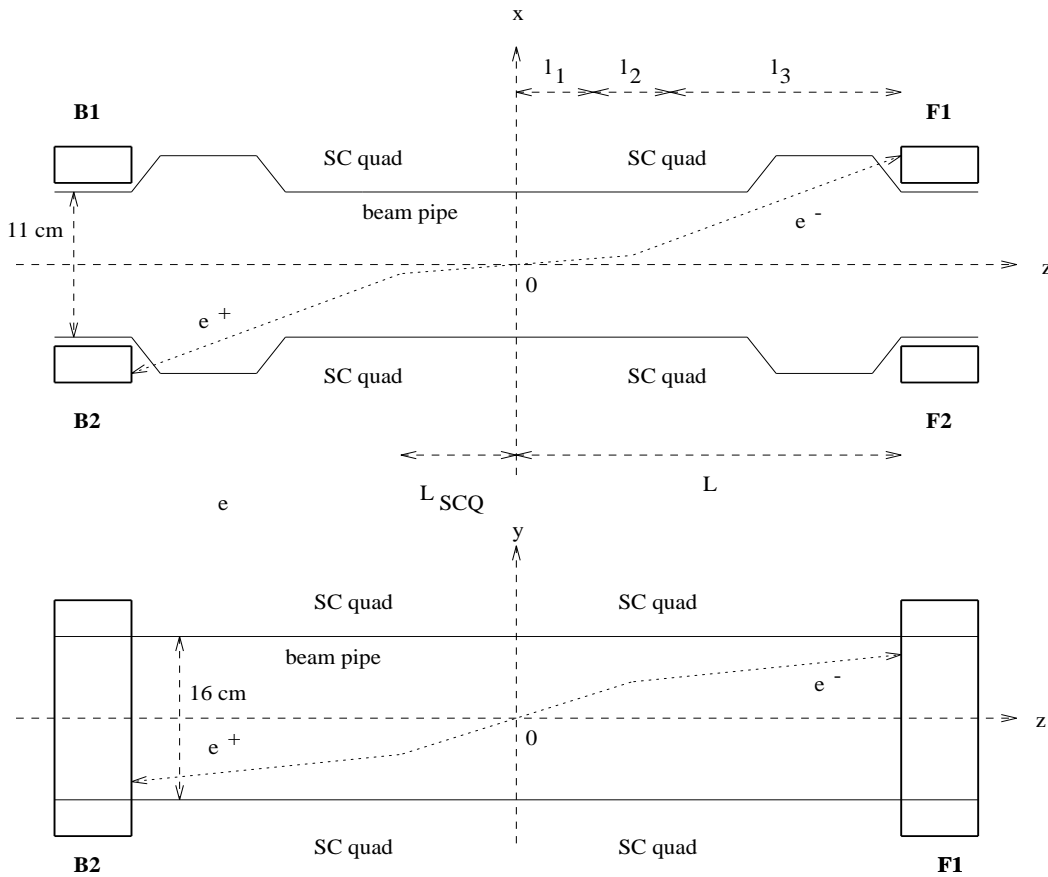

Figure 5.1: The VSAT module positions in the horizontal (top plot) and the vertical planes (bottom plot). The distances were: L=7.7 m, L_{SCQ}=3.7 (from the IP to the quadruple centre), l_2=2.0 m (the length of the quadruple), l_1=2.7 m and l_3=3.0 m.

5.2   VSAT module construction

Each detector module (B2, B1, F2, F1) was a sandwich calorimeter as shown in Fig. 5.2, made up by tungsten absorbers and silicon detectors. There were 11 silicon diodes or FAD (Full Area Detector) planes and three strip planes (two for the X and one for the Y coordinate).

Both types of silicon detectors had a thickness of 300 μm (0.3 mm). All FADs were separated by tungsten absorbers with a size of 5.12 cm x 5 cm and with a two radiation length thickness (0.38 cm). The FADs had a full depletion voltage of -30 V (operational voltage around -25 V) with a capacitance of 500 pF. A lead shield was installed behind the last FAD plane in order to stop background from off-momentum leptons entering the calorimeter from the back.   The three silicon strip planes called X1, Y and X2 were 5x5
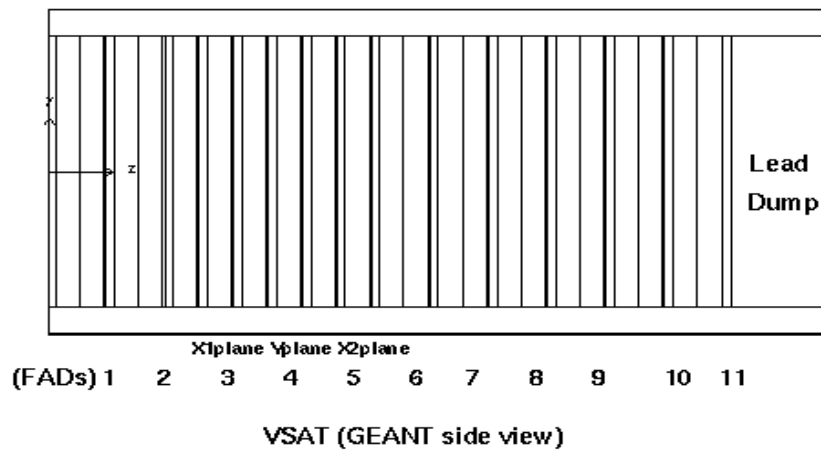

Figure 5.2: Side view describing the internal composition of a VSAT module (made with the GEANT 3.21 program)

cm^2 in size with a 1 mm pitch and they were placed after 5, 7 and 9 radiation length. They were used for the (X,Y) shower position measurement. There were two planes for the X measurement with 32 readable strips (each strip 1 mm wide, 50 mm high) and one for the Y measurement with 48 strips (each strip 50 mm wide, 1 mm high). Full depletion and operation voltages were +25 V for both types of strip planes.

The distance from the centre of the beam to the modules was decreased to about 5.7 - 5.9 cm after the LEP II upgrade of the beam pipe (end of 1997). The idea was to bring the detector modules as close as possible to the beams in order to increase the acceptance for gamma-gamma physics. Their horizontal displacement was not completely symmetrical. Therefore the change of position increased the acceptance of each module by a different amount. The position of the VSAT modules were basically defined by the shape of the beam-pipe section (Fig. 5.3).
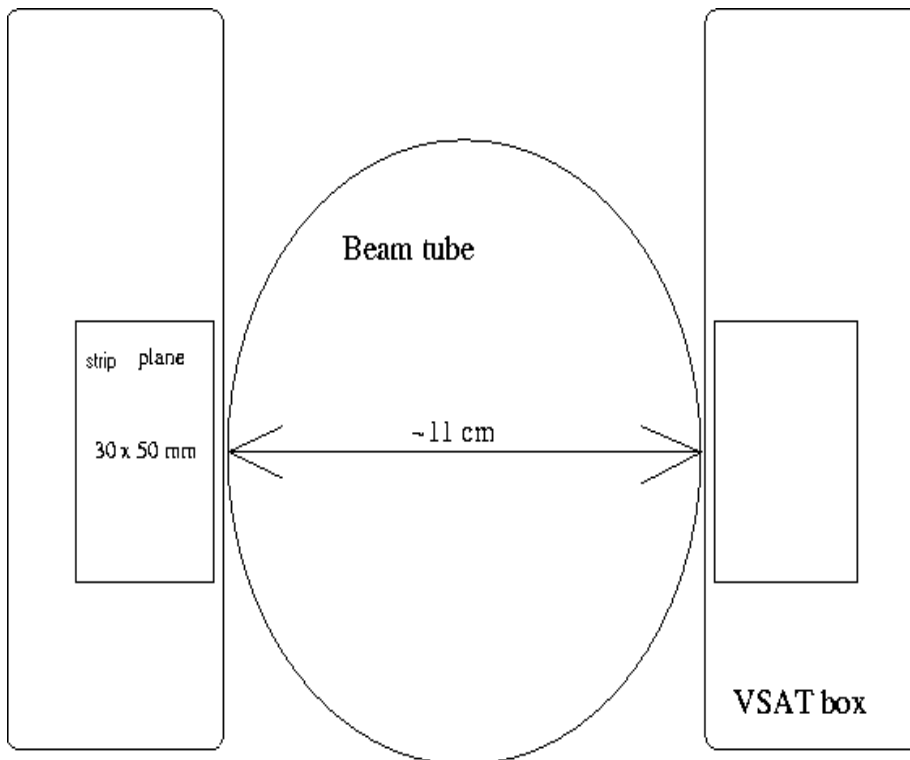

Figure 5.3: A plot of the location of one pair of VSAT modules with respect to the beampipe

Table 5.1: The position of the VSAT modules

$Years:$	Mod1(B2)	Mod2(B1)	Mod3(F2)	Mod4(F1)
$1994 - 97$	Mod 1	Mod 2	Mod 3	Mod 4
	-6.386 cm	6.178 cm	-6.343 cm	6.219 cm
	-1.677 cm	-1.675 cm	-2.231 cm	-2.335 cm
	-776.0 cm	-775.8 cm	775.9 cm	775.8 cm
$1998 - 00$	Mod 1	Mod 2	Mod 3	Mod 4
	-5.728 cm	5.915 cm	-5.915 cm	5.800 cm
	-2.399 cm	-2.245 cm	-2.245 cm	-2.377 cm
	-776.10 cm	-776.07 cm	776.07 cm	775.55 cm
$1998 - 00$	Mod 1	Mod 2	Mod 3	Mod 4
	-5.78 cm	5.96 cm	-5.97 cm	5.85 cm
	-2.35 cm	-2.19 cm	-2.20 cm	-2.33 cm

Events which had the largest transversal shower profile in the first X strip (a so-called first strip hit or strip error) were always cut away in the off-line reprocessing since the x-measurements requires data from two neighboring strips to the strip with the largest signal in order to extract an accurate position of the shower maximum. If the 1st strip had the largest signal then a leakage correction of the energy was also impossible.

The leakage correction was used to evaluate the missing part of the energy of the electromagnetic shower. Photons and leptons from electromagnetic showers are sometimes completely stopped in a calorimeter volume. And sometimes they leak energy through the side walls. The closer the maximum of the shower was to the upper, lower, left or right edge of the module the greater the energy loss and the greater the correction. In the case of a first strip hit the correction was not possible to calculate due to the fact that the shower maximum position was undefined if the 1st strip had the largest signal. As a result the acceptance of the coordinates was 0.5 mm shorter for X than is shown in Table 5.1.

5.3   Electronic Hardware

The signals from the VSAT silicon detectors were readout using a track-and-hold method where the peak value was recorded by an ADC. The sample time of the signals was 500 to 650 nanoseconds. All of the 124 ADC channels in each module (12 from FADs, 64 from two X planes and 48 from one Y strip plane) had 16 binary digits.

The track-and-hold circuits were located in the tunnel while the rest of the logic was located in the counting barrack D2 some 50 meters away. Problems with VSAT were similar to that of all DELPHI sub-detectors: electromagnetic noise from electrical and radio-wave sources, heating, unstable cooling, mechanical instability in connectors due to a partial dismounting of the VSAT and due to the fact that it was necessary to switch off a lot of systems during each winter shutdown period.

VSAT, as all DELPHI sub-detectors, has its own homepage available at the DELPHI sub-detector description page at [120].

The VSAT electronics worked well until the end (10 years) with only 4-6 strips and 1 FAD plane dead at the end of data-taking in 2000. This is a decent performance when considering that the other 448 strip and 44 FAD planes worked well and needed only a re-calibration once or twice per year.

All voltages, bias currents and temperatures in the modules were monitored constantly during data-taking and during test periods by the slow control system of VSAT which was connected to the DELPHI Slow Control database [130]. This was a very important feature which gave a lot of useful warnings when the background conditions were dangerously high. The synchrotron radiation and the off-momentum electron background proved to be very hard to reduce in spite of big efforts which were made by the DELPHI and the LEP teams [131]. During September 15, 1995 one essential part of the protection system, closest to the DELPHI collimators, was not closed on one side of DELPHI due to an operator error. This incident [130] lead to a severe radiation exposure of the VSAT inner and outer backward modules. The damage produced an increase of the bias currents by a factor of two to four and the energy resolutions of these modules were decreased in some places and they did not return to the initial performance until the last days of DELPHI.

The VSAT electronics could record three kinds of events:

Bhabha (BH) - defined as a coincidence between hits in two diagonal modules with signals above threshold. The threshold was typically at 25 GeV for the fills with a beam energy above 45 GeV.

Single electron (SE) - defined as energy deposition above the low energy threshold in any of the four modules. It could be down-scaled with different factors for outer and inner modules (for different SE background conditions).

False Bhabha (FB) or Accidental Bhabha - defined as a coincidence between one module and its diagonal module but delayed by four LEP bunch crossings. This trigger took too much time - 4 periods of 22 microseconds each after a Beam Cross Over signal arrival (BCO). The trigger was therefore switched off prior to the LEP II phase (False Bhabhas were selected in off-line mode instead). Energy thresholds were the same as for Bhabha triggers.

The VSAT hardware composition and the overall picture of the data flow is shown on the next page (see Fig. 5.4).
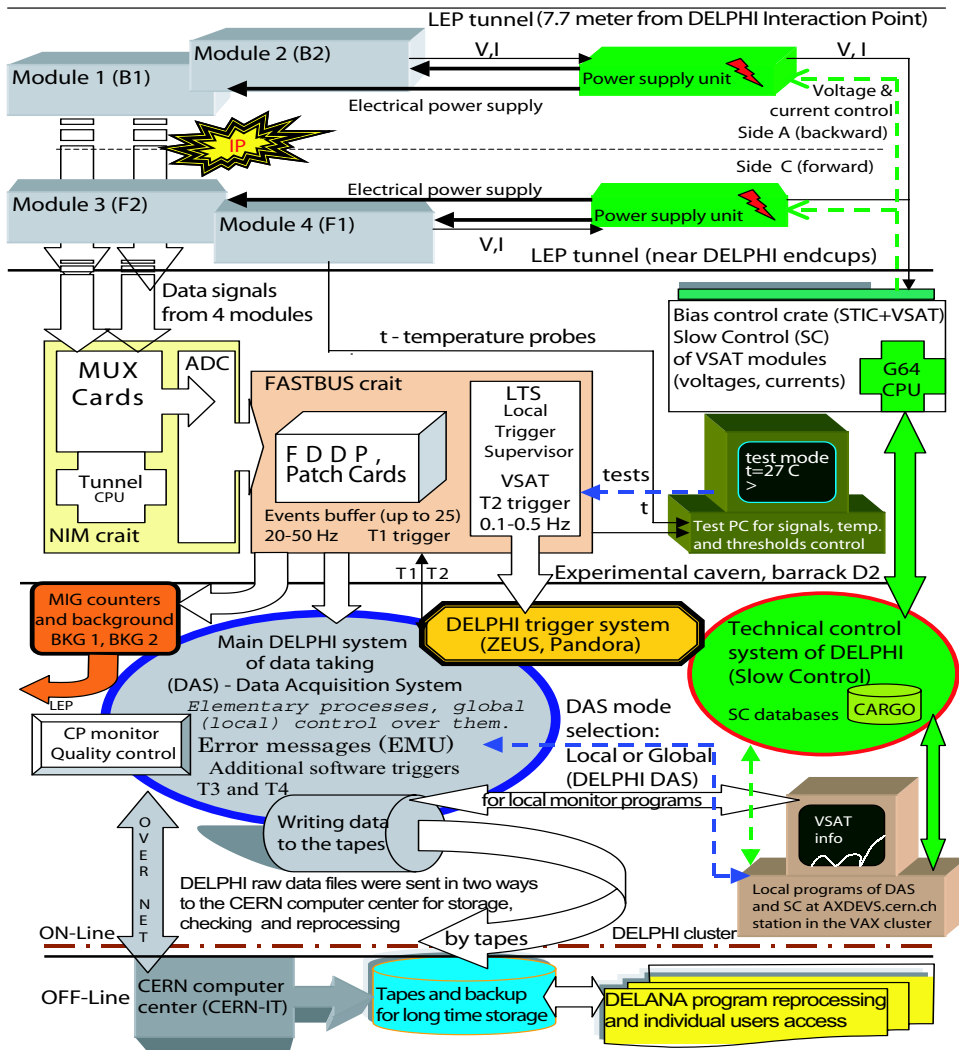
Figure 5.4: VSAT hardware and data flow map.

The triggering and data acquisition system of the VSAT detector was untypical for DELPHI due to the high rate of events and the positions of the modules. It was almost independent of the main data acquisition system of DELPHI, i.e., it had its own buffer in order to avoid triggering the entire DELPHI data acquisition. The basic T1 trigger required hits in double modules with the criteria discussed above (Bhabha trigger) or single hits (Single electrons). These single electron events were downscaled and were used in the analysis as a background sample.

The VSAT T1 level triggered events were stored in the VSAT data storage buffer. Initially it was designed to store up to 20 events. Since the rate was high, an efforts was made to compact the data in this buffer and this gave it a larger capacity. The maximum capacity of the VSAT T1 events bank was 28 events by 2000. When the buffer was full, VSAT made a T2 event signal and sent a trigger to the whole of DELPHI (transferring the events in the buffer to DELPHI). One can see from the distribution below (Fig. 5.5) that this did not happen very often - usually some other sub-detector triggered DELPHI (and VSAT) before our buffer was full. The VSAT buffer was transfered to the central DELPHI partition and was written on tape. The buffer length was maximum 12-20 events long in the beginning of DELPHI and 25-28 events long during last two years of the DELPHI operation.
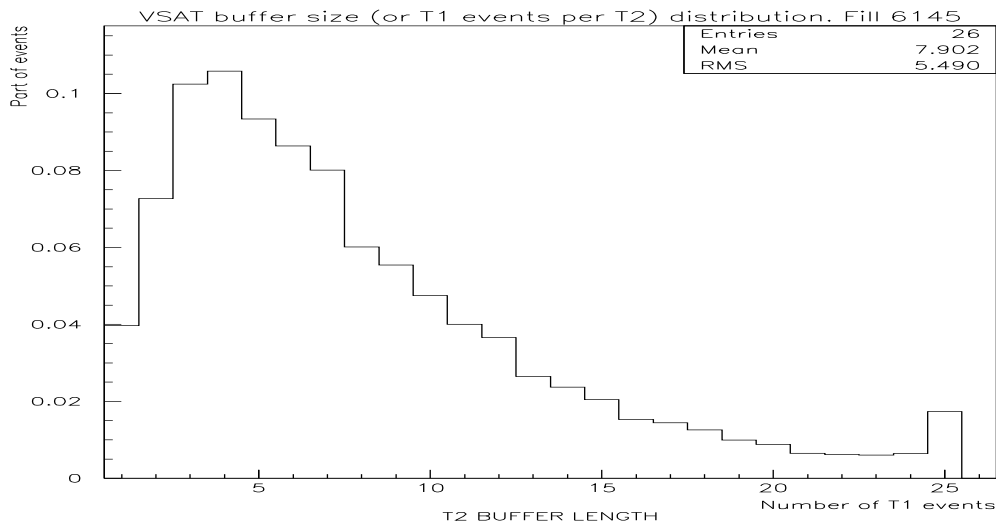

Figure 5.5: The VSAT buffer size (the number of T1 events per T2 event) during the physics fill 6145 (19.08.1999) with a 99.828 GeV beam energy. The picture was made by PAW using a file created by the VSAT on-line local monitor.

5.4   VSAT on-line tasks and the data acquisition

VSAT provided data for both on-line and off-line processes. VSAT was the only sub-detector in DELPHI which could provide on-line background and luminosity measurements during LEP filling, acceleration and adjusting of the beams. This feature was based on the direct connection from the VSAT Local Trigger Superwiser (LTS) electronic unit to the DELPHI scaler logical box and processors. VSAT signals were processed there together with important direct signals from other DELPHI sub-detectors affected by beam parameters and background.

The data from the LTS provided signals to so-called MIG scalers: Bhabha counters (BH1 for events in modules 1-4 and BH2 for events in modules 3-2) - integral (per fill) and differential (per second) number of Bhabha hits in each diagonal, False Bhabha (FB) counters - integral and differential number of coincidences in both diagonals, Single Electrons (SE1 - SE4) counters - integral and differential number of single hits in each of the four VSAT modules. Before the LEP II phase, the False Bhabha counters were abandoned since DELPHI could not afford to wait 3 minibunch periods of 22 microseconds each for such a coincidence at the high collision rate of LEP II (the dead time became too long). The False Bhabhas rate could, however, be calculated off-line from the Single Electron rates.

Some scaler values/numbers were sent to the so called LEP101 program (running in the DELPHI VAX cluster) which showed the up-to-date parameters and conditions of the LEP collider and the four LEP experiments.

A combination of Single electron counters formed the Bg2 counter which could be accessed by the same LEP101 program and on the LEP Information webpage as well as the TV picture which showed the real-time LEP activities on the LEP TV-sets at CERN. Bg2 mainly measured electrons (and positrons) but VSAT had the possibility to evaluate the X-ray background by using the signal from FAD plane No 1. The Bg2 number was made by summing the single electron hits in all four VSAT modules (for a beam energy above 95 GeV the rate was about 2000 Hz). This sum was multiplied by a factor to get the Bg2 number in a 0 - 5 unit range. The Bg2 in such a form, represented the level of radiation risk for the detectors (especially to the gas and silicon detectors). The Bg2 rate was provided to LEP at all times even if DELPHI was not in a data-taking mode. A Bg2 rate less than 1.0 meant that the background condition was calm, if it was 5.0 or more that meant that data-taking was impossible due to the high background and the high voltage for the detectors was switched off.

The method to measure an instant online luminosity was somewhat more complicated:

$$L = \frac{(Bhabha_{14} + Bhabha_{23}) - (SE1 \cdot SE4 + SE2 \cdot SE3)}{\sigma(500nb)} \qquad (5.1)$$

where $Bhabha_{14}$ and $Bhabha_{23}$ were the Bhabha counter values and $SE1-4$ were the Single Electron counters. The constant σ (equal to 500nb) represents the averaged cross-section of Bhabha events for the typical LEP conditions.

The Data Acquisition operator (DAS Maestro and shift leader) at DELPHI received a traceplot of the background and the luminosity. These traceplots helped to define the right time for the collimators to be closed (opened) and for the start of the DELPHI data-taking. The sum of the single electrons rate was called the traceplot of differential Single Rate and the sum of Bhabhas was called the traceplot of differential Luminosity (see Fig. 5.6)
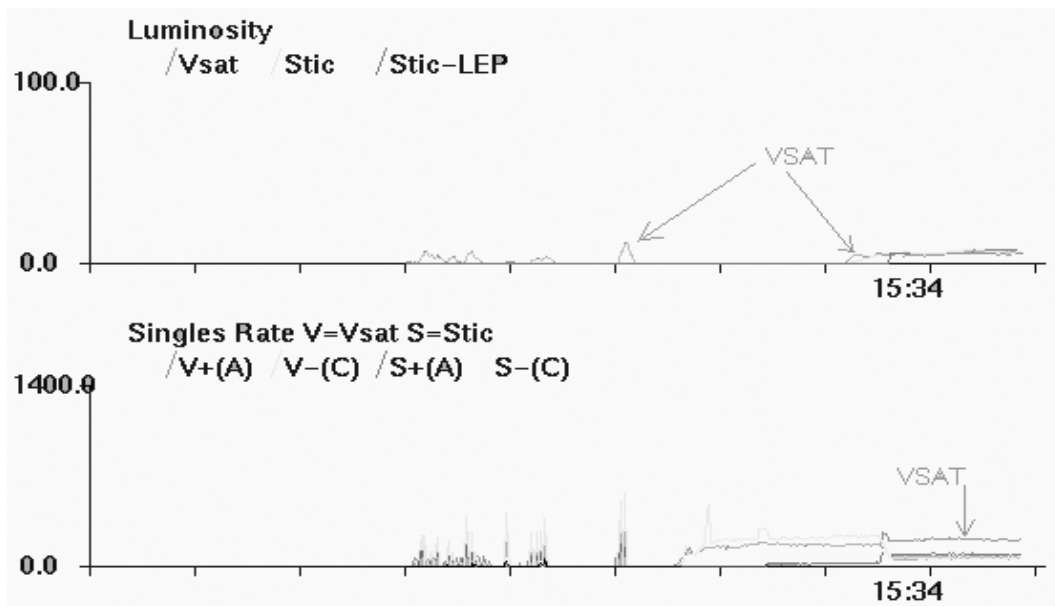
Figure 5.6: On-line traceplots of the VSAT single electron rates and the Bhabha rates from the screens used by the DAS (Data Acquisition System) Maestro in the DELPHI control room.

5.5 The VSAT off-line data

The VSAT data was written on the same cassettes as the rest of the DELPHI data stream. The data was transferred by a local network to the CERN computer centre instantly during data-taking. The raw data was processed and stored temporary there. In order to reprocess the VSAT part of the data, a separate set of files with VSAT information from each event was needed. All these files should be available to the VSAT team at any time, i.e., be stored on our own disks and cassettes. Such files were provided by the DELANA [67] program which used to run in the CERN-DELPHI computer centre at all times during the data-taking periods and afterwards. DELANA checked the raw data files, selected the real physics events, decoded them, calculated the energy response and produced tracks. It gave in other words a reconstructed picture of the event as it was seen by the DELPHI hardware.

In DELANA there was a part called LUMANA (connected with luminosity) which extracted, checked and wrote special VST files in a common DELPHI directory. From this directory, files were transferred to the VAX station which belonged to the VSAT team. Here the real reprocessing started more or less automatically as DELANA (LUMANA) provided the files. The monitoring program THOR (Total Handling Off-line Re-processing) created by Andreas Nygren [121] looked for new VST files and if they were available with the requested size (enough to process one physics fill) then the ODEN program started. ODEN was made by Per Jonsson [122] and had as a task to make summary ntuple files with basic parameters from one LEP fill (energy, beam intensity, background, luminosities) and the corresponding DELPHI runs (time, detectors status, etc). ODEN also did an important task

based on a COMPACT command file which was coded by Eric Vallazza in 1992. The task of COMPACT was to archive, compact and combine several big VST files into one FX file per fill. After that it could be stored on local disks, cassettes (using Exabyte connected to the same VAX station) and common HPSS (High Performance Storage System, now changed to CASTOR), i.e., a high capacity storage system based on disks or cassette drivers driven by robots.

The FX files could be used several times with summary ntuples. Both FX and summary ntuples were necessary for the next reprocessing phase which was performed by the VSDIAG program. The program was originally written by several people [123] but it needed to be modified a lot each year and for each new DELANA version. The DELPHI software team produced 4-8 versions of DELANA each year and only the last one was processing the whole set of raw data.

After the VSDIAG program had finished one fill it was possible to receive information about the Single electrons (for background checks), Bhabha events (for beam parameters and the luminosity estimation) and gamma-gamma events (for two-photons physics analysis). The information came as histograms and ntuple files (two per fill) and gamma-gamma text files with event numbers.

Corrections had to be done during the start of each year of data-taking and for new beam energy fills. The VSAT modules normally had to be removed during long shutdowns in order to give access to the LEP beam pipe near the superconducting quadrupoles on both sides of the DELPHI barrel. After each installation of the VSAT modules a new survey of their exact location was needed. This was carried out by the Milano group and its engineer Pietro Negri. There were small differences each time after a module had been removed and this had to be entered in the LUMANA geometrical database. This was done for both real data processing and for Monte-Carlo simulation.

An overview of the off-line parameters (short term results were obtained after two to six weeks after data-taking), the final luminosity and the gamma-gamma reprocessing can be seen on the next page (see Fig.5.7).
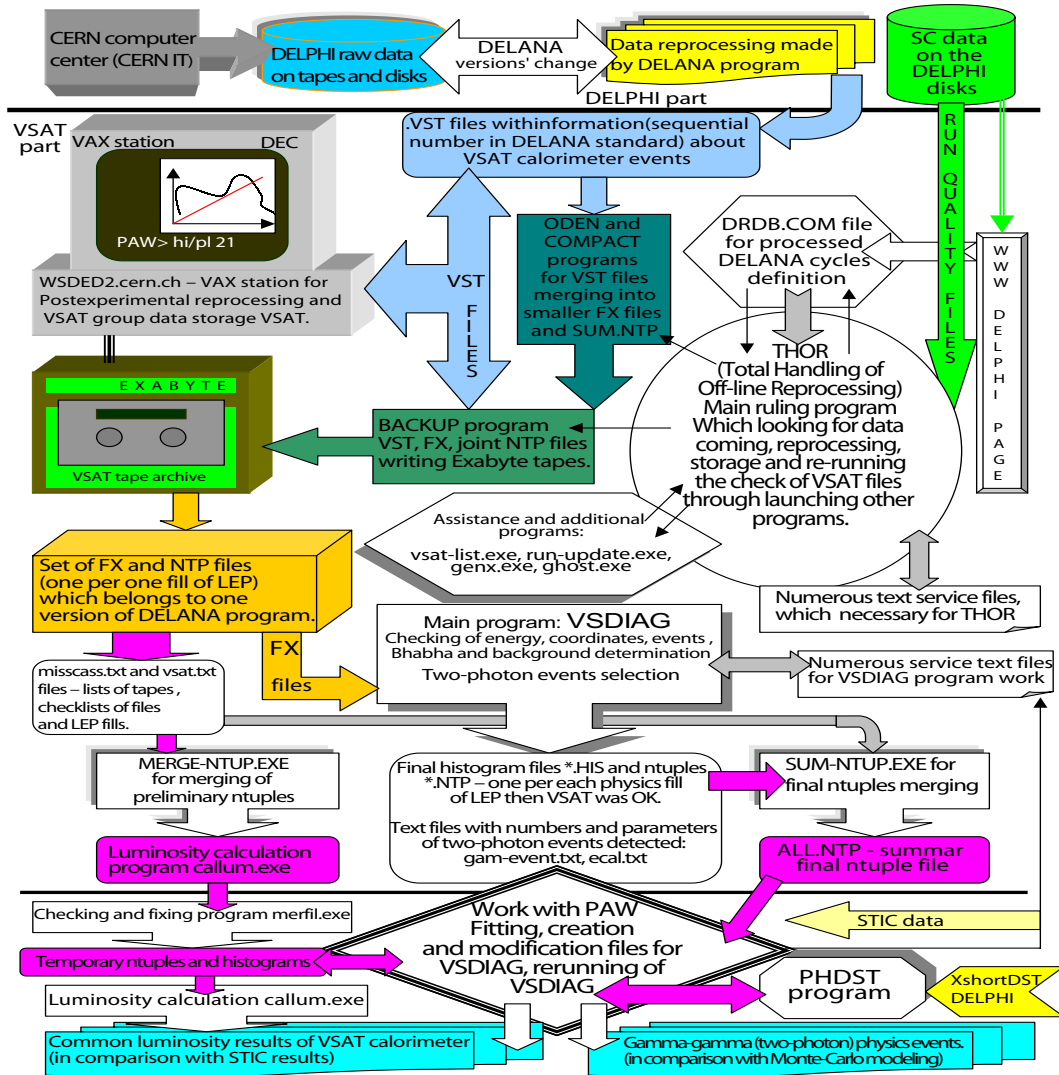
Figure 5.7: Map of VSAT off-line data reprocessing.

5.6   Luminosity measurement using Bhabha scattering

The luminosity is a crucial quantity for any high energy physics experiment. The luminosity (L) is obtained from the number of collisions (N) per unit time: $L = N/\sigma$ where σ is the cross-section in barn units (1 barn = $10^{-28}m^2$). The cross-section gives the probability for a specific process to occur and in the collider case the probability P of a specific process is given by:

$$P = \frac{N_x N_y \sigma}{2\pi \cdot s_x \cdot s_y} \tag{5.2}$$

N_x, N_y are here the number of beam particles (electrons and positrons in the LEP collider case), σ is the process' cross-section and $2\pi \cdot s_x \cdot s_y$ represents the total intersection area of the beams at the interaction point. One should keep this area as small as possible and the number of particles in the beams as high as possible to obtain a maximum events rate.

The integrated luminosity is given by:

$$\int L dt = \frac{N_X}{\sigma_X} \tag{5.3}$$

where N_x is the number of events produced in any reaction X during a time period dt and σ_X is the cross-section for that process. A high precision measurement of the luminosity therefore allows the accurate determination of the absolute cross section of other processes from their rate. Because of its large cross-section, especially at small angles, the Bhabha scattering ($e^+e^- \rightarrow e^+e^-$) is very useful for determining the luminosity at e^+e^- colliders. The theoretical cross-section has to be known with high accuracy. At LEP energies, the contribution to the cross-section from weak and higher order effects is non-negligible and the lowest order QED calculation does not suffice, but those effects have been calculated with a high accuracy.

In pure QED, Bhabha scattering can to the lowest order be visualised by two Feynman diagrams that describe the leptons interacting by exchanging either a space-like or a time-like photon propagator. At small angles the latter graph dominates. At high energies the electron mass can be neglected and the centre-of-mass differential cross-section is easily calculated and is found to be:

$$\frac{d\sigma_0^{QED}}{d\Omega} = \frac{\alpha^2}{4s}((1 + c^2) + 2\frac{(1+c)^2 + 4}{(1-c)^2} - 2\frac{(1+c)^2}{1-c}) \tag{5.4}$$

where $c = \cos\theta$, s is the centre-of-mass energy squared and $d\Omega$ is the solid angle element $d\cos\theta \, d\phi$. The angles θ and ϕ are defined as the polar and azimuthal scattering angles of the positron. The three terms in the equation correspond to the annihilation diagram (s channel),the exchange diagram (t channel), and the interference term (between both of them). A small scattering angles (θ less than 1 degree), the exchange term will dominate since it has a pole at $\theta = 0$ due to the infinite range of the Coulomb potential.

Equation 5.4 can be reduced to the simpler form:

$$\frac{d\sigma_0^{QED}}{d\Omega} = \frac{\alpha^2}{4s}\left(\frac{3+c^2}{1-c}\right)^2 \tag{5.5}$$

and for θ less than 1 degree, i.e. a longitudinal momentum much larger than the electron mass (the so called extreme relativistic limit [84]), it can be simplified further to

$$\frac{d\sigma_0^{QED}}{d\Omega} \approx \frac{\alpha^2}{4s}\frac{(3+cos^2\theta)^2}{4sin^4(\theta/2)} \tag{5.6}$$

from which the forward peaking of the cross-section can be clearly understood.

The systematic error in a relative luminosity measurement during LEP II was 1% after off-line, end-of-the-year processing using the STIC data for comparison and control (Fig. 5.8). During the LEP I period, when backgrounds were less severe, a relative luminosity error of 1 permill was achieved by the VSAT.
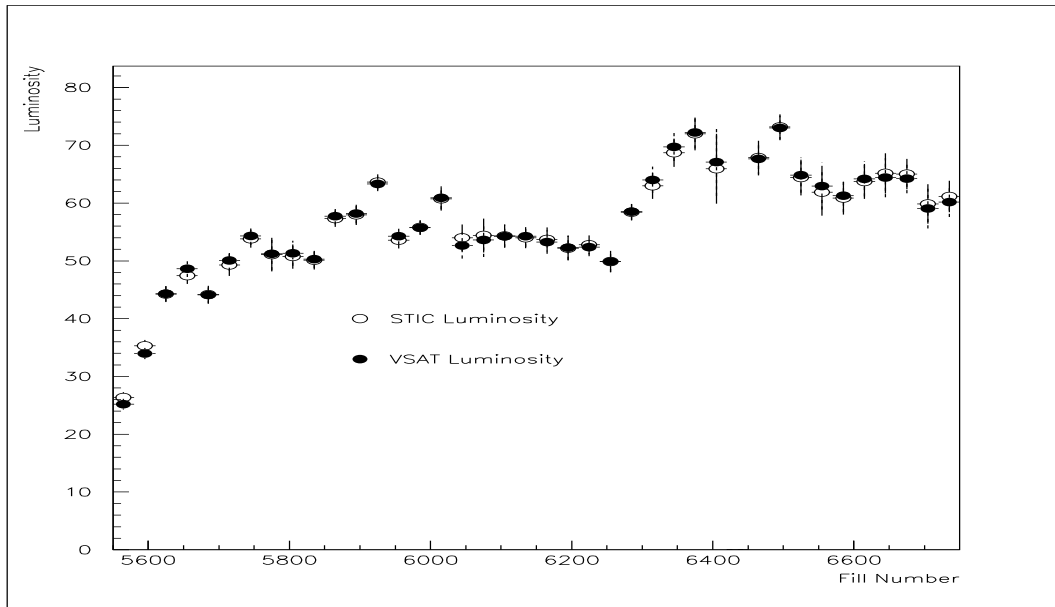
Figure 5.8: VSAT (closed circles) and STIC (open circles) luminosity per fill in nb^{-1} during year 1999.

5.7   The energy resolution

The energy resolution of VSAT at 45 GeV was 5% and at 95 GeV it was around 4% (it followed the parameterization formula $R = 35\%/\sqrt{E}$ there E is in GeV). The resolution was usually worse for the outer modules (1 and 3).
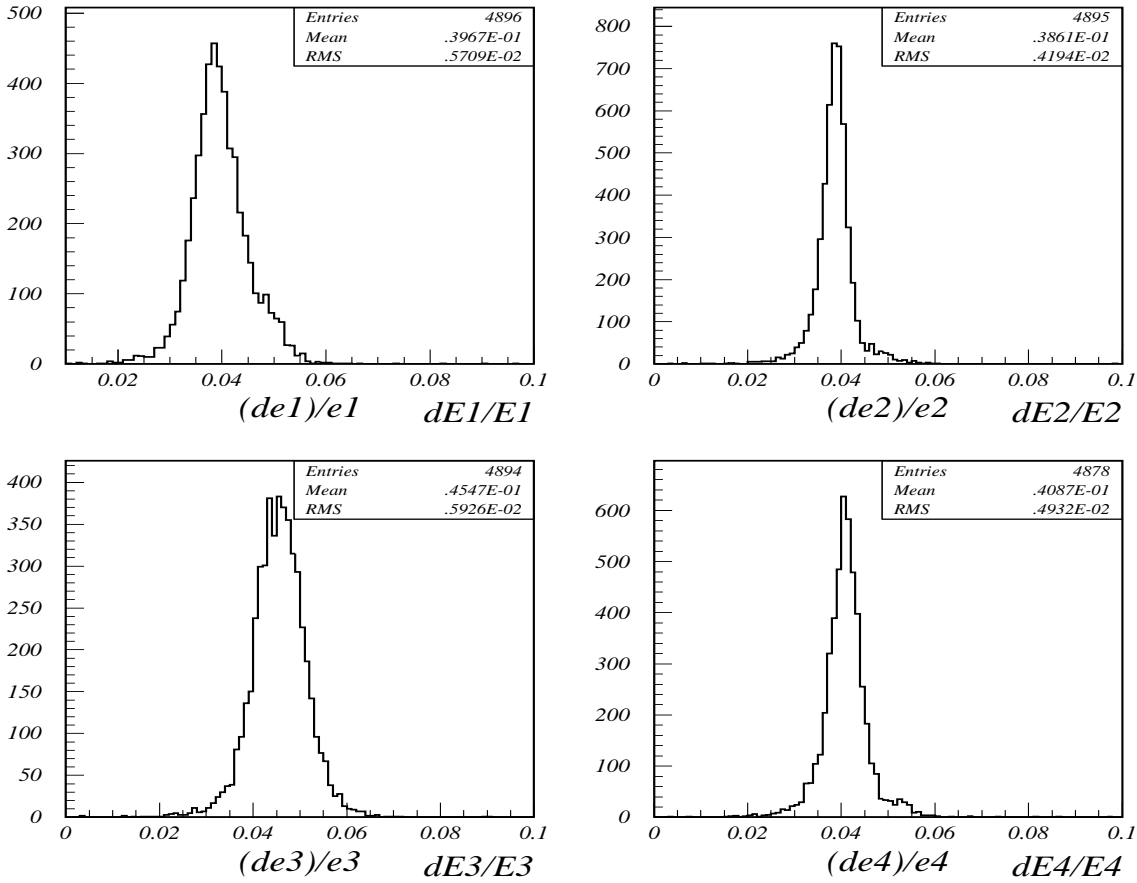
Resolution (dE/E) distribution for all modules

Figure 5.9: The VSAT energy resolution distributions for 95 GeV beam energy (1998).

The VSAT energy resolution was very stable for the inner modules and showed a small rise (about 1% between the beginning and the end of the year) in the outer modules due to a higher background. High background spikes, radiation damage of the FAD and the strip planes affected the energy distribution by making the energy resolution worse. The damage due to severe background storms had the longest effect and usually lasted all during the year of datataking or even longer (Fig. 5.10). This could be seen by monitoring bias currents and the resolution through long periods of time. Long pauses (like data-taking stops due to repair and the winter period) when bias voltage were not applied gave the detectors a possibility to recover.
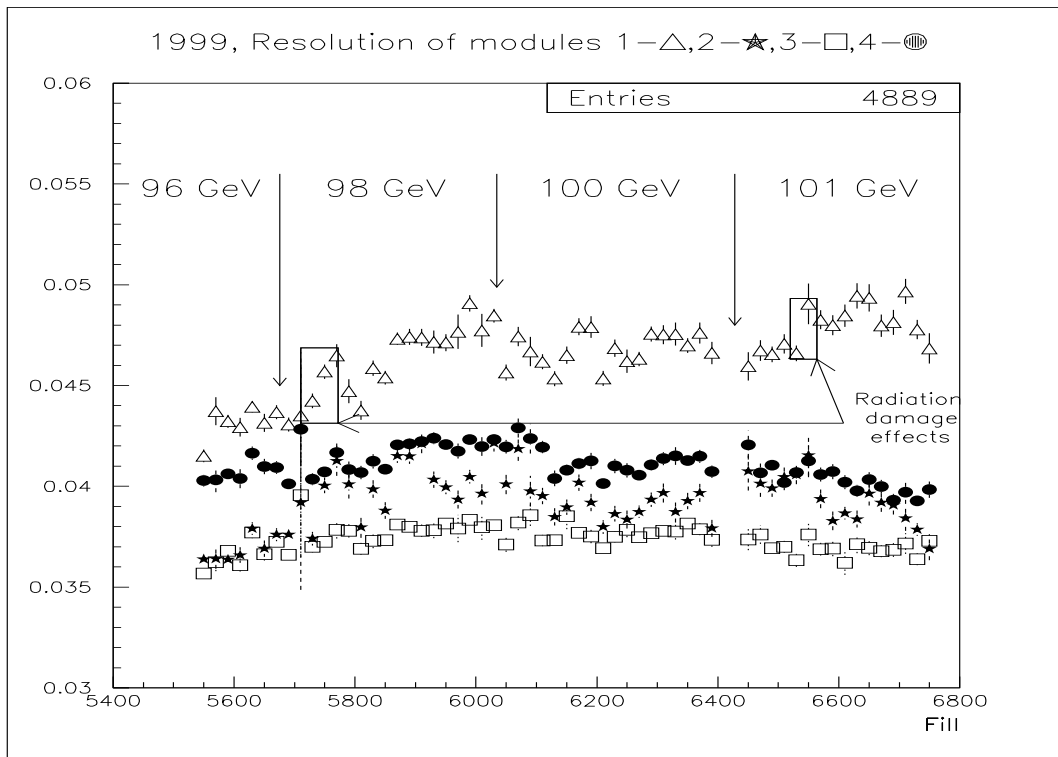
Figure 5.10: The VSAT energy resolution during year 1999. Module 1 - triangles, Module 2 - stars, Module 3 - squares, Module 4 - circles

The resolution of the silicon strips in the X and Y coordinate measurements was about 170 microns (1 mm pitch). Only the first X1 silicon strips plane was used for the determination of X coordinate of the electromagnetic shower maximum. The second plane X2 was used only in case of problems with the peak determination.

Some of the strips died during the 10 year operation of VSAT. This problem was worse for module 1 where sometimes two nearby strips were dead. An example of this effect can be seen in Fig. 5.11 which represents the shower maximum distributions for all four modules in a 3D view. It is clearly seen how a temporary dead strips in Y strip planes of modules 2 and 4 can produce a holes in the shower maximum coordinates. A nearby strip likelyhood algorithm was introduced and added to the reprocessing program and this algorithm closed the holes by using the working neighboring strips.
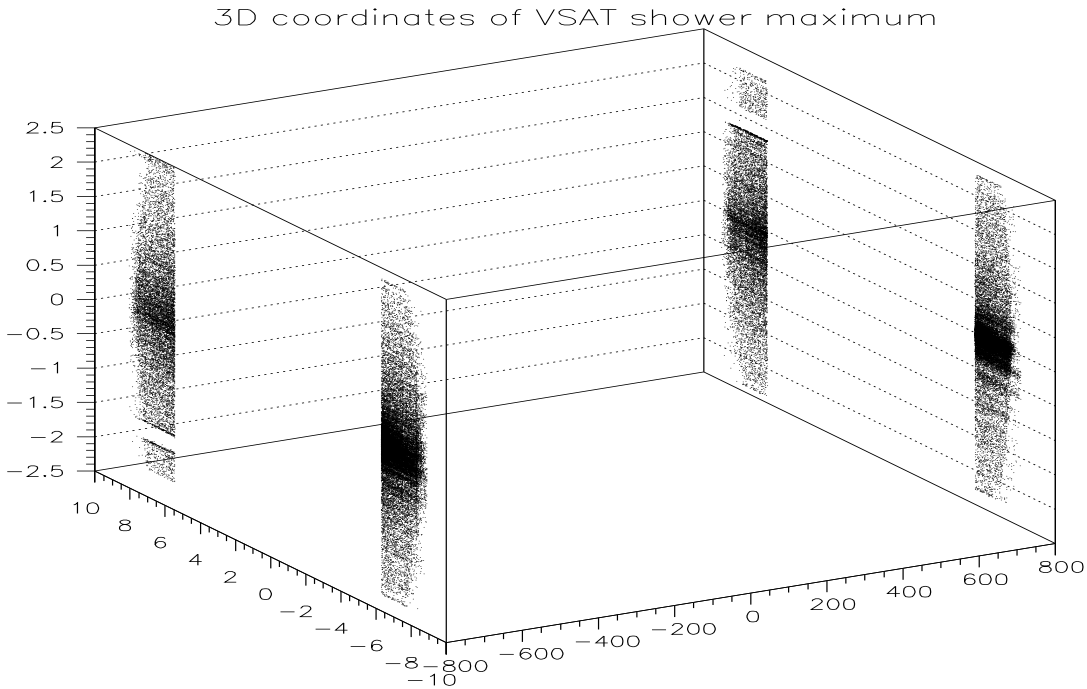
Figure 5.11: The VSAT shower maximum coordinates for all four modules. The Z-axis goes from -800 to 800 cm, the horizontal X-axis goes from -10 to 10 cm and the vertical is Y-axis goes from -2.5 to 2.5 cm.

5.8   The operation of VSAT

The use of VSAT off-line data became more complicated at LEP II since the background rose dramatically (especially during June of 2000). The VSAT suffered from some radiation damage, electronic noise and an increase of bias currents. The software needed to deal with background spikes, corrupted events and difficulties with separating good events from background. It was, however, still possible to calculate the luminosity with a precision of 1%. The beam parameters were calculated as well. The parameters which were estimated were the following:

1. The diagonal asymmetry (Fig. 5.12) which is $A_D = \frac{(N_1 - N_2)}{(N_1 + N_2)}$, where N_1 and N_2 are the number of Bhabha events in the diagonal 1 (modules 1 and 4) and diagonal 2 (modules 2 and 3).

2. The sum of x-positions of Bhabha hits for each diagonal: $\Delta X_1 = x_4 + x_1$, $\Delta X_2 = x_2 + x_3$ where x_i is the coordinate of Bhabha hits in module i.

3. The sum of y-positions for Bhabha hits in each diagonal: $\Delta Y_1 = y_4 + y_1$, $\Delta Y_2 = y_2 + y_3$ where y_i is the coordinate of Bhabha hits in module i.

These values together with the precise knowledge of the VSAT position with regards to the DELPHI interaction point made it possible to calculate the beam tilt in the horizontal and the vertical plane ($\pm 100 \mu$rad and $\pm 50 \mu$rad), the X-accollinearity ($\pm 50 \mu$rad), the Y-accollinearity ($\pm 200 \mu$rad) angles and the beamspot positions in X (around ± 3 mm) and Y (around ± 0.2 mm).
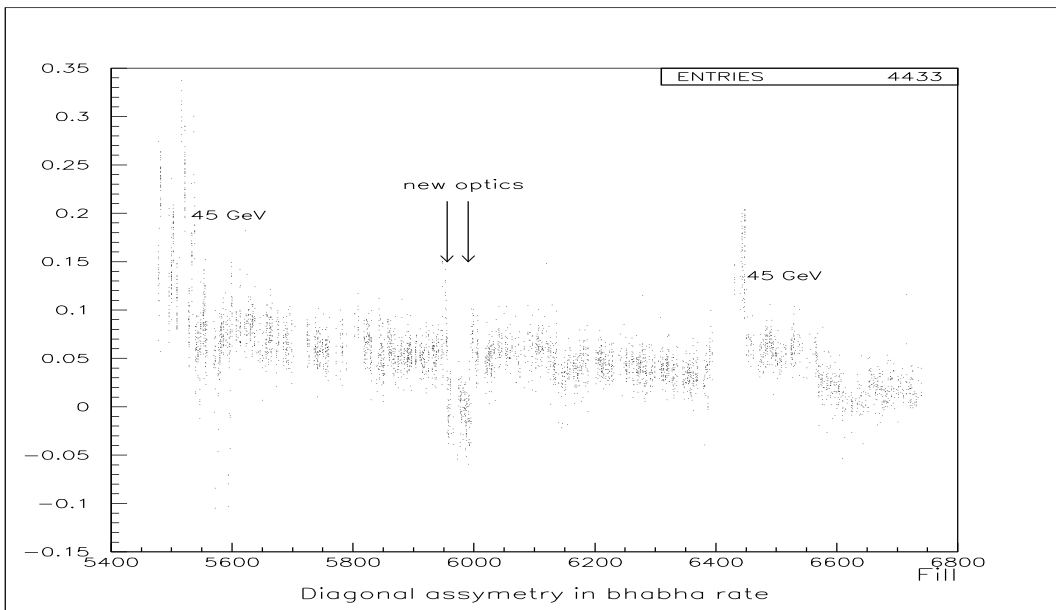

Figure 5.12: The diagonal asymmetry of the Bhabha hits in VSAT modules during year 1999.

A comparison of these parameters with data from the Vertex Detector (VD) of DELPHI was made. The study of the beam parameters are discussed in details in [126] and in Appendix D.

The on-line values provided by VSAT were the luminosity and the single electron background (Bckg 2). These values were within 5-10% of those from STIC and the LEP beam monitor detectors.

During the summer of 1999 a simulation was made by using the programs FASTSIM [124] (based on the DELPHI Monte-Carlo simulation standard) and GEANT [135] (a general purpose Monte-Carlo simulation package). The aim of this study was to estimate the energy reconstruction problems which VSAT could face with lepton energies above 100 GeV. The results showed that the electromagnetic shower stayed within the calorimeter and that leakage was still negligible (especially through the back of the module) in spite of the fact that

VSAT was designed for energies well below 95 GeV. The last year of data-taking confirmed the results of this simulation.

The last data-taking period of DELPHI (as well as for the other three LEP experiments) was stopped on November 2nd, 2000. VSAT was dismounted soon afterwards and checked for induced radiation. The detector itself proved to be robust and survived years of harsh radiation environment and millions of leptons (as is shown in Appendix C). Due to the very short decay periods for the radioactive elements created by the LEP beam background, the modules proved to be very little radioactive (less then the concrete walls of the DELPHI cavern). Two modules with a section of the beampipe was transported to Lund to be exposed in the museum of physics equipment.

The geometry of VSAT was changed prior to the LEP II phase. It was done by changing the beampipe section between the VSAT modules to a more narrow one. The increased acceptance gave a larger Bhabha and off-momentum electron flux as well as a larger number of electrons from gamma-gamma events. This change gave a two fold rise of gamma-gamma rates and in the same time increased the VSAT trigger rate because of an increased rate of the False Bhabhas trigger. The quality of the selection and the checks of the Bhabha events (the separation from background Single Electrons) remained the same as before and the final gamma-gamma event sample was not affected by background too much since most of it was located in the beam plane.

The apparent VSAT trigger rate was also decreased by increasing the T1 event buffer length, so that the VSAT T2 trigger rate was low enough to keep the DELPHI trigger system working with an acceptable dead-time. The number of corrupted events was around 0.2% during all years of data-taking except for the last two months when it was around 1% due to more unstable conditions of the beams and background. The VSAT raw data needed more than 30 Gb of disk space over the last three years (LEP II phase).

The VSAT data reprocessing and storage had a problem of format which made signals from some strips corrupted due to the change of the T1 buffer size but this was not a significant problem. Small temporary problems due to a shortage of disk space, when the DELANA versions were changed, occurred as well. The Y2K bug and a requirement of new run numbers (8 digits instead of 7), were a standard problem common to the whole DELPHI experiment.

Chapter 6

Background in the VSAT data

6.1   Off-energy background, its origin and effects.

Most gamma rays from synchrotron radiation could not reach VSAT or any other DELPHI sub-detector because the DELPHI interaction point was situated in the middle of long straight sections of the collider, far away from the curved sections. Some low energy radiation hitting the VSAT was intercepted by the first tungsten absorber (two radiation length thick) in front of the first FAD plane.

   The main source of background in VSAT was the single electrons. The single off-momentum electrons were produced by beam particles interacting with molecules or atoms of gas in the beampipe. Their production depended mostly on the density of residual gas in the beampipe but scattering on the walls and flanges were also possible. The LEP vacuum complex could reach a vacuum of about 10^{-10} Pa. This pressure is about 10^{15} times lower than the atmospheric pressure at sea level and close to the pressure in the outer space. During physics running the pressure increased and this lead to background increases as well.

   When the electrons and positrons were injected into the LEP ring and acceleration started, the vacuum pressure could unfortunately not be kept at the initial level since radiation pressure was created. This is caused by the synchrotron radiation from the beam. It hit the beampipe walls, which then were heated up and emitted particles. This so-called dynamic pressure increased with the radiated power of the beam. Such an effect was very large in the beginning of the year 2000 data-taking period because of the very high energy, the unusual beam acceleration schedule and cooling problems. Most experiments were unsatisfied with the quality of data-taking until the situation with the dynamic pressure got better thanks to the stabilization of the beams and the work done by slow but very efficient sublimation pumps.

Other sources of gas in the beampipe such as small leaks and off-momentum beam particles (i.e. beam electrons slowed down to a lower energy) could contribute to the static pressure in addition to the beam-gas particles that reside in the vacuum tube.

During operation with a four mA beam, LEP II therefore had an average pressure of about 10^{-7} Pa. In the proximity of the interaction point, the LEP ring was straight and the beampipe was pumped more, reducing the pressure with about a factor of ten.

Beam particles that interacted with the rest gas in the beampipe lost some of their energy. Particles that were off the beam energy usually experienced directional changes in the bending magnets and created a beam halo and some beam losses. This was called the off-energy background. This background could come from far away, have a high energy and it was focused in the vertical plane (Fig. 6.1).
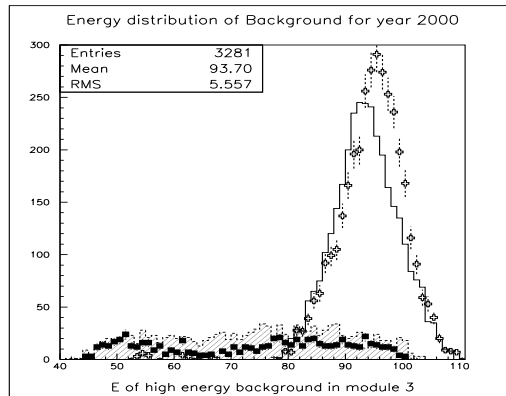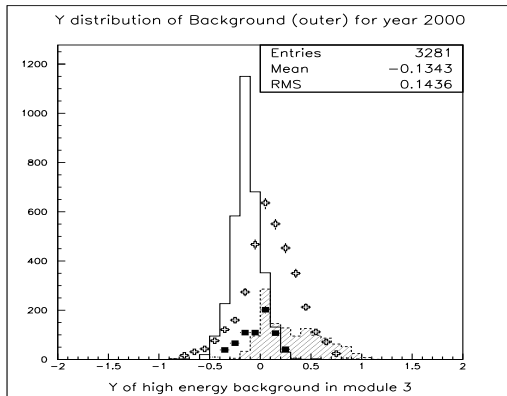

Figure 6.1: The Y coordinate measured by VSAT for background events, year 2000 (mean beam energy ∼103 GeV). Module 1 shown as crosses, Module 2 - filled, Module 3 - line, Module 4 - black rectangles.

Figure 6.2: The VSAT energy for background events in year 2000 data (mean beam energy ∼103 GeV). Module 1 - crosses, Module 2 - filled, Module 3 - line, Module 4 - black rectangles.

If the energy loss due to the beam-gas interaction was large, the resulting background would be more deflected. Such background came from regions close to DELPHI as it could not travel very far before it hit the beampipe walls. The low energy background was seen in all of the four VSAT modules, whereas the high energy background was concentrated in the outer modules 1 and 3 (Fig. 6.2). The VSAT detector therefore had about a factor 5 lower background in the inner modules 2 and 4 than in the outer ones (Fig. 6.1).

From what has been mentioned above it is also clear that the background at Z^0 running (beam energy $\sim$ 45 GeV) was much lower, with a total trigger rate of about 300-400 Hz compared to about 1200-1400 Hz at high energy running. The amount of background at LEPII would require a lot of storage space and dead time if it was recorded. The background trigger was therefore downscaled and only a small fraction of the events was read out.

The rise of beam energies from 94.5 GeV during year 1998 to 103 GeV during the last year of LEP operation (2000) together with some changes of the beam configuration change caused a visible difference in the background composition. One can see it quite clear by comparing the signal (selected events after all criteria have been applied) and background selected by cut-maps (look section 6.3 of this chapter) plots (Fig. 6.3 and 6.4). The background events' energy during year 1998 was widely distributed along the energy interval down to 50 GeV and the peak was broad. For year 2000 only a narrow peak of background was observed at the higher energies, starting from just 80 GeV and the peak itself was shifted to the higher energies as well.
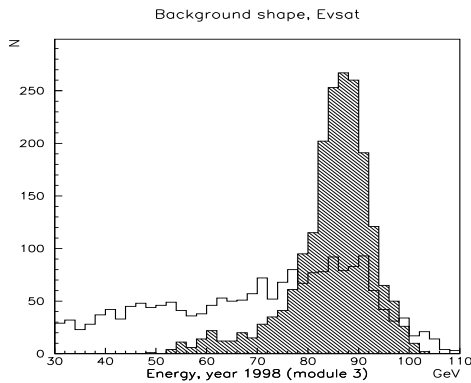

Figure 6.3: The VSAT energy for background events (hatched area) and for signal events (solid line) in Module 3 (outer) for year 1998 (mean beam energy 94.5 GeV).
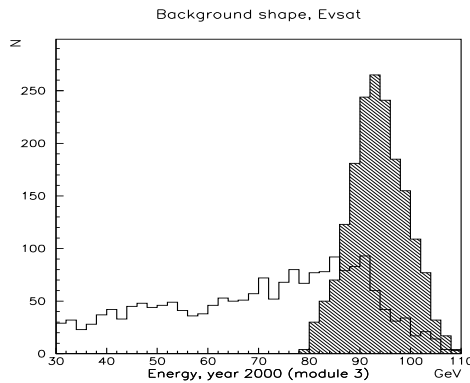
Figure 6.4: The VSAT energy for background events (hatched area) and for signal events (solid line) in Module 3 (outer) for year 2000 (mean beam energy $\sim$103 GeV).

The beampipe section where the VSAT modules were situated, connected to the main LEP ring beampipe by means of thick flanges which were quite close to the beam. Therefore the halo of the single electron background interacted with the flanges producing so-called "flange Bhabhas". A flange in front of the VSAT modules shadowed the active detector area and restricted the outer angle to 8 mrad.

Bhabhas and "flange Bhabhas" could only appear as diagonal hits, whereas the off-energy background was mainly concentrated in the outer modules. The flange Bhabhas could be removed by requiring that the electron hit the VSAT module within a certain box (not further away than 8cm from the beam). The bulk of off-energy electrons at low energy could be removed by rejecting events with an energy below 30 GeV. A VSAT tagged event would thus be limited to an energy above 30 GeV and a x-position less than 8 cm.

The background from off-energy electrons could not be completely eliminated, however, and the remaining background had to be subtracted afterward. To get this subtraction correct, it was necessary to know how much background was expected and how much of the background and the signal that were cut away. A number of different methods were used to

estimate the total expected off-energy background.

The off-energy electron background that typically satisfied the VSAT Bhabha trigger was a coincidence between two off-energy electrons. This "false Bhabha" rate normally stayed below 30% of the Bhabha triggers, but could at times go above 50%. Most of the false Bhabhas could be removed with tight cuts due to the well defined properties of a true Bhabha event (such as equal and opposite momenta, time and direction of the hits).

The remaining background can be parameterized by a linear combination of four different measurements [85]:

$$E_{cut}/(\frac{S_1 \cdot S_2}{SE_1 SE_2} - 1)\frac{SE_1 \cdot SE_2}{\delta T}B_{soft} - B_{hard}FB_{scal} \qquad (6.1)$$

Here E_{cut} means the number of events cut away by the Bhabha energy cut, S and SE are the numbers of downscaled off-energy electron triggers (1 and 2 are diagonal numbers) with and without the energy cut applied. The duration of the data measurement is given by δT and B_{soft}, B_{hard} is the difference between the normal Bhabha sample and one with harder background cuts. The FB_{scal} is finally the on-line delayed Bhabha rate (taken as the coincidence of two opposite hits separated by four bunch crossings).

A $\gamma\gamma$-event is selected by requirements on the hadronic system in the DELPHI detector. If an off-energy electron coincided with the hadronic trigger, it could result in any of the following VSAT $\gamma\gamma$-event:

1. If the off-energy electron trigger was in coincidence with a no-tag $\gamma\gamma$-event, it would be classified as a single tag event instead of background.

2. If the off-energy electron was in coincidence with a true single tag $\gamma\gamma$-event, it would result in a fake double tag trigger.

3. The coincidence of two off-energy electrons would be considered to be a double tag $\gamma\gamma$-event.

The most troublesome background for this analysis was the second one, when the off-energy background was mixed up with true $\gamma\gamma$-events. The other two background triggers could in principle be completely removed by hard cuts, without too much loss of the signal. This was unfortunately not the case for the second type and sometimes it produced both fake two-photon events and fake Bhabha events.

6.2 Background probabilities and features.

The most straight forward way to calculate the size of the off-energy background is to measure the probability to have an off-energy electron in any of the modules. The expected number of background events in the signal sample can then be calculated as the probability multiplied with the number of hadronic triggers. The easiest way to measure the off-energy electron probability was to measure the coincidence rate with Bhabha events.

For this purpose both the coincidence of a STIC and a VSAT Bhabha with an off-energy electron was measured [86]. The analysis of the STIC Bhabha triggers used only DELPHI events, whereas the VSAT Bhabha triggers used also the VSAT information. The two individual measurements provided a cross-check. Unfortunately the background conditions varied strongly and rapidly over a year. When the final data was selected the average probability obtained by the STIC and VSAT Bhabha measurements therefore might not be completely equal.

The background shapes in different modules were different (Fig. 6.5 and 6.6) and this made the evaluation of the background quite complex.
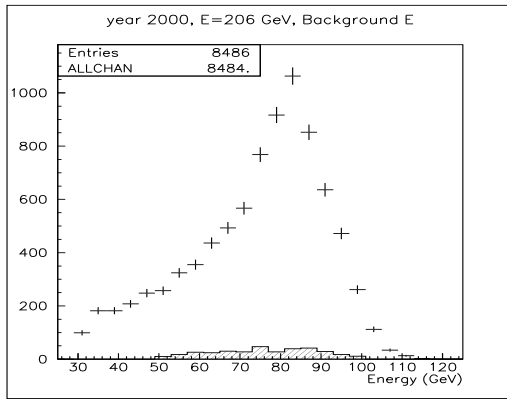

Figure 6.5: The VSAT energy for background events in inner Module 2 for year 2000 (mean beam energy ∼103 GeV). The background is shown as the filled area, the whole data sample before selection (signal+background) as crosses.
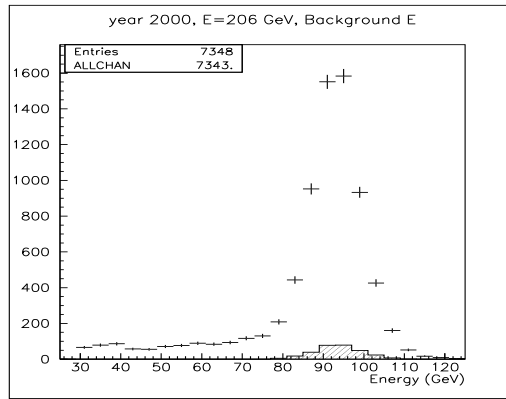
Figure 6.6: The VSAT energy for background events in outer Module 3 for year 2000 (mean beam energy ∼103 GeV). The background is shown as the filled area, the whole data sample before selection (signal+background) as crosses.

The probability to have two off-energy electrons in the VSAT was determined as the combined probability of the two modules. The coincidence with a single tag $\gamma\gamma$-event was calculated in a similar fashion.

6.3   Background selection using Cut-maps.

In order to achieve a good purity in the final $\gamma\gamma$ sample, it was necessary to impose hard and precise cuts on the data. All background could not, as mentioned before, be removed, but the analysis of the final sample needed a signal purity of at least 70% (i.e. the background should be well below 30%). This required a background rejection in the order of 90%, and at the same time it was desirable not to loose more than 50% of the signal.
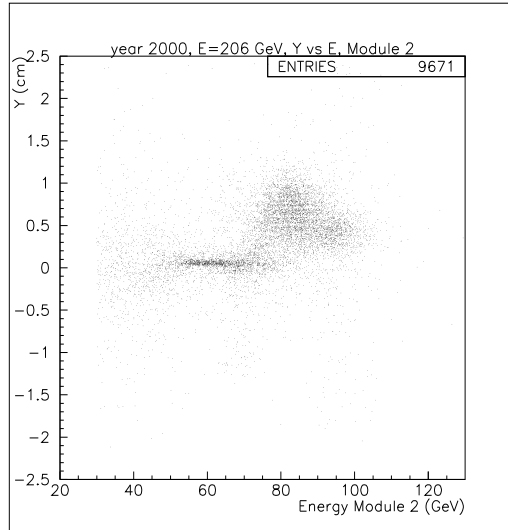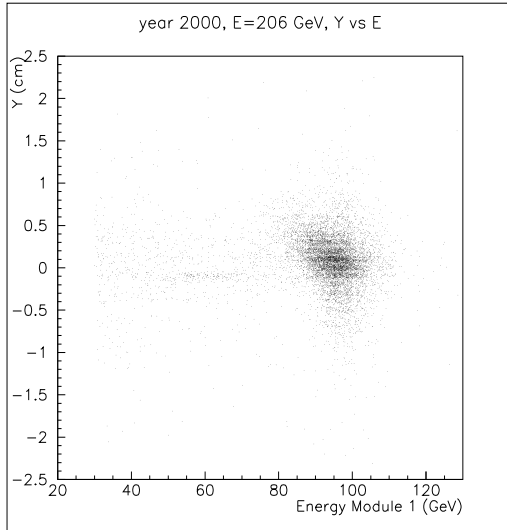

Figure 6.7: The VSAT background in the outer Module 1 for year 2000 (mean beam energy ∼103 GeV).

Figure 6.8: The VSAT background in the inner Module 2 for year 2000 (mean beam energy ∼103 GeV).

The off-energy background was spread out in the whole horizontal plane of the detector i.e. it was not confined in x. The high energy background (mainly in the outer modules) was, however, very well confined in the y-plane of the beam (Fig. 6.8) as well as in certain energy regions. That fact had been used previously [128] to introduce a two-dimensional selection criteria, called cut-maps.

Unfortunately the y-position of the background changed frequently during LEP-running (Fig. 6.9) making the whole rejection procedure ever more complicated and the cut-maps had to be recalculated for different data sets.

In Fig. 6.8 one can see two separate dense background regions and it is clear that no trivial mathematical expression can be used to define the rejection region of the off-energy background. Instead a cut has been defined as a grid map, i.e., as a function of the VSAT energy and the y-position measurement [132]:

$$Y_{map} = (y_{pos} - y_{off} + 1.6) \cdot 25 + 1, X_{map} = E_{beam} - E + 11 \qquad (6.2)$$

To improve and narrow down the criteria, the y-position of the background (y_{off}) shown in Fig. 6.9 and 6.10 were implemented on a run by run basis (blocks from 20 to 60 minutes data taking in DELPHI). The grid size of the maps was set to 80, which is the origin of the constant numbers in the expressions. A map was then created by filling it with off-energy electron events from the single electron trigger [132]. A map was defined for each module and energy interval of LEP, resulting in a total of 24 different maps.
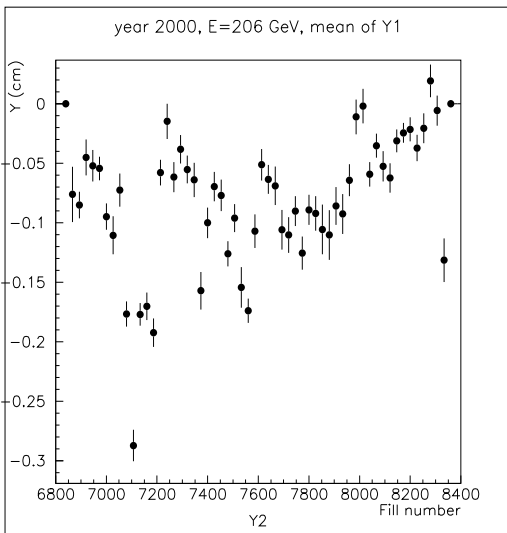

Figure 6.9: The average Y position of the hits in the outer Module 1 during year 2000 (mean beam energy ∼103 GeV).

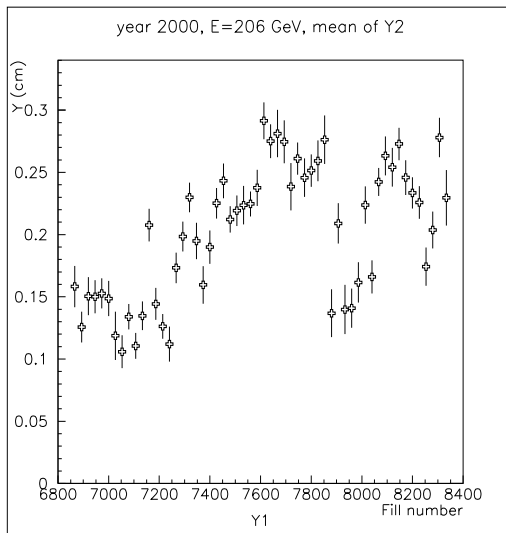Figure 6.10: The average Y position of the hits in the inner Module 2 during year 2000 (mean beam energy ∼103 GeV).

The height of each bin in the maps was defined as the relative probability (in permill) for an off-energy electron to enter that bin. The total sum of all the bins is thus equal to one. The cut was then implemented by specifying a horizontal cut limit in the map, removing all events that were in bins that have a height above that limit.
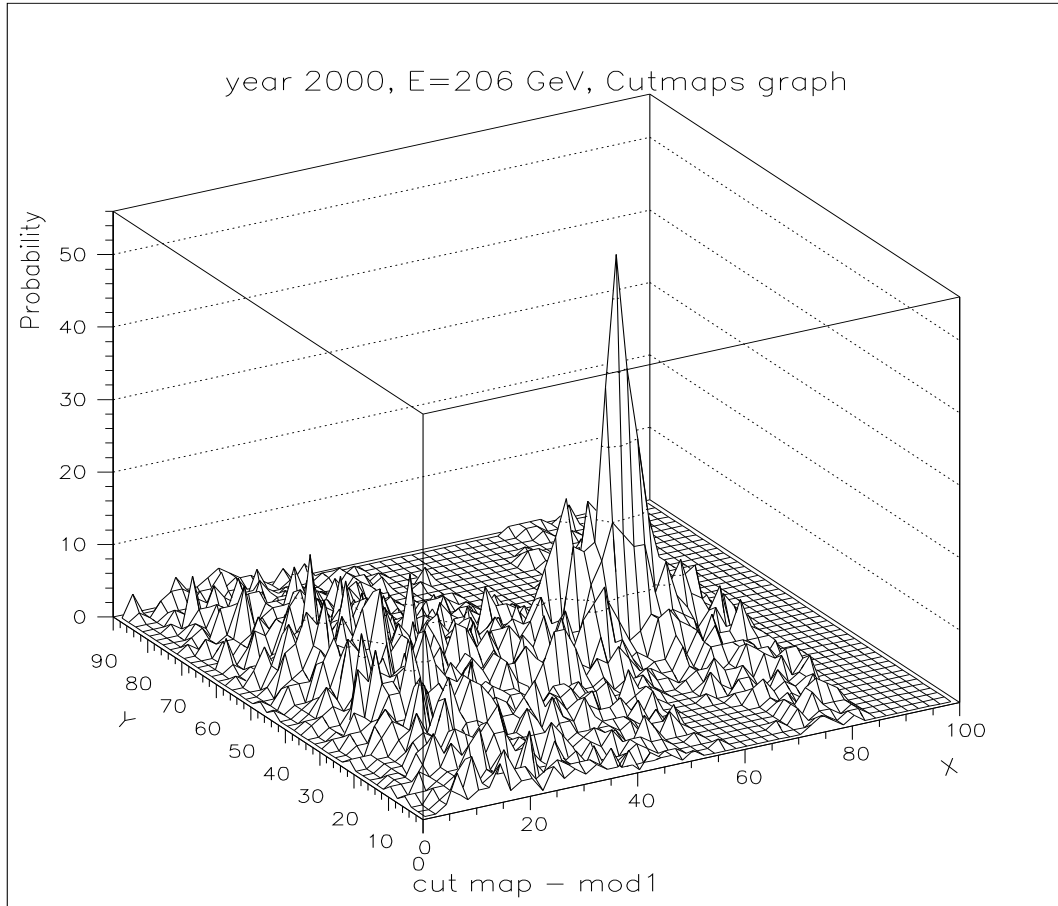

Figure 6.11: A cut-map for module 1 during year 2000 (mean beam energy ~103 GeV). The Z coordinate represents the probability of a background hit, X and Y have been calculated as X_{map} and Y_{map} as defined in the text above.

As the outer modules had a more confined background than the inner modules, the cut limits had to be set separately for each module. The impact of adjusting the cut limit is shown in Fig. 6.11, where a cut limit of about 0.2 permill is needed for a background rejection of 90% in the outer modules. The background rate in the inner modules was smaller and less background had to be cut away (a cut limit at about 0.4-0.6 was normally enough for the inner modules).

6.4 The procedure of background subtraction.

The procedure of the background subtraction used three different event samples which were stored in three different ntuples: one for data, one for Monte-Carlo and one for background.

First the hadronic invariant mass distribution was plotted for all events in the data sample. The applied selection criteria were:

1. checking the number of the module that was hit;

2. checking the tagging criteria (i.e. correct X,Y positions and requiring an energy above 30 GeV);

3. applying the Bhabha rejection criteria to purify the $\gamma\gamma$ events sample from Bhabhas (i.e. checking for diagonal events with the same energy in both modules);

4. the invariant mass of the hadronic system should be larger than 3 GeV;

5. the number of charged tracks should be more or equal to 4 for single and 3 for double tag;

6. the transversal momentum of the hadronic system should be more than 0.2 GeV.

Histograms of the data events with all criteria applied except the cut-maps were produced. The number of entries in the histograms are given in Table 6.1 as N_{tot} i.e. the total number of events in the data sample before the cut-map selection.

The cut-map selection process was done next. If the cut-map value for a certain event was lower than the $lim1$ value (which was tuned for each module and energy region) then the event was selected. The number of entries in these histograms gave the number of selected events - N_{sel} (Table 6.1).

To eliminate any possible background from leptonic $\gamma\gamma$ production in the hadronic event sample it was required in addition:

1. $3 \leq N_{Charged} \leq 18$ and that each charged track must have a momentum of at least 0.3 GeV and be in the angular region $10^o \leq \theta \leq 90^o$;

2. The maximum number of neutral and charged tracks had to be 20 and the total energy of the hadronic system had to be less than 45 GeV and have a transverse momentum less than 5 GeV;

3. The minimal invariant mass of the hadronic system should be larger than 3 GeV;

4. Anti-tag criteria were applied to ensure that the second electron had indeed disappeared in the beampipe;

5. The energy of the charged particles had to be below 30 GeV in the whole DELPHI detector and less than 25 GeV for neutral particles.

In the next step the Monte-Carlo sample was used to produce two sets of histograms. One with all criteria applied except the cut-maps and the second set with all events rejected by the cut-maps. The number of selected events could be calculated by subtraction $N_{sel}MC = N_{tot}MC - N_{rej}MC$ or by plotting the histogram with the opposite cut-maps criteria. The numbers of entries gave the selection ratio: $S_{mc} = N_{sel}MC/N_{tot}MC$ and the ratio of rejection: $R_{mc} = 1 - S_{mc}$. The same kind of procedure was also done with the background sample and the same ratios for the background selection and rejection were obtained: S_{bg} and $R_{bg} = 1 - S_{bg}$.

The number of gamma-gamma events ($N_{\gamma\gamma}$) and the number of background events (N_{bg}) in the preselected data (N_{tot}) were then calculated. This could be done by using the two equations: $N_{tot} = N_{\gamma\gamma} + N_{bg}$ and $N_{sel} = S_{mc} \cdot N_{\gamma\gamma} + S_{bg} \cdot N_{bg}$ with the solution: $N_{\gamma\gamma} = (N_{sel} - S_{bg} \cdot N_{tot})/(S_{mc} - S_{bg})$ and $N_{bg} = N_{tot} - N_{\gamma\gamma}$. The event purity could then be calculated as: $Pur = S_{mc} \cdot N_{\gamma\gamma}/(S_{mc} \cdot N_{\gamma\gamma} + S_{bg} \cdot N_{bg}) = S_{mc} \cdot N_{\gamma\gamma}/N_{sel}$ i.e. the fraction of the signal in the final sample.

By knowing all these numbers one can subtract the background from the final sample. In an initial step the Monte Carlo rejected events were subtracted from the rejected events which belonged to the data sample. One needed of course to normalize these histograms to the data sample. It was done by calculating the factor $K1 = N_{\gamma\gamma} \cdot S_{mc}/N_{rej}MC$ where $N_{rej}MC$ could be obtained as the number of entries of the histograms with rejected Monte Carlo events. The histograms in Fig. 6.12 and Fig. 6.13 were the result. They represent the pure signal after subtraction of the background.
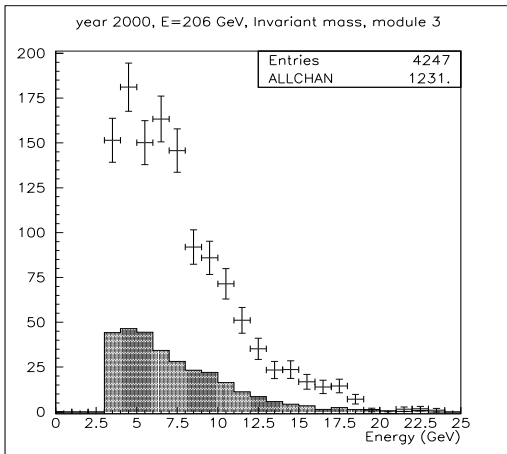

Figure 6.12: The invariant mass distribution in module 3 after the background subtraction (crosses) and the background itself (hatched area). Year 2000 data, mean beam energy ~103 GeV).
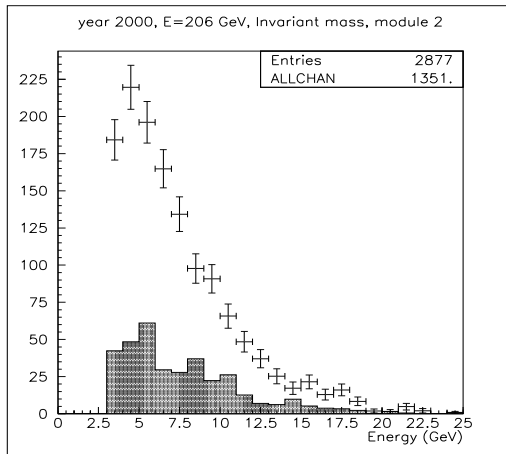
Figure 6.13: The invariant mass distribution in module 2 after the background subtraction (crosses) and the background itself (hatched area). Year 2000 data, mean beam energy ~103 GeV).

The subtraction of the background requires a normalization factor $K2 = S_{bg} \cdot N_{bg} / N_{pure} Bg$ where $N_{pure} Bg$ is the number of entries in the background histograms. With these factors one can get a histograms which have data without background. To get the background that was rejected from the resulting invariant mass histograms one had to normalize the pure background histograms with the factor $K2$ multiplied by the total number of events in the corresponding invariant mass histogram.

Table 6.1: Factors and statistic for the background subtraction in year 2000 data at E=206 GeV. The variables are defined in the text.

	mod1	mod2	mod3	mod4
lim	0.2	0.5	0.3	0.5
N_{tot}	3635	1876	3499	1750
N_{sel}	1696	1261	1712	1338
N_{rej}	1939	615	1787	412
S_{mc}	0.80	0.74	0.91	0.77
S_{bg}	0.19	0.27	0.21	0.43
$N_{\gamma\gamma}$	1648	1605	1396	1722
N_{bg}	1987	271	2103	28
Pur	0.78	0.94	0.74	0.99
$K1$	0.1727	0.124	0.1346	0.093
$K2$	0.2252	0.2535	0.2422	0.0546
$Norm$	308.5	348.6	300.6	75.

Chapter 7

A comparison of simulation with data

Comparisons of Monte Carlo predictions with data can help to improve the theoretical models that are implemented in the event generators. This is especially important in the very low Q^2 region ($Q^2 \leq 1 GeV^2$). The data from the DELPHI VSAT detector studied in this analysis explore for the first time this low Q^2 region at LEP II energies. Recent results obtained by ALEPH [15–17], DELPHI [69], L3 [21–23] and OPAL [28–30, 32], as well as combined results [5] show a good agreement in the high Q^2 region (at a $< Q^2 >$ above 10 GeV^2) and a poor agreement in the lower Q^2 region (at a $< Q^2 >$ around 3 to 10 GeV^2). These results got an explanation in the theoretical studies by [4, 6, 7]. Several steps were taken by all collaborations to deal with this disagreement and new versions of the Monte Carlo generators were introduced. For example, the HERWIG [61, 73, 74] and the JAMVG [11] programs were used by the ALEPH and L3 collaborations respectively. Among these two, HERWIG (versions 5.9 and higher) is the most advanced program since it is based on a general-purpose QCD generator with implementation of Hadron Emission with Interfering Gluons, while JAMVG is based on the BFKL equation [75]. The version of the general purpose generator HERWIG with a modified transverse momentum distributions of quarks in the photon was used in the two-photon studies.

The $\gamma\gamma$ events generator mostly used by DELPHI is the TWOGAM [72] as well as the PHOJET [62, 71] and the PYTHIA [63, 70] programs.

These three generators used in this analysis (PHOJET, PYTHIA, TWOGAM) have different approaches to the event simulation which requires some preadjustment of Monte Carlo parameters before the results can be compared. Certain variables were used for comparison: the total hadron multiplicity, the hadronic invariant mass (W_{inv}), the energy measured by VSAT ($Evsat$), the Q^2 and the transversal momentum P_t.

The selection of VSAT events was done as described in the previous chapter 6 and the same criteria were used for selecting both the data and the simulated events.

All generated samples passed the full event simulation using the standard DELPHI simulation program called DELSIM [68]. Scattered electrons and positrons that were measured by VSAT were treated by a specially developed version of the FASTSIM program [124] which trace particles through the quadrupoles with acceptable precision until they hit the VSAT modules. The DELPHI standard reconstruction program DELANA [67] was then applied on all the simulated events to get the reconstructed samples.

7.1 The Monte Carlo generators
7.1.1 TWOGAM

TWOGAM simulates only $\gamma\gamma$ interactions. Version 2.04 of the program [72] was successfully tested in previous DELPHI studies [100]. The generator uses three "classic" models which produce their classes of events: the Vector Dominance Model (VDM), the Quark Parton Model (QPM) and the Resolved Photon Contribution model (RPC).

The QPM part is based on the exact decomposition of the matrix element of the process and the exact differential cross-sections [105]. The quark masses are taken to be 0.3 GeV for u and d quarks, 0.5 GeV for s and 1.6 GeV for c quarks.

For the RPC perturbative part, the lowest order cross-section is used. There is no initial or final state parton showering. Strings are formed following the color flow of the sub-processes. The remnant of a quark is an antiquark (and vice versa), and the remnant of a gluon is a $q\bar{q}$ pair. The program is interfaced to PDFLIB [107], and thus can use any leading order parton density parameterization of the photon. The Gordon-Storrow [108] parton density function set 2 is used in this study. The kinematics of the partonic system is exact for any photon virtuality. This allows for a smooth suppression of the parton densities of resolved photons as their virtuality increases, according to a theoretically motivated ansatz. A transverse momentum cutoff, $p_t^{cut} = 1.8 GeV/c$, is applied to the partons of the resolved photons to separate soft from hard processes.

In this analysis a so called Generalized Vector Dominance Model GVDM [109] is used. The multihadronic final state is generated as a $q\bar{q}$ pair according to the quark P_t distribution $d\sigma/dp_t^2 \approx exp(-5p_t^2)$ in the $\gamma\gamma$ centre-of-mass system. The fragmentation is done using JETSET with $\sigma_q = 450 MeV/c$ (the width of the Gaussian transverse momenta distribution for primary hadrons).

TWOGAM treats the kinematics of the scattered electron and positron exactly and uses exact (unfactorized) expressions of the two-photon luminosity function.

An advantage of the TWOGAM generator is that the initial state radiation and final state radiation corrections have been implemented in its last version (version 2.04) for the first time in a $\gamma\gamma$ generator. It means that it is only the TWOGAM generator that has two modes: with radiative correction (RST) and without radiative corrections (non-radiative state NST). Numerous comparisons between them showed that the RST gives in general a larger cross-section (by around 10%) but that the shapes of all distributions are similar. Since the other generators have no radiative corrections, the TWOGAM NST mode was used in all comparisons with them.

It was shown by DELPHI at LEP 1 energies [100], that the simulation agreed better with data when the Gordon-Storrow parameterization (GS II) [108] of the parton distribution function of the photon was used in the QCD-RPC model. Therefore the GS II parameterization was used in the generation of $\gamma\gamma$ events by TWOGAM in this analysis. Two other parameterizations, the GRV [106] and SaS [104] have similar properties and the GRV and SaS 1D parameterization were therefore used in PHOJET and PYTHIA respectively.

Also shown in the previous studies [100] at LEP1 energies was that parameterizations of the parton density functions of the photon such as Drees-Grassie [114], Duke-Owens [115] and Levy-Abramowizc-Charchula [103] gives a poor agreement with data and they were not used in the present analysis.

7.1.2   PHOJET

The second event generator used was the PHOJET (version pre-1.12) program [71]. This version includes an exact photon flux calculation of photon-photon processes in lepton-lepton collisions. The ideas, methods and algorithms used in the program are based on the Dual Parton Model (DPM) [110]. In order to combine the DPM, which describes soft processes with the well-known perturbative QCD, the event generator is shaped as a two-component model (one component for soft and one component for hard components). On the basis of the optical theorem, Regge phenomenology is used to parameterize the total and elastic cross-sections as well as a number of partial inelastic cross-sections. In order to conserve s-channel unitarity, Gribov's Reggeon approach was implemented. Using all these implementations, the model predicts so-called "multiple parton interactions" in one event. Thus, multiple soft and hard interactions may be generated simultaneously since the unitarization of soft and hard processes was treated in a unified way in this program. Hard scattering processes are simulated using lowest-order perturbative QCD. Initial state and final state parton showers are generated in the leading-log approximation. Some coherence effects (angular ordering in the emissions) are taken into account as well. The JETSET 7.4 program is used for the fragmentation of parton configurations. The GRV [106] parameterization of the parton density function of the photon was used in this analysis. A transverse momentum cutoff, $p_t^{cut} = 2.5 \ GeV$, was applied to the partons of the resolved photons to separate soft from hard processes. The program can run only in the hadronic invariant mass region above 5 GeV.

7.1.3   PYTHIA

The third event generator used in this analysis is the PYTHIA program [70], which is a general purpose generator in high energy physics since many years but $\gamma\gamma$ physics was only recently implemented in details. The program uses six event classes for two-photon collisions based on the three-component model of the photon. Version 6.143 has been used in preference to more recent versions because it describes well Deep Inelastic Scattering (DIS) data. In this program different kinds of events are distinguished as: direct events, VDM events and anomalous events [102]. In order that the above classification is smooth and free of double counting, the cutoff parameters are introduced at the level of the real photon fluctuation $\gamma \to q\bar{q}$ and the final hadronic system creation $\gamma\gamma^* \to q\bar{q}$. The VDM and anomalous events are together called resolved events. These two classes differ in the structure of the underlying event and in the appearance of soft events. The superposition of events mentioned above applies separately for each of the two incoming photons and forms six distinct classes of events: direct-direct, VDM-VDM, anomalous-anomalous, direct-VDM, direct-anomalous and VDM-anomalous. In the case of deep inelastic scattering, only one of the photons is resolved and hence only direct-direct, direct-VDM and direct-anomalous components are used in the model. These three contributions are similar to the TWOGAM and PHOJET classifications.

7.2 The samples of data and simulated events

7.2.1 Single tagged events sample

The data collected by the DELPHI detector at LEP II during 1998-2000 have been used in this analysis. The integrated luminosity as well as the number of recorded (i.e. written on tape) and preselected events are given in Table 7.1. Here the preselected events are the ones which have no acquisition errors and fulfill the selection criteria described in the previous chapter 6. Only runs during which the VSAT detector was fully operational are included in the table.

Table 7.1: The number of data events selected for single tag analysis and the luminosity.

Year	Luminosity Total	Luminosity Preselected	E_{cms}	recorded/preselected events	selected events
1998	149.9 pb^{-1}	146.2 pb^{-1}	189 GeV	96387/86624	4763
1999	225.8 pb^{-1}	220.0 pb^{-1}	192 GeV	18370/17523	2355
			196 GeV	50900/49734	
			200 GeV	47577/45856	
			202 GeV	20189/19688	
2000	158.3 pb^{-1}	153.1 pb^{-1}	206 GeV	90736/84024	4608

A simulated event sample was also produced. The number of events simulated by the TWOGAM program is given in Table 7.2. It is given separately for the three different models used by TWOGAM.

Table 7.2: Number of events produced with the TWOGAM program

Year	mode	Lumin.	E_{cms}	VDM Model	QPM Model	GSP Model
2000	RST	450 pb^{-1}	206 GeV	40218	5953	48551
2000	NST	450 pb^{-1}	206 GeV	38886	5708	47539
1999	NST	450 pb^{-1}	200 GeV	38747	5679	46358
1998	RST	450 pb^{-1}	189 GeV	39387	5692	35443
1998	NST	300 pb^{-1}	189 GeV	25418	3677	23216

The number of events produced by PHOJET and PYTHIA are given in the Table 7.3 and Table 7.4 respectively. One can see from the tables that the simulated samples corresponded to a luminosity that was a factor 2-3 larger than that of the real data samples.

Table 7.3: The number of events produced with the PHOJET program

Year	Lum. $[pb^{-1}]$	E_{cms} [GeV]	N simulated/preselected
2000	382.1 pb^{-1}	206 GeV	85828 / 80419
1998	411.0 pb^{-1}	189 GeV	90223 / 84554

Table 7.4: The number of events produced with the PYTHIA program

Year	Lum. $[pb^{-1}]$	E_{cms} [GeV]	N simulated/preselected
2000	494.3 pb^{-1}	206.5 GeV	148222 / 108929
1999	552.6 pb^{-1}	199.5 GeV	171522 / 123039
1998	512.8 pb^{-1}	188.6 GeV	167211 / 113929

7.2.2   Double tagged events sample

Only 323 double tag events (for years 1998, 1999 and 2000) passed all selection criteria mentioned in chapter 6. The numbers are presented in Table 7.5. The same simulated sample that was used in the single tagged analysis was used in the double tagged analysis.

Table 7.5: The number of events selected in the double tagged data and the luminosity.

Year	Luminosity Total	Luminosity Preselected	E_{cms}	recorded/preselected events	selected events
1998	149.9 pb^{-1}	146.2 pb^{-1}	189 GeV	96387/86624	103
1999	225.8 pb^{-1}	220.0 pb^{-1}	192 GeV	18370/17523	127
			196 GeV	50900/49734	
			200 GeV	47577/45856	
			202 GeV	20189/19688	
2000	158.3 pb^{-1}	153.1 pb^{-1}	206 GeV	90736/84024	93

7.2.3 Renormalization of single tagged events

All simulated samples were normalized to the data luminosity. The TWOGAM sample was found to be in the best agreement with the data after normalization. The other generators agreed fairly well with the data when the shape of the simulated distributions were compared but not in the absolute values of the cross-section. Renormalization factors for the TWOGAM, PHOJET and PYTHIA program were calculated. These were needed to make the generated cross-section equal to the data cross-section and the renormalization factors are given in Table 7.6. The factors were estimated for the single tag events by using the distribution of the energy measured by VSAT. The distribution of the total hadron multiplicity were used as a crosscheck.

Table 7.6: The renormalization factors for the simulated single tag events.

Generator / Year:	1998	1999	2000
TWOGAM	1.10	1.00	0.90
PHOJET	0.58	-	0.47
PYTHIA	0.72	0.67	0.52
Ecms :	189 GeV	198 GeV	206 GeV

It is clear from Table 7.6 that the cross-section predicted by all the generators increase more rapidly with the c.m.s. energy than what is the case for the data.

The TWOGAM and PHOJET generators give, however, a more stable prediction (a 20% change from 189 to 206 GeV compared to a 30% change for PYTHIA). TWOGAM has an absolute normalization that is almost correct in this very low Q^2 region measured by VSAT while PYTHIA and PHOJET tend to overestimate the number of single tag events by some 40% and 50% respectively.

The effect of the normalization is illustrated in Fig. 7.1 where the energy distribution before normalization is shown and Fig. 7.2 where the normalization was done.
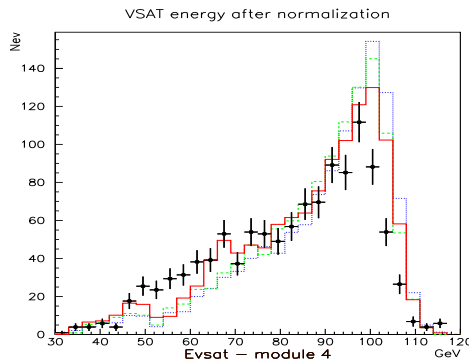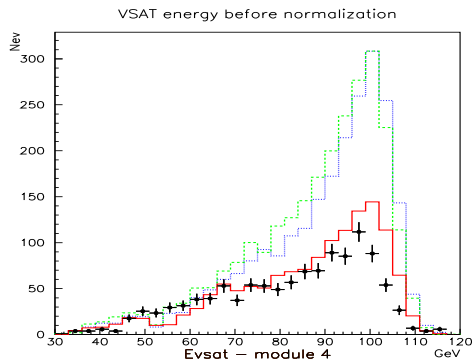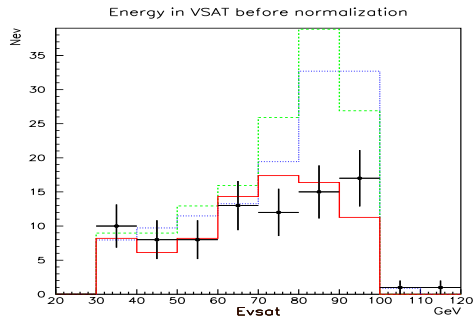

Figure 7.1: The energy distribution of single tag events measured by module 4 of VSAT in year 2000 before normalization. The points are data, TWOGAM is shown as a solid line, PHOJET as a dashed line and PYTHIA as a dotted line.
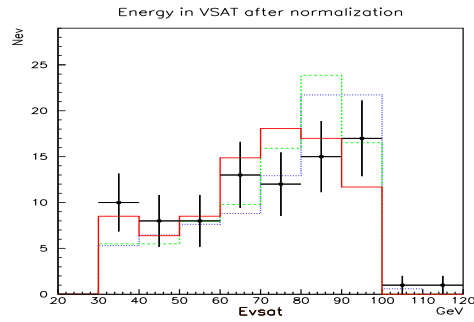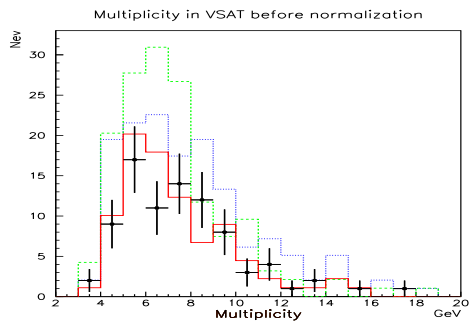
Figure 7.2: The energy distribution of single tag events measured by module 4 of VSAT in year 2000 after normalization. The points are data, TWOGAM is shown as a solid line, PHOJET as a dashed line and PYTHIA as a dotted line.

Similar plots are shown in the Figure 7.3 and 7.4 of the multiplicity distributions. The figures clearly show how superior TWOGAM is in its prediction of the absolute number of events compared to PHOJET and PYTHIA.
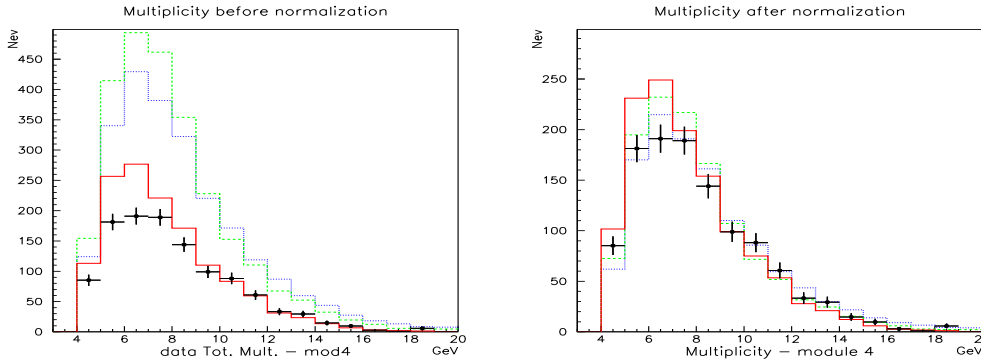
Figure 7.3: The multiplicity distribution of single tag events measured by module 4 of VSAT in year 2000 before normalization. The points are data, TWOGAM is shown as a solid line, PHOJET as a dashed line and PYTHIA as a dotted line.

Figure 7.4: The multiplicity distribution of single tag events measured by module 4 of VSAT in year 2000 after normalization. The points are data, TWOGAM is shown as a solid line, PHOJET as a dashed line and PYTHIA as a dotted line.

7.2.4   Renormalization of double tagged events

The comparison of the renormalization factors for the double tag events showed a similar picture as the single tagged events. TWOGAM again predicted well the absolute cross-section while PHOJET and PYTHIA overestimated it with 30-40%. The same procedure of renormalization that was used for single tagged events were also used for double tagged events. The result is given in Table 7.7. Due to the lack of statistics the data for 1998, 1999 and 2000 had to be combined to extract the common renormalization factor. The factors are similar to what was obtained in the single tagged case.

Table 7.7: The renormalization factors for the simulated double tag events.

Generator	mean factor for three years
TWOGAM	1.0
PHOJET	0.6
PYTHIA	0.7

The effects of the renormalization on the double tagged energy and multiplicity distributions are shown in Fig. 7.5, 7.6, 7.7 and 7.8.

Figure 7.5: The energy distribution of double tag events measured by all modules of VSAT in year 1998 before normalization. The points are data, TWOGAM is shown as a solid line, PHOJET as a dashed line and PYTHIA as a dotted line.

Figure 7.6: The energy distribution of double tag events measured by all modules of VSAT in year 1998 after normalization. The points are data, TWOGAM is shown as a solid line, PHOJET as a dashed line and PYTHIA as a dotted line.

Figure 7.7: The multiplicity distribution of double tag events measured by all modules of VSAT in year 1998 before normalization. The points are data, TWOGAM is shown as a solid line, PHOJET as a dashed line and PYTHIA as a dotted line.
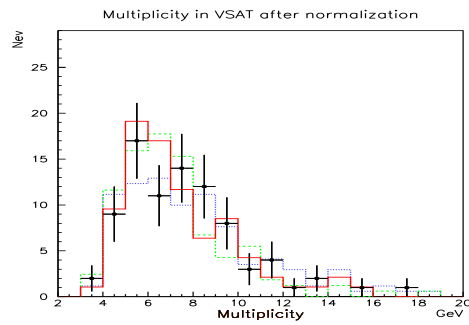
Figure 7.8: The multiplicity distribution of double tag events measured by all modules of VSAT in year 1998 after normalization. The points are data, TWOGAM is shown as a solid line, PHOJET as a dashed line and PYTHIA as a dotted line.

7.3   Data - Monte Carlo comparison of single tag events

7.3.1   The tag energy distribution

The renormalized plots of the scattered electron and positron energy as measured by VSAT are shown in Fig. 7.9 and Fig. 7.10.
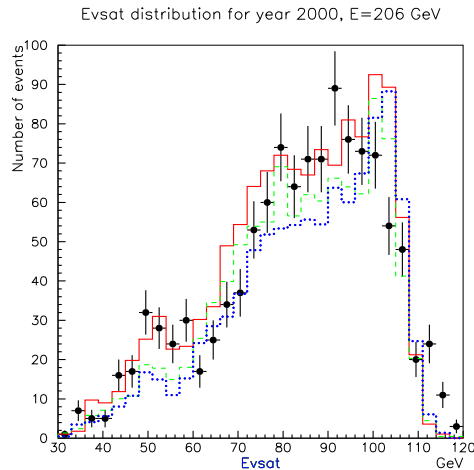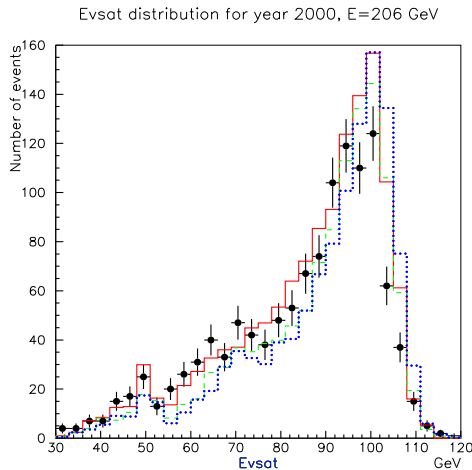
Figure 7.9: The energy distribution measured by module 2 of VSAT in year 2000. The points are data, TWOGAM is shown as a solid line, PHOJET as a dashed line and PYTHIA as a dotted line.

Figure 7.10: The energy distribution measured by module 1 of VSAT in year 2000. The points are data, TWOGAM is shown as a solid line, PHOJET as a dashed line and PYTHIA as a dotted line.

The agreement of the energy distributions between data and simulated events is better for the inner modules (2 and 4) than for the outer modules (1 and 3) where the background was very high.

Another important conclusion is that for the inner modules the shapes of the energy distributions are similar to the generated ones, i.e., they are less deformed by the background rejection procedure.

Comparisons have also been made for three VSAT energy regions (30-60 Gev, 60-90 GeV and 90-120 GeV) between the generated and reconstructed Monte Carlo samples. The comparison consisted of calculating and plotting distributions of $(E_{gen} - E_{rec})/E_{rec}$, i.e., the relative difference between E_{gen} and E_{rec}.

The results of such a comparison is presented in Table 7.8.

Table 7.8: A comparison of the energy generated by TWOGAM (E_{gen}) with the reconstructed one (E_{rec}) by the mean value and RMS of $E = (E_{gen} - E_{rec})/E_{rec}$

For year 1998, beam energy 94.5 GeV				
E [GeV]	Module 1	Module 2	Module 3	Module 4
30-60	0.00 ± 0.06	-0.01 ± 0.05	0.00 ± 0.05	0.00 ± 0.05
60-90	-0.01 ± 0.04	-0.01 ± 0.04	-0.01 ± 0.04	-0.01 ± 0.04
90-120	-0.03 ± 0.03	-0.03 ± 0.03	-0.03 ± 0.03	-0.03 ± 0.03
For year 2000, beam energy about 103.0 GeV				
E [GeV]	Module 1	Module 2	Module 3	Module 4
30-60	0.00 ± 0.06	0.00 ± 0.06	0.00 ± 0.05	0.00 ± 0.05
60-90	-0.01 ± 0.04	-0.01 ± 0.04	-0.01 ± 0.04	-0.01 ± 0.04
90-120	-0.02 ± 0.04	-0.02 ± 0.04	-0.02 ± 0.04	-0.02 ± 0.04

    The reconstructed mean energy is in all cases within 3% from the generated energy and the RMS is less than 6%. This shows that the energy measurement by VSAT is not biased by the reconstruction procedure.

7.3.2   The distribution of the hadronic multiplicity

The multiplicity distributions of particles from the hadronic system as measured by barrel and forward detectors of DELPHI are in a good agreement with the predictions, except in the low multiplicity region as shown in Fig. 7.11 and 7.12.
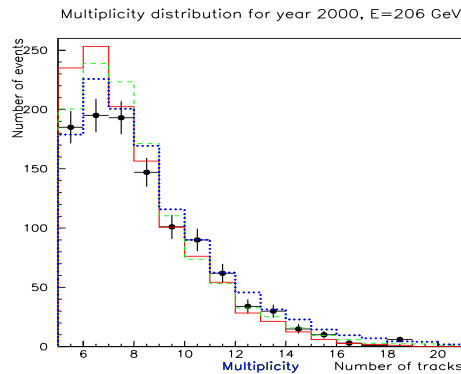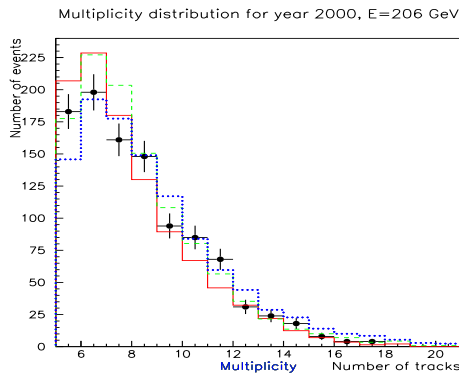
Figure 7.11: The multiplicity of hadronic particles in Module 3 using the year 2000 data (mean beam energy ∼103 GeV). The points are data, TWOGAM is shown as a solid line, PHOJET as a dashed line, PYTHIA as a dotted line.

Figure 7.12: The multiplicity of hadronic particles in Module 4 using the year 2000 data (mean beam energy ∼103 GeV). The points are data, TWOGAM is shown as a solid line, PHOJET as a dashed line, PYTHIA as a dotted line.

7.3.3 Reconstruction of the hadronic invariant mass W_{inv}

An unfolding procedure [36] has been used as a tool to reconstruct a so-called "true" invariant hadronic mass (W_{inv}) and photon structure functions since many years [17, 26, 35, 69]. It has been reconsidered and reevaluated recently with the appearance of the LEP II data and the new event generators for which a separation of the generated events into subgroups is difficult or even impossible.

In this analysis, mainly the W_{inv} variable was used, but in many cases when the structure function is reconstructed it is preferred to use the relative variable x_{true} which is defined as

$$x_{true} = \frac{Q^2}{(Q^2 + W_{inv}^2 + P^2)} \tag{7.1}$$

where P^2 is the transverse momentum squared of leptons lost in the beampipe. It is usually set to zero.

In order to check that the unfolding procedure has worked properly it is not enough to study W_{inv} and x_{true} but also other variables which are less correlated to the invariant mass.

The unfolding is usually taking part after all the distributions have been checked so that the data are known to be in agreement with the model predictions.

A certain amount of disagreement between the data and the Monte Carlo distributions can be accommodated by the unfolding procedure. It is, however, difficult to know how much of a disagreement that can be allowed before the unfolding procedure breaks down.

Another problem with the unfolding procedure itself is the limitation of the type of events it can handle. Correct unfolding can be done only for events with a similar final state topology (i.e. the same angular distributions of the quarks and the fragmentation products). The unfolding procedure cannot for example be used on a VDM-like event sample if it was trained on a QPM-like sample since the dependence of the event selection efficiency on x_{true} is very different for these different samples. The problems with the unfolding procedure means that it is not prudent to assume that the unfolding results are model independent.

For this reason a simplified calculation of the W_{inv} variable was introduced. For simulated events we know both the "true" variables which are possible to measure in experiment and those that are not possible to measure. For single tag events the "true" invariant mass W_{inv} is impossible to measure but the energy deposition in VSAT, the invariant mass of the hadronic system and many others variables can be measured.

After a study of different correlations between the "true" W_{inv} and other variables an expression was derived that was found to be giving a good estimation of the "true" invariant mass in the simulated samples:

$$W_{inv} = a_0 \cdot (E_{beam} - E_{VSAT}) + a_1 \cdot W_{had} \pm a_2 \cdot (\theta_{had} - 90)/10 \tag{7.2}$$

where W_{had} is the invariant mass of the hadronic system measured by the barrel and forward subdetectors, $\pm$ mean that the last element $(\theta_{had}-90)/10$ is positive for the forward modules (1 and 2) and negative for the backward modules (3,4). a_0, a_1, a_2 are coefficients which were estimated for each years data in order to have the best possible determination of the "true" W_{inv}.

Fig. 7.13 and Fig. 7.14 show the distribution of W_{inv} calculated by expression 7.2. The TWOGAM program seems to give a wider W_{inv} distribution than the PHOJET and PYTHIA generators. All of the generators seems to perhaps be shifted to lower values of invariant mass in comparison with data.
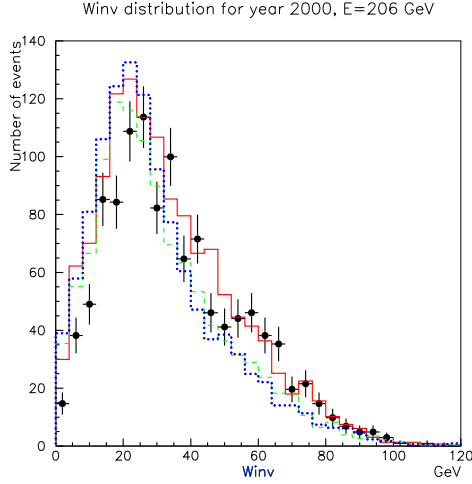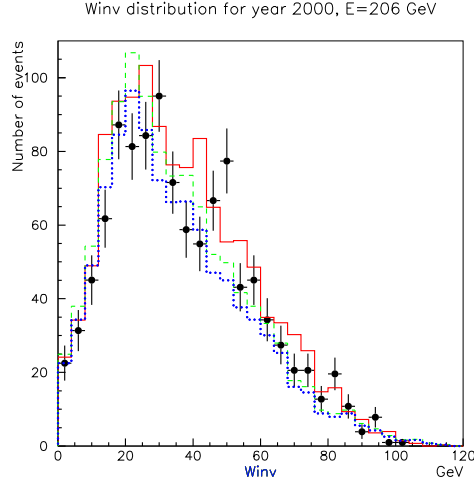

Figure 7.13: The W_{inv} distribution measured by module 2 using year 2000 data (mean beam energy ~ 103 GeV). The points are data, the TWOGAM distribution is shown as a solid line, PHOJET as dashed and PYTHIA as a dotted line.

Figure 7.14: The W_{inv} distribution measured by module 1 for year 2000 data (mean beam energy ~ 103 GeV). The points are data, the TWOGAM distribution is shown as a solid line, PHOJET as dashed and PYTHIA as a dotted line.

To estimate the accuracy of the reconstruction a similar procedure of comparisons as for E_{VSAT} in different regions of W_{inv} was applied for W_{inv}. The results are given in Table 7.9 and they give an indication of the uncertainty in the determination of the W_{inv} variable.

Table 7.9: Standard derivation (RMS) in % for $< W_{inv} >= (W_{inv}^{gen} - W_{inv}^{rec})/W_{inv}^{rec}$, TWOGAM simulation for Module 4.

W_{inv} [GeV]	30 - 36	36 - 42	42 - 50	50 - 60	60 - 75	75 - 120
Year	$\sigma_{<W_{inv}>}$	$\sigma_{<W_{inv}>}$	$\sigma_{<W_{inv}>}$	$\sigma_{<W_{inv}>}$	$\sigma_{<W_{inv}>}$	$\sigma_{<W_{inv}>}$
1998	58 %	53 %	52 %	50 %	40 %	38 %
1999	63 %	59 %	55 %	49 %	45 %	37 %
2000	60 %	57 %	55 %	50 %	44 %	36 %

These results give an estimation of the uncertainty when an individual event is measured. The analysis was, however, made with large samples of events and that greatly improves the uncertainty in the determination of the average W_{inv}.

In the case of double tag measurements, the "true" invariant mass W_{inv} can be calculated from the energies of the tagged leptons. The formula for the calculation of the "true" W_{inv} is:

$$W_{inv} = 2 \cdot \sqrt{(E_{beam} - E_1) \cdot (E_{beam} - E_2)} \qquad (7.3)$$

where E_{beam} is the beam energy, E_1 is the energy of the first lepton and E_2 the energy of the second one.

For an individual measurement the unsertainty (RMS) is changed from 10to 4% when energies measured by VSAT are changed from around 35 Gev to 100 Gev.

Additional distributions of W_{inv} have been made where the data from all VSAT modules are combined and with a larger binning so that statistical fluctuation becomes smaller. The data were divided into several different size W_{inv} intervals and then the number of events in each interval divided by the width of the interval itself was plotted. The study was made with unequal intervals in order to have a statistically significant number of events in each interval. Later the data in these intervals were used in the extraction of the total $\gamma\gamma$ cross-section. The result is presented in Fig. 7.15 and 7.16. While there are statistically significant differences between the shape of the distributions of the three renormalized Monte Carlo programs there are no significant difference between the data and any of the simulation.
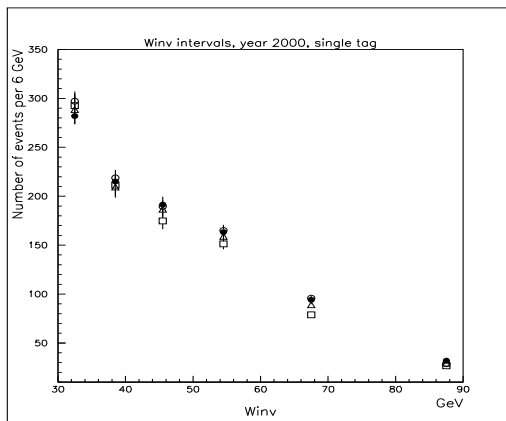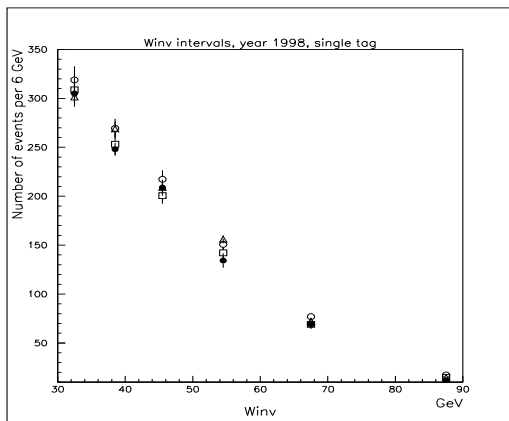
Figure 7.15: Single tag W_{inv} distribution (with 6 intervals) for 1998 data (mean energy 189 GeV). Data is shown as points, the TWOGAM as open circles, PHOJET as open rectangles and PYTHIA as open triangles.

Figure 7.16: Single tag W_{inv} plot (with 6 intervals) for year 2000 (mean energy $\sim$ 206 GeV). Data is shown as points, the TWOGAM as open circles, PHOJET as open rectangles and PYTHIA as open triangles.

7.3.4 The Q^2 distribution

The Q^2 distribution simulated by all generators agreed less well with data than the energy distribution. The background rejection with the help of cutmaps cut differently into the signal distribution in the inner and outer modules and the Q^2 distributions measured by the inner and outer modules therefore looks very different (Fig. 7.17 and 7.18). It is particularly visible in the intermediate Q^2 where the efficiency for the signal is lower in the outer modules.

There seem in addition to be a difference in the level of agreement between data and Monte Carlo in the outer and inner modules. One has to remember that the Monte Carlo events have been re-normalized to the data and so a comparison of the absolute levels are difficult but the difference in shape between data and Monte Carlo still indicate that there are more events in data than in the simulation at the very lowest Q^2 in the outer modules. The situation is if anything the reverse for the inner modules. The likely cause for why at very low Q^2 the Monte Carlo underestimate the data in the outer modules is that there is still some background remaining in the outer module distribution. Due to this discrepancy between data and and Monte Carlo, the data from the outer modules was not use in the final cross-section determination.
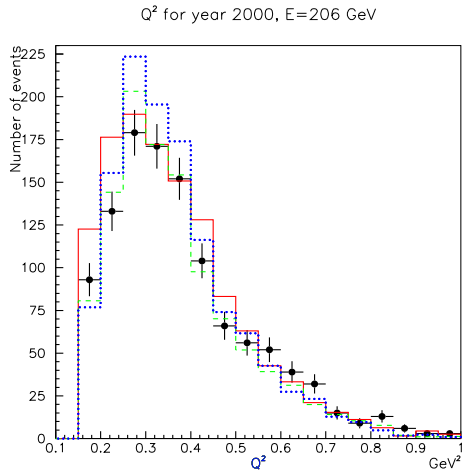
Figure 7.17: The distribution of Q^2 measured by the VSAT module 2 (year 2000 data). The points are data, the TWOGAM distribution is shown as a solid line, PHOJET as a dashed line and PYTHIA as a dotted line.
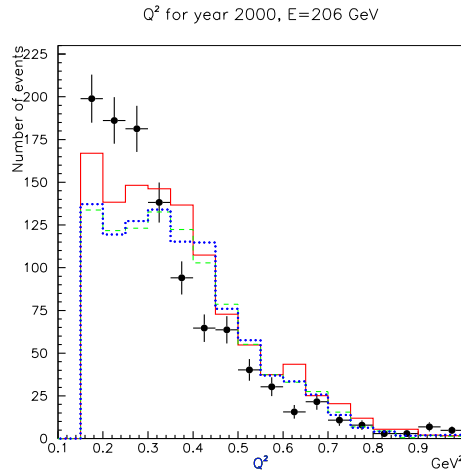
Figure 7.18: The distribution of Q^2 measured by the VSAT module 1 (year 2000 data). The points are data, the TWOGAM distribution is shown as a solid line, PHOJET as a dashed line and PYTHIA as a dotted line.

7.3.5 The P_t distribution

The transverse momentum distributions of hadrons created in single tagged $\gamma\gamma$ collisions are given in Fig. 7.19 and 7.20. The predictions from all generators agree well with each other. The Monte Carlo distributions are narrower for all VSAT modules due to the number of simulated secondary particles in the forward region that is larger in simulation than in the data.
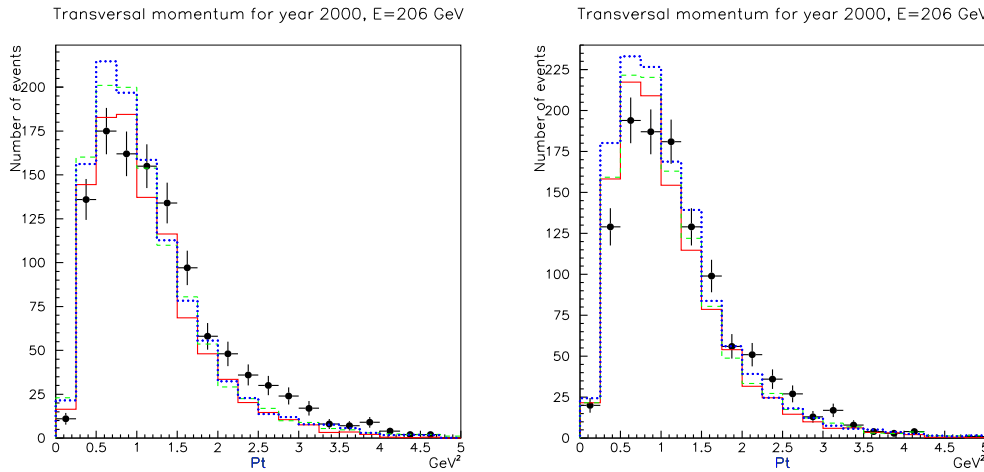

Figure 7.19: The transverse momentum distribution of particles where the event was tagged by Module 3 in year 2000 (mean beam energy ∼ 103 GeV). The points are data, the TWOGAM is shown as a solid line, PHOJET as a dashed line, PYTHIA as a dotted line.

Figure 7.20: The transverse momentum distribution of particles where the event was tagged by Module 4 in year 2000 (mean beam energy ∼ 103 GeV). The points are data, the TWOGAM is shown as a solid line, PHOJET as a dashed line, PYTHIA as a dotted line.

Most events in the transverse momentum distributions are at low P_t. This is due to the fact that the VSAT modules were hit only by scattered leptons which were very close to the beam and therefore had very small transverse momentum. In a previous study single tag events tagged by the STIC and FEMC subdetectors were used to extract the photon structure function at larger P_t [69].

7.4 Comparison of Double tagged events

The W_{inv} and Q^2 distributions were also studied with the double tag sample where W_{inv} was reconstructed from the energy of the both measured leptons. The low statistics of the double tag samples made it necessary to combine all data from the years 1998 and 2000 in one plot. All Monte Carlo generators have a similar Q^2 distribution (Fig. 7.21). PHOJET seems to be higher than all others, but all simulations agree with the data within the large statistical uncertainties.
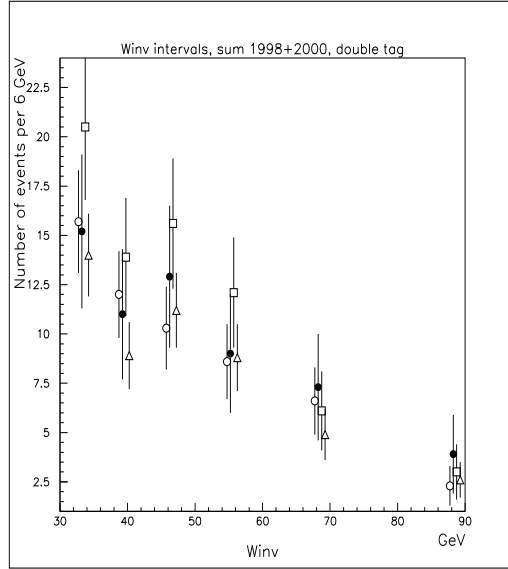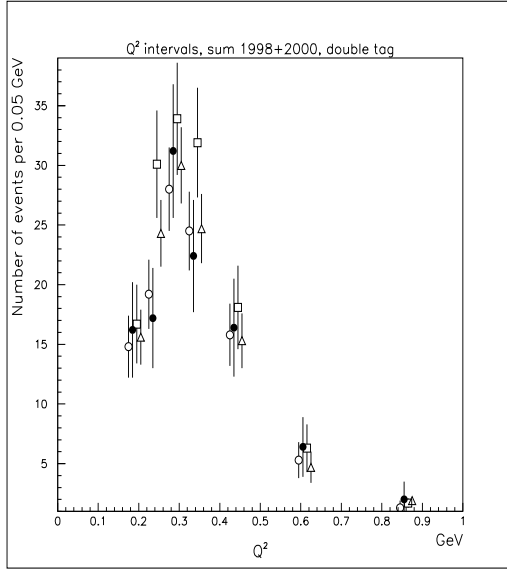
Figure 7.21: The Q^2 distribution (7 intervals) of double tag events recorded during the years 1998+2000. Data is shown as points, TWOGAM as open circles, PHOJET as open rectangles and PYTHIA as open triangles.

Figure 7.22: The W_{inv} distribution (6 intervals) of double tag events recorded during the years 1998+2000. Data is shown as points, TWOGAM as open circles, PHOJET as open rectangles and PYTHIA as open triangles.

Fig. 7.22 shows the W_{inv} distribution for double tagged events. Due to the poor statistics it is again difficult to draw any conclusions but perhaps the PHOJET distribution is above the PYTHIA one.

Chapter 8

Results

8.1 The final sample of single tagged events

Studies were made to check the consistency of data samples from different years. The following run-time dependencies were studied and implemented in the reconstruction procedure of the tagged lepton:

    a) the beam-spot position (for each run);
    b) the inclination of the incoming beams (for each run);
    c) the beam energy (for each fill);
    d) the leakage corrections (for each beam energy);
    e) the geometrical position of the VSAT modules (for each year).

The hadronic system created in the $\gamma\gamma$ collisions was reconstructed with the standard reconstruction procedure of DELPHI. The final reprocessed samples with all the corrections applied for individual tracks and neutral particles have been used in the present analysis.

The overlapping geometrical acceptance of the different detectors provided a substantial redundancy between the different trigger conditions which ensured a high and stable efficiency over long running periods.

This redundancy made it possible to determine both the trigger efficiency and its error with good precision. Thus, it was found that the global trigger efficiency for electron-positron and muon pairs created in e^+e^- collisions is consistent with 1 at the level of 10^{-4} for polar angles between 20° and 160°. For single tracks, provided their momentum transverse to the beam exceeds 1 GeV, the efficiencies in the barrel ($42^o < \theta < 138^o$) and forward ($10^o < \theta < 32^o$) and backward ($148^o < \theta < 170^o$) regions exceeds 95%. It means that for $\gamma\gamma$ events with a relatively low multiplicity (6-8 charged particles, see Fig. 7.11 and 7.12) and relatively low transverse momentum (see Fig. 7.19 and 7.20) the global event trigger efficiency was found to be 97% with possible variations of 2% during long running periods.

After all corrections mentioned above were applied, the samples from different years were compared. All the distributions were found to be consistent with each other. The combined distributions of the single tag events for all years are shown in Fig. 8.3. They were compared and found to be in a reasonable agreement with the simulation.

The final sample of single tag data events which passed all criteria with averaged purity estimated 81% are shown in Table 8.1 together with the samples of simulated events.

Table 8.1: Summary of the number of selected single tag events in VSAT after all cuts were applied.

Data set:	1998	1999	2000
Data	4763	2355	4608
TWOGAM	8969	15178	15107
PHOJET	19263	-	20269
PYTHIA	23191	27796	28902

8.2 The final sample of double tagged events

Only 103+127+93=323 double tag events (for years 1998, 1999, 2000 respectively) passed all the selection criteria with an averaged purity estimated at 75%.

The background rejection in the double tag analysis is based on the same cut-maps as for the single tag events. The background to be subtracted generally follows the shape of the signal distribution or is shifted to lower energies (see also sections 6.1 and 6.4). Two typical examples of this is the energy of the leptons measured by VSAT and the reconstructed invariant mass as shown in Fig. 8.1 and 8.2.
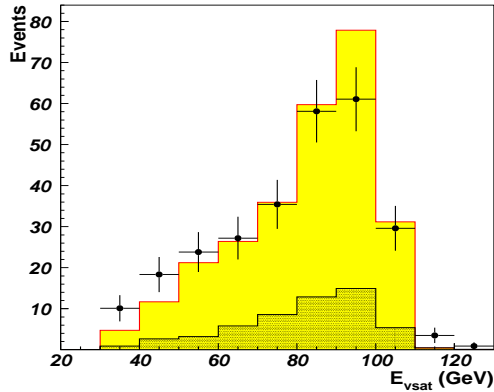
Figure 8.1: The E_{vsat} distribution of double tag events (sum of three years data). The crosses are data and the TWOGAM simulation is shown as a solid line and shaded area. The hatched area is the background.
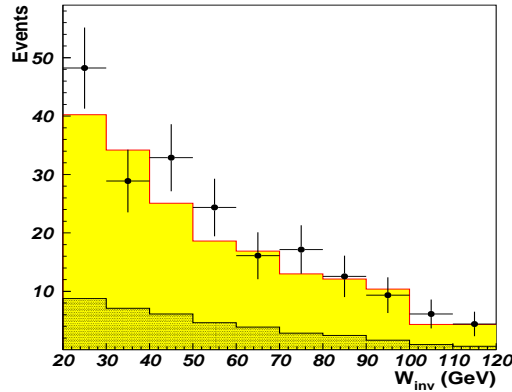
Figure 8.2: The W_{inv} distribution of double tag events (sum of three years data). The crosses are data and the TWOGAM simulation is shown as a solid line and shaded area. The the hatched area is the background.

Quantities such as the total multiplicity, energy in VSAT, W_{inv} and P_t agree well for all three years after background subtraction. The double tag samples from all years were therefore also combined into one and the total number of double tag events from data and Monte Carlo simulations are presented in Table 8.2.

Table 8.2: Summary of simulated and real data samples for double tag events in VSAT with all cuts applied.

Sample	1998	1999	2000	Total
Data	103	127	93	323
Data background subtracted	85	105	77	267
TWOGAM	347	245	330	922
PHOJET	784	-	412	1196
PYTHIA	576	705	591	1872

Data and the Monte Carlo predictions for double tag events shown in Fig. 8.4 agree within the statistical errors. It is difficult to distinguish between the performance of the Monte Carlo programs but perhaps TWOGAM is in a better agreement than the other two programs. This is partly due to the requirement that both scattered particles have a measured Q^2 (i.e. > 0). It means that all generators work better when both particles have a scattering angle far from zero. In the single tag case there is a large subsample of events with very low $Q^2 \approx 0$ (which is impossible to reach if both leptons are tagged). For such events there is an indication that the simulation disagree increasingly with a decreasing Q^2. Therefore the differences between simulated and data samples are larger in the single tagged case.
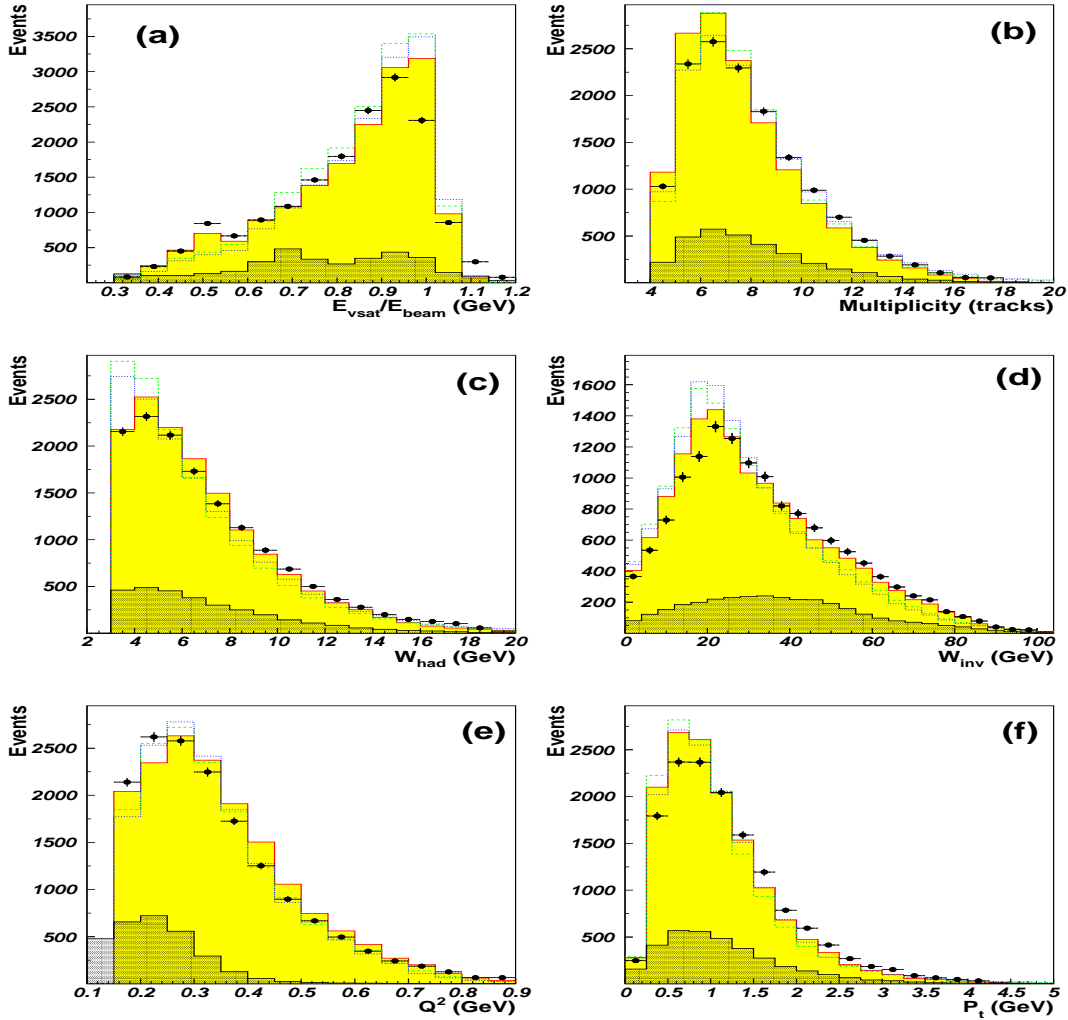
Figure 8.3: Single-tag events: a) The relative energy of scattered e^+ and e^- measured in VSAT, b) The event multiplicity, c) The invariant mass of the hadronic system, d) Reconstructed invariant mass, e) The distribution of Q^2, f) The transverse momentum of the hadronic system. Points are data, hatched area is the background, lines show Monte Carlo: solid line and shaded area is TWOGAM, the dashed line is PHOJET and the dotted line is PYTHIA.
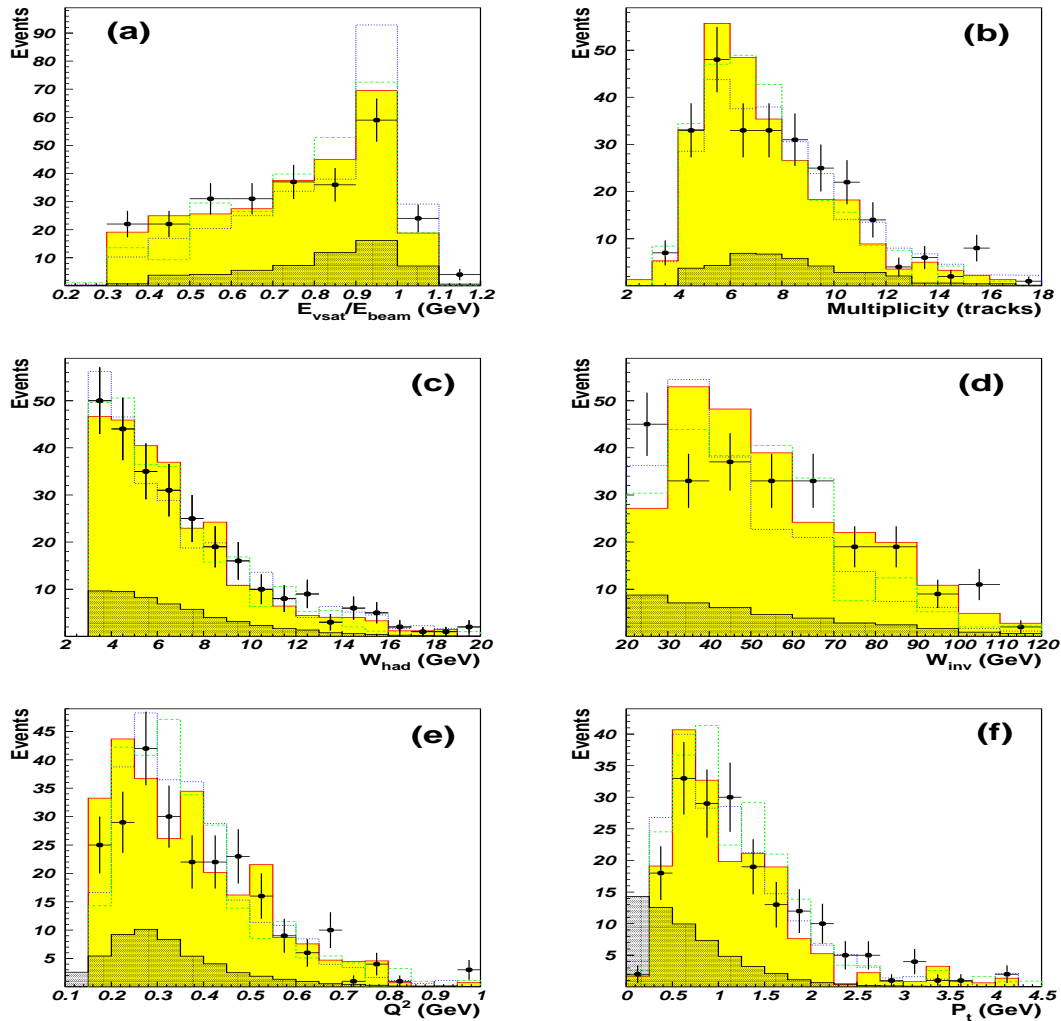
Figure 8.4: Double tag events: a) The relative energy of scattered e^+ and e^- measured in VSAT, b) The event multiplicity, c) The invariant mass of the hadronic system, d) Reconstructed invariant mass, e) The distribution of Q^2_{max}, f)The transversal momentum of hadronic system. Points are data, the hatched area is the background, lines show Monte Carlo: solid line and shaded area is TWOGAM, the dashed line is PHOJET, and the dotted line is PYTHIA.

8.3 Total cross-section

In order to extract the total $\gamma\gamma$ cross-section it is necessary to calculate the luminosity function of the photon flux (see section 2.12, formula 2.19). The luminosity function of the photon flux gives the probability of having a $\gamma\gamma$ collision with a certain W in the e^+e^- interaction. To calculate the luminosity function it is in principle necessary to know the kinematical variables of both photons. For $Q_i^2 \to 0$ and $Q_i^2 \ll W^2$ and low scattering angles the photon luminosity function can be, however, determined as a product of two fluxes based on the kinematics of only one vertex [38] (since $W^2 \simeq 4E_1^\gamma E_2^\gamma$ i.e. W depends only on the energy of the photons). One can therefore obtain the factorized luminosity function:

$$\frac{d^2L_{12}}{d\omega_1 d\omega_2} = \frac{dN_\gamma(\omega_1)}{d\omega_1}\frac{dN_\gamma(\omega_2)}{d\omega_2} \tag{8.1}$$

where $\omega_i = E_i^\gamma/E_{beam}$.

After the pioneering work of V.M. Budnev et al. [57] the equivalent photon approximation for two-photon production was widely used. A considerable improvement to this approximation was recently done by Schuler [60], where the previously used forms of the equivalent photon approximation were critically examined.
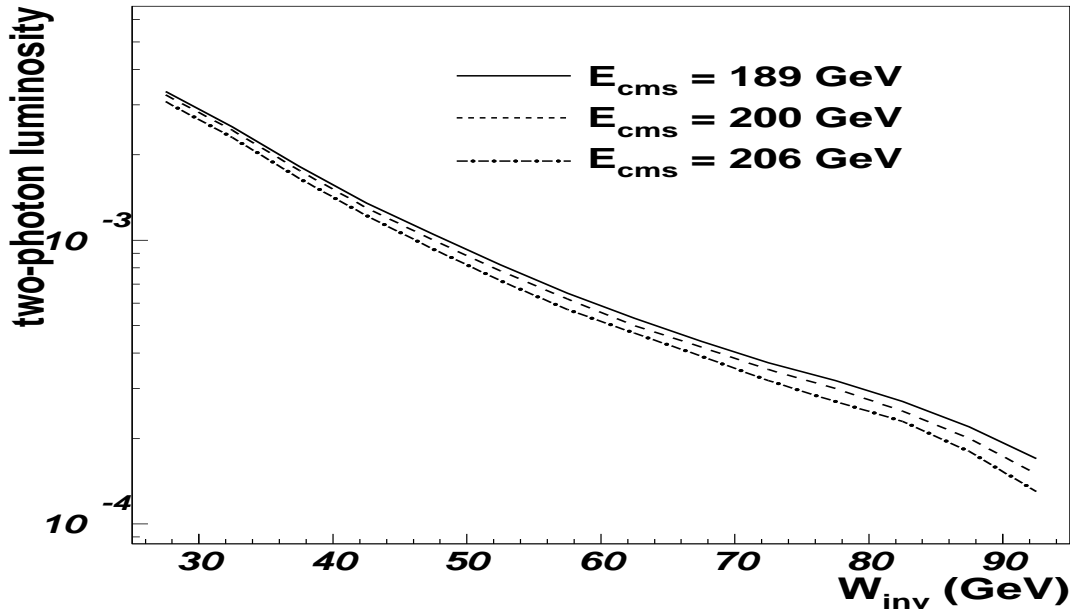
Figure 8.5: The two-photon luminosity function versus W_{inv} for different beam energies (189 GeV is shown as a dash-dotted line, 200 GeV as a dashed line and 206 GeV as a solid line). The so-called "two-photon luminosity" is the probability to have a $\gamma\gamma$ interaction.

The improved calculation of the two-photon luminosity function which includes beyond-leading-logarithm effects is implemented into the GALUGA program [66], which was used to calculate the photon flux in this study. It is important to note that the improved two-photon luminosity function is better calculated for both single tag and double tag topologies. It should of course be calculated for them separately. The example of such a calculation for the single tag case is shown in Fig. 8.5. These luminosity functions (and similar ones for double tag events) were used in the extraction of the total $\gamma\gamma$ cross-section.

Another very important task in order to get the total $\gamma\gamma$ cross-section extracted correctly is the transformation from the effective cross-section $e^+e^- \rightarrow hadrons$ measured in the experiment to the real cross-section of this physics process. The level of complexity of this problem is clearly shown in Fig. 8.6 and 8.7 where the generated invariant mass distributions are shown for all generated events and those that passed all the selection criteria.

Both the single and double tag distributions can be seen in comparison with the initial distribution of the generated W_{inv} in Fig. 8.6 and then after selection in Fig. 8.7. It is clear from the plots that it is necessary to carefully take into account the acceptance and other features of the experimental setup, to separate the physical process studied from other processes and to reject different backgrounds. Due to the small acceptance of the VSAT detector (including the cut-maps in the background subtraction procedure) the selection of events introduces a drastic change in the shape of the distribution of the reconstructed W_{inv}.
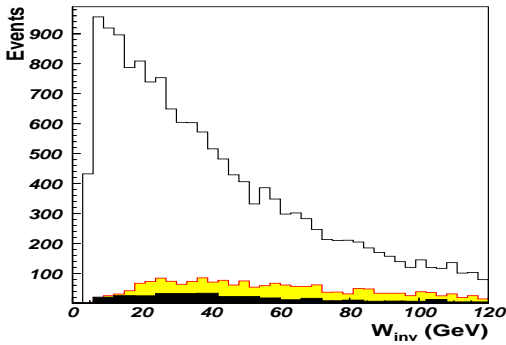

Figure 8.6: The simulated W_{inv} distribution (for module 2) of year 2000 data (mean beam energy $\sim$103 GeV). The solid line is W_{inv} before selection, after single tag selection it is shown as a shaded area. The dark area is the double tag events in all modules.
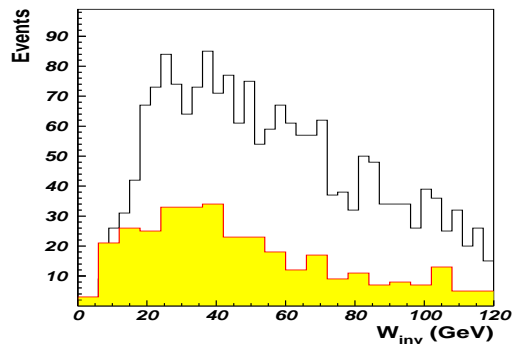
Figure 8.7: The simulated W_{inv} distribution after the selection of single tag events (module 2) and of double tag events (all modules) for year 2000. The solid line is for single tag data while double tag is shown as a shaded area.

Since the simulated samples agree well with data (after renormalization of PYTHIA and PHOJET) all of them have been used to calculate the detection efficiency at different invariant masses W_{inv} of the hadronic states and with all effects of the event selection included.

The efficiency was calculated separately for the single tag and double tag samples. An efficiency averaged over all simulated samples was finally used in the total $\gamma\gamma$ cross-section calculations. The TWOGAM generator showed again a better agreement with data for both the absolute values and shapes of the compared distributions. Specially generated samples by TWOGAM for no-tag conditions were therefore used to transform the cross-section in single and double tag topologies to the total effective $\gamma\gamma$ cross-section of the process $\gamma\gamma \rightarrow hadrons$. This was done for the same W_{inv} intervals that were used in the extraction. As the inner VSAT modules were considerably less affected by the background conditions, only events tagged by those modules have been used for the cross-section extraction in the single tag case. Final results are given in in Table 8.3, The total error was calculated as the quadratic sum of the statistical and systematical error.

Table 8.3: The number of events in different samples before normalization and the effective $\gamma\gamma$ hadronic cross-section for single tag events.

W_{inv},GeV	30-36	36-42	42-50	50-60	60-75	75-100
Data	1071	815	901	803	672	267
TWOGAM	1514	1222	1227	1228	1222	510
PHOJET	2472	1851	1883	1621	1203	473
PYTHIA	2769	2055	1800	1575	1184	531
Statistical error, %	3.1	3.5	3.3	3.5	3.9	6.1
Systematical error, %	2.6	2.7	2.7	2.8	2.9	3.3
Total error, %	4.0	4.4	4.3	4.5	4.9	7.0
σ_{tot}, nb	370	406	437	474	513	604
Statistical error, nb	11	15	15	17	20	37
Systematical error, nb	10	11	12	13	15	20
Total error, nb	15	18	19	21	25	42

The average contributions to the systematic errors from different sources were estimated as follows:

- the background rejection procedure: $\sim 2.0\%$;

- the event selection procedure: $\sim 0.9\%$;

- the generation of no-tag samples: $\leq 0.7\%$;

- the calculation of the photon luminosity function: $\leq 0.2\%$.

The uncertainties due to the limited Monte-Carlo statistics used in the determination of the detection efficiency in different invariant mass W_{inv} intervals are also included in the systematic errors. The total systematic error (calculated as the quadratic sum of the individual systematic errors) is therefore different for different W_{inv} intervals.

The total effective $\gamma\gamma$ cross-section was extracted in the same fashion from the double tag events. Due to the lower statistics, the event sample was only split into 4 intervals of invariant mass W_{inv}. All four VSAT modules were used as tagging devices. Thus both the diagonal (inner and outer modules) and the parallel (inner-inner or outer-outer) combinations contributed to the final data sample. To increase the Monte Carlo statistics, both the NST and RST samples generated by the TWOGAM program have been used in the determination of the detection efficiency. Final results for the double tag case are shown in Table 8.4. The total error was calculated as the quadratic sum of the statistical and systematical error.

Table 8.4: The number of events (before normalization) in different samples and the effective $\gamma\gamma$ hadronic cross-section for double tag events.

W_{inv},GeV	20-34	34-50	50-72	72-100
Data	89	76	77	81
TWOGAM	310	238	208	266
PHOJET	256	208	176	92
PYTHIA	574	302	238	148
Statistical error, %	10.6	11.5	11.4	11.1
Systematical error,%	5.4	6.0	6.4	7.2
Total error, %	11.9	13.0	13.1	13.2
σ_{tot}, nb	344	412	478	624
Statistical error	36.5	47.4	54.5	69.3
Systematical error	18.6	24.7	30.6	44.9
Total error, nb	41	54	63	83

The systematic errors were estimated in the same manner as in the single tag analysis. For each W_{inv} interval the averaged uncertainties were as follows:

- the background rejection procedure: $\sim 4.0\%$;

- the event selection procedure: $\sim 1.0\%$;

- the generation of no-tag samples: $\leq 0.7\%$;

- the calculation of the photon luminosity function: $\leq 0.2\%$.

These systematic errors are different for each W_{inv} interval as was the case in the single tag analysis.

The results of the extrapolation of the total $\gamma\gamma$ cross-section for both the single and double tag case are shown in Fig. 8.8 together with a compilation of measurements from L3 and OPAL. The results were found to be in a good agreement with earlier preliminary DELPHI [128] results based on double tag events only. The total $\gamma\gamma$ cross-section predicted by the TWOGAM generator is also shown. The VSAT measurements are consistent with each other but seem to be higher than what has been obtained by L3 [26] and OPAL [33].
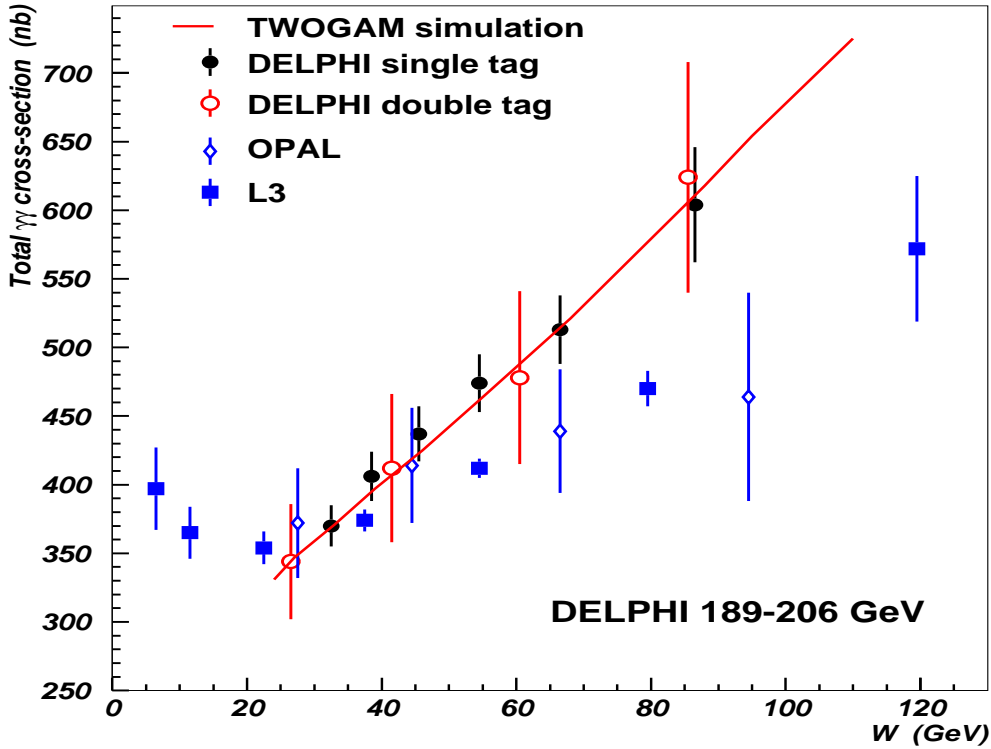
Figure 8.8: The total hadronic $\gamma\gamma$ cross-section measured by VSAT for single tag events (filled circles) and double tag (open circles), TWOGAM (line), OPAL (open rombs) and L3 (filled rectangles).

The statistical uncertainty in the new VSAT double tag measurement is smaller than in the previous work [128] based on a small sample of VSAT double tag events. The errors from the VSAT single tag events are of course noticeably smaller than those of the double tag events. Results from all experiments clearly show an approximately linear rise of the cross-section as a function of the invariant mass W_{inv} of the hadronic system. Fig. 8.9 shows the dependence of the cross-section as predicted by TWOGAM for all the $\gamma\gamma$ subprocesses implemented in the program.

At the very low Q^2 studied in this analysis, the VDM process gives a constant and large contribution to the $\gamma\gamma$ cross-section while the RPC cross-section increases almost linearly with W. This explains why the data distribution in Fig. 8.8 looks flat for $W \leq 30 \ GeV$ and then increases linearly at higher W. It is also worth to notice that it is the VDM process which dominates the cross-section for W less than $\sim 70 \ GeV$ and it is only for very high W that the RPC process gives the largest contribution to the cross-section. The QPM process gives a negligible contribution for all values of W.
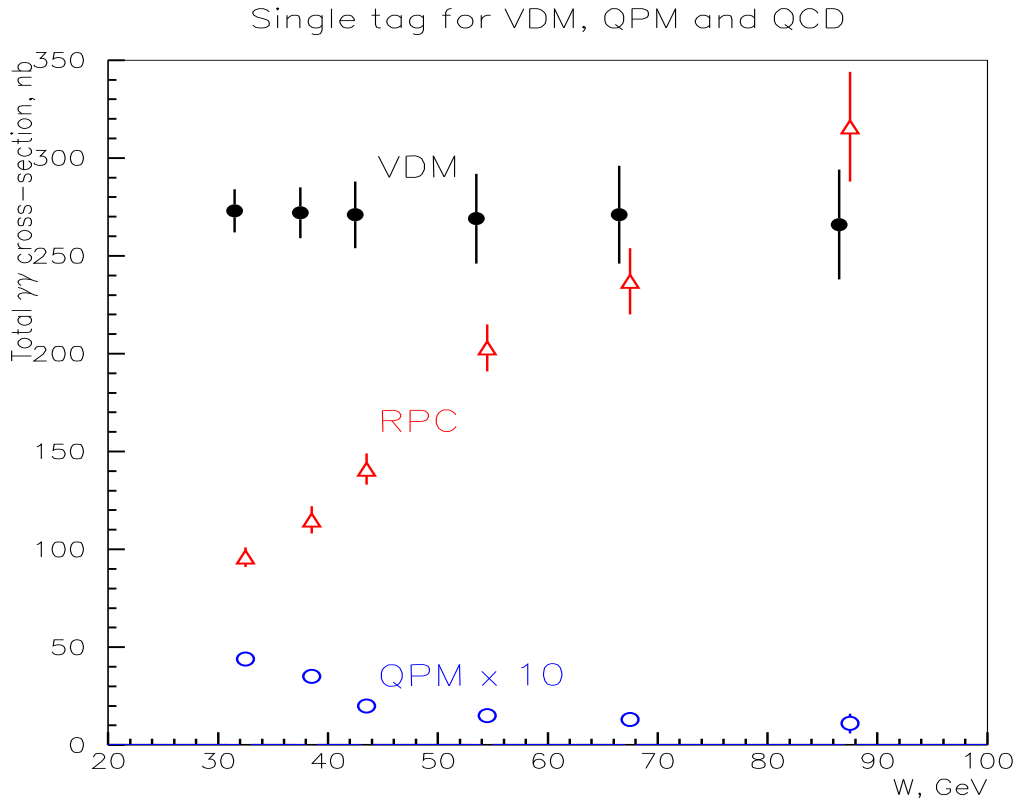
Figure 8.9: Contributions to the total hadronic cross-section in $\gamma\gamma$ interaction from three processes included in the TWOGAM generator for the single tag events: Vector Dominance Model (filled circles), Resolved Photon Contribution from QCD (open triangles) and Quark Parton Model (open circles multiplied by a factor of 10 in order to be seen in the plot).

Chapter 9

Conclusion

The topic of this study is an analysis of hadronic events produced in two-photon collisions in single and double tag modes at e^+e^- centre-of-mass energies between 189 and 206 GeV. The VSAT (Very Small Angle Tagger) detector was used to tag scattered electrons and positrons and the whole DELPHI detector information was used in the analysis of the hadronic part of the events.

Unfortunately, due to the very small distance between the VSAT modules and the beam, the background conditions caused by off-energy electrons were difficult to master. A large effort has been made to reject it as much as possible and to estimate and subtract the remaining background.

Different experimental distributions were reproduced by simulation. The three Monte Carlo generators TWOGAM, PYTHIA and PHOJET were compared with data and with each other. The shape of the various distributions was similar for all generators and the data but the overall prediction of the cross-section was too high from the PYTHIA and PHOJET programs.

Measurements of the effective total $\gamma\gamma$ cross-section were made at a very low Q^2 (much closer to Q^2=0 in comparison to other results obtained by other LEP experiments). It was done for $\gamma\gamma$ centre-of-mass energies from 30 GeV to 100 GeV. The cross-section determination using VSAT single tagged events was consistent with the determination using double tag events The rise of the $\gamma\gamma$ cross-section with W_{inv} is somewhat steeper in this study than in previous measurements by the L3 and OPAL collaborations. This rise can be explained by the RPC process which starts to dominate at high W.

Chapter 10

Acknowledgments

Bibliography

[1] D.Sperber, *Phys. Scr.,* **10 A**, 115, (1974)

[2] PHOTON 2001, Proceedings of the International Conference on the Structure and Interactions of the Photon, Including the 14th Intemational Workshop on Photon-Photon Collisions,
Ascona, Switzerland,Copyright 2002 by World Scientific Publishing Co. Pte. Ltd. ISBN 981-238-053-1.

[3] R. J. Taylor, Measurement of the hadronic photon structure function at LEP2.
PHOTON 2001, Ascona, Switzerland.

[4] P. Achard, V. Andreev, S. Braccini et al. Comparison of deep inelastic electron-photon scattering data with the HERWIG and PHOJET Monte Carlo models.
Geneva, CERN, 3 Jul 2000, internal report CERN-EP-2000-109, hep-ex 0010041.

[5] M. Drees and R.M.Godbole, J. Phys. **G21** (1995)1559

[6] L.E. Gordon and J.K. Storrow, Z. Phys. **C52** (1992)307

[7] M. Gluck, E. Reya and A. Vogt, Phys. Rev. **D45** (1992)3986

[8] H. Abramovicz, K. Charchula and A. Levy, Phys. Lett. **B269** (1991)233

[9] G.A. Schuler and T. Sjostrand, Z. Phys. **C68** (1995) 607.

[10] DELPHI Coll., P. Aarnio et al., Nucl. Instr. and Meth., A303 (1991)233

[11] OPAL Coll., Jan A. Lauber, Proc. of the 28th Int. Conf. on High Energy Physics, World Scientific Publising Co. Pte. Ltd., (1996)725

[12] PLUTO Collaboration, Ch. Berger et ai, Z. Phys. **C26**(1984)353

[13] TPC/2γ Collaboration, H. Aihara et al., Phys. Rev. Lett. **58**(1987)97
TPC/2γ Collaboration, H. Aihara et al., Phys. Rev. **D41**(1990)2667

[14] AMY Collaboration, R. Tanaka et ai, Phys. Lett. **B277**(1992)215

[15] ALEPH Collaboration, D. Buskullic et ai, Phys. Lett. **B313**(1993)509

[16] U. Sieler, A. Bohrer, A.Finch, Measurement of the D^{*+} Production in Two Photon Events in the ALEPH Detector at LEP II energies
(Inclusive $D^{*\pm}$ Production in Two-Photon Events)
Geneva : CERN, 21 Jul 2000, internal report CERN-ALEPH-2000-07,
30th International Conference on High Energy Physics, Osaka, Japan, 2000

[17] A. Wright, A. Finch, Two-photon analyses with the ALEPH detector
Geneva, 1998 : CERN internal report CERN-ALEPH-98-085

[18] P. Hodgson, M.H. Lehto, A. Finch, A measurement of the di-jet cross section in $\gamma\gamma \rightarrow$ hadrons with ALEPH MeasDi-jet production in untagged two photon events at LEP 2, Geneva: CERN, 21 Jul 2000. - CERN internal report: CERN-ALEPH-2000-052, Presented at: 30th International Conference on High Energy Physics,
Osaka, Japan, 2000

[19] U. Sieler, Charm production in two-photon collisions measured by the ALEPH detector at LEP II energies.
AIP Conf. Proc.: 571 (2001) pp.245-251

[20] R. Garisto, J.N. Ng, What can the L3 $\gamma\gamma ll$ events be?
Phys. Lett., **B317** (1993) 462-466

[21] L3 Collaboration, O. Adriani et. al., Phys. Lett. **318B**(1993)575

[22] R.R. McNeil, Hadron production in $\gamma\gamma$ collisions in the L3 detectors at $\sqrt{s}$=130 - 140 GeV, 9th Annual Meeting of the Division of Particles and Fields of the American Physical Society,
Minneapolis, MN, USA , 11-15 Aug 1996 - pp.576-579

[23] P. Achard, Inclusive π^0 and K_S^0 in $\gamma\gamma$ reactions at L3
Geneva : CERN, 2001 . - mult. p. Published in: AIP Conf. Proc.: 571 (2001)172-178

[24] S. Saremi, Charm and bottom production in two photon collisions at LEP with the L3 detector
AIP Conf. Proc.: 571 (2001)266-75

[25] D. Haas, Cross section measurement of tau pairs in two photon collisions with the L3 detector at LEP 2
AIP Conf. Proc.: 571 (2001)339-44

[26] M. Acciarri et al. (The L3 Collaboration), Total Cross Section measurement in $\gamma\gamma$ Collisions at LEP 2.
CERN-EP/2001-012, January 30, 2001

[27] V.P. Andreev, Resonance production in two photon collisions at LEP with the L3 detector
AIP Conf. Proc.: 571 (2001) pp.380-7

[28] OPAL Collaboration, R. Akers et. al., Z. Phys. **C61**(1994)119

[29] OPAL Collaboration, K. Ackerstaff et al., Phys. Lett. **B411**(1997)387-401

[30] OPAL Collaboration, K. Ackerstaff et al., Phys. Lett. **B412**(1997)225-234

[31] OPAL Collaboration, K. Ackerstaff et al., Z. Phys. **C74**(1997)33-48

[32] OPAL Collaboration, Total Hadronic Cross-Section of Photon-Photon Interactions at LEP,
     CERN preprint CERN-EP-99-076, Eur. Phys. J., **C 14** (2000)199-212

[33] OPAl Coll., K. Ackerstaff et al., Eur. Phys. J., **C 14** (2000)199

[34] J. Patt, Production of D* mesons in photon-photon collisions at $\sqrt{s}_{ee} = 183$ GeV and 189 GeV using the OPAL detector at LEP
     Published in: Nucl. Phys. B, Proc. Suppl. 82 (2000) 200-5

[35] Akos Csilling, Hadron production in two-photon collisions at LEP-L3.
     hep-ex/9910051 pres. at: Central European Triangle Symposium on Particle Physics, Zagreb, Croatia, June 1999

[36] V. Blobel, In Proceedings of the CERN School of Computing,
     Aiguablava, Spain, (1984), CERN 85-09.

[37] F.M. Renard, Basics of Electron Positron Collisions, Editions Frontieres, 1981

[38] H. Kolanoski, Two-Photon Physics at e+e- Storage Rings, Springer, 1984

[39] H. Kolanoski, P. Zerwas, High Energy Electron-Positron Physics,
     Eds: A. Ali, P. Soding, World Scientific, Singapore, 1998

[40] M. Feindt, CERN-PPE/91-90

[41] J.S. Steinman, Thesis, UCLA-HEP-88-004, 1988

[42] F. Naraghi, Thesis, Univ. Paris VII, 1992

[43] H.-U. Martyn, DESY 89-121 PITHA 89/20

[44] PLUTO Collaboration, Ch. Berger et al., Phys. Lett. **Bl49**(1984)421

[45] TASSO Collaboration, M. Althoff et al, Z. Phys. **C31**(1986)527

[46] CELLO Collaboration, H.J. Behrend et al., Z. Phys. **C51**(1991)365

[47] J. Rosner, NBL Report 17522 (1972)316

[48] J. Rosner, Brookhaven Report CRISP 7126 (1971)

[49] I.F. Ginzburg, V.G. Serbo, Phys. Lett. **B109**(1982)231

[50] J.J. Sakurai, D. Schildknecht, Phys. Lett. **B41**(1972)489

[51] TASSO Collaboration, M.Althoff et al., Z. Phys. **C31**(1986)527
     CELLO Collaboration, H.J.Behrend et al., Z. Phys. **C51**(1991)365
     DELPHI Collaboration ,P.Abreu et al., Phys.Lett.**B342**(1995)402

[52] A. Nygren, DELPHI 2001-002 Talk 021 (2001).

[53] DELPHI Collaboration, P.Abreu et al., Z. Phys., B **69** (1996) 223
A measurement of the photon structure function F_2^γ at average Q^2 of 12 GeV^2/c^4.
CERN PPE/95-87

[54] DELPHI Collaboration, P.Abreu et al., Z. Phys., C **62** (1994) 357-366
Study of hard scattering process in multihadron production from $\gamma\gamma$ colisions at LEP.
CERN PPE/94-04

[55] T. Alderwereld et al. Event Generators for $\gamma\gamma$ physics, CERN OPEN-2000-141.

[56] V.M. Budnev et al., Phys Rep **15** (1975)181

[57] V.M. Budnev, I.F. Ginzburg, G.V. Meledin and V.G. Serbo,
Physics Reports (Section C of Physics Letters) 15, no. 4 (1975)181-282

[58] DELPHI Collaboration, P.Abreu et al., Phys. Lett. **B491** (2000)67-80
Determination of the $e^+e^- \rightarrow \gamma\gamma(\gamma)$ cross-section at centre-of-mass energies ranging
from 189 GeV to 202 GeV. CERN-EP/2000-094

[59] DELPHI Collaboration, Abreu, P. et al., Eur. Phys. J., **C 17** (2000)53-65
Photon Events with Missing Energy at $\sqrt{s} = 183$ to 189 GeV, CERN-EP-2000-021

[60] G.A. Schuler, CERN-TH/96-297 (1996).
Improving the equivalent-photon approximation in electron-positron collsions.

[61] I.G. Knowles et al., QCD Event Generators, hep-ph/9601212
G.Cooorcella et al., hep-ph/9912396.

[62] R. Engel. Hadronic interactions of photons at high energies.
PhD thesis, Universitat Siegen 1997.

[63] T. Sjostrand, Computer Phys. Commun **82** (1994)74

[64] S. Nova et al., DELPHI 90-35(1990).

[65] DELPHI Collaboration, DELPHI 89-67 PROG 142(1989).

[66] Gerhard A. Schuler. Two-photon physics with GALUGA 2.0.
Computer Physics Communications 108 (1998)279-303

[67] DELPHI collaboration,
DELPHI data analysis program (DELANA) user's guide.
DELPHI 89-44 PROG 137(1989).

[68] DELPHI Collaboration.
DELSIM. DELPHI event generation and detector simulation. version 3.4 User's Guide.
DELPHI 89-67 PROG 142, 10 July 1989.

[69] Study of the hadronic photon structure function at LEP2.
CERN-EP/2003-018

[70] T. Sjostrand, PYTHIA Status Report.
Lunds Univ. Dept. Theor. Phys., 15 Dec 2000 report: LUTP-2000-54, hep-ph/0012188.
T. Sjostrand, L. Lonnblad, S. Mrenna, PYTHIA 6.2 Physics and Manual.
Lunds Univ. Dept. Theor. Phys., 31 Aug 2001 report: LUTP-2001-21, hep-ph/0108264.

[71] A.J.   Finch,   Nucl.   Phys.   B,   Proc.   Suppl.   82   (2000)156-61
http://lepton.bartol.udel.edu/ eng/phojet.html

[72] T. Alderweireld, S. Todorovova, P. Verdier,
Study of the hadronic $\gamma\gamma$ interactions at $\sqrt{s}$=200 GeV
Geneva, CERN, 1 Sep 2000, CERN-DELPHI-2000-163-PHYS-878, CERN-OPEN-2002-
032

[73] G. Marchesini, Bryan R. Webber, G. Abbiendi, I. G. Knowles, Michael H. Seymour, L.
Stanco,
HERWIG : a Monte Carlo event generator for simulating hadron emission reactions
with interfering gluons (version 5.1 - April 1991)
Hamburg : DESY, May 1991 report: DESY-91-048.

[74] S. Moretti, HERWIG an event generator for e^+e^- Linear Colliders
Geneva, CERN, 18 Sep 2002 internal report: CERN-TH-2002-237.
Presented at: 5th International Workshop on Linear Colliders, Jeju Island, Korea, Aug
2002

[75] L. Del Duca, BFKL : a minireview, Edinburgh : Edinburgh Univ., 1 Jul 1997, internal
report: EDINBURGH-97-8. hep-ph/9706552
Presented at: 5th International Workshop on Deep-Inelastic Scattering and QCD ,
Chicago, IL, USA , Apr 1997

[76] T.Alderweired et al., Proc of the Int. Conf. on High Energy Physics, Tokio, 2000. Also
a DELPHI report: DELPHI 2000-072 CONF 371, 30 June, 2000.

[77] A. Bonifas, Ch. Nuttall, G. Rau, Environmental monitoring for the LEP project :
measuring results of preoperational background parameters during 1985
Geneva, LEP Note 558 and CERN internal report, 12 March 1986.

[78] P.E. Faugeras, Performance Of An Electron-Positron Facility Using LEP And SPS
Geneva, LEP Note 303 and CERN internal report, June 1981.

[79] L. Maiani (chairperson), G. Becker, U. Michelini, Aldo Steinberger, Jack Amaldi, Ugo
Hubner, LEP experiments - From ideas to reality.
LEPFest Meeting , CERN, Geneva, Switzerland , Oct 2000 - Presentation at LEP-
Fest2000, Geneva, CERN, Oct 2000.

[80] G. Thubes, Carlo Rubbia and the discovery of the W and the Z.
Phys. World: 16 (2003) no. 1, pp. 23-8

[81] S.Naganiya, Proceedings of the Conference "Quark Matter '91", Gatlinburg, Tennessee,
USA (1991).

[82] R.Ghetti, *et al., Nucl. Phys. A* **674**, 277, (2000).

[83] S.E.Koonin, *Phys. Lett* B **70**, 43 (1977).

[84] Otto Nachtmann, Elementary Particle Physics. Concepts and Phenomena. Springer-Verlag, Berlin, Heidelberg, New York, 1990. ISBN 3-540-51647-6.

[85] A. Nygren, DELPHI 2000-054 PHYS 857 (2000)

[86] S. Ask, V. Hedberg, P. Niezurawski, A. Nygren, P. Tiapkine, N. Zimin
LEP machine background and noise in the DELPHI calorimeters.
DELPHI 99-157 LEDI 12 (1999) (look Appendix B)

[87] Christopher K. Bowdery(ed.) The ALEPH handbook : 1995
Geneva, CERN, 1995 . - 2 v
ISBN: 92-9083-072-7 : v.1
ISBN: 92-9083-073-5 : v.2

[88] R.R. White, Search for the Standard Model Higgs Boson at the ALEPH Detector
9th International Conference on Hadron Spectroscopy,
Protvino, Russia , 25 Aug - 1 Sep 2001 - pp. 829-832

[89] A.Garcia-Bellido, Searches for gauge mediated supersymmetry breaking at ALEPH
with centre-of-mass energies up to 209 GeV
Geneva, CERN, 10 Dec 2002 - internal report: CERN-THESIS-2002-041

[90] J. M. Pascolo, Recherche independante de saveur du boson de Higgs neutre avec le
detecteur ALEPH a LEP2
Clermont-Ferrand 2. Lab. Phys. Corpusc. Cosmol., 21 Dec 2001.

[91] P. A. McNamara, S. L. Wu (dir.). The Search For The Standard Model Higgs Boson
At Aleph
Madison, WI, Wisconsin Univ., 2002 . - 255 p, ISBN: 0-493-63950-0

[92] DELPHI : technical proposal
Geneva, CERN, 1983, internal report: CERN-LEPC-83 and DELPHI-83-66 and LEPC-P-2.

[93] Letter of intent : DELPHI detector (DEtector with Lepton Photon + Hadron Identification)
Geneva, CERN, 1982 - internal report: CERN-LEPC-82-8 and LEPC-I-6 . - 21 p

[94] J. Rubio, The L3 experiment,
CAS - CERN Accelerator School : Accelerator Physics , Salamanca, Spain , Sep 1988,
168-193

[95] L3 Collaboration, L3 Experiment
Published in: Experim. CERN: (1997)322-328

[96] D. Teyssier, J.P. Martin (dir.), Recherche du boson de Higgs standard et non-minimal
a LEP2 dans l'experience L3
Lyon : CNRS Lyon. Inst. Phys. Nucl., Mar 2002.

[97] OPAL Collaboration, Letter of Intent : "OPAL DETECTOR"
Geneva, CERN, 1982 - internal report: CERN-LEPC-82-4, LEPC-I-2, CM-P00043634,
28 p

[98] P. Rapp, The OPAL detector at LEP
College Park, MD : Maryland Univ. Dept. Phys. Astron., Jun 1985.

[99] OPAL collaboration: G.Abbiende et al. Search for the standard model Higgs boson
with the OPAL detector at LEP
Published in: Eur. Phys. J., **C 26** (2003) 479-503

[100] DELPHI collaboration,
Study of the hadronic photon structure function at LEP2
CERN-EP/2003-018 (submited to Eur. Phys. J. C)

[101] M. Drees and R.M.Godbole, J. Phys **G21** (1995)1559

[102] Workshop on Physics at LEP2, CERN 96-01 v2 (1996).

[103] H. Abramowicz, K. Charchula and A. Levy, Phys. Lett. **B269** (1991)458

[104] G.A. Schuler and T.Sjostrand,
Phys. Lett. **B300** (1993) 169;
Nucl. Phys. **B407** (1993) 539.

[105] V.N.Baier et al., Phys. Rep. **78** (1981)293

[106] M. Gluck, E. Reya and A. Vogt, Phys. Rev. **D46** (1992)1973

[107] H. Plothow-Besch, PDFLIB: A Library of all available Parton Density Functions of
the Nucleon, the Pion and the Photon and the corresponding α_s calculations, CERN-
PPE-92-123.

[108] L.E. Gordon and J.K. Storrow, Z. Phys. **C56**(1992) 307.

[109] J.J. Sakurai and D. Schildknecht, Phys. Lett. **B41** (1972)489;
Phys. Lett. **41B** (1972) 489.
I.F. Ginzburg and V.G. Serbo, Phys. Lett. **B109** (1982)1

[110] A. Capella, et al. Phys. Rep. **D46** (1992)1973

[111] V.N. Gribov Sov. Phys. JETP 26 (1968) 414;
V.N. Gribov and A.A. Migdal Sov. J. Nucl. Phys. 8 (1969)583

[112] Bernd Surrow, The structure of the photon and its interactions.
Proc. of the workshop on Photon Interactions and the Photon Structure, Lund, 10-13
September, 1998, p.83

[113] Marco Stratmann, The Parton Content of Virutal Photons.
Proc. of the workshop on Photon Interactions and the Photon Structure, Lund, 10-13
September, 1998, p.183

[114] M. Drees, K. Grassie
Parametrizations of the photon structure and applications to supersymmetric particle production at HERA
DO-TH-84-13.- Dortmund : Dortmund Univ. Inst. Phys., May 1984.

[115] D.W. Duke, J.F. Owens, The photon structure function as calculated using perturbative quantum chromodynamics
FSU-HEP-80-24-01. Tallahassee, FL : Florida State Univ. Dept. Phys., Jan 1980.

[116] R. Bailey, C. Benvenuti, S. Myers, D. Treille, The LEP collider
Compt. Rend. Acad. Sci. Paris, 4: 3 (2002) no. 9, 1107-20

[117] R.W. Assmann, M. Lamont, S. Myers, A Brief History of the LEP Collider
Geneva, CERN, 30 Apr 2002 - internal report: CERN-SL-2002-009-OP
and published in: Nucl. Phys. B, Proc. Suppl. 109 (2002)17-31.

[118] S. Almehed et al.
Beam parameter monitoring and interaction point measurement in DELPHI with the VSAT. DELPHI 94-77 PHYS 453

[119] S. Almehed et al.
A silicon-tungsten electromagnetic calorimeter for LEP
NIM, A305 (1991) p. 320-330, North-Holland

[120] http://delphiwww.cern.ch/∼offline/physics/delphi-detector.html

[121] Andreas Nygren, THOR
Technical Report, Lund University, 1999 LUNFD6/(NFFL-7152)

[122] Per Jonsson, Luminosity measurements and two-photon physics with DELPHI VSAT at LEP. Technical Report, Lund University, 1998, LUNFD6/(NFFL-6151)

[123] Andreas Nygren
VSAT analysis tools.
Technical Report, Lund University, 1999
LUNFD6/(NFFL-7271)

[124] J. Cuevas, J. Marco, A. Ruiz, F. Richard, F. Simonetto
Fast Simulation for DELPHI, Version 2.0
DELPHI 87-26 PROG 71
J. Cuevas, J. Marco, A. Ruiz, F. Richard, F. Simonetto
Fast Simulation for DELPHI Reference Manual, Version 2.0
DELPHI 87-27 PROG 72

[125] I. Tyapkin, Study of the hadronic photon structure function with the DELPHI detector at LEP. PHOTON 2001 Conf. Proc., Ascona, Switzerland.

[126] Christina Zacharatou Jarlskog, Luminosity evaluation and fragmentation studies for the DELPHI experiment at LEP.
Lund University doctoral dissertation: LUNFD6(NFFL-7193)2001. ISBN 91-7874-126-2

[127] Jonas Bjarne, Two-Photon Physics and Online Beam Monitorin Using the DELPHI
      Detector at LEP.
      Lund University doctoral dissertation: LUNFD6(NFFL-7089)1994. ISBN 91-628-1388-9

[128] Andreas Nygren, Hadronic Structure Measurements of the Photon by DELPHI at LEP
      II. Lund University doctoral dissertation: LUNFD6(NFFL-7199)2001.
      ISBN 91-628-4932-8

[129] Ch. Jarlskog, Interaction point estimation and beam parameter variation in DELPHI
      with the VSAT.
      LUNF D6/(NFFL-7110)/1995, Lund University

[130] I. Kronkvist
      Data Base and Slow controls of DELPHI VSAT and Two-Photon Physics using DELPHI
      at LEP.
      Lund University doctoral dissertation: LUNFD6/(NFFL-7128)1996.
      ISBN 91-682-2182-2

[131] G.Von Holtey and M.Lamont
      Protection of LEP Experiments against Particle Background at Highest Beam Energies
      CERN SL-99-022 EA

[132] Sverker Almehed, Andreas Nygren, Nikolai Zimin
      $\gamma\gamma$-Physics Background in VSAT
      DELPHI 2000-173 PHYS 884

[133] A. Hakansson
      Beam dependent correction applied to VSAT relative acceptance
      DELPHI 93-49 PHYS 279

[134] S.J.Alvsvaag et al.
      The system for on-line monitoring of LEP beam background and luminosity at the
      DELPHI interaction point
      DELPHI 93-3 DAS 137

[135] P.Tyapkin, VSAT detector simulation by using GEANT and FASTSIM
      Lund University internal report LUNFD6/(NFFL-7163)1999

Appendix A

1998 running review workshop, the VSAT project

1998 running review workshop, the VSAT project

**Goran Jarlskog, Ulf Mjoernmark, Andreas Nygren, Pavel Tyapkin,
Nikolai Zimin**

Experimental Elementary Particle Physics department of Physics Institute, Lund University

Abstract

This report gives a brief account of the performance of the VSAT hardware and software during 1998. Overall, the detector was very reliable and there are no serious problems of operation.

1 Hardware

1.1 Improvements made in the shutdown 97/98:

A smaller elliptical beam pipe was installed at ± 7.5 m from the collision point (the VSAT group had requested a cylindrical subsection of the beam pipe with a 10 mm reduction in horizontal radius). Compared to the old beam pipe the new one has a 5 mm smaller radius in the horizontal plane while the vertical radius is the same as before [1]. Resulting increase of the geometrical acceptance is shown in the Fig. 1.
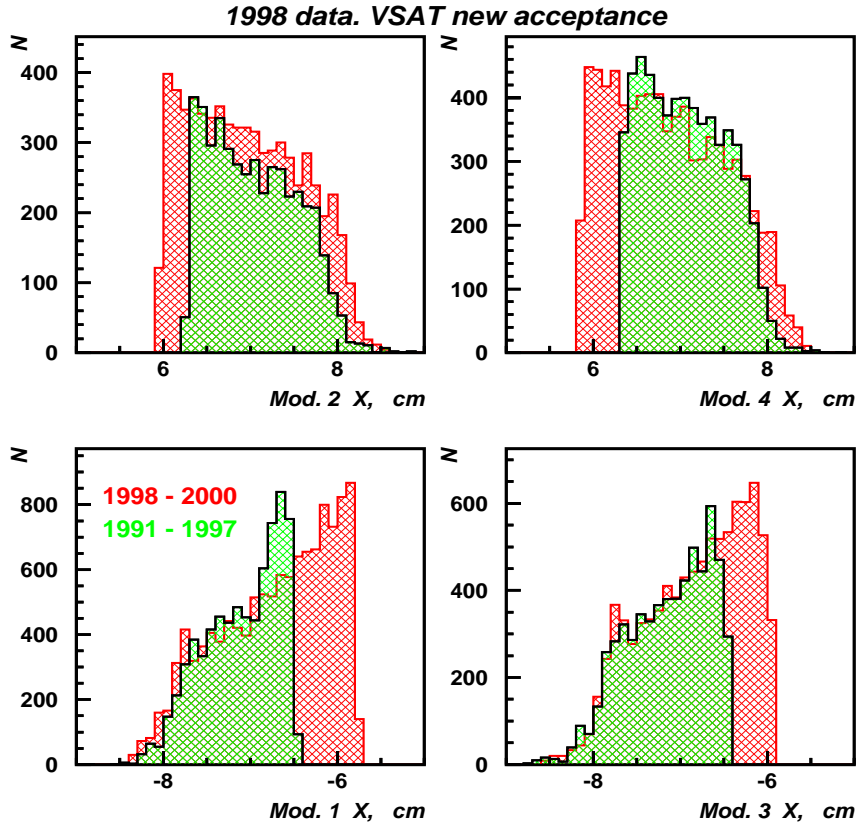
Figure 1: VSAT geometrical acceptance in X plane before (97) and after move (98)

Preliminary results from the current analysis show that the VSAT acceptance is significantly improved after last year upgrade. Unfortunately the new beam pipe pieces were produced with a bit larger x-dimension than specified. The specification was an increase of the acceptance of 5 mm in each module, and as can be seen above this clearly not the case. For this reason the statistics available for double tagged events is increased only by a factor 1.8 instead of 2.

The final number of events depends also from the procedure of background rejection which is now under revision. For single tagged events the increase in statistics is a little less than 1.5. What is important is that the kinematical range in Q^2 (up to 0.6 GeV^2) and invariant mass W (up to 100 GeV) of the gamma-gamma system W (up to 100 GeV) are obtained as predicted and give us an opportunity to get results in this range for the first time.

At high energy some amplifiers of the FADs (full area silicon planes), located at the depth of 6 to 10 radiation length, were saturating at the peak of the shower. This was caused by a limitation in the amplifiers to reproduce the true rise time of the signals. Since the readout is a sample and hold the exact timing of the hold is crucial – a shift of the hold signal to 250 ns later removed the saturation (see Fig. 2 and Fig. 3). This was implementation in June 1998. For data taken before that date the signals from the strip planes, which are also located around shower maximum, can be used for a correction of the energy in the saturated FADs.
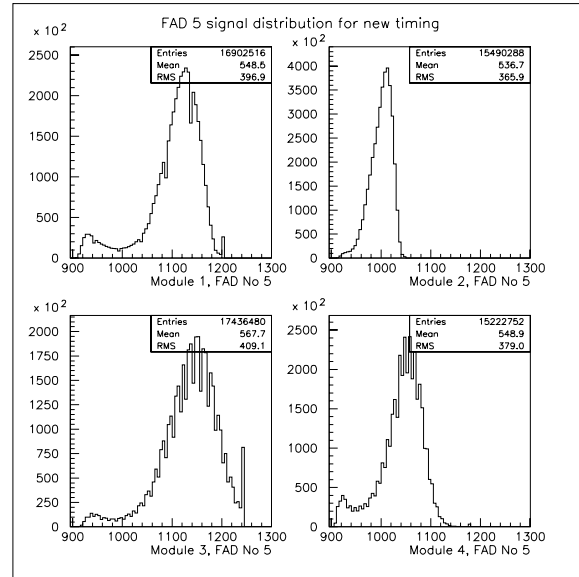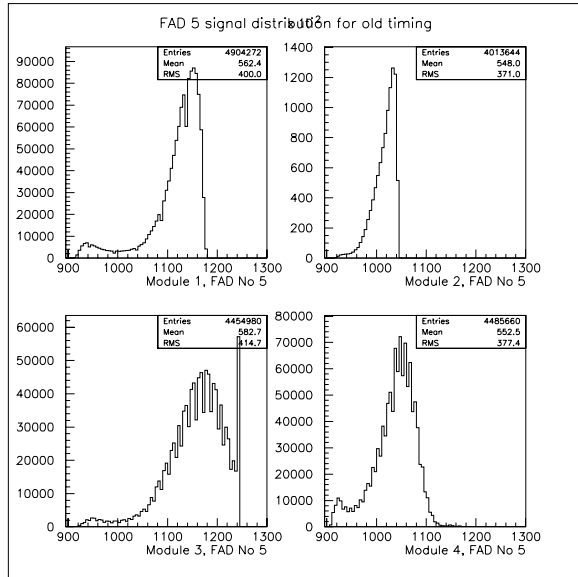

Figure 2: FAD plane Number 5 amplitude distribution for all modules (1,3 - outer modules, 2,4 - inner modules) with old timing - 5.55 μs

Figure 3: FAD plane Number 5 amplitude distribution for all modules (1,3 - outer modules, 2,4 - inner modules) with new timing - 5.80 μs

1.2 Major problems/damages:

In May a FASTBUS card (LURFB) designed to handle the minibunch scheme of LEP burned. For the repair we had to send for the engineers from Sweden who made the card and lost about 5 days of running, mainly at the Z. A bad connector was also found which prevented downloading the programs to a DSP handling minibunches (this was repaired in October 1998). In May also a NIM crate handling the trigger information broke down, about 1 day was lost. None of the problems above affected the central data acquisition of DELPHI.

1.3 Backgrounds:

The VSAT is built to measure the off-momentum background in LEP and can cope with various conditions. VSAT have a background rate of about 500 electrons per second in the outer modules and about 100 for the inner. These are down-scaled by a factor 400 and 130 respectively, so that they in total consist about 10% of our readout triggers. The number of accidental Bhabha triggers from the off momentum background increased with the luminosity of LEP (False Bhabha to real Bhabha rate is given on Fig. 4), but did not affect the data-taking adversely.
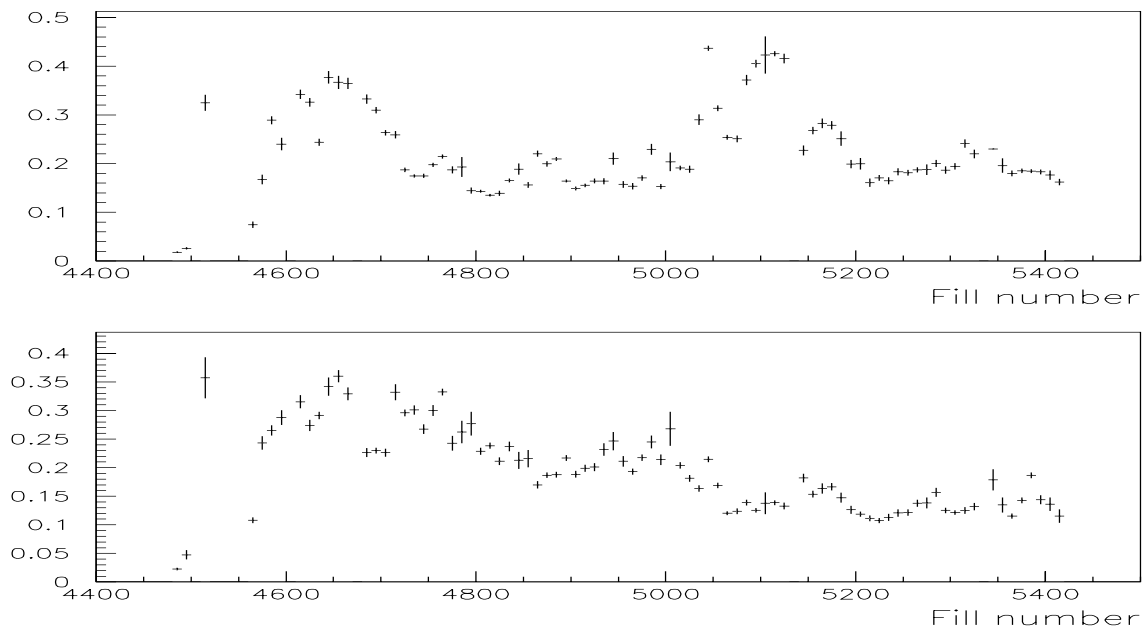

Figure 4: False Bhabha to real Bhabha rate

1.4 Spares:

The VSAT electronics is unique and does not have spares. If faults occur they have to be investigated by our engineer on call (from Sweden). Minor problems can be handled by the physicist in charge of the VSAT at CERN.

1.5 Future:

The LURFB card used now to handle minibunches will get a spare that can be used for the high energy running with only one bunch. A second LURFB for minibunches is built but not yet tested (we are not sure when this will be done since the engineer who designed it has left). We do not plan any changes but cross our fingers that things will keep running as nicely as in 1998 (after May).

2 Software

2.1 Improvements made 97/98:

The output from DELANA was modified to include the information from the x- and y-strips of the silicon planes in order to improve determination of the shower position at DST level. All preamplifiers were carefully calibrated (again). The information in the XSDST was extended to be used for two-photon physics analysis.

As the VSAT is shadowed by a flange in the beam pipe, the movement resulted in a pure increase of the active detector area. This new region of the detector was never used and had to be calibrated. The VSAT modules is of limited size and at the edges the energy shower leaks out of the detector. Before the shadow of the flange prevent particles to reach out on the far side in x, and only leakage calibration on the inner edge were done. With the move of the modules it is necessary to correct for leakage on the other side as well(fig 5). Leakage correction were also applied in the Y direction(fig 6), even if very few events reach the edges in y.
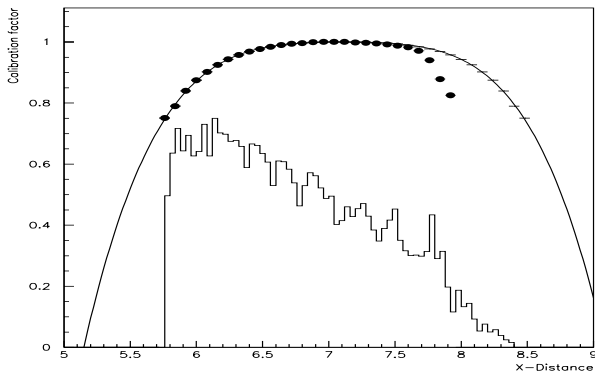
Figure 5: VSAT energy leakage calibration in X (dots=data) and the X-distribution for all events.
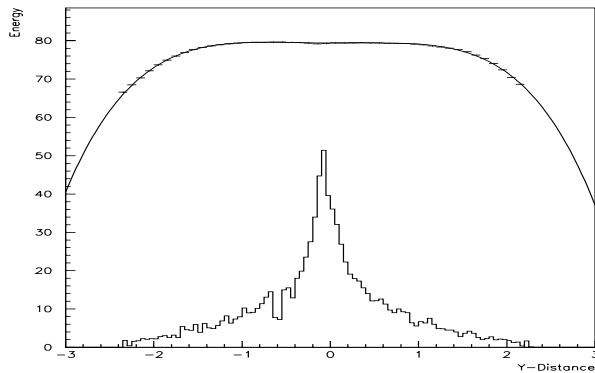
Figure 6: VSAT energy leakage calibration in Y (bars=data) and the Y-distribution for all events.

A four degree polynomial was used as a leakage correction function. The drop of the data on the far side of X is energy losses due to interaction with the flange and have nothing to due with detector leakage.

2.2 Major problems/bugs:

There are no major problems. The disk storage space is critical and must be watched carefully. At high energy there is some longitudinal leakage from the modules that we have not made a correction for so far, this will be investigated. During the data taking for 1998 a resident bug from beginning of LEP was found in DELANA. In the event that all four modules in VSAT get hit at the same time, some of our counters get out of phase and causes some corruption. The likelihood for this was vanishing small up to 1998 and no effect could be seen on the data. With the increase of background an luminosity in LEP and the movement of the detector closer to the beam, this effect became visible in our data sample. A fix has already been implemented and the data should be corrected next time DELANA runs on it in the end of 1999.

4

2.3 Monitoring:

We are quite happy with the (automatic) monitoring system introduced by Andreas Nygren [3]. It is easy to spot problems in the offline data stream. The central online monitor had a mysterious problem throughout the year, with strange spikes appearing in the data now and then. These effects could not be reproduced when the central monitor was run stand alone in playback on the data. A fix to work around the problem was implemented in the central monitor, which now works fine.

3 Performance

Higher background and luminosity in from the LEP beam in addition to the increased crossection due to the movement of the modules, heavily increased the radiation hitting VSAT during 1998 in comparison to previous years. The main part of the radiation comes from the off-momentum background, which is concentrated in the outer modules. We have therefor bigger degradation of the detector silicon planes in these modules, clearly visible in fig 8.

The resolution jump in module two around fill 4640, is due to the fact that we temporarily lost the signal from one of our fad-planes. We lost about 0.6-0.9 % of resolution in the outer modules and about 0.2-0.3% in the inner. With just two more year of running this is acceptable without any intervention to improve the situation. The average resolution for the whole year is shown in fig 7.
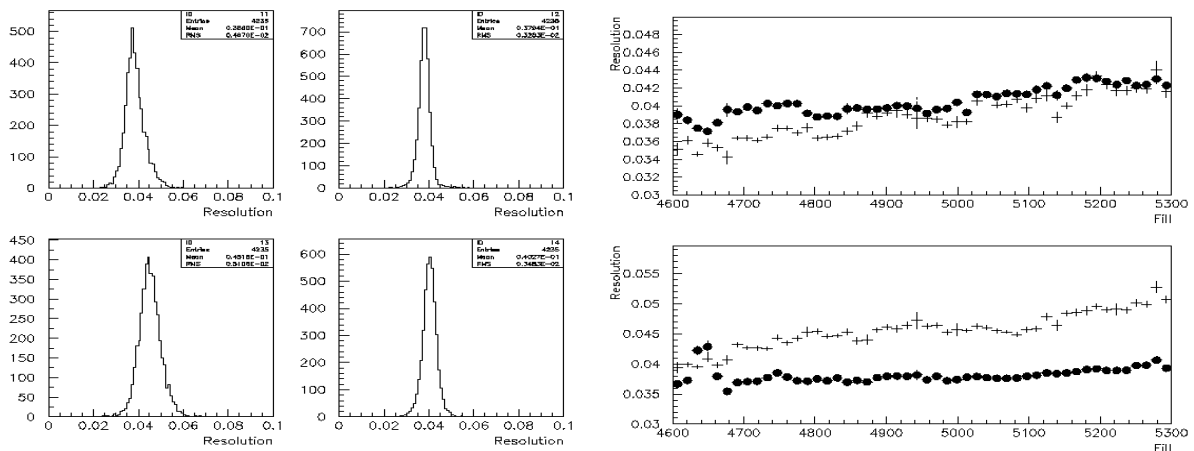
Figure 7: Energy Resolution R=dE/E of each module (Note: 1, 3 - outer modules, 2, 4 - inner modules)

Figure 8: Resolution development during 1998 running, crosses=outer modules and dots=inner

Every year a luminosity analysis is made to check the stability of the STIC detector for shorter periods of time. VSAT can not measure the absolute luminosity, and therefor have to be normalized to STIC data for normally 3 to 5 periods of running. After normalisations and corrections STIC and VSAT luminosity can be compared as shown in Fig 9.

VSAT crossection also have to be calibrated in correspondence to certain beam-parameters that can be measured with the X- and Y-strip planes. For example Fig. 10 shows the center Y-coordinates of the beam as measured in each detector (about usual procedure look at [4]).There has clearly been a gradual shift in Y-position during 1998.
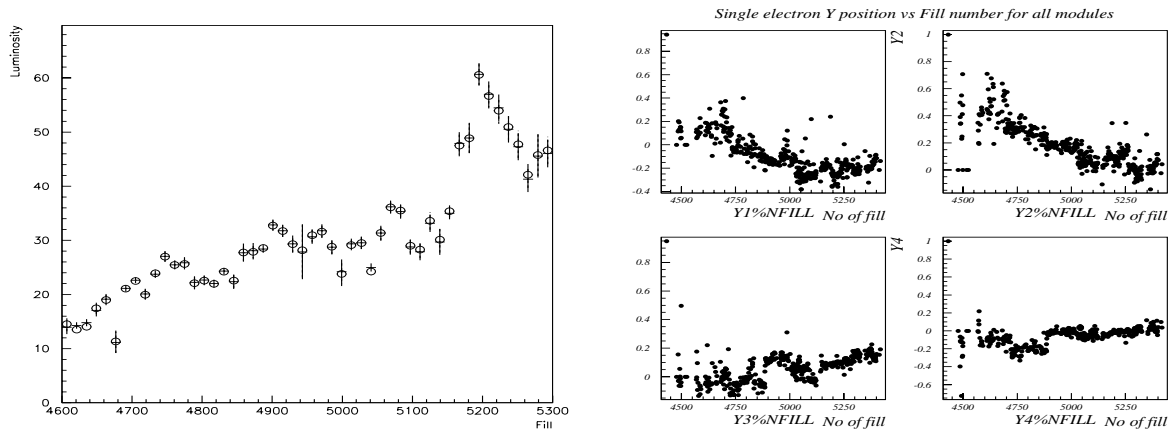

Figure 9: VSAT (circles) and STIC (crosses) luminosities in nb^{-1}

Single electron Y position vs Fill number for all modules

Figure 10: Y position of the beam (cm) in each module

The energy signal from the FAD-planes is calibrated every fill. Changes in these calibration constants is normally an indication of that something have happened with beam energy or VSAT electronics. As the FAD timing was changed, the energy calibration constant was changed also. This can be clearly seen on Fig. 11 - big step from 0.97 to 0.85. Some other correlated steps in the graphs is also clearly visible, probably as a result of a power cut.

After calibration we have a very nice and clean bhabha peak at a very stable energy. The energy variations on the bhabha peak for all the year is shown in fig 12. We have a energy variation of less than one permill, which is very satisfactionary.
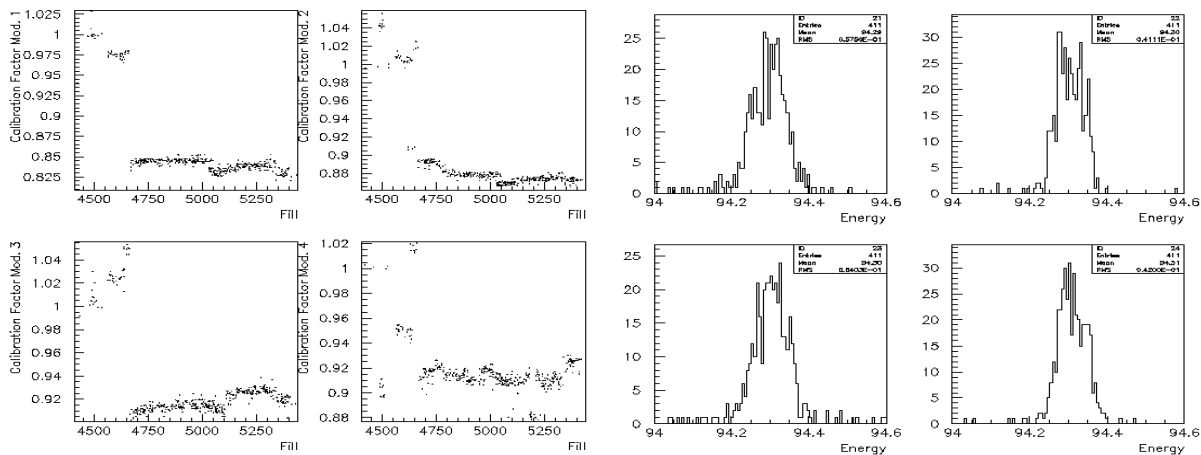

Figure 11: Energy calibration constants during 1998

Figure 12: Bhabha Energy (in GeV) deposited in all modules during 1998

6

4 Manpower

The Lund group has one physicist stationed at CERN in charge of the VSAT (in 1997/98 it was Andreas Nygren, in 1999/00 it will be Pavel Tyapkin). Weekly checks on the raw data quality is done in Lund by Ulf Mjornmark. For each year of running the beam parameters of LEP are determined and the acceptance of the VSAT is recalculated using those inputs. If the range of parameters change too much new simulations [5, 6] are done in order to have the correct coverage in parameter space (by Sverker Almehed). The main VSAT analysis effort is on tagged electrons/positrons for two-photon physics. Nikolai Zimine is coordinating this effort [1]. It is unsatisfactory to have only one person in charge at CERN for the entire remaining period.

5 Trigger rate

The VSAT T1 trigger rate was low during LEP I, which in turn produced a neglectable amount of T2 triggers. In the beginning of LEP II the T1 rate increased mainly due to our delayed Bhabha trigger. This was removed during 1996 and since then we have had a T1 rate of about 10-20 Hz. Due to this removal the false Bhabha background has to be estimated off-line from the single electron rate (about 10% of the VSAT triggers are read out from the single electron off momentum background). This estimated rate of false Bhabhas is normalized (see Fig. 13) to the STIC [7] and VSAT luminosity difference. This works pretty satisfactory as can be seen Fig 14, where the STIC and VSAT luminosity difference before and after false Bhabha subtraction is plotted.
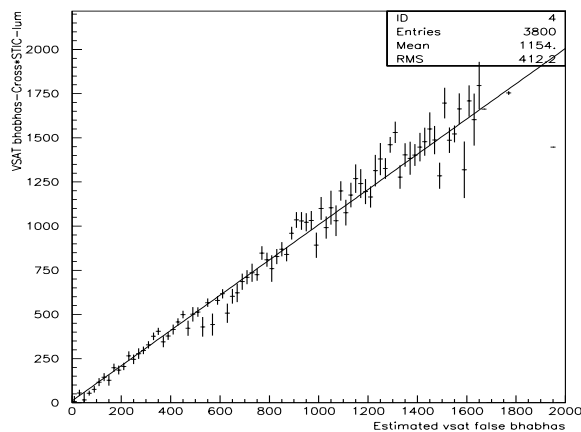

Figure 13: The difference between VSAT and STIC luminosity versus VSAT estimated number of false Bhabhas
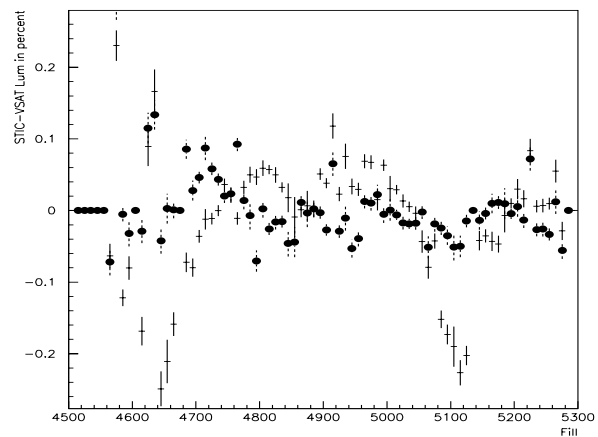
Figure 14: The difference between STIC and VSAT luminosity before (crosses) and after (dots) false Bhabha subtraction

The movement of the detector closer to the beam pipe and the increase of luminosity, background and energy of the beam pushed up both T1 and T2-trigger rate rapidly during 1998. Many long discussions were ignited during several pit-meetings about our trigger system. Two solutions to deal with the problem were pursued by the VSAT group.

VSAT events are recorded in an internal buffer which is read out each DELPHI Event and causes a DELPHI trigger only if it becomes full. The internal event buffer length was increased from 12 to 20 events at the start of fill 5162, which pulled down the T2 rate with a factor 4 in the critical period at beginning of the fills (see Fig. 15 and 16).
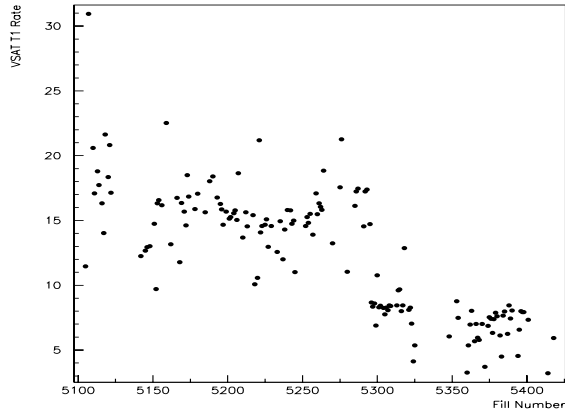

Figure 15: The VSAT T1 trigger rate in Hz versus fill. T1 down-scaling with a factor 2 at fill 5296 can clearly be seen.
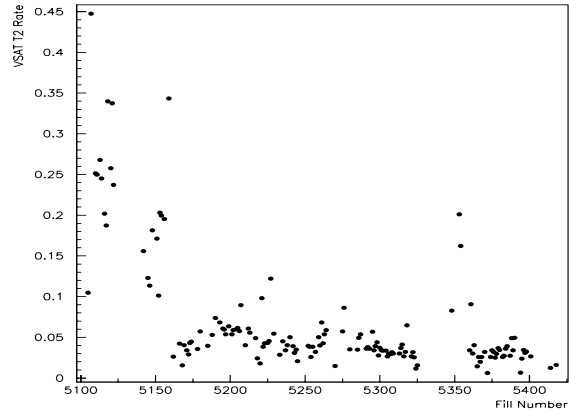
Figure 16: The VSAT T2 trigger rate in Hz versus fill. Buffer length increase at fill 5162 is clearly visible, but no effect from the T1 downscaling.

To improve the situation further the VSAT T1 trigger rate was down scaled by a factor two at fill 5296. This worked fine for our T1 trigger, but the T2 rate continued to be the same(clearly visible around fill 5350 were the buffer length by mistake were set to 12 again). This is due to an error in the logic of the hardware, which in turn also caused some troubles(correctable, but undesirable) in the running of DELANA as well. The people who built the hardware system have left the VSAT group and we will therefore not correct it. Instead we will run with no down scaling and increase our buffer length to 25.

References

[1] S.Almehed, G.Jarlskog, F. Kapusta, U.Mjornmark, A. Nygren I. Tyapkin, N. Zimin,
Forthcoming results in two-photon collisions at very low Q^2 from LEP2
DELPHI 98-175 PHYS 814, 7 December 1998

[2] Ivan Kronkvist,
Data Base and Slow Controls of DELPHI VSAT and Two-Photon Physics using
DELPHI at LEP
ISBN 91-628-2182-2 LUNFD6/(NFFL-7128) 1996

[3] Andreas Nygren,
THOR
LUNFD6/(NFFL-7151), Lund, 1997

[4] Jonas Bjarne,
Two-Photon Physics and On-line Beam Monitoring Using The DELPHI Detector at
LEP
LUNFD6/(NFFL-7089), Lund, 1994

[5] A. Håkansson,
Beam dependent correction applied to the VSAT relative acceptance
DELPHI 93-49 PHYS 279

[6] A. Håkansson,
Luminosity Measurement at LEP using the Very Small Angle Tagger of DELPHI
ISBN 91-628-1091-X LUNFD6/(NFFL-7077), 1993

[7] E. Falk, V. Hedberg, P.Ferrari, C. Matteuzzi,
Photon Analysis with STIC
DELPHI 98-147 PHYS 791, 3 August 1998

Appendix B

LEP machine background and noise in the DELPHI calorimeters

LEP machine background and noise in the DELPHI calorimeters.

S. Ask [1], V. Hedberg [2], P. Nieżurawski [3], A. Nygren [2], P. Tiapkine [2,4], N. Zimin [2,4]

[1] Summer student, Luleå University of Technology
[2] Dept. of Physics, University of Lund, Sweden
[3] Dept. of Physics, Warsaw University, Poland
[4] JINR, Dubna, Russia

Abstract

The LEP machine background and noise in the DELPHI calorimeters have been studied in four independent analyses. The main purpose of this work is to estimate the probability of a shower from these sources in coincidence with a genuine physics event and to see how best to reject this type of background. Both the 1998 and the 1999 high energy data have been used in this study.

1 Introduction

LEP machine background and noise in the electromagnetic calorimeters can affect many DELPHI analyses. Particularly sensitive are the analyses of two photon interactions [1] and events with a single photon in the final state [2] since these analyses select or trigger on energy in the calorimeters. However, analyses which veto on energy in the calorimeters e.g. STIC also need to take this background into account.

In this note several different studies of calorimeter background have been compiled. At low angles, i.e. in VSAT and STIC, the most troublesome background comes from off-energy electrons caused by bremsstrahlung from beam particles on rest-gas molecules. This background has been simulated in DELPHI [3]. The simulation has given a better understanding of the production and origin of the background but cannot be used for quantitative estimates, since it needs as input the vacuum pressure in LEP, which is not known in detail.

The only way of estimating the off-energy background is to use real data. Any sample of events which is not expected to give electrons in VSAT can be used to estimate the probability of an off-energy electron in VSAT. A few basic questions need to be answered: What is the rate of the background (normalized to luminosity) and how does it vary with time ? What is the probability that an off-energy electron is recorded together with a genuine physics event ? How can the background best be rejected ?

The off-energy background in VSAT has been estimated with three different data samples: VSAT Bhabha events, STIC Bhabha events and muon events. All the analyses were done with 1998 high energy data.

Three different event samples were also used for the study of off-energy electrons in STIC: the STIC single arm events, the STIC Bhabha events and random triggered events. Data from both 1998 and 1999 have been studied.

In the other DELPHI calorimeters such as FEMC, HPC and HAC, there is no off-energy electron background but noise can cause spurious showers. This problem was studied with the 1999 random triggered events.

2 Background in VSAT

At LEP2, VSAT is used mainly to measure the energy and position of the scattered electrons in $\gamma\gamma$ collisions. The main background in this type of analysis comes from the enormous off-energy electron background. The probability of having an off-energy electron faking the scattered electron from a $\gamma\gamma$ event can be calculated with any sample of events which does not give electrons in VSAT. The largest sample available is the VSAT Bhabha sample and it can be used to calculate the probability with a minute statistical error. To estimate the systematic error, other event samples such as muon events and STIC Bhabha events have also been studied.

In the following discussion, the standard DELPHI coordinate system is used with the x axis pointing towards the centre of LEP, the y axis pointing upwards and the z axis pointing in the direction of the electron beam. θ is the polar angle in relation to the z axis and ϕ is the azimuthal angle around the z axis. In this coordinate system, the numbering

of the four VSAT modules is as follows:

Module 1	Module 2	Module 3	Module 4
$x < -5$cm, $z < -775$cm	$x > 5$cm, $z < -775$cm	$x < -5$cm, $z > 775$cm	$x > 5$cm, $z > 775$cm

which means that module 1 and 3 are on the outer circumference of the LEP ring and module 1 and 2 are on the DELPHI A-side while 3 and 4 are on the C-side.

2.1 VSAT scalers and Bhabha events

The most direct way to investigate the probability of having an off-energy electron in a VSAT module is to count them and compare the number to the number of bunch crossings during the same period. The VSAT detector is hit by an enormous quantity of off-energy background electrons, so, in order to save disk-space for more interesting processes, only a small fraction of these events are read out.
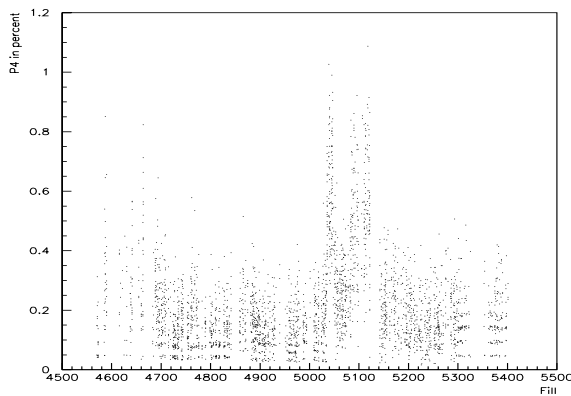

Figure 1: The probability of an off-momentum electron in module 4 for each cassette of 1998 data.
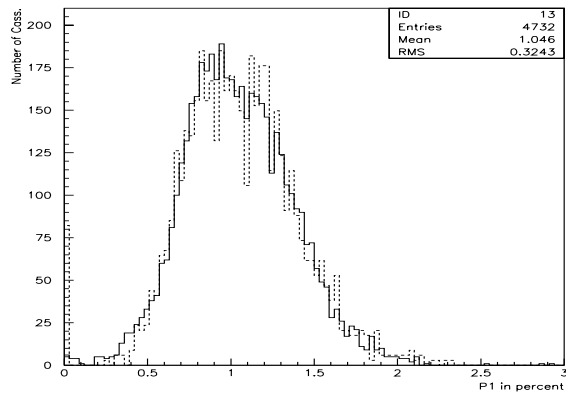
Figure 2: The distribution of the number of cassettes as against the probability of a single electron in module 3, calculated from the scalers (full line) and from the Bhabha events (dotted line).

The VSAT is also equipped with scalers that count the number of hits in each module and the number of Bhabha triggers. The scaler values can be used offline to estimate the probability of background in an individual modules. Since the scalers count all events, the Bhabha scaler value was subtracted to get the true number of single electrons.

The beam and vacuum conditions vary during the year, which alters the VSAT background rate. This is shown in Figure 1, where the probability of a single electron in module 4 have been calculated for each cassette and plotted against the fill number. The increase between fill 5050 and 5100 is due to a LEP vacuum leak.

The full line in Figure 2 shows the probability distribution of single electrons in module 3, as calculated from the scalers on each cassette of 1998 data and Table 1 gives the probability of an off-energy electron in VSAT averaged over all the 1998 data.

Off-energy electrons coinciding with Bhabha events can be used to measure both the probability and the energy and position distributions of this background. The dotted line in Figure 2 shows the probability of each cassette having an electron in module 3 at the

2

$\mathcal{P}_1[\%]$	$\mathcal{P}_2[\%]$	$\mathcal{P}_3[\%]$	$\mathcal{P}_4[\%]$
1.105±0.00002	0.167±0.00001	1.046±0.00002	0.234± 0.00001

Table 1: The probability of an off-energy electron in the four different VSAT modules. The VSAT scalers were used in this study and the minimum energy required in the trigger was ∼15 GeV.
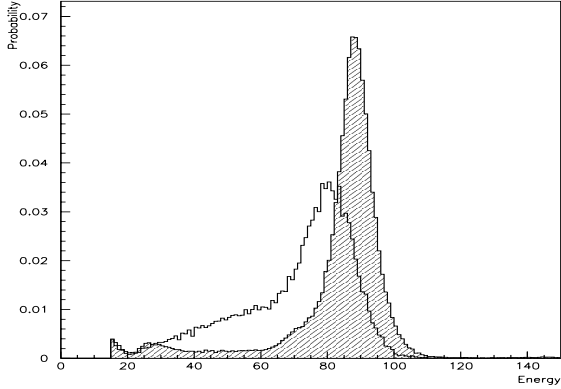

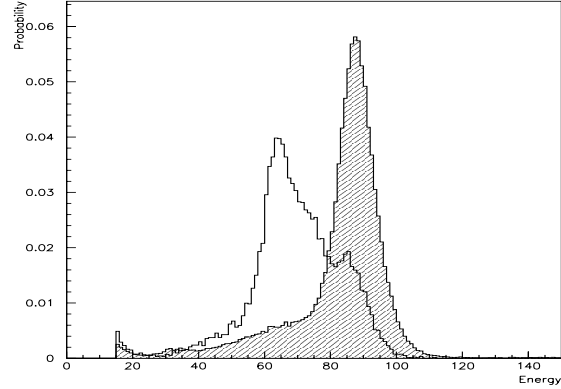Figure 3: Off-momentum background energy distribution for module 1 (shaded) and module 4.

Figure 4: Off-momentum background energy distribution for module 3 (shaded) and module 2.

same time as a pair of Bhabha electrons in module 1 and 4. In this study an energy cut of 15 GeV on the electron in module 3 was made, since this corresponds to the cut in the trigger used by the scalers. The cassettes were required to contain at least 3000 Bhabha events, which reduced the number of cassettes from 4700 to 1600. The distribution in Figure 1 from Bhabha events has therefore been rescaled so that it can be compared to the distribution from the scalers. The two methods seems to be in perfect agreement, with the probability of an off-energy electron in Module 3 varying between 0.2-2.3% .

E_{min} [GeV]	$\mathcal{P}_1[\%]$	$\mathcal{P}_2[\%]$	$\mathcal{P}_3[\%]$	$\mathcal{P}_4[\%]$
15	1.017±0.002	0.1601±0.0008	1.053±0.002	0.2076±0.0009
20	1.005±0.002	0.1580±0.0008	1.044±0.002	0.2049±0.0009
50	0.949±0.002	0.1482±0.0008	0.999±0.002	0.1769±0.0008
70	0.901±0.002	0.0740±0.0006	0.896±0.002	0.1309±0.0007
80	0.803±0.002	0.0354±0.0004	0.784±0.002	0.0744±0.0005

Table 2: The probability of an off-energy electron with energy larger than E_{min} in the four different VSAT modules. The measurement was done with VSAT Bhabha events.

From the energy distributions of the off-energy electrons (Figure 3 and Figure 4) the probability of an off-energy electron in VSAT as a function of an energy-cut can be calculated. The energy is not properly calibrated in the XSDST data and the data used here are taken from the VSAT offline processing with all the corrections applied. The background in the outer modules (1 and 3) has a higher energy as it is produced in a region further away from DELPHI [3]. The probabilities of an off-energy electron in the
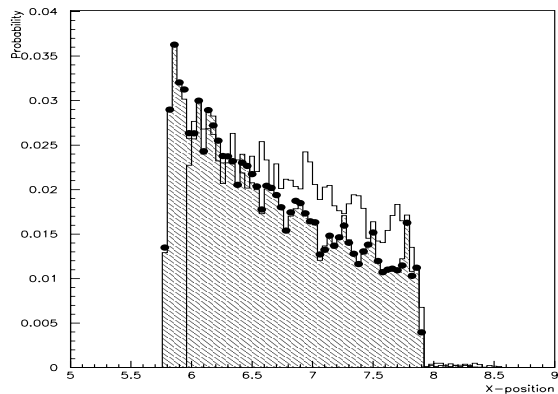
3

Figure 5: The X distribution of VSAT single electrons in module 1 (shaded) and 2. Comparison is made with a full readout single electron sample in module 1 (dots).
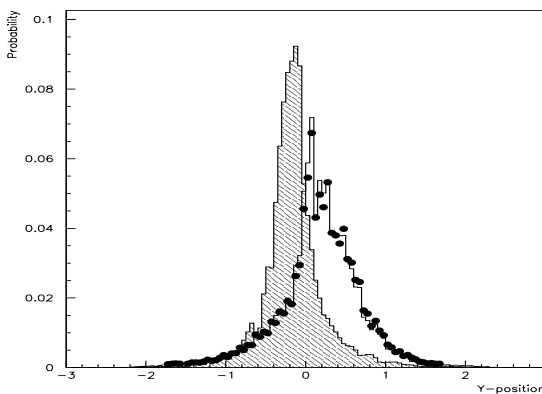
Figure 6: The Y distribution of VSAT single electrons in module 1 (shaded) and 2. Comparison is made with a full readout single electron sample in module 2 (dots).

four VSAT modules are given in Table 2 and are calculated from a sample consisting of $47.5 \cdot 10^6$ Bhabha events, of which 578782 events had an additional off-energy electron in VSAT with energies higher than 15 GeV.

The best way of removing the background is by a cut on the position of the showers, since the background is concentrated in the horizontal plane. The x and y distributions of the single electrons are shown for both inner and outer modules in Figure 5 and 6. In the outer modules the y-distribution has a sharp peak since it is produced closer to DELPHI. A comparison was made of the position distributions with the single electrons NOT in coincidence with a Bhabha event. This sample contains more events although it has been downscaled. These distributions are shown as dots in Figure 5 and 6 and are in a good agreement with those obtained from the Bhabha events.

E_{min} [GeV]	N_{VSAT}	$\mathcal{P}$ [%]	$\mathcal{P}_1$[%]	$\mathcal{P}_3$[%]	$\mathcal{P}_4$[%]
15	13	4 ± 1	1.6 ± 0.7	1.4 ± 0.6	0.5 ± 0.4
50	12	3 ± 1	1.6 ± 0.7	1.4 ± 0.6	0.3 ± 0.3
60	10	2.7 ± 0.9	1.4 ± 0.6	1.1 ± 0.5	0.3 ± 0.3
70	8	2.2 ± 0.8	1.4 ± 0.6	0.8 ± 0.5	-
80	8	2.2 ± 0.8	1.4 ± 0.6	0.8 ± 0.5	-

Table 3: The probability of an off-energy electron with energy higher than E_{min} in the four different VSAT modules. The measurement was done with dimuon events. N_{VSAT} is the number of events with energy in the VSAT greater than corresponding E_{min}. $\mathcal{P}_i$ means the probability for module $i = 1, 2, 3, 4$. There was no events with a signal in module 2.

2.2 Dimuon events

A sample of $e^+e^- \to Z^0(n\gamma), Z^0 \to \mu^+\mu^-$ events was also selected to study the probability of having off-energy electrons in VSAT. In this study the 1998 data[2] was used and the
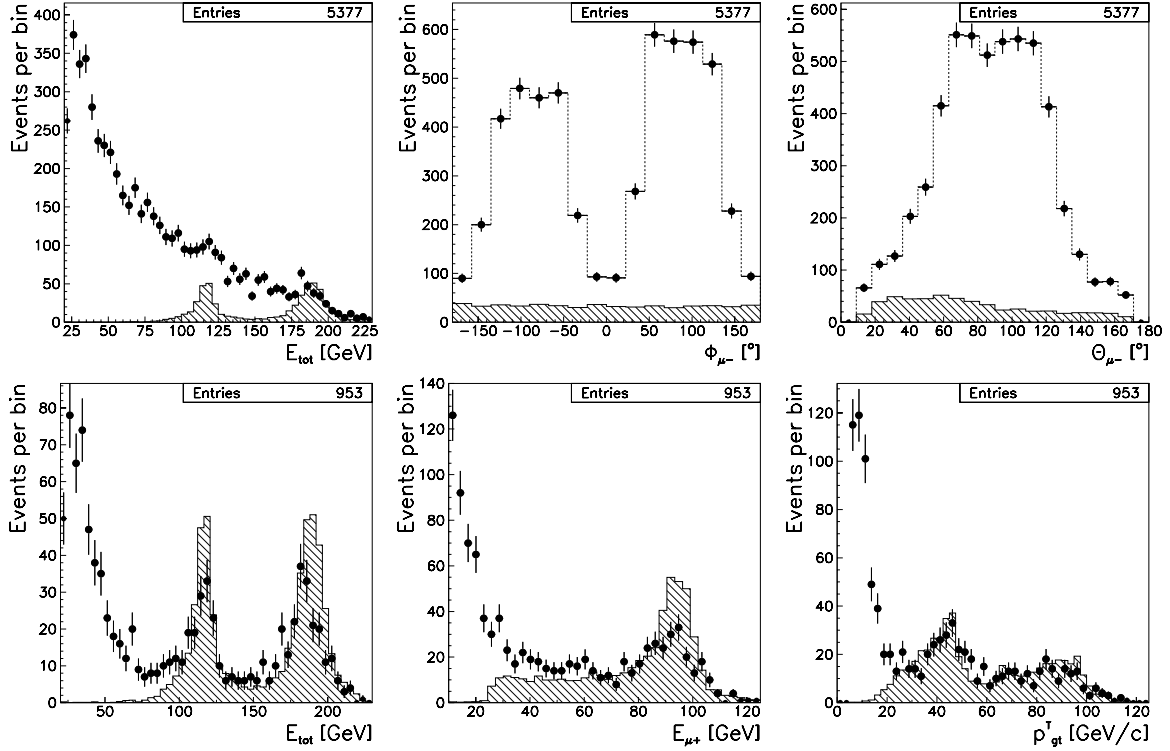
Figure 7: Distributions of E_{tot}, θ_{μ^-} and ϕ_{μ^-} . Points represent data and the hatched histograms represent MC. The top row of plots shows events which fulfil conditions 1, 2 and 3 and the bottom row those fulfilling conditions 4 as well.

selection criteria was optimised with the help of a KORALZ4.2 [4] Monte Carlo sample[3].

To suppress the background, which was mainly due to cosmic muons, it was required that:

1. Two muons were found, one positive and one negative, with no other particles in the event. The muons should be identified as "very loose" or better.
2. The energy of each muon should be $10 < E_{\mu^\pm} < 125$ GeV.
3. The azimuthal angles were required to fulfil $||\phi_{\mu^+} - \phi_{\mu^-}| - 180^0| < 3^0$.
4. Both muons should come from the primary vertex (Q(LPV+4)=0).
5. The transverse momentum of the muons should have $p_{gt}^T > 35$ GeV/c , where $p_{gt}^T \equiv \max(p_{\mu^+}^T, p_{\mu^-}^T)$.

The upper three plots in Figure 7 show the distributions of E_{tot}, θ_{μ^-} and ϕ_{μ^-} after conditions 1, 2 and 3 were satisfied. At this stage 4741 events remained, with 495 expected. The angular distributions had broad peaks at $\theta \approx 90^0$ and around $\phi = \pm 90^0$ which were not predicted by Monte Carlo. The reason is of course the large contamination of cosmic muons. Many of the cosmic events can be rejected by the requirement on the primary vertex (condition 4). The bottom three plots in Figure 7 depict the distributions of
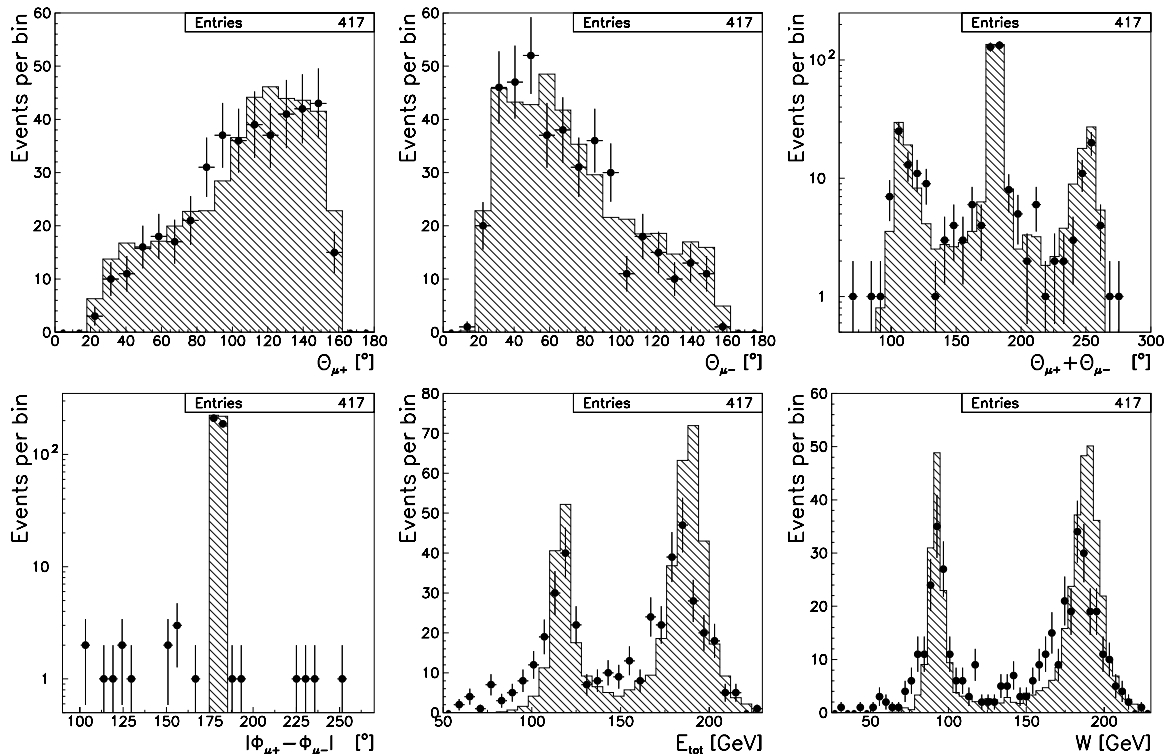
5

Figure 8: Distributions of polar angle (θ_{μ^+} and θ_{μ^-}), the sum of polar angles ($\theta_{\mu^+} + \theta_{\mu^-}$), the difference of azimuthal angles ($|\phi_{\mu^+} - \phi_{\mu^-}|$), and the total energy of the muons (E_{tot}) and their invariant mass (W).

E_{tot}, E_{μ^+} and p_{gt}^T after the vertex cut. 800 events remained in the data with an unchanged number of expected events.

The last cut on p_{gt}^T removes softer muons coming from $e^+e^- \to \gamma^*(n\gamma), \gamma^* \to \mu^+\mu^-$, $\gamma\gamma$ collisions or $Z^0 \to \tau^+\tau^-$ events. After this cut 369 ± 19 events remained in the data, with $408 \pm 7 \pm 3$ expected from the Monte Carlo study (the second error is due to the uncertainty in the cross section). Good agreement between data and predictions was obtained, as can be seen in Figure 8, which shows different angular distributions such as the polar angle of each muon ($\theta_{\mu^\pm}$), the sum of polar angles ($\theta_{\mu^+} + \theta_{\mu^-}$) and the difference in azimuthal angles ($|\phi_{\mu^+} - \phi_{\mu^-}|$). The total energy ($E_{tot} = E_{\mu^+} + E_{\mu^-}$) and invariant mass of the muons ($W = \sqrt{E_{tot}^2 - (\vec{p}_{\mu^+} + \vec{p}_{\mu^-})^2}$) are also presented in Figure 8. The overall impression from the data-Monte Carlo comparison is that the efficiency is somewhat too high in the simulation and that the energies are slightly high.

Out of the 417 selected events, only 18 had an electron in the VSAT. In all of these events, only one module scored a hit. The energy measured by VSAT was corrected using the offline VSAT programs. The total probability and probabilities for each module derived from this sample are shown in Table 3.

2.3 Cosmic muon events

The cosmic muon events, rejected in the previous analysis, can also be used to look for off-energy electrons in VSAT. The following cuts were made to select the events:
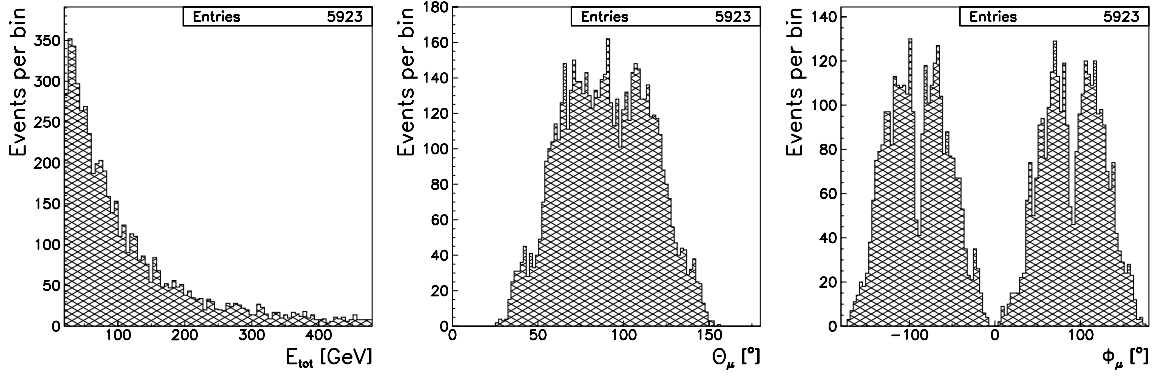
6

Figure 9: Distributions of E_{tot}, θ_μ and ϕ_μ for events fulfilling conditions 1–4.

E_{min} [GeV]	N_{VSAT}	$\mathcal{P}$ [%]	$\mathcal{P}_1$[%]	$\mathcal{P}_2$[%]	$\mathcal{P}_3$[%]	$\mathcal{P}_4$[%]
15	113	2.1 ± 0.2	0.9 ± 0.1	0.15 ± 0.05	0.9 ± 0.1	0.11 ± 0.05
50	94	1.7 ± 0.2	0.7 ± 0.1	0.09 ± 0.04	0.8 ± 0.1	0.11 ± 0.05
60	84	1.6 ± 0.2	0.7 ± 0.1	0.04 ± 0.03	0.8 ± 0.1	0.09 ± 0.04
70	75	1.4 ± 0.2	0.6 ± 0.1	0.04 ± 0.03	0.7 ± 0.1	0.08 ± 0.04
80	31	0.6 ± 0.1	0.19 ± 0.06	-	0.35 ± 0.08	0.04 ± 0.03

Table 4: The probability of an off-energy electron with energy greater than E_{min} in the four different VSAT modules. The measurement was done with cosmic muon events.

1. Two muons had to be found, with no other particles in the event. The muons should be identified as "very loose" or better.
2. The energy of each muon had to fulfil $E_\mu > 10$ GeV.
3. Neither of the two muons should come from the primary vertex (Q(LPV+4)$\neq$0).
4. It was required that $|\theta_n + \theta_m - 180^0| < 1^0$ and $||\phi_n - \phi_m| - 180^0| < 1^0$ where n and m can be a positive μ^+ or a negative μ^- .

After this selection, 5396 events were found, 337 $\mu^+\mu^+$ pairs, 336 $\mu^-\mu^-$ and 4723 $\mu^+\mu^-$ events. Distributions of the total energy of the muon pair (E_{tot}) and of the azimuthal angle (ϕ_μ) and polar angle (ϕ_μ) of the individual muons are shown in Figure 9.

Of the 5396 events, there was one VSAT off-energy electron in 136 events and two off-energy electrons in 5 events. The probability of an electron in VSAT computed from these events is presented in Table 4.

2.4   VSAT background in STIC Bhabha events

A sample of back-to-back Bhabha events in STIC was selected by requiring a single shower in each calorimeter with $2.5° < \theta < 8°$ and $0.97 < E_e/E_{beam} < 1.05$. The angle between the two showers was required to be larger than $179.85°$. In all, 925445 events from the 1998 data satisfied these requirements, 22433 of them having at least one shower in VSAT with an energy larger than 20 GeV. Most of the events (22072) had a shower in only one module, while a small fraction had a hit in two (359) or three (2) modules.
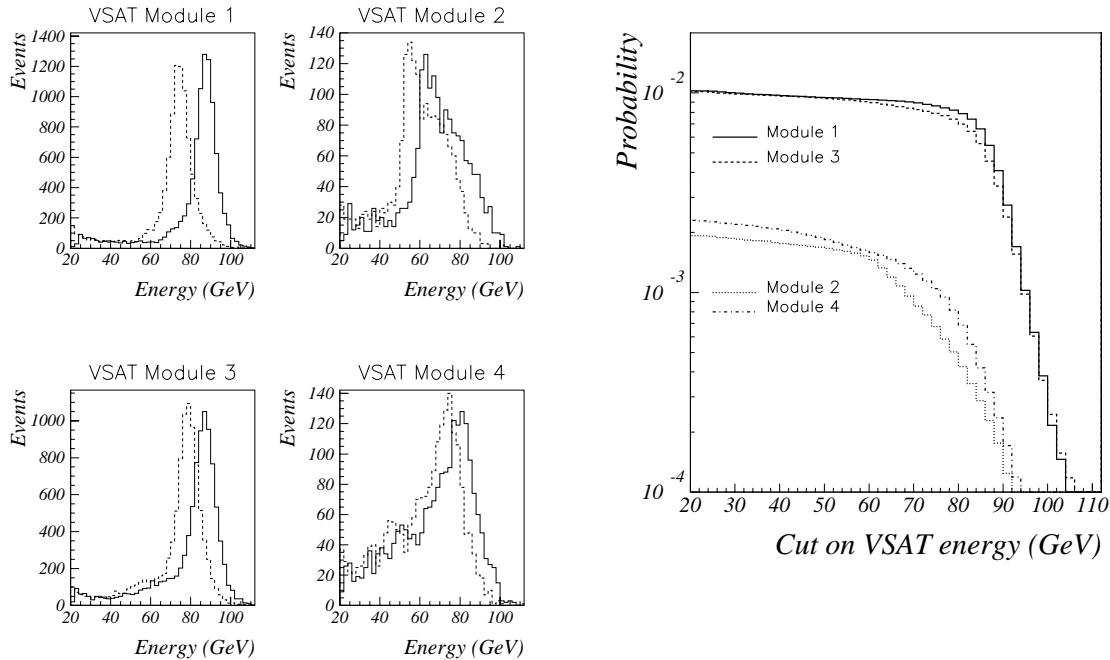
Figure 10: Left: Energy distribution of the showers in the four VSAT modules. The dotted line shows the uncorrected and the full line the corrected spectrum. Right: The probability that an off-energy electron shower will be found in VSAT, as a function of an energy cut.

Figure 10 shows the energy distribution of the showers seen in the four VSAT modules. The energy spectrum is shown both directly from the XSDST and after offline corrections. The VSAT modules at the outer circumference of the LEP ring (module 1 and 3) shows 5 times as much background as those on the inner circumference and the energy of the off-energy electron peaks close to the beam energy. In the inner modules the energy distribution is also peaked but broader. Since the energy of the background peaks at high energy, this background cannot be rejected with an energy cut. That is shown in Figure 10 and Table 5 which give the probability of having an off-energy electron in the different VSAT modules as a function of a cut on energy. Both for the inner and outer modules, the cut has to be made at very high energies in order to achieve a sizable reduction in background.

Since the off-energy background is concentrated in the horizontal plane, the best way

E_{min} [GeV]	$\mathcal{P}_1[\%]$	$\mathcal{P}_2[\%]$	$\mathcal{P}_3[\%]$	$\mathcal{P}_4[\%]$
20	1.025 ± 0.011	0.193 ± 0.005	1.017 ± 0.010	0.230 ± 0.005
50	0.947 ± 0.010	0.166 ± 0.004	0.936 ± 0.010	0.184 ± 0.004
70	0.890 ± 0.010	0.085 ± 0.003	0.824 ± 0.009	0.124 ± 0.004
80	0.788 ± 0.009	0.042 ± 0.002	0.699 ± 0.009	0.069 ± 0.003

Table 5: The probability of an off-energy electron with energy greater than E_{min} in the four different VSAT modules. The measurement was done with STIC Bhabha events.
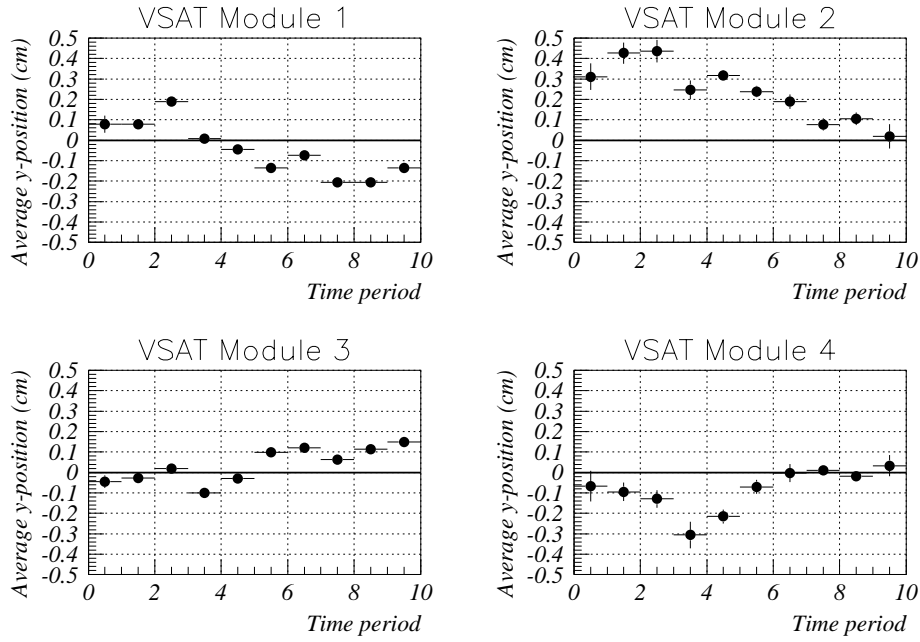
Figure 11: The average y-position in VSAT of the off-energy electron background during different time periods.

to reject it is by a cut on y (i.e. the vertical coordinate). However, differences in the magnetic fields in LEP during different time periods mean that the background peak in y moves during a LEP run. To study this, the 1998 data was divided up into 10 time periods as indicated by Table 6 and the average y-position was plotted (Figure 11). Variations of up to 5 mm of the average y-position were observed during the year, considering that each VSAT module has an active area which is only 5x5 cm, this is a significant effect.

Period	Fills	$\mathcal{Y}_1[mm]$	$\mathcal{Y}_2[mm]$	$\mathcal{Y}_3[mm]$	$\mathcal{Y}_4[mm]$
0	4550-4600	0.78 ± 0.42	3.10 ± 0.65	-0.45 ± 0.30	-0.67 ± 0.76
1	4601-4675	0.78 ± 0.21	4.26 ± 0.52	-0.27 ± 0.13	-0.95 ± 0.45
2	4676-4725	1.88 ± 0.14	4.35 ± 0.55	0.20 ± 0.09	-1.30 ± 0.43
3	4726-4750	0.09 ± 0.10	2.47 ± 0.46	-0.99 ± 0.11	-3.05 ± 0.65
4	4751-4875	-0.45 ± 0.09	3.16 ± 0.27	-0.29 ± 0.07	-2.16 ± 0.33
5	4876-4950	-1.36 ± 0.08	2.38 ± 0.28	0.98 ± 0.07	-0.70 ± 0.34
6	4951-5000	-0.73 ± 0.12	1.89 ± 0.35	1.21 ± 0.08	-0.03 ± 0.44
7	5001-5120	-2.06 ± 0.08	0.77 ± 0.31	0.64 ± 0.07	0.09 ± 0.21
8	5121-5330	-2.05 ± 0.09	1.05 ± 0.31	1.15 ± 0.06	-0.18 ± 0.24
9	5331-5500	-1.35 ± 0.17	0.18 ± 0.60	1.49 ± 0.13	0.33 ± 0.51

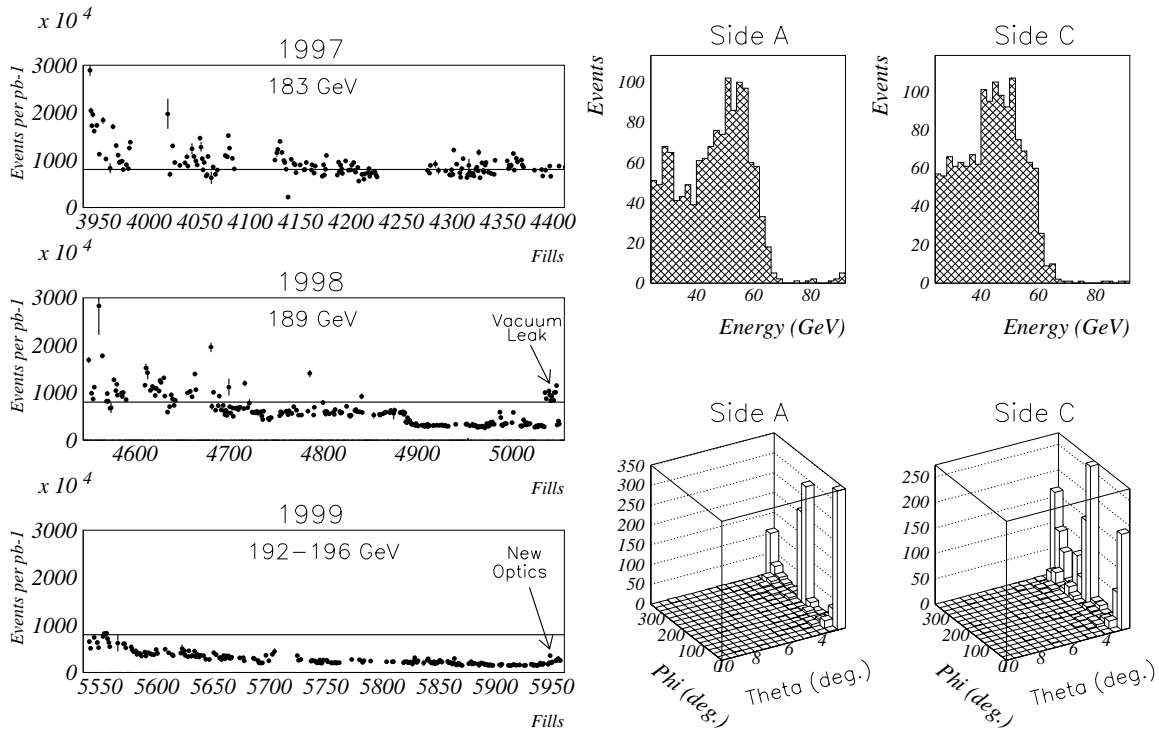Table 6: The average y-position of the off-energy electrons during 10 time periods.

9

Figure 12: Left: The number of off-energy electrons in STIC per pb^{-1}. Only the first 400-500 high energy fills during each year are shown. Right: The energy and theta-phi distributions of events recorded by the STIC single arm trigger. Data from fill 5941 were used.

3 Background in STIC

3.1 STIC single arm triggers

The STIC single arm triggered events can be used to measure the rate of off-energy electrons in STIC [5]. This trigger requires a shower with an energy greater than $\sim 0.25 \cdot E_{beam}$ in one of the two calorimeters. The trigger is dynamically downscaled to a constant trigger rate, and this has to be taken into account in the estimation of the rate. Figure 12 shows the rate of off-energy electrons in STIC normalized to luminosity. In 1997 the typical rate of off-energy electrons in STIC was $8 \cdot 10^6$ per pb $^{-1}$. The rate has decreased each year and it is now $< 2 \cdot 10^6$ per pb $^{-1}$.

The energy and angular distributions of the off-energy electrons in STIC are shown in Figure 12 for 1999B data from fill 5941. Most of the background has a large energy and is in the horizontal plane, which results in peaks in the theta-phi distribution. This horizontal background component can, however, be removed by a cut on the polar angle since it does not extend much above 3°.

3.2 STIC Bhabha events

To calculate the probability that an off-energy electron is recorded together with a physics event, the same basic selection of events as in the VSAT study was used, i.e., the events had to have one shower in each calorimeter with $2.5° < \theta < 8°$ and $0.97 < E_e/E_{beam} < 1.05$.
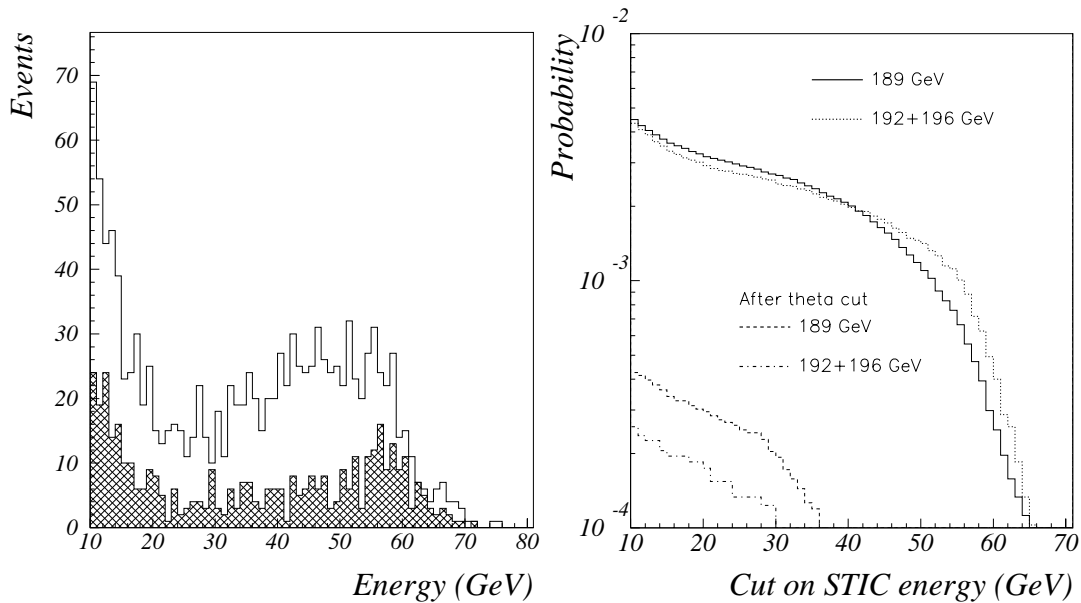
10

Figure 13: Left: Energy distribution of the third shower in the selected STIC events. The unshaded histogram is 1998 data and the shaded histogram 1999 data. Right: The probability that an off-energy electron shower will be found in STIC as a function of an energy cut.

The angle between the two showers had to be larger than 179.85°. A third shower was required in the event and this shower has to be separated by at least 45° in azimuth from the closest shower. The angular requirements meant that radiative Bhabha events with a photon energy of at most ∼8 GeV could survive the selection; the final sample of Bhahbas + an off-energy electron was selected by requiring the third shower to have an energy larger than 10 GeV.

The energy distribution of the third shower in the selected events are shown in Figure 13 for both 1998 and 1999 high energy data. The probability of an off-energy electron in STIC as a function of an energy-cut is also shown in Figure 13. The probabilities in 1998 and 1999 are very similar.
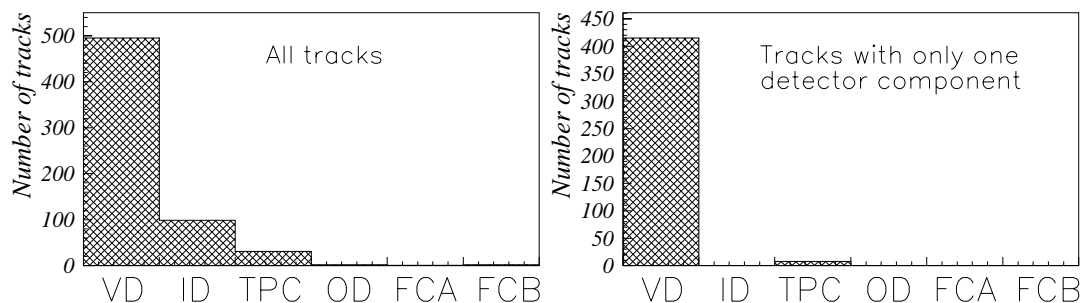

Figure 14: The different detectors used in track reconstruction for all tracks (left) and tracks with only one detector used in the reconstruction (right). 1999B data was used in this study.

11

E_{min} [GeV]	189 GeV		192-196 GeV	
	$\mathcal{P}[\%]$	$\mathcal{P}_{\theta>3°}[\%]$	$\mathcal{P}[\%]$	$\mathcal{P}_{\theta>3°}[\%]$
10	0.449±0.013	0.0425±0.0039	0.434±0.021	0.0257±0.0051
15	0.360±0.011	0.0341±0.0035	0.334±0.019	0.0195±0.0045
20	0.318±0.011	0.0295±0.0032	0.292±0.017	0.0174±0.0042
25	0.292±0.010	0.0249±0.0030	0.270±0.017	0.0133±0.0037
30	0.267±0.010	0.0193±0.0026	0.246±0.016	0.0092±0.0031
40	0.201±0.008	0.0081±0.0017	0.198±0.014	0.0072±0.0027
50	0.110±0.006	0.0025±0.0009	0.142±0.012	0.0021±0.0015
60	0.025±0.003	–	0.040±0.006	–

Table 7: The probability of an off-energy electron with energy higher than E_{min} in STIC. The measurement was done with STIC Bhabha events.

The most effective way of removing showers from off-energy electrons is not by an energy-cut but by a cut on the polar angle. By requiring $\theta > 3°$, most of the background in the horizontal plane is rejected. The probability of having an electron after this θ-cut is given in Table 7 and Figure 13 and it can be seen that the cut reduces the background by at least one order of magnitude.

One surprising observation is that more than a third of the events (36% in 1998D and 43% in 1999B) are accompanied by charged tracks. This is in contrast to Bhabha events without off-energy electrons, where less than 1% of the events are accompanied by charged tracks. Most of the tracks in the off-energy electron sample survive the standard cuts on impact parameters and momentum error and are not concentrated in the forward region. They are, however, short (average length = 27 cm) and have a low momentum (average p = 0.4 GeV). A study of the detectors used in the reconstruction of the tracks (Figure 14) showed that most of the tracks are seen in the VD only.

E_{min} [GeV]	$\mathcal{P}[\%]$	$\mathcal{P}_{\theta>3°}[\%]$
0.1	3.65±0.15	0.39±0.05
0.5	2.89±0.14	0.16±0.03
2.5	1.52±0.10	0.05±0.02
5	1.03±0.08	0.03±0.01
10	0.53±0.05	0.01±0.01
15	0.38±0.05	–
20	0.35±0.05	–
25	0.33±0.05	–
30	0.31±0.05	–
40	0.23±0.04	–
50	0.16±0.03	–
60	0.05±0.02	–

Table 8: The probability of a shower with energy larger than E_{min} in STIC. The measurement was done using random triggered events recorded in 1999.
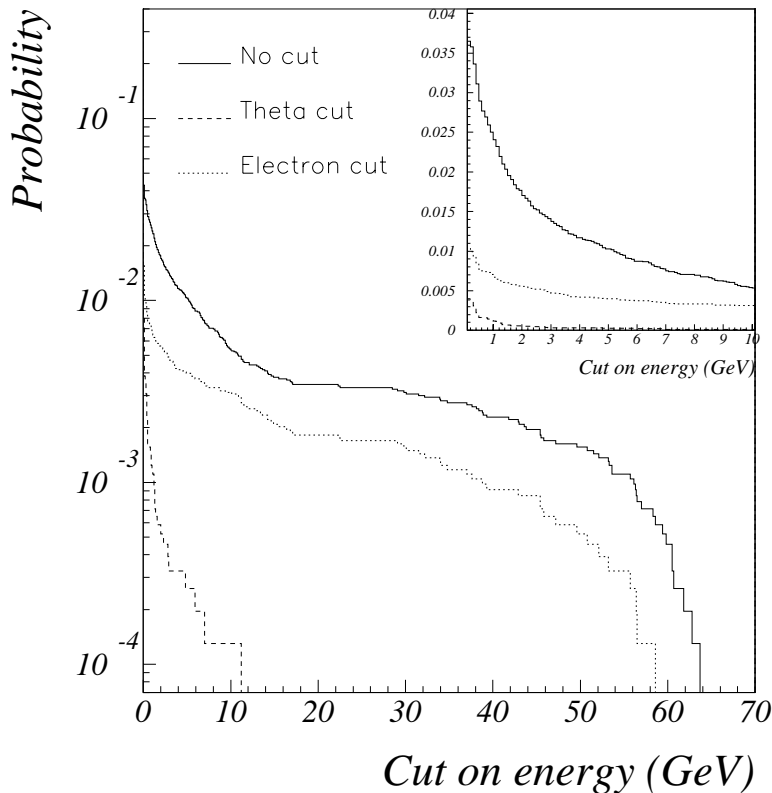
Figure 15: The probability of a STIC shower in a random triggered event as a function of a cut on the STIC energy. The probability has been calculated for all events with a shower in STIC and for the sub-samples when the veto scintillator counters identify the incoming particle as an electron and when the shower has a polar angle larger than 3 degrees.

3.3   Random triggers

The random trigger in DELPHI is caused by a signal from a scintillator placed close to a radioactive source. It is used to select an unbiased sample of events when no real interaction has occurred. The events taken with the random trigger during the first part of the 1999 LEP run ($\sim$40pb^{-1}) has been studied. Both the A- and the B-processing has been used.

The advantage of using random triggers compared to Bhabha events is that it makes it possible to go down to lower energies. The disadvantage is a smaller event sample. There is also the possibility that the off-energy electrons background is correlated in time to interactions and that the random sample therefore underestimates the off-energy background.

The probability of a STIC shower in a random triggered event as a function of a cut on the STIC energy is depicted in Figure 15. The probability has been calculated for all events with a shower in STIC and for the subsamples when the veto scintillator counters identify the incoming particle as an electron [6] and when the shower has a polar angle of more than 3 degrees. The most effective way of removing the off-energy background is, as stated previously, by a cut on the polar angle. This is illustrated in the right plot in Figure 16 which shows the theta-phi distribution of the off-energy electrons in the random triggered sample.
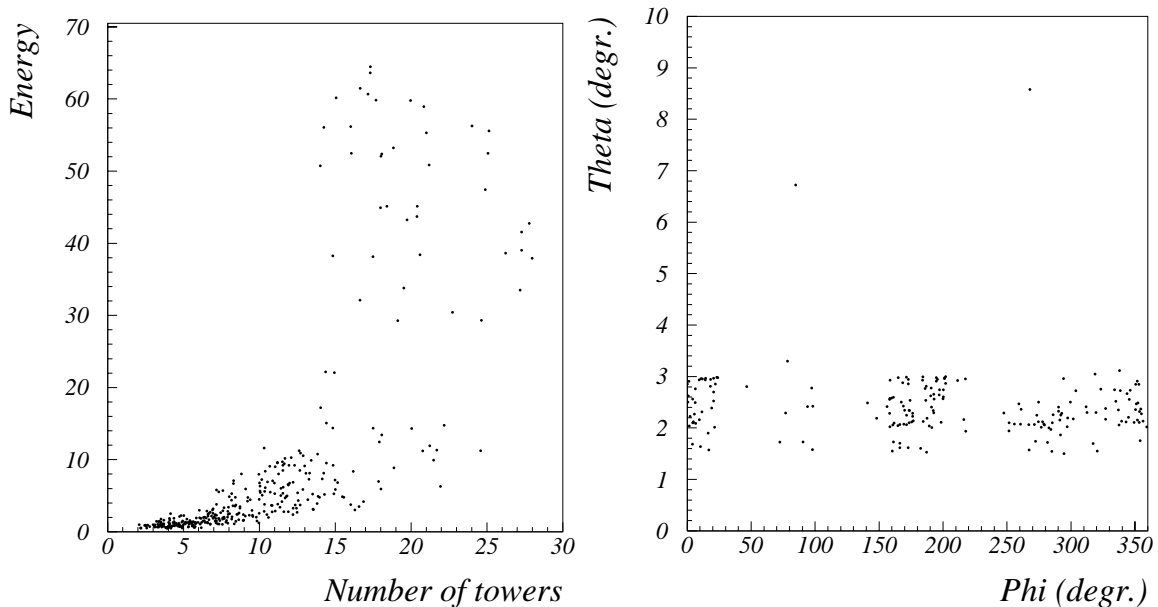
Figure 16: Energy versus the number of towers in the shower (left) and the theta versus phi distribution (right). Showers with an energy greater than 0.5 GeV were used in these plots.

By requiring a confirmation of the electron from a signal in the veto-counters a sizeable part of the background may be rejected. The reason is that many of the off-energy electrons enter STIC from behind or below the tungsten shield. In principle, the reason could also be that the STIC showers are caused by noise and not by off-energy electrons. That this is not the case can be seen in the left plot of Figure 16, which shows the energy of the showers versus the number of towers used in the shower reconstruction. A shower caused by noise has only one tower in the reconstruction and no showers like this were found with an energy larger than 0.5 GeV.

Table 8 gives the probability for an off-energy electron in STIC for different cuts on energy. An analysis which veto events with more than 0.5 GeV in STIC will lose 3% of the signal. In a search analysis which ends with 10 candidate events the probability of at least one off-energy electron in the events with more than 2.5 GeV is 15% while the probability of such a shower higher than $\theta > 3°$ in the 10 events is only 0.5%.

The probability of charged tracks in the events is 52%±6%, when the energy in STIC is larger than 10 GeV. The tracks are similar to the ones found in the Bhabha sample.

A comparison of the probability obtained at E_{min}=10 GeV with the Bhabha sample ($\mathcal{P} = 0.43 \pm 0.02$) and the random triggered sample ($\mathcal{P} = 0.53 \pm 0.06$) shows a barely significantly higher value for the random sample (contrary to naive expectations). This could be due to the fact the time period studied in the two analyses was not exactly the same.

4   Noise in the other calorimeters.

The other DELPHI calorimeters have also been studied by using the random triggered sample. At angles above STIC the calorimeters do not see any of the off-energy electron

background. Instead they suffer from noise showers and occasional showers created by cosmic rays. In the 1999A data, a noisy area in HCAL which created high energy showers was observed, but was removed in the 1999B processing (Figure 17). The left plot in Figure 18 and Table 9 gives the probability of a noise-shower in different calorimeters as a function of a cut on the shower energy.
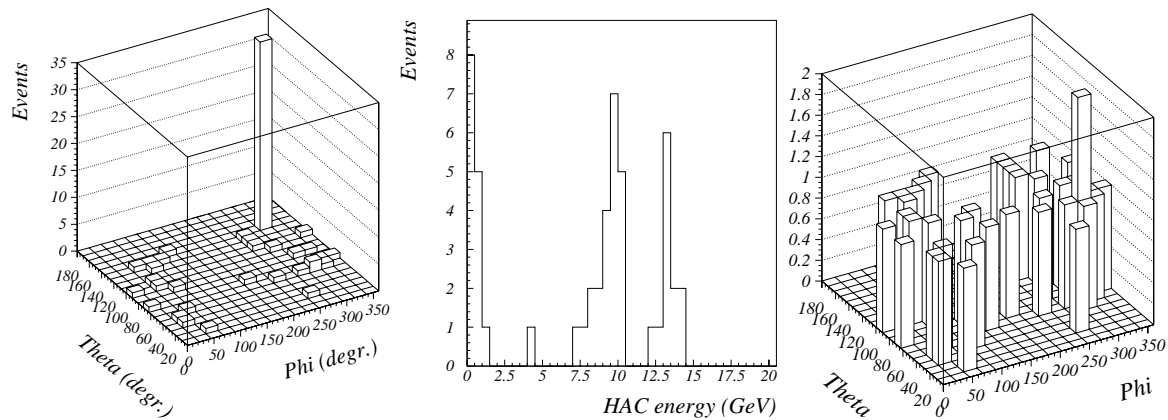
Figure 17: The theta-phi distribution of noise showers in HAC in the 1999A data (left) and the 1999B data (right). The middle plot shows the energy distribution of the peak in the theta-phi distribution.
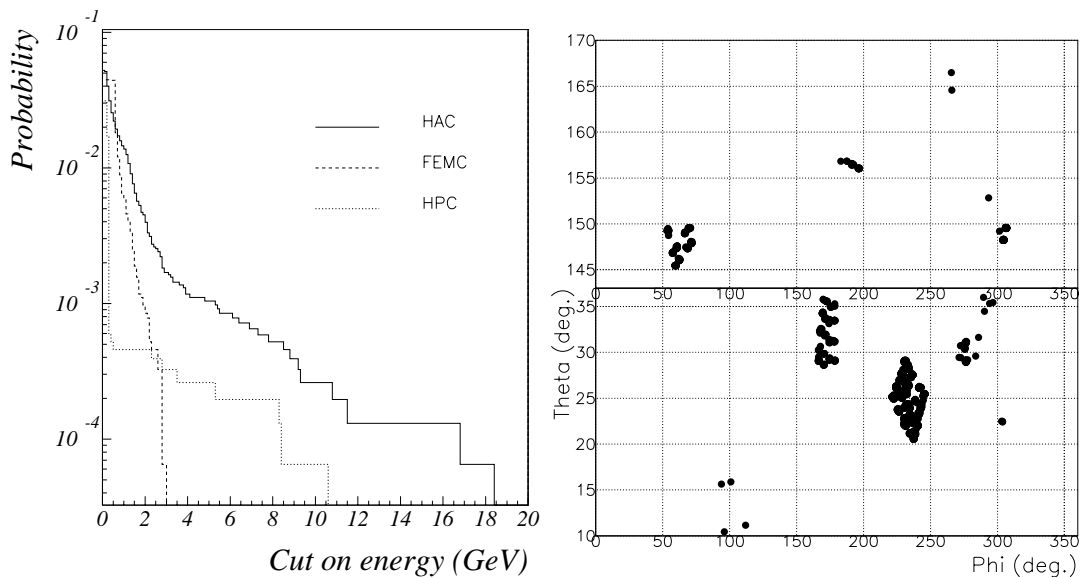
Figure 18: Left: The probability of a shower in different calorimeters as a function of a cut on the shower energy. The data used were triggered by the random trigger and come from the 1999 B-processing. Right: Noisy areas in the FEMC calorimeter during the 1999 data taking.

The probability plots in Figure 18 are of course only useful for analyses which does not select events based on energy in the calorimeters. If one takes the FEMC as an example,

15

E_{min} [GeV]	$\mathcal{P}_{HAC}$[%]	$\mathcal{P}_{FEMC}$[%]	$\mathcal{P}_{HPC}$[%]
0.1	5.15±0.18	4.47±0.17	3.12±0.14
0.5	2.21±0.12	4.42±0.17	0.05±0.02
2.5	0.25±0.04	0.05±0.02	0.04±0.02
5.0	0.10±0.03	–	0.03±0.01

Table 9: The probability of a shower with energy higher than E_{min} in HAC, FEMC and the HPC.

the probability of a noise-shower with energy larger than 2.5 GeV on top of a physics events is completely negligible. If on the other hand single photon events are selected by triggering on energy in FEMC and by not requiring any signals in any other DELPHI detectors (which would confirm the event to be a genuine physics event), events caused by noise in FEMC are selected. In this way one can find hundreds of single photon events in FEMC caused by fake showers. This is illustrated in the left plot of Figure 18 which shows noisy areas in the 1999B FEMC data. In this plot, only noisy areas producing showers larger than 2.5 GeV which survive the Margoni offline noise algorithm are included.

5   Summary and conclusions.

VSAT:

The VSAT Bhabha sample has been used to estimate the probability of an off-energy electron in VSAT on top of a genuine physics events such as an untagged $\gamma\gamma$ event. The statistical precision of this measurement is unbeatable. In an independent analysis a muon sample was selected and the probability to have an off energy electron in VSAT calculated. The result agreed with the VSAT Bhabha measurement within large statistical errors. Finally, a STIC Bhabha sample was used. All features of the background were the same in the STIC and VSAT Bhabha samples. Comparing the probabilities in the four modules by taking the ratio $\mathcal{P}_{VSAT} - \mathcal{P}_{STIC}/\mathcal{P}_{VSAT}$ for E_{min}=20 GeV -0.02±0.01, -0.22±0.03, +0.03±0.01 and -0.12±0.02 are obtained, i.e. a significant difference in the measurement of probability in the outer modules.

The best way of removing the background is by a cut on the measured y-coordinate since the off-energy electrons are concentrated in the horizontal plane.

STIC:

For STIC, a Bhabha sample has been used to measure the background of off-energy electrons. It is limited to electrons with an energy larger than 10 GeV and has therefore been supplemented by an analysis of random triggered events with which the low-energy off-energy electrons can be studied. At 10 GeV the difference $\mathcal{P}_{Bhabha} - \mathcal{P}_{Random}/\mathcal{P}_{Bhabha}$ is -0.23±0.15 .

The most effective way of removing the background is to discard any STIC showers with a polar angle less than $\sim 3°$.

FEMC:

The probability of a FEMC shower with energy above 0.5 GeV is sizeable (4.6%) but it drops off quickly with energy and for $E_{min} > 2.5$ GeV there is no need to take the detector noise into consideration (except in problematical analyses like single photon

analyses which select noise events).

HPC:

The energy spectrum due to noise is very steep and with an energy cut of $E_{min} > 0.5$ GeV the probability to have a noise shower in an event is at the level of 0.05%.

HAC:

The hadron calorimeter is noisier than the electromagnetic calorimeters and certain noisy areas can produce showers with energies of up to 10-15 GeV. However, by a cut of $E_{min} > 2.5$ GeV the probability of a noise shower is reduced from 5% (without the cut) to 0.3% (with the energy cut).

References

[1] The DELPHI collaboration. Phys. Lett. 342B(1995)402.

[2] E. Falk et al, DELPHI NOTE 98-147 PHYS 791.
    E. Falk et al, DELPHI NOTE 98-76 CONF 144.
    P. Checchia et al, DELPHI NOTE 99-77 CONF 264.

[3] E. Falk, V. Hedberg and G. von Holtey, CERN SL/97-04(EA).

[4] S. Jadach *et al.*, Comp. Phys. Comm. **66** (1991) 276;
    S. Jadach *et al.*, Comp. Phys. Comm. **79** (1994) 503.

[5] S.J. Alvsvaag *et al.*, Nucl. Inst. and Meth. **A425** (1999) 106.

[6] P. Ferrari et al, DELPHI NOTE 98-49 CAL 141.

Appendix C

Radiation damage and background monitoring by VSAT

Radiation damage and background monitoring by VSAT.

Pavel Tiapkine

University of Lund

Abstract

This paper reviews the main properties of the VSAT (Very Small Angle Tagger) detector which is used to provide a background measurement in DELPHI, in addition to monitoring luminosity. The events are dominated by Bhabha and single electrons and during filling, tuning and occasional beam loss the particle flux is high enough to produce short and long term radiation damage. The VSAT particle flux rates and acceptance is affected by beam parameters and the changes in geometry made in 1997. Radiation damage are evaluated for 1998 and 1999. A short description of problems connected with the LEP beam configuration in year 2000 is included.

1 Introduction

1.1 Position and Geometry

The background conditions at DELPHIs outer regions (i.e. outside the DELPHI super-conducting solenoid) are monitored partly by the LEP operation group using their detectors installed inside horizontal collimators at 8.5 meters distance [4,5] from the DELPHI Interaction Point (IP) and partly by the VSAT (Very Small Angle Tagger) detector. The main difference of the VSAT (Very Small Angle Tagger) detector compared to other DELPHI sub-detectors is the position very close to the beam. It is also far away (7.7 meters) from the interaction point and background conditions are different compared to the inside part of DELPHI Fig.1. A small change in collimators and/or quadrupoles operation parameters can cause a tremendous effect on VSAT counting rates and data-taking [2]. The VSAT detector consist of four calorimeter modules placed just next to the beam-pipe. The distance from the beam centre to the modules was about 6.4-6.2 cm prior to the LEP2 operation upgrade. By the end of 1997 the beam tube was upgraded to bring the modules closer to the beam. The recent position (5.7-5.9) of the VSAT modules is mainly defined by the beam-pipe shape and dimension than by design - the idea was to bring detectors as close as possible to the beam in order to increase the acceptance of leptons from two-gamma collision events. The symmetry of the modules was slightly broken by the upgrade but the gamma-gamma event rate become twice as large and the Bhabha cross-section increased by 50%.
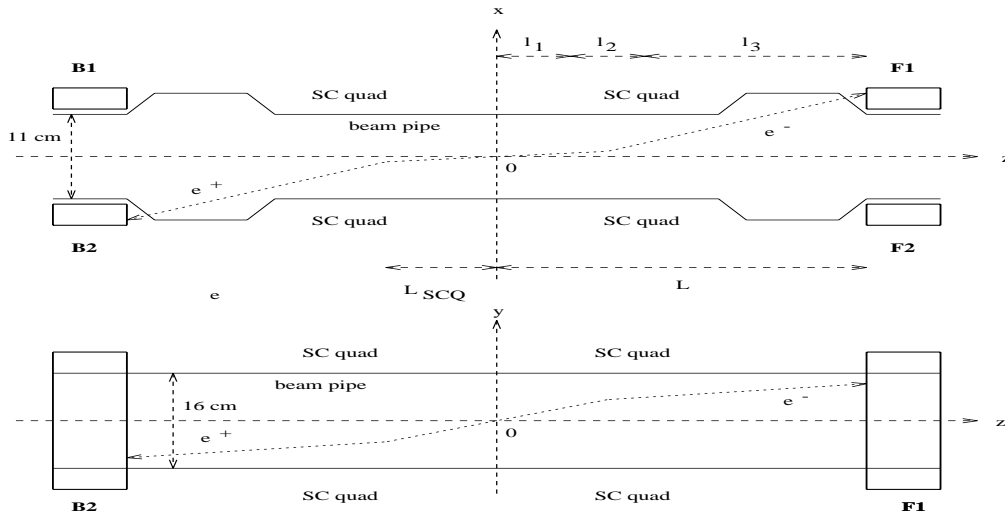

Figure 1: Cross-sections of the VSAT modules positions in horizontal (top) and the vertical (bottom) planes. The distances are: L=7.7 m, L_{SCQ}=3.7 (from the IP to the quadrupole centre), l_2=2.0 m - length of quadrupole, l_1=2.7 m, l_3=3.0 m

The change of position increase the acceptance of each module in different ways. Positions prior and after the upgrade are shown in Table 1. Here the XXIN is the distance from the beam center to the closest edge of the sensitive area of VSAT along the horizontal plane, YYLO - the lower edge of the sensitive area in vertical plane with respect to the beam level and ZZFR is the distance from the IP to the closest of the VSAT sensitive elements. Modules are called LUM1-LUM4 with: LUM1 and LUM2 (also called B2 and B1) belonging to the backward side (or A side of DELPHI setup), LUM3 and LUM4 (also called F2 and F1) are situated on the forward side (or side C). It should be mentioned also that events which has a maximum transversal shower profile in the 1st X strip (so-called first strip hit or strip error) always have been removed from the off-line re-processing since the leakage correction (estimation of the shower energy which escaped from the calorimeter through it side) of the event energy is impossible. The Bhabha instrumental acceptance coordinates are different for X as shown in Table 1.

Table 1: Position of the VSAT modules

$Years:$	Description	LUM1	LUM2	LUM3	LUM4
$1994 - 97$	geometry (in cm)	Mod 1	Mod 2	Mod 3	Mod 4
	DATA XXIN94	-6.386	6.178	-6.343	6.219
	DATA YYLO94	-1.677	-1.675	-2.231	-2.335
	DATA ZZFR94	-776.0	-775.8	775.9	775.8
$1998 - 00$	geometry (in cm)	Mod 1	Mod 2	Mod 3	Mod 4
	DATA XXIN98	-5.728	5.915	-5.915	5.800
	DATA YYLO98	-2.399	-2.245	-2.245	-2.377
	DATA ZZFR98	-776.10	-776.07	776.07	775.55
$1998 - 00$	Bhabha acceptance (in cm)	Mod 1	Mod 2	Mod 3	Mod 4
	DATA XBIN98	-5.78	5.96	-5.97	5.85
	DATA YBLO98	-2.35	-2.19	-2.2	-2.33

1.2 Detectors Hardware

The main sensitive elements of the four calorimeter modules are the FAD (Full Area Detector) planes. FAD has the typical thickness of 300 microns for semiconductor detectors, with full depletion voltage around -30 V (p type). Their operation voltage is -25 V. The strip planes (two X planes with 32 strips and one Y plane with 48 strips) (n type) have a full depletion voltage around +25 Volts and the operation voltage is also +25.

Both crucial parameters, voltage and current (which should be close to zero for ideal undamaged detector), are under Slow Control survilliance. The bias voltages and currents for FADs are distributed in two groups in an uneven way: FAD 1 is the only one in the first group and FADs 2-11 are in the second bias supply group. Such a distribution was chosen because of a concern that forward FAD 1 (which was also used for special X ray monitoring) would suffer more damage from low energy particles. This was not exactly what happened - as shown in Table and Figure 2 the bias leakage currents in the forward FAD was always less than 10 % of the total bias current in the other 10 FADs (inside that ten FADs the currents can be different but it is uncheckable).

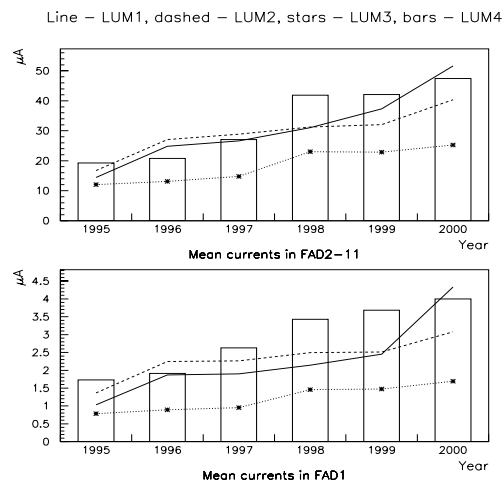| $Year$	FADs	LUM1	LUM2	LUM3	LUM4
1995	1	1.035	1.369	0.783	1.728
1995	2-11	14.44	16.76	12.01	19.27
1996	1	1.867	2.245	0.891	1.912
1996	2-11	24.80	27.09	13.15	20.76
1997	1	1.898	2.261	0.956	2.630
1997	2-11	26.65	28.90	14.78	27.06
1998	1	2.144	2.496	1.457	3.427
1998	2-11	31.02	31.26	22.99	41.90
1999	1	2.455	2.510	1.477	3.686
1999	2-11	37.33	32.08	22.88	42.08
2000	1	3.334	3.076	1.692	3.996
2000	2-11	51.61	40.35	25.26	47.46

Figure 2: Bias Currents.

Voltage (in Volts) and bias currents (in microAmpers [μA]) values are stored in the CARGO database which can be accessible by using program DPLOT at the DELPHI on-line cluster.

1.3 Logic

The trigger criteria of the VSAT trigger system is based on a Local Trigger Superwiser (LTS) processor operated in the FASTBUS crate and producing two kinds of triggers.

- The first is a Bhabha (BH) trigger i.e. two simultaneous hits in diagonal modules with energy greater than the threshold (roughly equal to 20 GeV).

- The second one is the Single Electron (SE) trigger: one hit in a module without coincidence with the diagonal module (using the same threshold around 20 GeV).

- The third trigger is a False Bhabha (FB) trigger or a so called Accidental Bhabha coincidence. It was used before the spring of 1996 and it was designed to select an

3

event with two hits in diagonal modules but separated in time by several (up to three) bunch collisions periods. Of course, the VSAT hardware in this case needs to wait several BCO periods for a second hit to happens and this dead time was the reason for switching off this kind of trigger when the interaction rate became too high.

The information which is produced by the VSAT operation can be described as two nearly independent streams which use the same trigger criteria - Physics data and on-line MIG scalers.

The physics data events are produced only when the global DELPHI or the local VSAT Data Acquisition System (DAS) is running. With each T2 from DELPHI or when the local buffer has no more free space all information (i.e. FAD signals, strip signals, trigger type) are storing in the VSAT local buffer (with capacity up to 25 events) and written to the DELPHI DST for off-line re-processing.

There is a possibility to downscale any of the Physics data triggers by using different factors for different modules. This ability was used several times during the VSAT lifetime to reduce the VSAT T1 rate by downscaling Single Electron triggers.

The MIG scaler stream is giving only rate information (i.e. number of events per unit of time) for each type of trigger. These values can be synchronised with the DELPHI read-out (gated) or not (ungated). After multiplication by calibration factors and after integration they provide both on-line plots and off-line records for the CARGO data base (Background 2 and VSAT on-line Luminosity).

1.4   Types of background

The proximity to the beams exposed the VSAT to a very big flux of particles such as:

- synchrotron radiation photon from the arc sections of LEP with critical energy $E_c = 26.5$ keV for 45 GeV energy and $E_c = 253$ KeV for 90 GeV energy [4] (decreased by several orders of magnitude by horizontal collimators during the 250 meters of straight sections before the IP). Also synchrotron radiation photons from quadrupoles are produced with energy ranging from 20 keV (a limit due to the photons absorption by the beam-pipe surface) to 5-10 MeV and back and forward scattered photons from collimators.

- electrons and positrons at beam energy during beam adjustments (especially in outer modules).

- beam particles with a small energy loss from 1 % to 3 % of the beam energy due to bremsstrahlung. If the energy losses is smaller than 1 % the particle stays within the acceleration system range and if the energy loss is more than 3 % it leads to fast particles which are lossed in the LEP arc sections.

- off-momentum e^+ and e^- produced in the straight section which loose the energy due to the interaction with residual gas atoms and beam-pipe components such as collimators, flanges and narrowings. The main feature of this background is the growth rate which is equal to the square of the beam current. The rate also depends on the dynamical vacuum condition in the closest sections of the beam-pipe.

2 Background storm and spikes

High background events can be divide in two groups - long term background storms (more than several minutes long) and short background spikes. Long storms are usually the result of a vacuum leak somewhere or some mistake in the LEP operation. Unpurities and residual gas in the beam-pipe section close to the DELPHI site which was opened during the shutdown gave a lot of problems during the start of the 1999 data-taking. The background was 3-4 times bigger than usual (Fig.3) but it has a tendency to decrease to a normal value by the end of each fill (Fig.3-5).
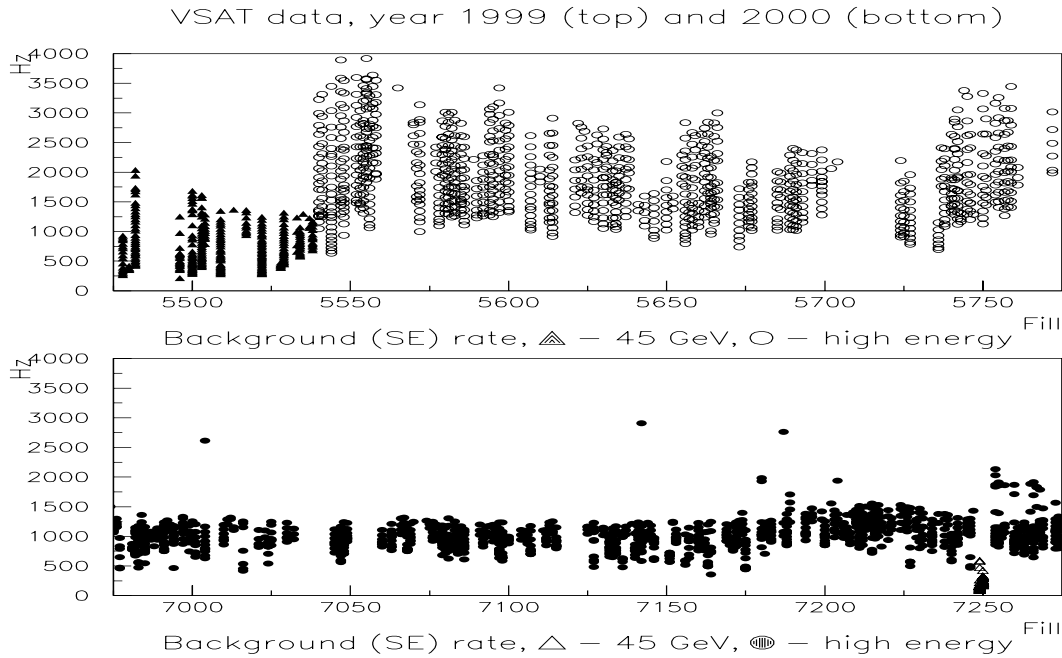
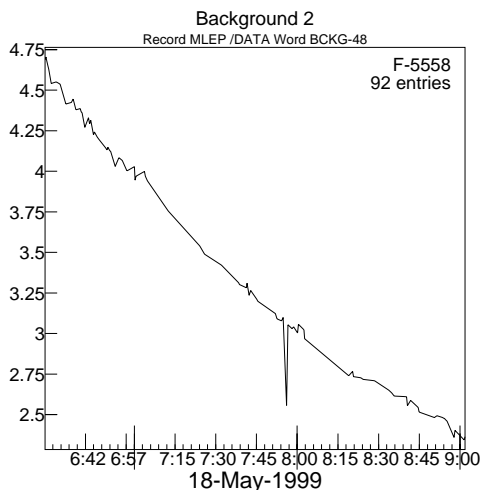Figure 3: Single electrons rates - start of 1999 and 2000.

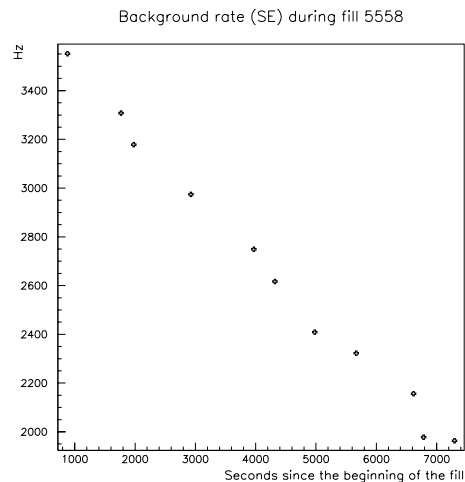Figure 4: On-line background rate during fill 5558 (1999).

Figure 5: Off-line background rate during fill 5558 (1999).

Short spikes are common during beam adjustment, closing of collimators or when beams are brought into collision as well as during minor malfunction of the RF or the magnets of the LEP. They can always be expected before beam loss or dumping.

VSAT had many incidents with high radiation levels during the last years but all dwarfed in comparison with one major radiation damage to both VSAT backward modules 1 and 2 (B2 and B1). This event took place on the 15th of September 1995 and has explained in detail in Ivan Kronkvist's thesis [3]. During that day, the fill 2989 was started around 17:30 with the collimators totally open during injection. The alarm which should dump the beam was silent due to malfunction of the automatic system and low background rate for the inside DELPHI detectors (shielded by the VSAT modules) was the reason that the situation remained the same until the the beams was lost at 18:15.

Two modules suffered damage. In terms of leakage currents the increase was up to 300 % - 11 to 42 for module 1, 13 to 38 for module 2. At the end of the year the currents stabilised at the levels 25 and 28 μA.

In recent years there were several spikes e.g. a series of spikes in modules 1,2,3 in July 96 (Fig.6). During three days (the 15th, 19th and 23rd of July, fills 3450-3940) there were several fast rises and drops of the bias currents (with magnitude up to 40 % of the usual current) in these modules but for all of them the normal level was back in one day.
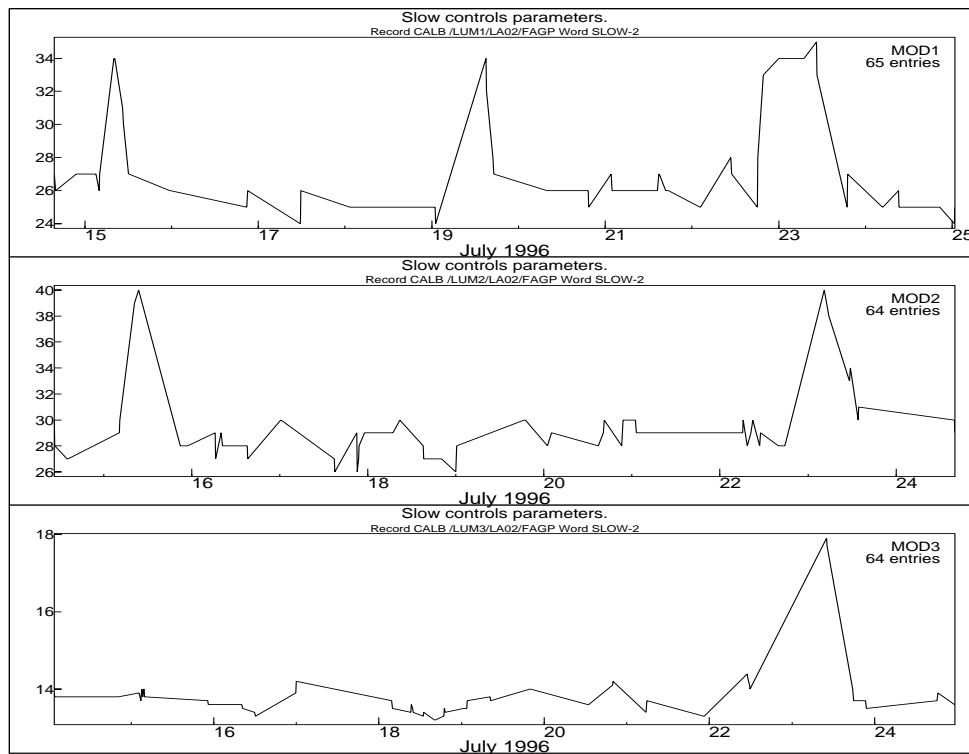
Figure 6: Bias currents in modules 1-3 (1996).

Table 2: Radiation damage and changes in VSAT modules

Energy :	97.79	99.83	100.83	100.86
Module	1,(2)	1,(2)	4	1,2
bias μ A:	28 to 40	36 to 46	42 to 48	40 to 50
% rise:	35 %	28 %	15 %	25 %
DELPHI background 2	100	120	6	70
duration	5 min	1 min	2 min	5 min
LEP background 2	35	6	225	3
duration	7 min	9 min	9 min	15 min
dates:	8.06.99	4.09.99	20.10.99	26.10.99
fills:	5673-5675	6261-6264	6574	6611-6620
runs :	102755-757	105831-842	107078	107233-268
Recuperation time:	8 days	6 days	2 days	10 days
Recuperation level:	100 %	80 %	90 %	50 %
nitrogen flow l/h:	400	500	500	800

The only possibility to treat the sensitive parts for radiation damage is by cooling. The detectors cooled by gaseous nitrogen. The flow of nitrogen is measured in units which varies from 0 to 1200. One unit is equal to 1 litre of nitrogen flow per hour if the temperature is about 20^0 C and the pressure is 1.21 bar. The typical nitrogen flow for year 1998 and 1999 was about 400 units. From august of 1999, the flow was increased to 500 and at 27th of October it was changed to 800 units.

The last change was made on the 10th of November 99 - after the end of physics at LEP. The flow increased to 1100 units per hour and module 1 showed a very fast and uniform recovery during one week (-2 microAmpers per day). The leakage current of the main group of FAD planes for module 1 was back to the desired level (40 μA) which was typical for that module before the last damage (26.10.99). The change was fast and stable also because LEP had no beam and no RF operation during that time. Unfortunately the DPLOT program can not use the data for that last period due to the cleaning of the CARGO database when LEP stopped.

All VSAT detector modules have temperature readout by two probes in each module. One of the probes is installed on the detector itself and another one sits on the preamplifiers which is housed in the same box close to the beam-pipe. Therefore the preamplifiers can also be damaged by radiation. A indirect evidence of such damage are the energy calibration changes (Fig. 7 and 8) and the malfunction of the temperature probe for preamplifiers in forward module F1 which gives an unstable zero temperature readout since 1998.
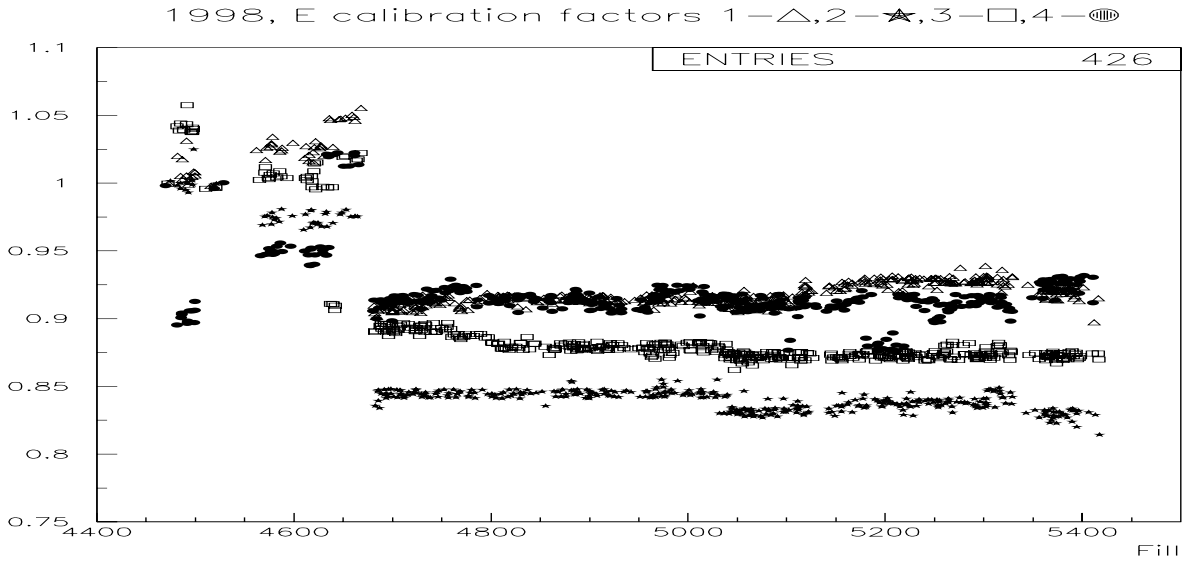

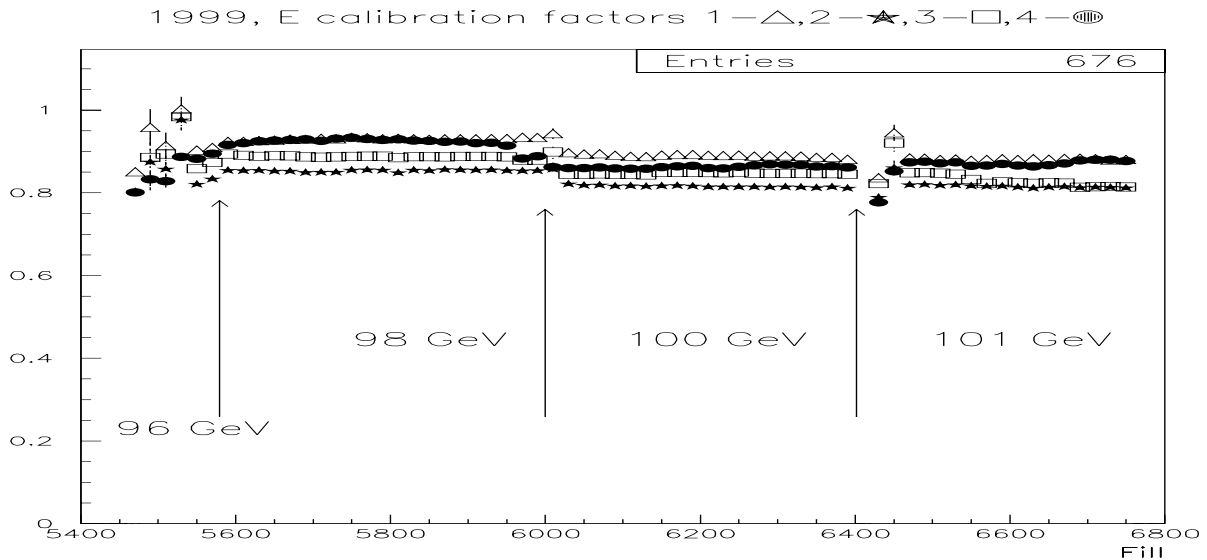Figure 7: Energy calibration coefficients during 1998.

Figure 8: Energy calibration coefficients during 1999.

8

3 Particle Rate and LEP operation

The downscaling factor for single electrons is now equal to 100 for the inside modules and 750 for the outside modules. These values were selected during 1999 in order to get the same number of single electrons per module for off-line processing (accidental coincidence subtraction by using single electrons to estimate a background). Around 10 % of all collected events are single electron events and this is enough to study typical parameters of the background particles for various cuts. During the year 1998 the downscaling factors was 130 and 400 and the single electrons sample had the same share of 10 %. A big difference between outside and inside modules is still seen but not between forward and backward modules as was the case for 1998 data between module 2 and module 4 (total hit rate 90 vs 120 Hz). Appendix A gives a total hit rate distribution in the VSAT modules.

After having the single electrons rate downscaled from hundreds of Hz to less than one Hz and after adding several Hz of Bhabha events we have a T2 rate from VSAT of around 3-6 Hz.

The dead time of VSAT can be divided in two parts: The first is caused by the DELPHI readout (during physics only) and can be evaluated by using live time variable which compare the number of WNG0 (WarNing Gate 0 - prepare for trigger) signals with the number of BCOs (Beam Cross Over - signal of collision between two bunches) itself (LIVTIM=ALLWNG/ALLCLK) in the VSAT DST. Mean dead time for 1999 was equal to 4.25 % and for 1998 it was 5.83 %.

The second is caused by the VSAT hardware itself. Such dead periods can be spotted by missing BCO (variable WNGBDT in the VSAT DST). The WNGDBT/ALLCLK ratio shows the relative dead-time which is negligible: $1.59 \cdot 10^{-8}$ for the 1999 and $2.4 \cdot 10^{-8}$ for the year 1998. This dead time affects ungated signal as well.

The "ungated" means only that it is not synchronous with the DELPHI read-out as it was stressed in DELPHI Note [8] where the last upgrade (1993) of the online system was described. Moreover the number of missing BCO signals is also counted to provide an estimation of the VSAT dead time.

To measure the overall particle flux obtained by VSAT only ungated signals from VSAT or so-called MIG scalers can be used. The rate of ungated signals is usually 5-10 % higher than the gated ones - i.e. the difference is mostly due to the dead time of the DELPHI read-out.

The problem is the flux of particles during long periods of LEP filling, acceleration etc. It should be stressed that the VSAT background rate (BACKGT) in the VSAT DST is different from the background 2 in the DELPHI on-line system and the CARGO database. The VSAT DST variable is defined by:

$$BACKGT = \frac{(seung1 \cdot seung4 + seung4 \cdot seung) \cdot 22 \cdot 10^{-6}}{\delta t}$$

The on-line Background 2 which is sent to LEP and can be seen on the LEP 101 page and TV monitors as a DELPHI BCKG 2 and in the CARGO database as well, is roughly equal to 800-1000 hits per second (Hz) for all four modules of VSAT and has no exact definition. It is renormalised from time to time in such a way that "1" means that background conditions are good and "5" means that the background is too high for data-taking. The Background 2 value has one very good feature it is updated outside physics mode of LEP and stored in the CARGO database.

Comparisons made using the DPLOT program shows that for the 100 GeV fills of August 1999 the integrated rate of Background 2 during the LEP setup (filling and acceleration) was twice that of the integrated Background 2 rate during physics period of LEP (which is accessible by using word W2 from record HEAD, tree MLEP). Therefore, Factor 3 should be used to evaluate the total particle flux since the VSAT DST gives one particle flux during physics only.

Table 3: Particle flux and LEP time distribution

Year	Particle flux	per inner module	per outer module
1998	during physics:	$N_{lep} = 0.4 \cdot 10^9$	$N_{lep} = 2.3 \cdot 10^9$
1998	total flux:	$N_{lep} = 1.2 \cdot 10^9$	$N_{lep} = 6.9 \cdot 10^9$

Year	Hours	Physics coast	Energy Calibration	Filling with coast	without coast
1998	4170	44 %	5 %	20 %	22 %

Year	Particle flux	per inner module	per outer module
1999	during physics:	$N_{lep} = 0.5 \cdot 10^9$	$N_{lep} = 2.7 \cdot 10^9$
1999	total flux:	$N_{lep} = 1.5 \cdot 10^9$	$N_{lep} = 8.1 \cdot 10^9$

Year	Hours	Physics coast	Energy Calibration	Filling with coast	without coast
1999	4460	36 %	8 %	21 %	19 %

All high energy fills was made with 4 bunches per beam. All 45 GeV (Z_0) fills has been made with 4 trains of 2 mini-bunches. 102/90 optics was used for acceleration with 102 degrees phase advance in the horizontal plane and 90 degrees phase advance in the vertical plane.

The unbalance in the single electron ungated mean rate for module 4 (in mean values: 120 Hz vs 90 Hz in module 2) is the most significant feature (Fig. 9):
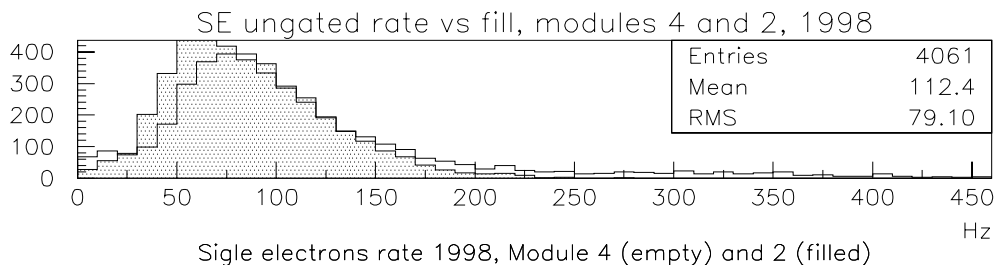

Figure 9: Single electrons hit rate in 1998, modules 2 and 4

and it was caused by a group of fills starting with fill 5082 (24 of August) and ended with fill 5122 (31 of August). LEP was working with horizontal/vertical beta function values 1.5m/0.05m respectively. But during this week the value of horizontal beta function was different in all points (1.7 / 1.45 / 1.2 / 1.5 in points 2(L3) / 4(ALEPH) / 6(OPAL) / 8(DELPHI) respectively) giving a great luminosity disbalance among the experiments (OPAL had +20% luminosity excess).

Such a drift of the horizontal beta function gave a factor 2.0 - 2.5 increase of the single electron rate (+400 Hz) in module 4 of VSAT. The opposite Module 3 single electrons rate shows no rise at all but it had a much bigger rate during the first Z^0 period.
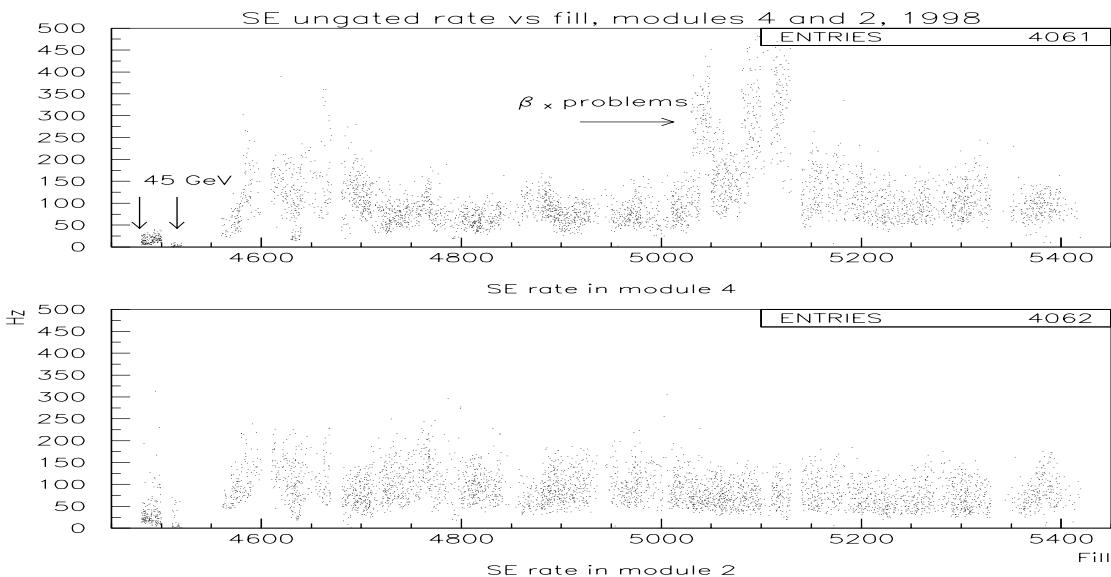

Figure 10: Single electrons rate in the outside modules 4 and 2

From early September the horizontal value of β was reduced to 1.25 m, and the vertical value was reduced to 0.04 m for the last three weeks of 1998 LEP physics. A decision was made for the future to check the beta function parameters in all points regularly.

11

3.1 Localisation of background

A comparison of the Single Electrons rate in different modules is in a certain way a description of geometrical properties of the background.

The upper plot of Fig. 11 shows much bigger variations between outer and inner modules than between backward and forward (lower plot). It is evident that the Z^0 fills provide a bigger asymmetry than the ones with high energy.
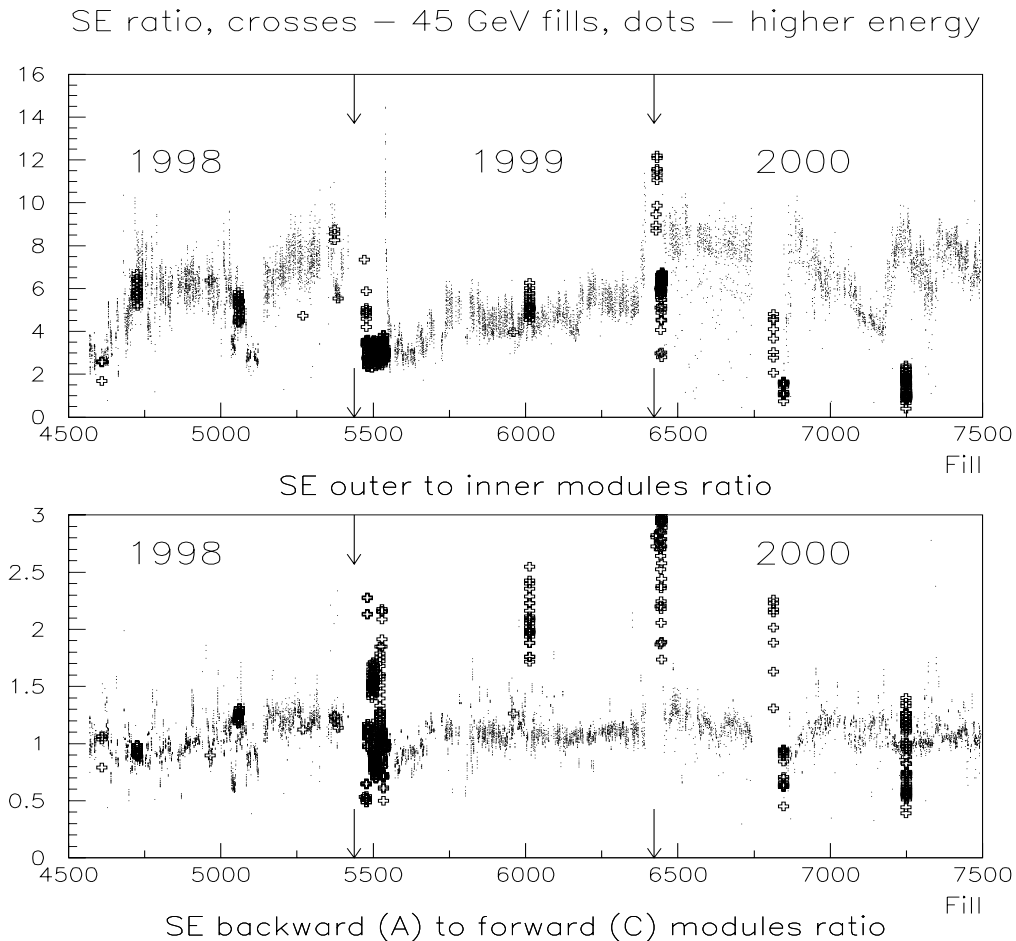

Figure 11: Ratio between SE hits in different group of modules

There were no big problems with the strip planes due to a radiation damage. All 32 strips of the X1 planes are working, the X2 planes have one dead strip in three modules (this is strip number 10 in module 1, strip 14 in module 14, strip 16 in module 4) and there is one dead strip in each of two Y planes (module 2 and 4, strips 7 and 40 respectively). Althought during the year 1998 module 4 had 2 dead strips in a row (40 and 41 in module 4).

The X distribution of Single Electrons are nearly the same for all four modules and as uniform as the total sample distribution. It has some maximum close to the beam-pipe and it decreases linearly to the outer edge of the detectors. During high energy fills the maximum at the inner edge is a little bit more evident.
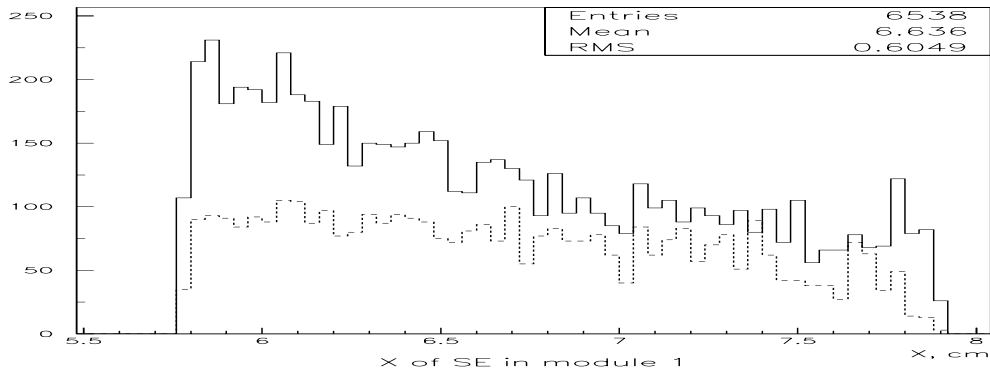

Figure 12: X distribution of Single Electrons in module 1 - solid 102 GeV, dashed 45 GeV beams

The Y distribution shows very different structures. For all modules the background tend to concentrate in a very narrow peak around the horizontal plane of the beam. Those peaks are oscillating around zero Y coordinate (within ± 0.5 cm). For 45 GeV fills the peaks are broad - up to 1 cm width. High energy fills have one more feature - a additional broad peak to the left of the main one. It is common in module 2 and quite rare in module 1 and 4.
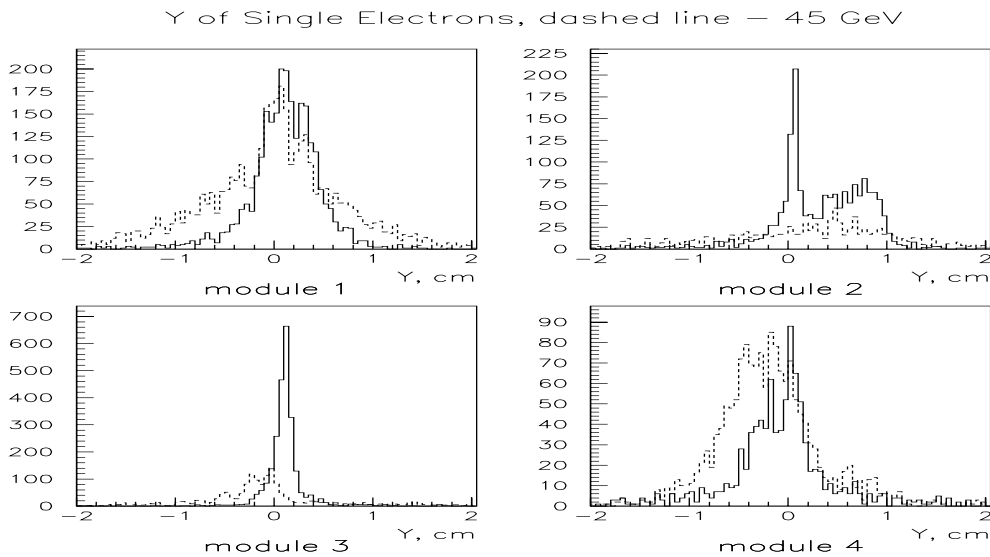

Figure 13: Y distribution of Single Electrons within each module

13

3.2 Energy resolution

The energy resolution at 45 GeV is 5 % and at 95 GeV it is around 4 %. The VSAT energy resolution is traditionally very stable for inner modules and shows a small rise (about 1 % between start and end of year - Fig. 14) in outer modules (1,3) due to the higher background.
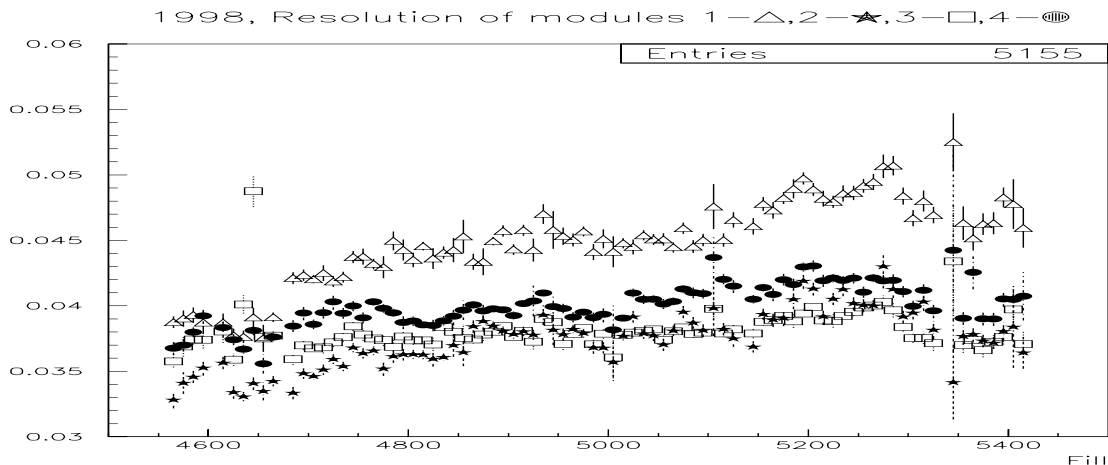

Figure 14: VSAT Energy resolution for high energy 1998

There is a trend of a resolution decrease during 1999 as shown on the second plot (Fig. 15). This is mainly connected with the energy change but the recovery after a damage is also possible. The resolution R depends on the energy E as described by the simple formula $R = 35\%/E^{1/2}$ where E is in GeV. Two regions of a fast increase of the energy resolution for module 1 and 2 can be interpreted as the result of the first and the last radiation damages mentioned in Table 2.
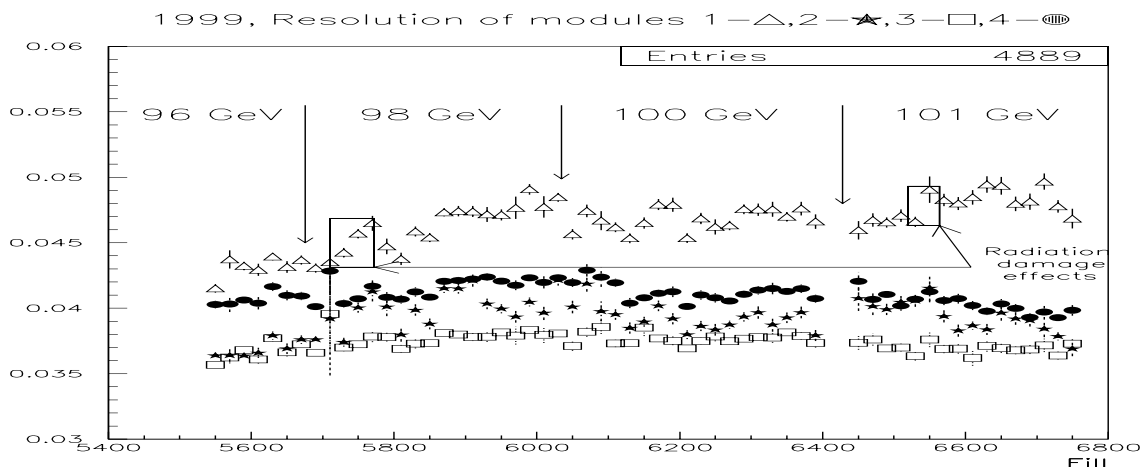

Figure 15: VSAT Energy resolution for high energy 1999

14

3.3 Radiation dose

The ionisation dose is measured in Grey $[Gy]$ which is equal to 1 Joule $[J]$ of energy loss in 1 kilogram of matter. Using the data about e^+ e^- flux obtained above and by using the mean particle energy we get an evaluation of the particle flux (particles per cm^2 - assumed surface is $S = 15 \ cm^2$) and the energy flux formula:

$$I_S = N_{lep} \cdot S \qquad I_E = \frac{(N_{lep} \cdot E \cdot 10^6 eV \cdot 1.602 \cdot 10^{-19} J/eV)}{m}$$

Here m can be the total mass (i.e. tungsten plus silicon) or the mass of the sensitive media only (which is more useful and correct). The largest part of total mass of the calorimeter is the mass of the tungsten blocks with dimensions: 5.12x5.0x0.38 cm^3 and density 18.24 g/cm^3 (this is an alloy). There are 22 of them in one module which gives a total mass of:

$$M_W = 9.728 cm^3 \cdot 18.24 g/cm^3 \cdot 22 = 3903.64 g \approx 3.9 kg$$

It is also possible to evaluate the mass of the sensitive elements only. There are 11 FADs, one Y plane and two X planes per one module. Each of the planes has a size: 50x50x0.03 mm^3 or 0.075 cm^3 (sensitive areas are smaller for the X and Y planes) . The mass of silicon elements is then:

$$m_{plane} = 0.075 \cdot 2.33 g/cm^3 = 0.175 g$$

and the total mass of the silicon elements is :

$$m_{Si} = 15 \cdot m_{plane} = 2.621 g \approx 2.62 \cdot 10^{-3} kg$$

Mean energy per particle (i.e. for total flux - background and trigger events) deposited in the outer module are 72.7 (69.8 for inner) GeV for 1998 and 73.3 GeV (70.8 for inner) for year 1999. The distribution is shown below: (Fig.16).
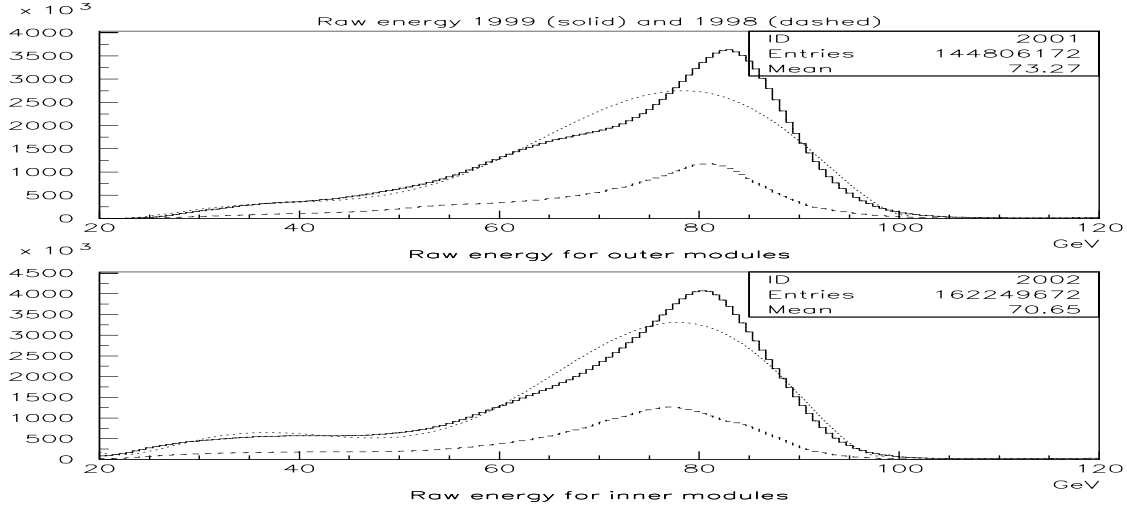

Figure 16: Energy distribution of all events in VSAT

Part of the energy deposited in the silicon can be derived from the ratio of silicon to total masses:

$$E_{Si} = E \cdot \frac{m_{Si}}{M_W + m_{Si}} = E \cdot 0.4095 \cdot 10^{-3}$$

By using that, the final formula is:

$$I_E = \frac{(N_{lep} \cdot E_{Si} \cdot 10^6 eV \cdot 1.602 \cdot 10^{-19} J/eV)}{m_{Si}} = \frac{(N_{lep} \cdot E \cdot 10^6 eV \cdot 1.602 \cdot 10^{-19} J/eV)}{M_W + m_{Si}}$$

And it gives the values represented here, in Table 4. It should be mentioned that only lepton background with energy above 20 GeV was used to calculate these results.

Table 4: Estimation of Radiation Damage of VSAT

position year	1998	1999	units
I_E, outer (1 and 3)	20.6	24.4	Gy
I_E, inner (2 and 4)	3.4	4.4	Gy
I_S, outer (1 and 3)	$4.6 \cdot 10^8$	$5.4 \cdot 10^8$	cm^{-2}
I_S, inner (2 and 4)	$0.8 \cdot 10^8$	$1.0 \cdot 10^8$	cm^{-2}

4 Year 2000 background

More radiation hits the module 1 (B2) since it is closest to the beam-pipe (5.7 cm from the beam centre in comparison to 5.8 and 5.9 for other modules) and the malfunction of the collimator at point 8. The horizontal collimator COLH.QS3B.L8 (on the left side from DELPHI - side C) 56.3 meters away from the IP has given some problems since 19:30 on the 7th of April.

The VSAT background was up to 34 at 9:30 on the 8th of April and the LEP background was around 7 at the same time. It should be mentioned that in spite of the proximity (LEP radiation monitors are 8.5 meters away from the IP vs 7.7 meters for the VSAT modules) and similar hardware [4] the background rate measured by them are often very different and strongly depends on the collimators.

Leak currents for module 4 are shown a big spike during the night 7-8th of April. Background storms during 16:00 - 19:00 with a magnitude of 7, might be the reason for the increase of leakage current or previous irradiation. Unfortunately the VSAT background is not available for these hours due to local tests with the VSAT at this time.

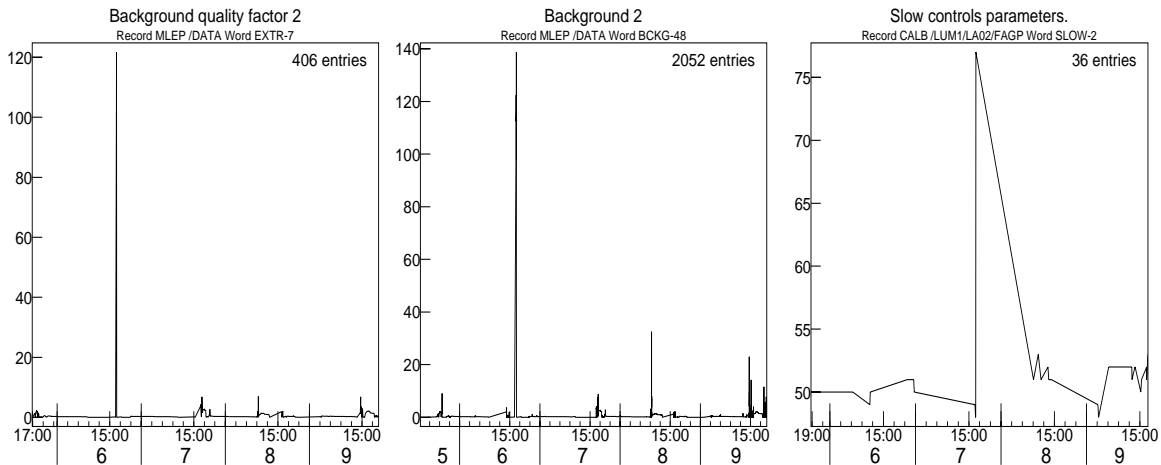| Background quality factor 2	Background 2	Slow controls parameters.

Figure 17: LEP Backgr.2   Figure 18: VSAT Backgr.2   Figure 19: I_{leak} mod 1

The big spike at 17:00 on the 6th of April (Fig. 19) was also connected with collimator problems. The background storm was around 30 minutes long for the VSAT background rate and only 5 minutes long (but the same amplitude as one can see from plots) for the LEP radiation monitors.

The collimator was needed to be moved several times but could be placed in almost nominal position after some attempts. On the 9th of April around 6pm it was stuck in the beam completely and was then repaired (an electro-motor contact problem). Beam operation delay caused by the magnet patrol and the LEP access gave a VSAT time to recover.

The VSAT survived much better (no spikes and leak current rise) at even more dangerous situation at the 7:00 on the 12 of April. The collimators were then opened during physics ! Even the internal DELPHI background 1 showed values of 60000 and both LEP and VSAT backgrounds showed nearly infinite numbers like $5 \cdot 10^5$. On the next day the off-momentum particle collimator was changed from 12 to 10 standard beam deviation to avoid background storms.

17

Module 1 has the greatest leak currents on the different components since the middle of April 2000. The FAD2-11 voltage group and the X2 strip plane even have a small leak currents (2.2 and 0.7 μA respectively) for some time after the bias voltage being switched off.

Sometimes the background consist mainly of the low energy leptons and photons. Such rare cases can be distinguished by a sudden rise of leakage bias current for the FAD plane number 1 (Fig. 22). One such event happened on the 30th of June and is shown in Fig. 20,21,22.
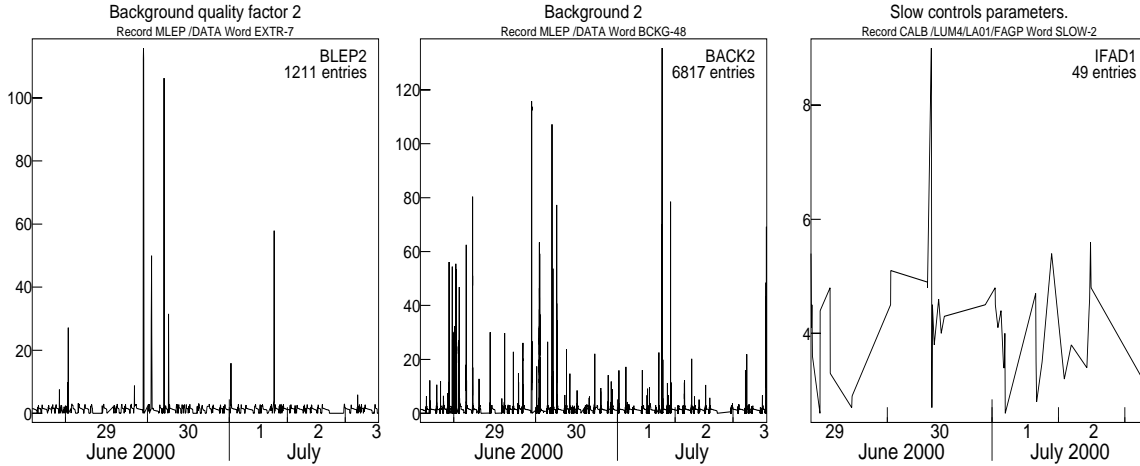

Figure 20: LEP Backgr.2   Figure 21: VSAT Backgr.2   Figure 22: I_{leak} mod 4

5   Conclusion

Analysis shows that the VSAT silicon detectors radiation damage affects the data in an indirect way. The main consequences are: first, an energy calibration shifts due to the damage to preamplifiers and second, an energy resolution degradation (from 4 to 5 %) which last for a periods from one week up to several months (i.e. until LEP shutdowns). The main criteria of how serious the damage was, is the rise of the bias currents which have a trend to self repair to nearly the same levels during a typical period of one-two weeks. The strip planes shows a good robustness. Only three Y and planes three X2 planes have a one dead strip each now amoung total number of 12 planes and 448 strips.

References

[1] S. Almehed et al.
Two-photon physics at LEP200 - what DELPHI can get with an upgraded position
for the VSAT detector.
Technical Report DELPHI 96-63 PHYS 624

[2] S. Almehed et al.
Beam parameter monitoring and interaction point measurement in DELPHI with
the VSAT
DELPHI 94-77 PHYS 453

[3] I. Kronkvist
Data Base and Slow controls of DELPHI VSAT and Two-Photon Physics using
DELPHI at LEP
(Lund University Thesis) ISBN 91-682-2182-2 LUNFD6/(NFFL-7128) 1996

[4] G.von Holtey and M.Lamont
CERN SL-99-022 EA
Protection of LEP Experiments against Particle Background at Highest Beam
Energies

[5] J.Y. Hemerly, F. Lemeilleur, G.von Holtey
CERN LEP-BI 86-5
An Interaction Rate Monitor for LEP

[6] S.Battisti et al.
Radiation Damage to Electronic Components
CERN 75-18 Laboratory II 19-Dec-1995

[7] G.Jarlskog, M.Jonker
Background and Luminosity Monitoring in DELPHI
DELPHI 89-59 MIG 3

[8] S.J.Alvsvaag et al.
The system for online monitoring of LEP beam background and luminosity at the
DELPHI interaction point
DELPHI 93-3 DAS 137

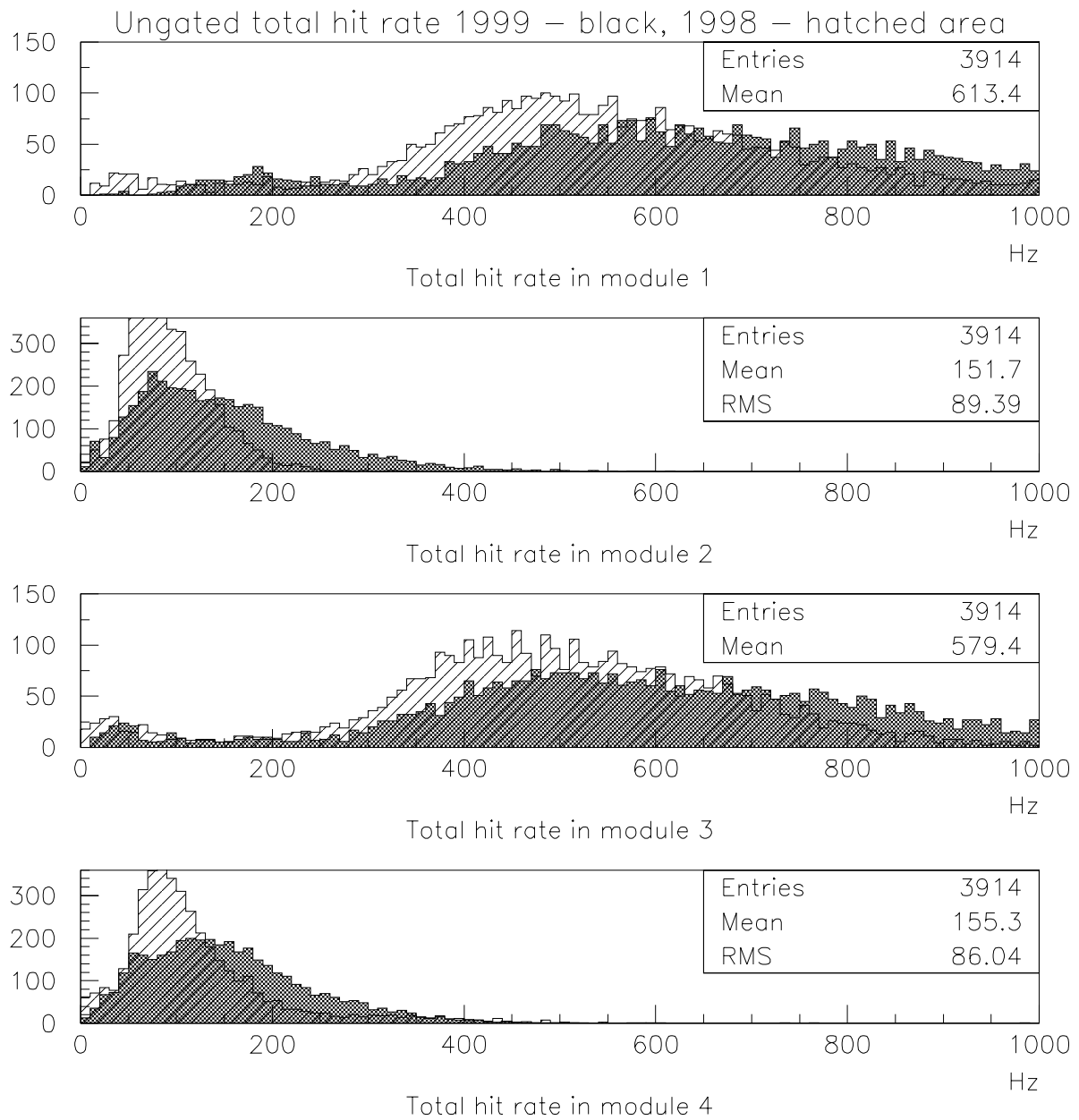# A   Appendix: Total Hit rate in VSAT (1998-1999)

Ungated total hit rate 1999 − black, 1998 − hatched area

Entries	3914
Mean	613.4

Total hit rate in module 1

Entries	3914
Mean	151.7
RMS	89.39

Total hit rate in module 2

Entries	3914
Mean	579.4

Total hit rate in module 3

Entries	3914
Mean	155.3
RMS	86.04

Total hit rate in module 4

Figure 23: Total particle hit rate in VSAT

Appendix D

Exact position of VSAT modules and LEP beam parameters measurements in 1998-2000

Exact position of VSAT modules and LEP beam parameters measurements in 1998-2000.

A. Nygren, P. Tyapkin, N. Zimin, G. Jarlskog
Elementary Particle Physics Department
Lund University

Abstract

This report presents detailed information of how the beam-pipe upgrade in 1998 has affected the geometry of the VSAT detector. The shift between DELPHI and VSAT coordinate systems has been determined and presented here along with a beam-parameter analysis with help of the VSAT detector. Finally methods are presented to correct for some errors occurring in the VSAT data base as well as a general shifts of the VSAT modules between 1998 and 2000.

1 Introduction

The VSAT (Very Small Angle Tagger) detector is one of three DELPHI sub-detectors which are able to provide beam related information. The position of VSAT is quite far away (7.7 meters) from the interaction point and its main purpose is to count Bhabhas events with a θ angle around 4-7 mrad. The detector is placed very close to the beam and therefore measurements are affected by the background and beams distortions, which makes the beam related information quite inaccurate. Good results can however be accomplished by using statistically significant amount of data (several thousands of events at least).

The VSAT detector consists of four identical modules, each with a 3x5 cm^2 active detector area. The distance from the LEP beam line to the VSAT modules is since the beam pipe upgrade at the end of 1997 to about 5.7-5.9 cm. The idea was to bring detector modules as close to the beamline as possible, in order to increase electron/positron acceptance for gamma-gamma physics.
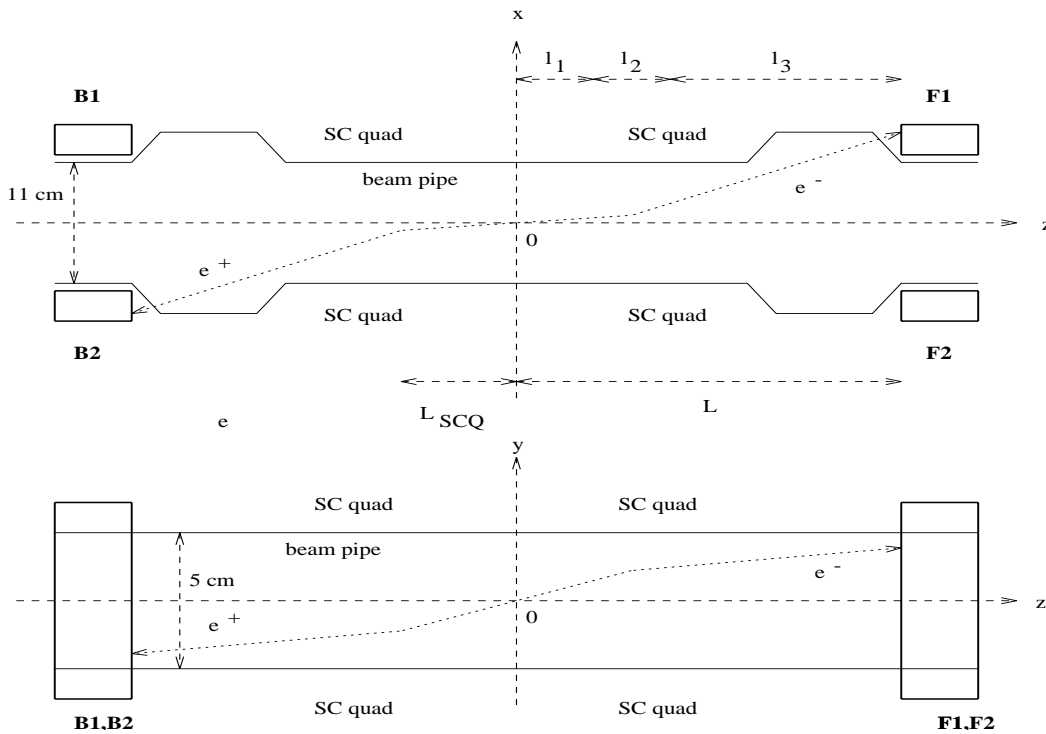

Figure 1: Transverse view of VSAT modules positions in horizontal (up) and vertical (down) planes. The distances given: L=7.7 m, L_{SCQ}=3.7 (from IP to the quadrupole center), l_2=2.0 m - length of quadrupole, l_1=2.7 m, l_3=3.0 m.

Moving the module closer to the beam in X directly increases the VSAT acceptance, as the outer edge of the detector is shadowed by a flange. Events that hit any of the edge strips of the VSAT detector can not be reconstructed and are cut away, reducing the acceptance with about 0.5 mm from the edges.

2 VSAT parameter fix in X

The VSAT has been positioned with precise mechanical measurements in relation to the LEP equipment (section 4), which is however not fixed with respect to DELPHI. The VSAT and DELPHI coordinate systems are thus not the same and have to be fixed in position before any beam parameter analysis can be performed. In order to get the most correct position of the VSAT modules it is necessary to use the symmetries of the Bhabha events recorded by VSAT. In the X-Z plane there are 3 beam-spot properties that influence the signals measured by VSAT, shown in Fig. 2 and 3.
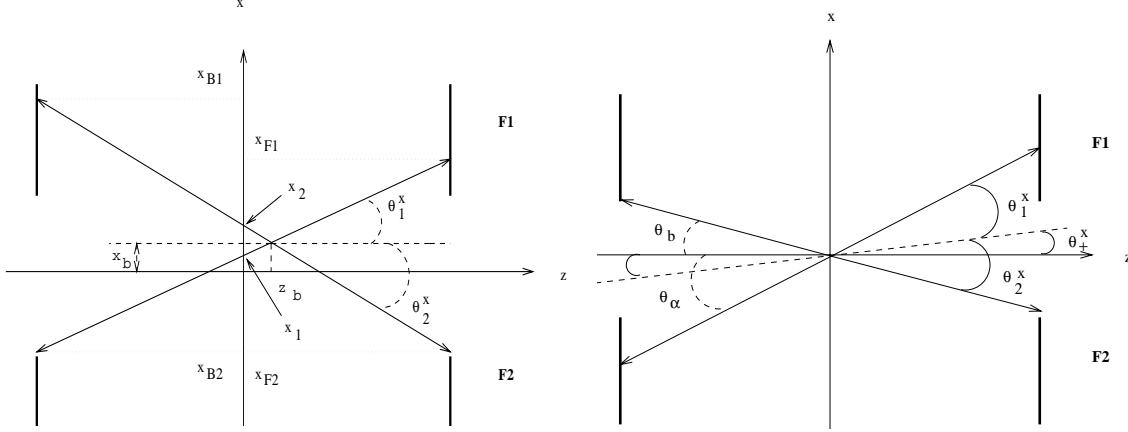

Figure 2: Event with zero tilt, nonzero beam spot displacement in both X and Z position.

Figure 3: Event with non-zero tilt (acollinearity), zero beamspot displacement in both axes.

As the electrons from an elastic Bhabha event are back to back symmetric, there is a distinct relation between the position measurements in the diagonal modules. The paths of the outgoing leptons are affected by a pair of quadrupoles, which however can be described by a simple focusing/defocusing factor and an effective magnetic length of the VSAT [1]. The relation between the beam-spot position, the relative position of the Bhabha electrons and the beam acollinearity can be expressed as [2]:

$$\Delta X_1 = x_4 + x_1 = 2f_x(x_b - z_b(\theta_1^x + \theta_x)) + \epsilon_x l_x \quad , \tag{1}$$

$$\Delta X_2 = x_3 + x_2 = 2f_x(x_b + z_b(\theta_2^x - \theta_x)) + \epsilon_x l_x \quad . \tag{2}$$

Here x_b is the beam spot position (from the beamline) and ϵ_x is the acollinearity between the beams. The quadrupole focusing factor is described by f_x and its magnetic length by l_x. Finally θ_1^x and θ_x (θ_+^x in Fig. 3) are the angles of the outgoing lepton and of the undisturbed LEP beam. The sum of the x-position of the leptons (ΔX_1 and ΔX_2) are the two VSAT observables for diagonal 1 and 2. If the VSAT coordinate system was fixed totally symmetrically around the beam-spot these would both be equal and have an average around 0.
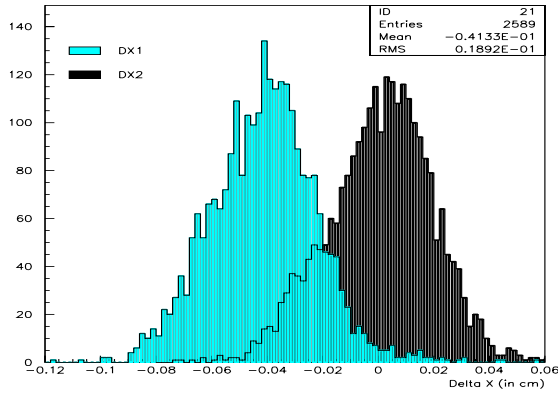
Figure 4: The ΔX (cm) distributions for diagonal 1 and 2. The 0.4 mm shift were found to be due to a database error.
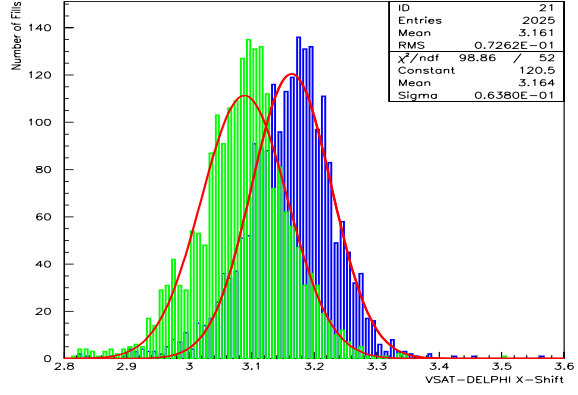
Figure 5: The uncorrected (left) and survey aligned X-shifts (right) between the DELPHI and VSAT coordinate system (in mm).

From Fig.4 it is clear that ΔX_2 is nicely centered around 0, whereas ΔX_1 has an average shift around -0.4 mm. There are two possible sources for this discrepancy, a general shift in the z beam-spot position (z_b) or an asymmetry in the position measurement of any of the modules. It is quite hard to separate the two effects, but they both have the same impact on the calculation of the DELPHI-VSAT X-coordinate system shift (Fig. 5). The f_x and l_x parameters were fixed by consistant fitting the VSAT data to the LEP acollinearity and the DELPHI beam-spot variations (Fig. 6 and 7).
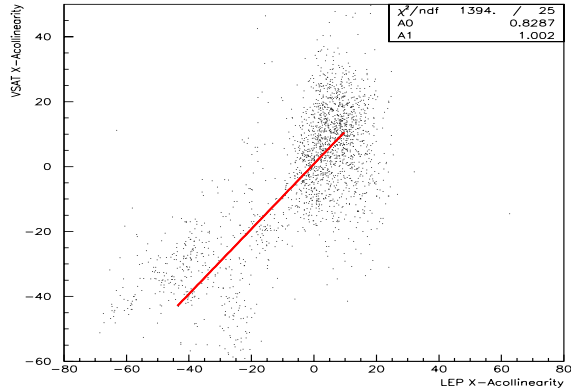

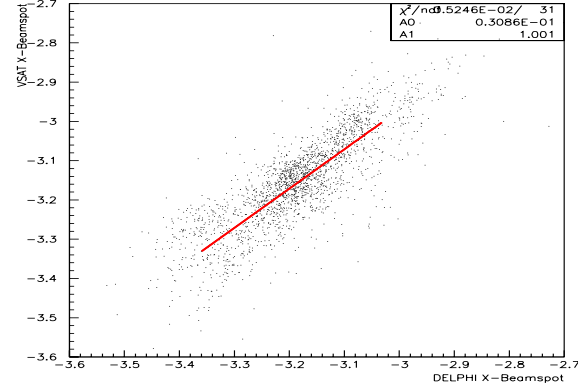Figure 6: Fitting the l_x parameter to the LEP acollinearity (in μrad) using the VD beamspot data.

Figure 7: Fitting the f_x parameter to the DELPHI beam-spot (in mm) using the LEP x-acollinearity (ϵ_x).

From equations (1) and (2) it is clear that the fits of f_x and l_x are not independent and a number of iterations were done to converge to the correct values. The final values of f_x and l_x for the LEP II data (1998-2000) were found to be 1.50 and 17.0 respectively. The f_x parameter slightly depends on the beam divergence and the width of the ΔX distribution [3], so f_x=1.5 should be considered as an average. The DELPHI beam-spot shift with respect to the VSAT is then easily extracted from equation (1). This was done in the left hand fit in Fig. 5, resulting in a shift of 3.09 mm.

3 VSAT parameter fix in Y

The transport equation in Y looks very similar to the one in X (equation (1) and (2)). There are however two important differences: first the quadrupoles are focusing in Y and secondly the angles in Y are centered around 0 (makes the z_b term neglectable). As the quadrupoles are focusing in Y (f_y is in the order of 0.3) VSAT is not very sensitive to Y-position changes of the beam.

$$\Delta Y_1 = y_4 + y_1 = 2 \cdot f_y \cdot y_b + \epsilon_y l_y \quad , \tag{3}$$

$$\Delta Y_2 = y_2 + y_3 = 2 \cdot f_y \cdot y_b + \epsilon_y l_y \quad . \tag{4}$$

The VSAT data were fitted (Figs. 8 and 9) to the LEP y-acollinearity data and DELPHI beamspot data, according to the equations above. This fit was done in a similar fashion as for x and the resulting l_y and f_y value was 3.40 and 0.25 respectively. It should be mentioned that this fit could only be made for 1999 and 2000, as the acollinearity files for ϵ_y data were unavailable for 1998.
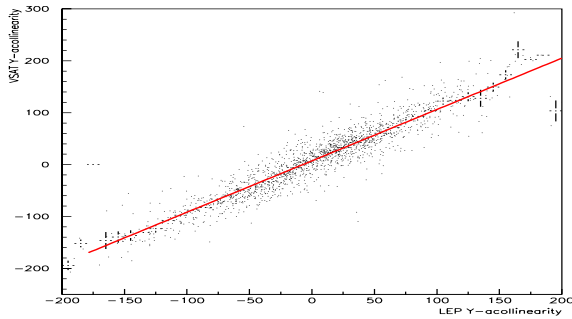

Figure 8: Fitting the l_y parameter to the LEP Y-acollinearity (μrad).
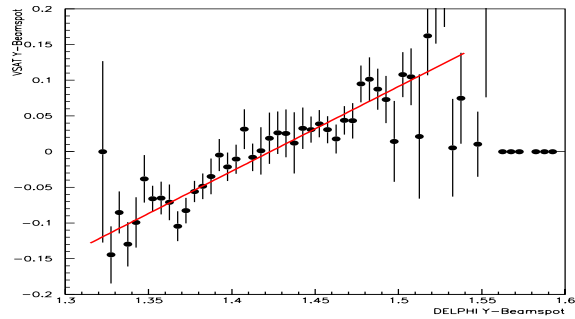
Figure 9: Fitting the f_y parameter to the DELPHI Y-beamspot (mm).

The two differences $\Delta Y_1 - \epsilon_y \cdot l_y$ and $\Delta Y_2 - \epsilon_y \cdot l_y$ should both be centered around zero, but from Fig. 10 it is clear that there is a large shift in both diagonals in opposite direction from the zero-point. This means that, not only the beamline is not in the center of the VSAT detector, but there is also a relative shift between the position measurement of the modules. Taking the difference between dy_1 and dy_2 over the LEP 2 period it is clear that this shift also changes from year to year (Fig. 11).
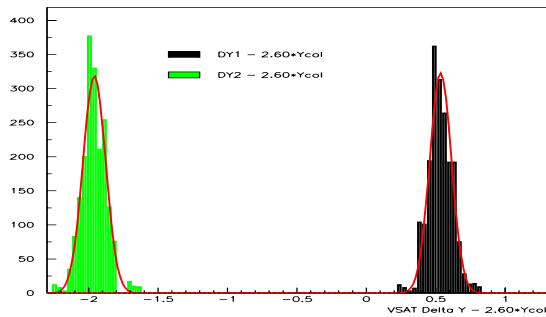

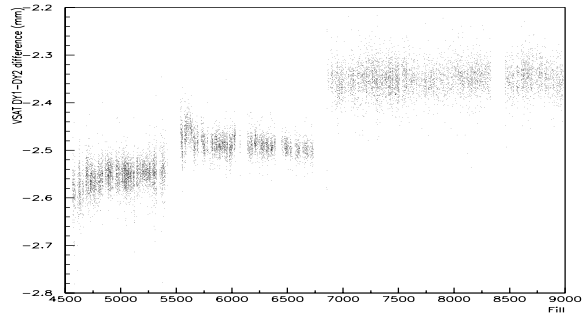Figure 10: The ΔY-shift (in mm) of the two VSAT diagonals (1999).

Figure 11: The difference of the ΔY-shift (mm) over LEP 2.

4

The relative shift from the ΔY measurement is quite accurate, but do not fix the system on its own. The off-energy electron background can however provide a second fix, as hits on the same side of DELPHI (backward or forward) should hit the outer and inner module on the same y-position (if magnetic deflection is neglected). This measurement is less accurate, as the inner modules suffer from a mix of low and high energy background. From Fig. 12 it is however clear that a distinct general shift of the modules can be extracted. These values together with the Bhabha ΔY measurement fix the relative position of the VSAT modules and are presented in the left hand part of Table 1.

$\Delta Module$ (mm)	Measured	Shift	Module	Off e^-	Bhabha	Estimated
$\Delta Y_1(1+4)$	-0.460	0.46	1	0.25	0.86	0.70
$\Delta Y_2(3+2)$	1.928	-1.93	2	-1.26	-0.12	-0.03
Forward (1-2)	-0.8	0.73	3	-2.59	-1.67	-1.90
Backward (3-4)	1.7	-1.66	4	-1.86	-0.13	-0.24

Table 1: The measured relative (Col 2) and absolute (Col 5,6) Y-shift (in mm) of the VSAT modules. From these measurements the module shift were estimated (Col 3,7).

The absolute Y-shift of the modules with respect to the beam-line is quite hard to extract. The general direction and size of any shift of the module position can however be estimated by looking on the peak-position of the Bhabha and off-energy electron distribution for a fill with zero acollinearity. For this purpose fill 6390 was chosen, and the resulting measurements can be found in right hand part of Table 1.

The numbers in Table 1 converge quite nicely (measured value in column 2 with the applied shift in column 3 is approximately 0) and it can be assumed that the absolute measurement of the module positions are more or less correct. If the VSAT coordinate system is corrected with the shifts above it will be centered around the beamline and the shift to the DELPHI beamspot can then be extracted according to equation (3) and (4). As will be shown in section 4 the position of module 3 was 2.87 mm wrong, which will correct most of the discrepancy between ΔY_1 and ΔY_2. The shift between VSAT and DELPHI coordinate system was then found to be 1.77 mm, shown in the left part of Fig. 13. If then the VSAT coordinate system is centered around the beamline and moved up 0.35 mm we finally find the shift to be 1.42 mm (right hand fit in Fig. 13).
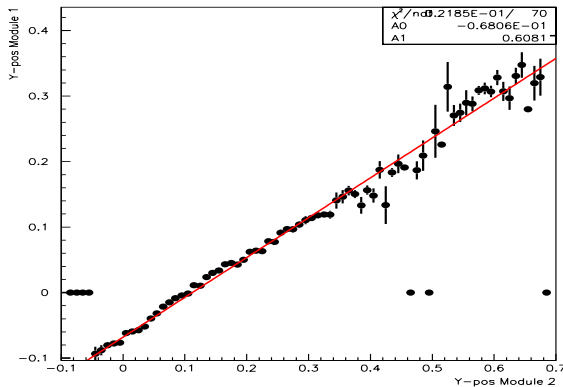

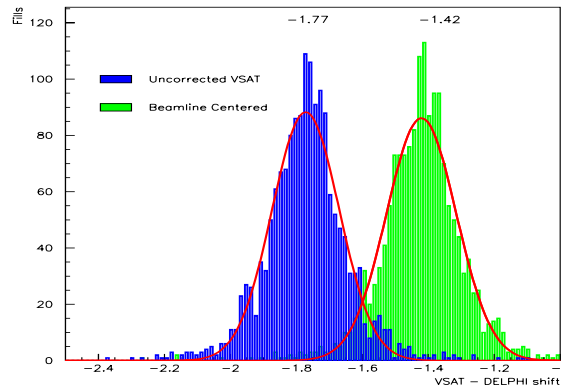Figure 12: The Y-position (cm) in module 1 and 2 for off-energy electrons.

Figure 13: The Y-shift (mm) between the DELPHI and the VSAT coordinate system.

4 VSAT survey measurements

Every time VSAT is put in place or removed, mechanical survey measurements are made. The position of each of the VSAT modules are measured with respect to a bottom plate, which is assumed to be fixed with respect to the beamline. The VSAT was not removed between 1998 and 2000, so the survey measurements at the time of insertion in 1998 should be the same as the measured at the point of VSAT dismantling in year 2000. As clear from the table here below this is however not the case.

Module	1 (B2)	2 (B1)	3 (F2)	4 (F1)
1998 X	-5.728	5.915	-5.915	5.799
1998c X	-5.728	5.915	-5.944	5.799
2000 X	-5.704	5.946	-5.921	5.825
X-Shift	+0.024	+0.031	+0.023	+0.026
1998 Y	-2.399	-2.245	-2.245	-2.377
1998c Y	-2.399	-2.245	-2.532	-2.377
2000 Y	-2.400	-2.247	-2.535	-2.381
Y-Shift	-0.001	-0.002	-0.003	-0.004
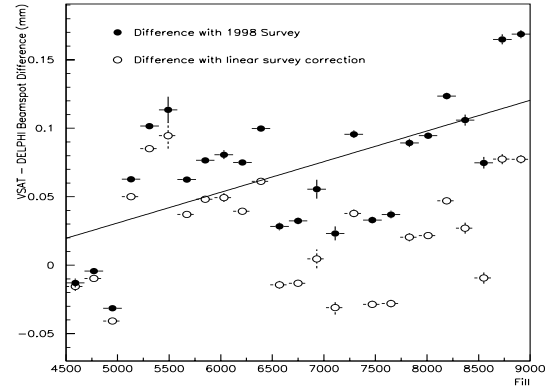
Geometrical surveys for 1998 and 2000, module 3 was miss-edited in database.

Figure 14: VSAT geometry X-shift (mm).

As seen from the table above the x and y measurement in 1998 for module 3 is wrong. By mistake the values for module 2 were inserted for module 3 as well. This error is the main reason for both the ΔX_1-ΔX_2 and ΔY_1-ΔY_2 differences discussed in section 2 and 3. All asymmetries are not solved by the correction of this error, but the situation definitely improves. The second thing to notice is that there is a general shift of about 0.26 mm in x between 1998 and 2000. If the difference between the DELPHI and VSAT beamspot is compared over the years it is clear that there is a small drift (Fig. 14). By linearly compensating for the survey shift, this drift almost fully disappears and the correspondence between VSAT and DELPHI data gets better. The VSAT - DELPHI shift then becomes 3.17 mm instead, as show in Fig. 5.

5 Beam Parameter measurement

The VSAT beam parameters measurements are based on the exactly opposite and equal momentum of the leptons from a Bhabha event in the interaction point. Only true Bhabha events (obtained after various cuts applied during off-line re-processing for the luminosity calculation) was used. One DELPHI cassette number (or file) was used as an elementary sample of data. This assures the number of Bhabha events is high enough to be significant and in the same time the beam parameters can be assumed to be more or less stable. The following quantities from the VSAT Bhabha measurement were used:

- Diagonal asymmetry of Bhabha events, $A_D = (N_1 - N_2)/(N_1 + N_2)$ - where N_1 and N_2 are the a number of Bhabha events per diagonal 1 and 2.

- The difference ΔX between modules in the two Bhabha diagonals $\Delta X_1 = x_1 + x_4$ and $\Delta X_2 = x_2 + x_3$ (Module 1 and 3 are the outside modules (w.r.t the LEP ring) and have negative X).

- The difference between the Bhabha Y coordinates (similar to that in X case) $\Delta Y_1 = y_1 + y_4$ and $\Delta Y_2 = y_2 + y_3$.

- Width of ΔX_1 and ΔX_2 distributions - the corresponding value for Y is not useful as the quadrupole field is focusing charged particles in the Y-plane (defocusing in X) resulting in a very narrow delta Y distribution.

Adding equations (1) and (2) as well as equations (3) and (4), results in that the ΔX and ΔY measurements easily can be combined and reduced into two important quantities:

$$\Delta X = \frac{\Delta x_1 + \Delta x_2}{2} = 2 \cdot f_x x_b + \epsilon_x l_x \qquad , \qquad \Delta Y = \frac{\Delta y_1 + \Delta y_2}{2} = 2 \cdot f_y y_b + \epsilon_y l_y$$

The z_b term lost in ΔX disappears as $(\theta_2^x - \theta_1^x - 2\theta_x)$ is very close to zero. If the VSAT data is combined with the beamspot measurement of the vertex detector (x_b), the beam acollinearity (ϵ_x) can be extracted. Naturally the vice versa is also true and both the beamspot position and beam acollinearity is calculated and shown in Figs. 15 and 16.

Figure 15: The beamspot position in X in the DELPHI reference system (in mm).

Figure 16: The X-acollinearity (μrad) of the two LEP beams.

The Y-beamspot measurements are quite insensitive due to the focusing effect of the quadrupoles. As shown in section 3, a dependence is however visible and the same procedure used for x can be performed on Y. This is shown in Figs. 17 and 18, and clearly VSAT parameters follow those extracted from DELPHI and LEP.
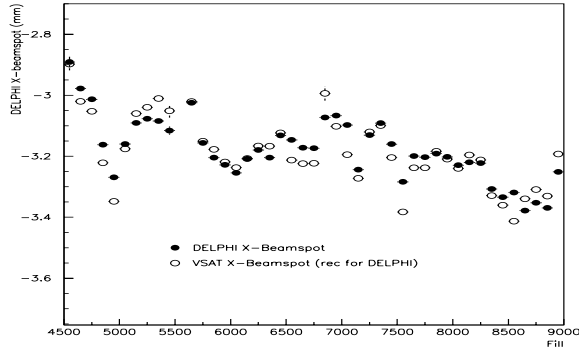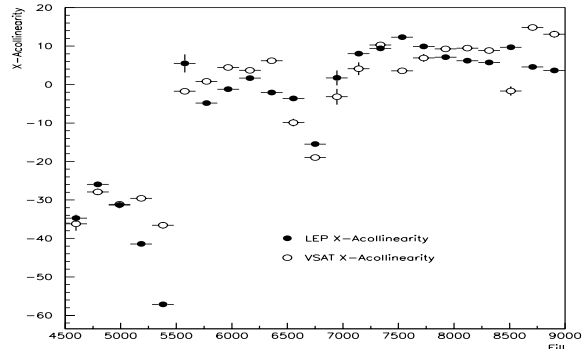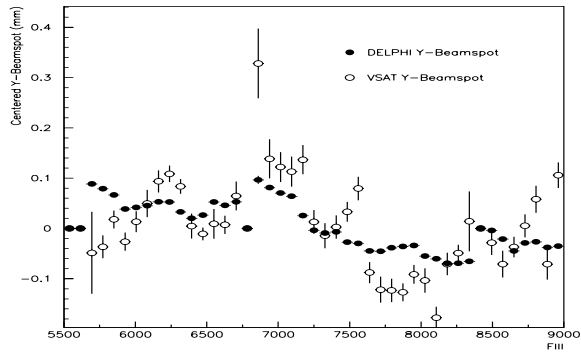
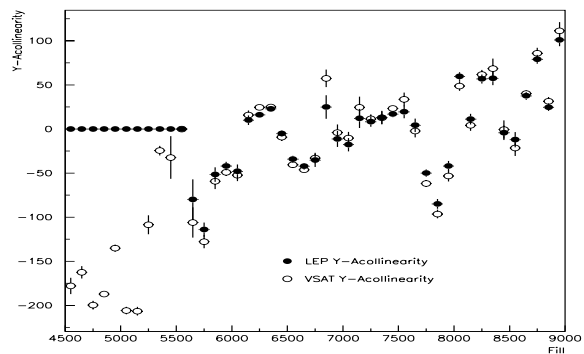Figure 17: The beamspot position in Y in the beamline reference system (in mm).

Figure 18: The Y-acollinearity (μrad) of the two LEP beams.

The Y-acollinearity files were not available for 1998, which is the reason for the zero acollinearity in Fig. 18 and the lack of data in Fig. 17. The average tilt of the LEP beams were also not available for Y, but can however be reconstructed with the help of VSAT data. The average tilts of the LEP beams in x and y can be expressed as:

$$\theta_x = \frac{\theta_+^x + \theta_-^x}{2} \sim 1.75 A_D \quad , \qquad \theta_y = \frac{\theta_+^y + \theta_-^y}{2} \sim \frac{Y_4 + Y_3 - Y_1 - Y_2}{4l_y}$$

Here A_D is the diagonal asymmetry for Bhabhas in diagonal 1 and 2, and $Y_1 - Y_4$ is the Bhabha y-position in module 1 to 4. Both θ_x and θ_y were calculated from the VSAT data over the years 1998-2000 and are shown in Fig. 19 and 20. The horizontal tilt of the beams were available from LEP over that period and the correlation with the VSAT data can be seen in Fig. 19.
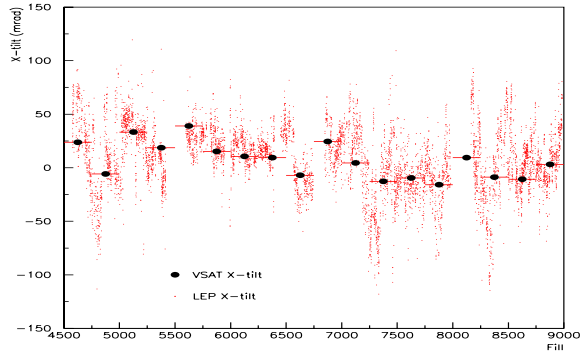
Figure 19: The average tilt (μrad) of the LEP-beams in the horizontal plane.
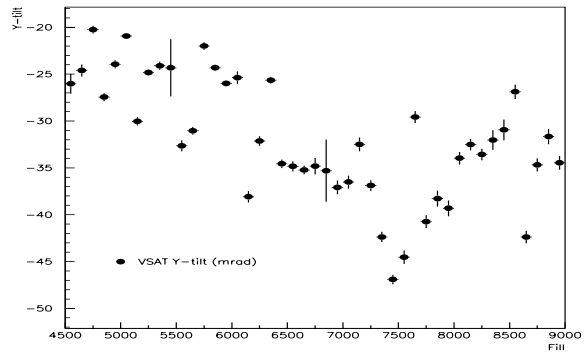
Figure 20: The average tilt (μrad) of the LEP-beams in the vertical plane.

The VSAT data can also be used to spot variations in the Z-beamspot position, but as there were no variations of significance (as seen by DELPHI) during 1998-2000, no information could be extracted. The beam divergence in x and y can be monitored by looking on the width of the ΔX and ΔY distributions. Once again there is however no other data to compare with, so a fix of the parameters is impossible.

8

6 Conclusion

The geometry of VSAT was changed in 1998 and the increased acceptance gives a bigger $\gamma\gamma$-, Bhabha- and off-energy- electrons flux than before. The data analysis shows good agreement between VD and LEP parameters and those calculated by VSAT. This is a verification that VSAT takes high quality data with high precision in both x and y.

The VSAT geometrical database has had a mistake since the beampipe upgrade in 1998. The VSAT module 3(F2) accidently got the same geometrical value as module 2, which has affected the whole DELANA processing. To correct for this, any analysis should include a subtraction of 0.29 mm from the VSAT X_3 value and 2.87 mm from the Y_3 value. Comparing the geometrical measurements from the surveys 1998 and year 2000, there seem to be a general horizontal shift of about +0.26 mm of all the VSAT modules. This corresponds quite nicely with DELPHI-VSAT X-shift change and for a high precision analysis a linear shift over the years should be applied to the data.

The geometrical changes presented here do absolutely not have any impact on the luminosity measurements performed by the VSAT. The online monitoring only depends on the MIG-scalers and do not use the position measurements at all. The offline analysis is always calibrated to the position of the Bhabha peak both in x and y, so any change in geometry will automatically be corrected for.

The general shift between the VSAT and DELPHI beamspot is however important for Monte Carlo generation of $\gamma\gamma$ events. The horizontal shift of the DELPHI beamspot varies from 3.03 to 3.3 mm from 1998 to year 2000. An average of 3.17 mm can be used without any visible impact on the data. The VSAT detector coordinate is slightly off the beamline in Y and needs to be moved up 0.35 mm (when the 2.87 mm shift has been applied in module 3). The DELPHI coordinate system in Y is then 1.42 mm above the VSAT coordinate system (1.77 mm for the uncorrected VSAT).

7 Acknowledgments

References

[1] S. Almehed et al. *Beam parameter monitoring and interaction point measurement in DELPHI with the VSAT*, DELPHI 94-77 PHYS 453

[2] S. Almehed et al., *Measurement of the beam parameter variations in DELPHI with the VSAT*, DELPHI 95-150 LEDI 2

[3] Ch. Jarlskog, *Interaction point estimation and beam parameter variation in DELPHI with the VSAT*, LUNF D6/(NFFL-7110)/1995, Lund University

Appendix E

A measurements of the Total Hadronic Cross-section in $\gamma\gamma$ collisions at very low Q^2 at LEP2

DELPHI Collaboration

DELPHI 2004-013-CONF-689
9 July, 2004

A measurements of the Total Hadronic Cross-section in $\gamma\gamma$ collisions at very low Q^2 at LEP2

S. Almehed [1], V. Hedberg [1], G. Jarlskog [1], P. Tyapkin [1,3], N. Zimin [2,3]
[1] Physics Department, University of Lund, Sweden
[2] CERN, Geneva, Switzerland
[3] JINR, Dubna, Russian Federation

Abstract

Results of an experimental study of both single and double tagged events measured in $\gamma\gamma$ collisions are presented. The data have been obtained with the DELPHI detector at LEP2 energies (from 189 up to 206 GeV) with the scattered e^+ and e^- measured by the VSAT detector. A good agreement between data and the full simulation is observed and the total $\gamma\gamma$ hadronic cross-section is estimated for a $\gamma\gamma$ centre of mass energy from 25 to 120 GeV.

Contributed Paper for ICHEP 2004 (Beijing)

1   Introduction

The multihadron production in the reaction $e^+e^- \rightarrow e^+e^- + hadrons$ has been studied for the first time at LEP2 energies with one or both scattered electrons (referred to as tags) detected at very low momentum transfer squared, Q^2, by the DELPHI Very Small Angle Tagger (VSAT). Such events are called single or double tagged events depending on the number of detected electrons. Previously, these types of measurements have been performed at lower energies [1–3] and at LEP2 [4, 5] at an intermediate range of Q^2 from data provided by luminosity detectors.

Data collected with the DELPHI detector during 1998-2000, corresponding to an integrated luminosity of 620 pb^{-1}, where hadronic final states were produced in $\gamma\gamma$ collisions were used in the following analysis.

The DELPHI VSAT [6] detector was the principal tool in these studies. It consisted of four identical modules, each with a 3x5 cm^2 active detector area. They were placed symmetrically $\simeq$7.7 m downstream of the DELPHI interaction point behind the superconducting quadrupoles at $\simeq$ 60 mm from the beam line, covering polar angles, θ, between 3-15 mrad. The energy resolution of the VSAT detector was about 4.5% at 100 GeV. It also had a precise measurement of the position of the incoming particles in x and y (about 200 μm), which allowed for an efficient separation of signal from background.

The double tag mode is attractive because the most complete information about the $\gamma\gamma$ process is obtained in this case. From the measured tags, the four-momentum of each virtual photon is known. Thus, in a small angle approximation, a direct reconstruction of the invariant mass, W, of the produced system becomes possible on an event-by-event basis, eliminating the need to infer the W spectrum from the hadrons detected with the use of some unfolding procedure, as it is necessary for no-tag [7] or single-tag events [8]. As a result, a total hadronic cross-section as a function of the $\gamma\gamma$ centre-of-mass energy, W, can be studied with double tag events with significantly smaller systematic errors. In the case of the VSAT detector, where the very low Q^2 range below 0.9 GeV^2/c^4 is covered, the errors coming from the extrapolation of the results to $Q^2 = 0$ are smaller than those obtained in previous experiments. Knowledge of both four-momenta of the tags also permits, in principle, measurements of the interference between photon helicity states [1]. Unfortunately, despite the low angles measured, the number of events are considerably reduced in the double tag case due to the very small acceptance of the modules and the very difficult background conditions which reduce the effective working area of the detectors. In the single tag mode, the available statistics is much larger.

2   The Monte Carlo

According to the current picture, established from studies of hadronic $\gamma\gamma$ processes at e^+ e^- colliders and γp interactions at HERA, a correct description of the experimental data has to use a three-component model: a soft interaction term described by the generalized Vector meson Dominance Model (VDM), a perturbative term described by the Quark Parton Model (QPM) with direct quark exchange, and a term for the hard scattering of the partonic constituents of the photon, the so-called Resolved Photon Contribution (QCD-RPC).

All these models were in one way or another implemented in the three generators used in the present study: TWOGAM (version 2.04) [9], PHOJET (version 1.12) [10] and PYTHIA (version 6.143) [11]. The TWOGAM generator describes DELPHI data reasonably well as has been shown in previous LEP1 analysis for both the no tag [12] and single tag case [3]. The QPM and VDM events are in the present study generated with the same parameters

as in previous DELPHI analyses [12]. The QCD-RPC process was treated by using leading order QCD factorization where a hard scattering subprocess gives the dominant p_T^2 scale, taken also as the factorization scale. Since such subprocesses are considered as perturbative, a single free parameter, p_T^{min}, the transverse momentum of the outgoing partons, has to be specified and used in order to separate the RPC from the non-perturbative contribution. The values of p_T^{min} were found for the parton density functions from the requirement to reproduce the visible experimental two-photon cross-section. The Gordon-Storrow (GS2) parameterization of the parton density functions with $p_T^{min}(GS2) = 2.05(1.88) \pm 0.020 \, GeV/c$ has been shown to reproduce the data better than other models and were chosen for the simulation.

The PHOJET generator (version pre-1.12) [10] was created for two-photon physics applications. This version includes an exact photon flux calculation of photon-photon processes in lepton-lepton collisions. The ideas, methods and algorithms used in the program are based on the Dual Parton Model (DPM). In order to combine the DPM, which describes soft processes, with the well-known perturbative QCD, the event generator is constructed as a two-component model (one component for soft and one component for hard processes). Thus, multiple soft and hard interactions may be generated simultaneously since soft and hard processes was treated in a unified way in this program. Hard scattering processes were simulated using lowest-order perturbative QCD. Initial state and final state parton showers were generated in the leading-log approximation. Some coherence effects (angular ordering in the emissions) were taken into account as well. The JETSET 7.4 program was used for the fragmentation of the parton configurations. The GRV parameterization of the parton density function of the photon was used in this analysis. A transverse momentum cutoff, $p_T^{cut} = 2.5 \, GeV$, was applied to the partons of the resolved photons to separate soft from hard processes. The program could run only in the hadronic invariant mass region above 5 GeV.

The PYTHIA generator [11] is a general purpose generator in high energy physics since many years but was only recently upgraded to simulate two-photon events. The program uses six event classes for two-photon collisions based on the three-component model of the photon. Version 6.143 has been used in preference to more recent versions because it describes well Deep Inelastic Scattering (DIS) data. In order to use different kinds of events and be free of double counting, the cutoff parameters are introduced at the level of the real photon fluctuation $\gamma \to q\bar{q}$ and the final hadronic system creation $\gamma\gamma^* \to q\bar{q}$. The VDM and anomalous events are together called resolved events. The superposition of events applies separately for each of the two incoming photons and forms six distinct classes of events: direct-direct, VDM-VDM, anomalous-anomalous, direct-VDM, direct-anomalous and VDM-anomalous. In the case of deep inelastic scattering, only one of the photons is resolved and hence only direct-direct, direct-VDM and direct-anomalous components are used in the model. These three contributions are similar to the TWOGAM and PHOJET classifications.

The generated events have been processed by the full detector simulation program and then been subjected to the same selection procedure as the experimental data. A description of the DELPHI detector together with basic criteria used to select tracks and the thresholds applied to neutral particles in the calorimeters can be found in reference [13].

2

3   The data

The final reprocessed samples with all the corrections applied to individual tracks and neutral particles have been used in the analysis. The scattered electrons were traced backwards in an iterative procedure from the VSAT detector, through the quadrupole and solenoid magnetic fields, to the interaction point by a special program made for VSAT called FASTSIM. The precision of this procedure is best for highly energetic particles that hit the detector close to its center. The accuracy of the angle reconstruction was checked by comparing the reconstructed angles with the generated angles in simulated events.

Studies were made to check the consistency of data samples from different years. The following run-time dependencies were studied and implemented in the reconstruction procedure of the tagged lepton:

- the beam energy (for each LEP fill);

- the leakage corrections (for each beam energy);

- the geometrical position of the VSAT modules (for each year);

- the beam-spot position (for each DELPHI data acquisition run);

- the inclination of the incoming beams (for each DELPHI data acquisition run).

The energy corrections were based on studies of the large sample of Bhabha elastic scattering events with hits covering the full area of the detector modules. The final calibration was done on a fill-by-fill basis correcting the single-arm energy of these events to the beam energy. The other type of corrections is connected to the leakage effect when particles hit the VSAT modules near the edge and some part of the electromagnetic shower escapes from the module. The size of the correction ranges from 0 to 8 GeV, depending on the reconstructed position of the particle. This is one of the largest corrections as can be seen in Table 1.

Correction	Size of corr.	Uncertainty	ϕ (degrees)	θ (mrad)
Energy leakage and calibration	≈ 5 GeV	7%	1°	0.15
Geometrical survey (x,y,z)	≈ 1 mm	200 μm	0.5°	0.07
Off-energy electron position(y)	≈ 1 mm	600 μm	1.5°	0.1
Beam spot correction(x)	≈ 3 mm	20 μm	-	0.03
Beam angle correction in y	≈ 1 mm	≈ 1 mm	2°	0.12
Angle reconstruction	-	-	5°	0.4

Table 1: Corrections applied to the VSAT part of the analyzed events and the resulting uncertainties in ϕ and θ. The beam spot variation have been corrected for in the y and z directions as well. For the beam-spot, the effect on θ and ϕ is small, so it has been ignored in this table. The correction of the beam angles is merely a way of treating a shift in angles as a shift in module-position.

The geometrical corrections are intended to fix the geometry of the VSAT with respect to the beams as accurately as possible, in order to be able to reconstruct the angles of the tagged electrons at the vertex with high enough precision. The geometrical survey measured the position of the VSAT modules with respect to each other with a precision of about 200

μm at the beginning and end of the each yearly data taking period. By studying the sharply peaked impact distribution of the off-momentum electrons in the horizontal-plane, it was possible to align the y-coordinate of the two outer modules with respect to the beam-axis. By further using the strict collinearity of the Bhabha events, the y-coordinate of the two inner modules could also be aligned. The accurate position of the beam spot is as essential to know as the position of the VSAT modules. The angle reconstruction was corrected for the position of the beam-interaction point, as given by the DELPHI beam spot measurements using the central tracking devices on a run-by-run basis. During 1998-2000 the spread in the relative angles of the beams was less than 100 μrads. The effect this had on the VSAT measurements corresponded to approximately 0.3 mm variations in the measured y-coordinate. This variation was treated by shifting the VSAT modules on a fill-by-fill basis, in order to align the y-position by using the off-momentum electrons and Bhabha events as described above. In this way the shift due to the beam tilt at the interaction point was translated into a correction of the position of the VSAT. The resulting error on the reconstructed angles is thus the same as before the operation, but the result is easier to compare to a simulation, where different beam-angles are not implemented.

Extensive studies were performed to eliminate the off-momentum electron background as much as possible, as an efficient rejection of the background is one of the major problems in this type of analysis. Independent studies performed by the CERN SL Division [14] at the DELPHI interaction point demonstrated that background conditions at LEP2 were much worse than those at LEP1. Using the LEP luminosity monitors they found that the background event rate normalized to the Bhabha events almost doubled when the energy increased up to 91.5 GeV. Later, during the last year of LEP operations (2000), the background was even higher. The main source of background came from random coincidences between two independent events incorrectly recorded as the same, i.e., the showers detected by the VSAT modules were not coming from the same process as the hadronic system detected by the main DELPHI detector.

When $\gamma\gamma$ events are studied in single tag mode, only one electron/positron is measured. The main background source to that process is the coincidence between an off-energy electron/positron and a no-tag $\gamma\gamma$ event.

For double-tagged $\gamma\gamma$ events, the background came mainly from three sources, i.e., when there were coincidences between:

a) a normal Bhabha event measured by VSAT and a hadronic activity from an untagged $\gamma\gamma$ event;

b) two off-momentum electrons hitting VSAT modules on opposite sides, again with hadronic activity from no-tag $\gamma\gamma$ events;

c) one off-momentum electron hitting a VSAT module while a scattered electron was hitting the opposite VSAT module (single tagged $\gamma\gamma$ event).

All these sources of background have different intrinsic features and they had to be treated separately.

In order to reject Bhabha events in the analysis, a set of cuts on the tagged electrons were applied to the data. These cuts were customized to eliminate the Bhabha background as efficiently as possible, thereby taking advantage of the strict collinearity of this elastic scattering process. Extensive studies of Bhabha events, revealed that they were confined to a narrow region in the plane of δX and δY, where δX denotes the difference in the measured X coordinates of the two electrons and δY similarly refers to the Y coordinates. For the true double tagged two-photon events the two quantities show significantly broader distributions than the Bhabha events. A cut on the two quantities was applied corresponding to 2σ of the measured Bhabha distribution. Events within this region and with a measured energy in the VSAT of more than 70% of the beam energy were marked as Bhabha events and rejected. The cut was applied on a fill-by-fill basis, since the quantities fluctuate with the specific beam-conditions. A cut on the total event energy was also applied, since any Bhabha event superimposed on a two photon event, will result in a higher energy than the beam-energy. The cut was set at 115 GeV.

Studies of Bhabha events showed that the δX and δY cuts, as described above, rejected 90% of the Bhabha background while the true two-photon events were not affected. The cut on total energy rejected 93% of the remaining background, while again the true two-photon events were not affected. It was thus possible to reduce the background by 99.3%, without losing any signal events.

The off-momentum background in the VSAT modules depended on the beam spot positions and the beam's inclination angles. The background (especially its high energy component) was concentrated in certain areas of the two dimensional plot showing the Y position as a function of the energy. A typical distribution of off-energy electrons in the Y-E plane is shown in Fig. 1. One can see from the plot that a trivial mathematical expression cannot be used to describe the background region and for this reason two-dimensional cut-maps were used.
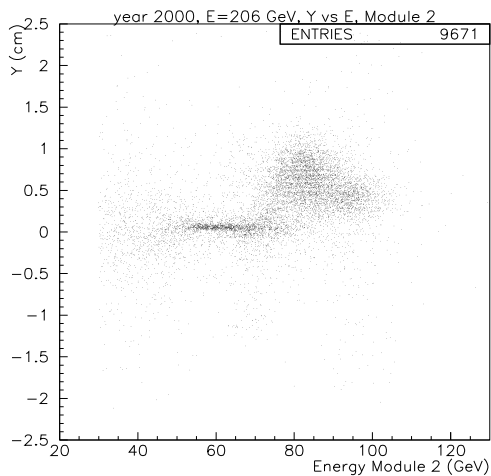

Figure 1: The VSAT high energy background distribution in the Y-E plane for VSAT module 2 for one fill during 1999.
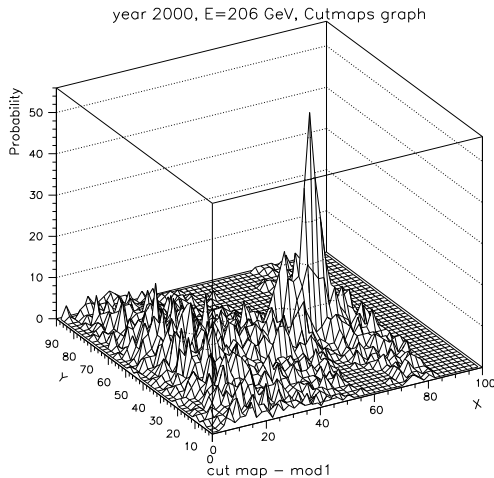
Figure 2: The probability of having a background event as a function of the energy (shown as X) and the Y position of the hit. The probability is given in units of permill.

5

The primary source of information used in constructing the cut-maps came from off-energy electron background events recorded by other DELPHI triggers. Due to the fact that the background usually changed both in size and position with changes of the LEP parameters, the cut-maps were created for each module and LEP energy (see Fig. 2).

The transformed variables $Y_{map} = (y - y_0 + 1.6) \cdot 25 + 1$ and $X_{map} = E_{beam} - E + 11$ were used for that. Here E_{beam} is the beam energy, y_0 is the average Y-position (in cm) of the off-energy background for each DELPHI run while Y and E are the Y-position (in cm) and energy (in GeV) of the measured electron. If the Y_{map} or X_{map} variable was outside the map border, the event was accepted. The probability of having a background electron in each bin was calculated and defined a third coordinate Z. The cut used was therefore a cut-off value in the horizontal plane in Fig. 2. All events above the cut-limit were rejected by the cut. The cut-limits were set differently for different modules (inner modules, for example, always had lower limits than the outer modules) and energy regions.

4 Data - Monte Carlo comparison

The final samples of two-photon events were prepared by a sequential selection procedure. The first step was to separate single from double tag events by the number of modules that were hit. For tag particles the following was required:

- the correctness of the X and Y position measurement;

- that the energy measured by the VSAT module was above 30 GeV;

- that the second electron was not seen in the experiment in the single tag case. It was therefore required that the energy of each individual particle was below 30 GeV (25 GeV for neutral particles) in the whole DELPHI detector;

- that the double tag events had passed the Bhabha rejection criteria;

- that the electrons had fulfilled the cut-map selection.

For particles in the $\gamma\gamma$ hadronic system the following selection criteria were applied:

- $4 \leq N_{Charged} \leq 18$ for single tag event and $3 \leq N_{Charged} \leq 18$ for double tag event for charged tracks which had a momentum of at least 0.3 GeV and were found in the angular region $10^o \leq \theta \leq 90^o$;

- the total energy of the hadronic system should be less than 45 GeV;

- the transverse momentum should be less than 5 GeV;

- the minimal invariant mass of the hadronic system should be larger than 3 GeV.

After all rejection and selection criteria were applied the residual background was found to be $\simeq 12\%$ in the final $\gamma\gamma$ sample of single tag events and about 35% in the double tag events sample. It was subtracted from the data in the final step.

An identical selection procedure was used also in the selection of the simulated double and single tagged events.

The numbers of events and corresponding luminosities for real data and simulated samples are given in Tables 2.

Sample	Luminosity pb^{-1}	E_{cms} GeV	Recorded/simulated number of events	Single tag selected	Double tag selected
1998 year					
Data	146.2	189	86624	4763	103
TWOGAM	300.0	189	52311	8669	347
PHOJET	411.0	189	84554	19263	784
PYTHIA	512.8	188.6	113929	23191	576
1999 year					
Data	29.0	192	17523		
	82.4	196	49734	Total	Total
	76.0	200	45856	2355	127
	32.6	202	19688		
TWOGAM	450.0	200	90784	15178	245
PYTHIA	552.6	199.5	123039	27796	705
2000 year					
Data	153.1	206	84024	4608	93
TWOGAM	450.0	206	92133	15107	330
PHOJET	382.1	206	80419	20269	412
PYTHIA	494.3	206.5	108929	28902	591

Table 2: The number of events and the luminosity in the data and the simulated samples.

The normalization to the data luminosity was done for all simulated samples. The number of events produced by the generators for each year were then multiplied by a factor to get the number of simulated events equal to the number of events in the corresponding data sample. This was done so one could better compare the shape of the distributions from the different simulations with each other and with real data.

The renormalization factors for the TWOGAM single tag sample were close to one: 0.90 - 1.10 (depending on the year). PHOJET and PYTHIA both tended to overestimate the number of single tag events and needed renormalization factors from 0.47 to 0.58 for PHOJET and from 0.52 to 0.72 for PYTHIA. A similar situation was observed for the double tag case: the renormalization factor for TWOGAM was 1.0, for PHOJET it was 0.6 and it was 0.7 for PYHTIA.

The renormalized plots of the scattered positron energy as measured by VSAT are shown in Fig. 3 and Fig. 4. The background in the outer modules (1 and 3) was much higher than in the inner modules (2 and 4) and the cut-map requirement therefore distorted more the energy distribution in the outer modules. This is the reason why only events tagged by the inner modules were used in the total hadronic cross-section calculations.

Comparisons have also been made for three VSAT energy regions (30-60 , 60-90 and 90-120 GeV) between the generated and reconstructed Monte Carlo samples.

The relative difference between E_{gen} and E_{rec} i.e. $(E_{gen} - E_{rec})/E_{rec}$, was in all cases less than 3% with an RMS less than 6%. This showed that the energy measurement by VSAT was not biased by the reconstruction procedure.
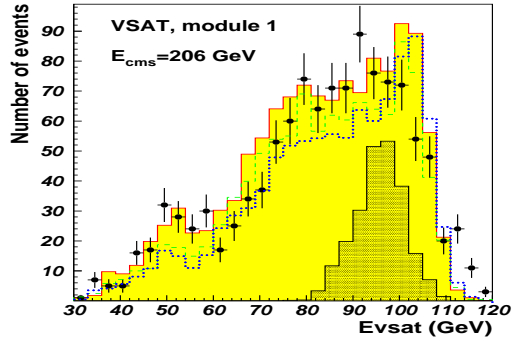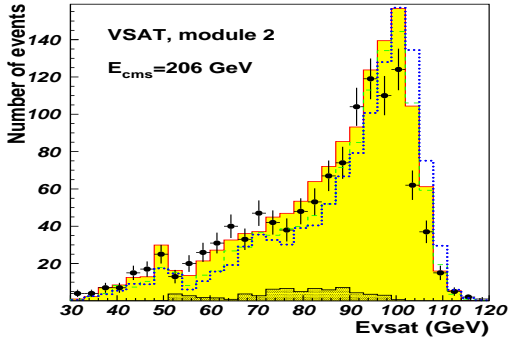
7

Figure 3: The energy distribution measured by module 2 of VSAT in year 2000. The points are data, TWOGAM is shown as a solid line and a shaded area, PHOJET as a dashed line and PYTHIA as a dotted line. The hatched dark area is the subtracted background.

Figure 4: The energy distribution measured by module 1 of VSAT in year 2000. The points are data, TWOGAM is shown as a solid line and a shaded area, PHOJET as a solid line and a shaded area, PHOJET as a dashed line and PYTHIA as a dotted line. The hatched dark area is the subtracted background.

After all corrections and the background rejection procedure were applied, the samples from different years were compared. All the distributions were found to be consistent with each other. The combined distributions of the single tag events for all years are shown in Fig. 5 - 7. They were compared and found to be in a reasonable agreement with the simulation. The subtracted background is shown in all distribution as hatched dark areas. The distribution of energy in VSAT relative to the beam energy (Fig. 5 a) shows a good agreement between data and simulation. Some disagreements with the simulated distributions is visible around the peak. The multiplicity distributions of particles in the hadronic system, as measured by the barrel and forward detectors of DELPHI, are also in a good agreement with the predictions of all generators, except in the low multiplicity region as shown in Fig. 5 b.
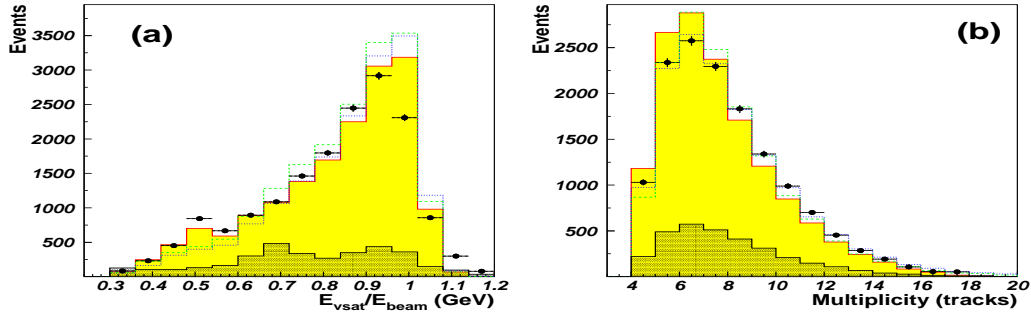

Figure 5: Comparison of data and normalized Monte Carlo for single-tag events: a) The relative energy of scattered e^+ and e^- measured in VSAT, b) The event multiplicity. Points are data, hatched area is the background, lines show Monte Carlo: solid line and shaded area is TWOGAM, the dashed line is PHOJET and the dotted line is PYTHIA.

8

Previously, an unfolding procedure [15] has been used as a tool to reconstruct a so-called "true" invariant hadronic mass (W_{inv}). In spite of the fact that it has been reconsidered and reevaluated recently with the appearance of the LEP II data and the new event generators, the unfolding procedure has many inherent problems mainly due to the different final topologies for the VDM, QPM and BCD-RPC type of $\gamma\gamma$ events [16].

All this means that it is not prudent to assume that the unfolding results are model independent. For this reason a simplified calculation of the W_{inv} variable was introduced in this analysis. After a Monte Carlo study of different correlations between the "true" W_{inv} and other variables, a fenomenological formula was derived that was found to be giving a good estimation of the "true" invariant mass in the simulated samples:

$$W_{inv} = K_0 \cdot (E_{Beam} - E_{VSAT}) + K_1 \cdot W_{Had} \pm K_2 \cdot (\theta_{Had} - 90^o)/10^o \qquad (1)$$

where $\pm$ before the last element $(\theta_{Had} - 90^o)/10^o$ must be positive for forward modules (1 and 2) and negative for backward modules (3 and 4). K_0, K_1, K_2 are the coefficients which were adjusted (to 1.0 - 1.1, 2.0 - 2.4, 1.2 - 1.4 respectively) so that the generated invariant mass W_{inv}^{gen} could be reconstructed from the measured variables such as hadronic invariant mass W_{Had} (invariant hadronic mass measured by DELPHI barrel detectors) and θ_{Had} (the resulting azimuthal angle of the total momentum of the particles detected in the barrel). The unsertainty (RMS) of the invariant mass reconstructed W_{inv} is changed from 60% to 40% for the W_{inv} changed from around 35 GeV to 75 GeV when individual event is measured.
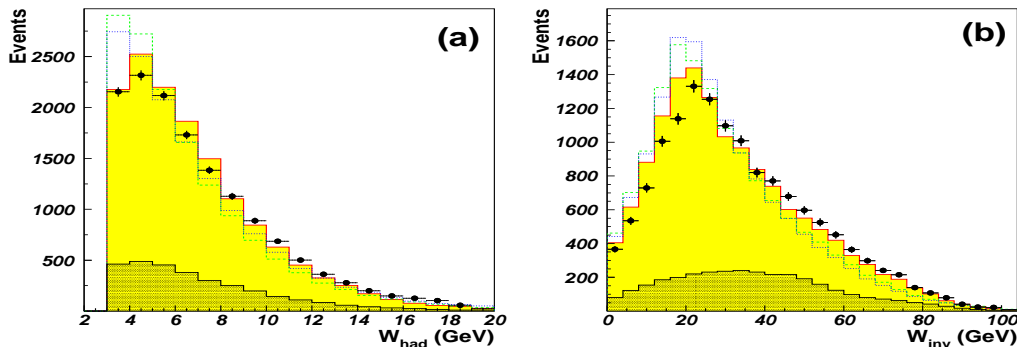

Figure 6: Comparison of single tag data and normalized Monte Carlo events: a) The invariant mass of the hadronic system, b) Reconstructed invariant mass. Points are data, the hatched area is the background, lines show Monte Carlo: solid line and shaded area is TWOGAM, the dashed line is PHOJET, and the dotted line is PYTHIA.

The TWOGAM program seems to give a wider W_{inv} distribution (see Fig. 6 b) which agrees better with data than the PHOJET and PYTHIA generators. All of the generators seems to be shifted to lower values of the invariant mass in comparison with data.

The distribution of the transverse momentum of the hadronic system in Fig. 7 b shows that all generators disagree somewhat with the data for a P_t below 1 GeV. There is also some disagreement between the Q^2-distribution in Fig. 7 a.
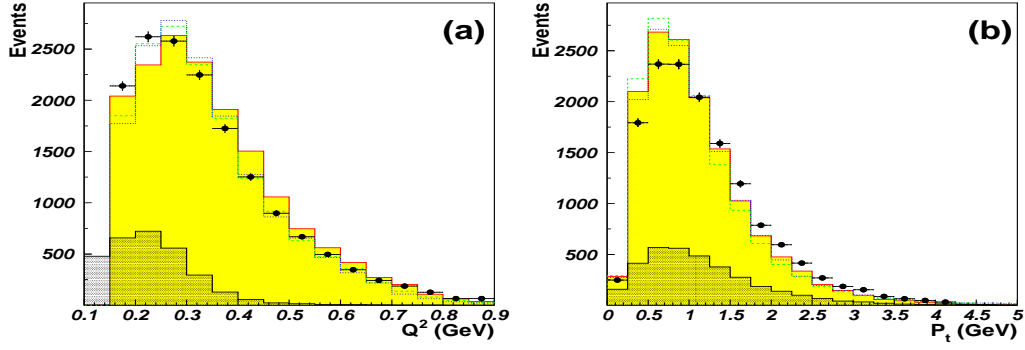
9

Figure 7: Comparison of data and normalized Monte Carlo for single-tag events: a) The distribution of Q^2, b) The transverse momentum of the hadronic system. Points are data, the hatched area is the background, lines show Monte Carlo: solid line and shaded area is TWOGAM, the dashed line is PHOJET, and the dotted line is PYTHIA.

The background rejection in the double tag analysis is based on the same cut-maps as for the single tag events with the averaged purity estimated to be 83%.

Data and the Monte Carlo predictions for double tag events are shown in Fig. 8, 9 and 10 and agree within the statistical errors. For an individual measurement the unsertainty (RMS) of the invariant mass reconstructed W_{inv} is changed from 10% to 4% when energies measured by VSAT are changed from 35 GeV to 100 GeV.
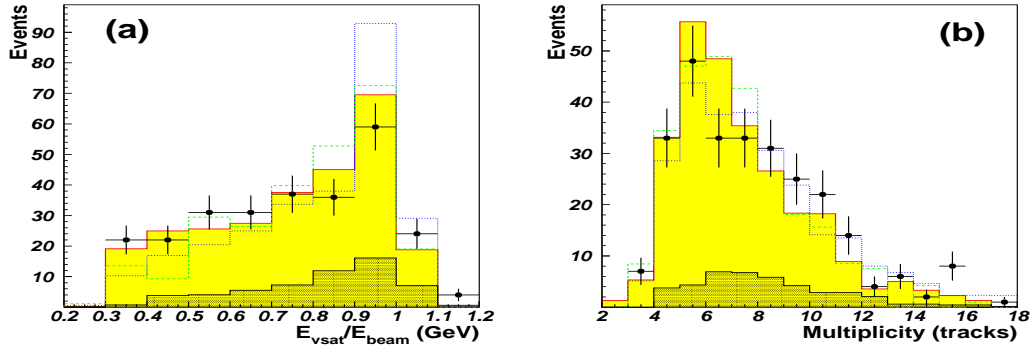

Figure 8: Comparison of data and normalized Monte Carlo for double tag events: a) The relative energy of scattered e^+ and e^- measured in VSAT, b) The event multiplicity. Points are data, the hatched area is the background, lines show Monte Carlo: solid line and shaded area is TWOGAM, the dashed line is PHOJET, and the dotted line is PYTHIA.
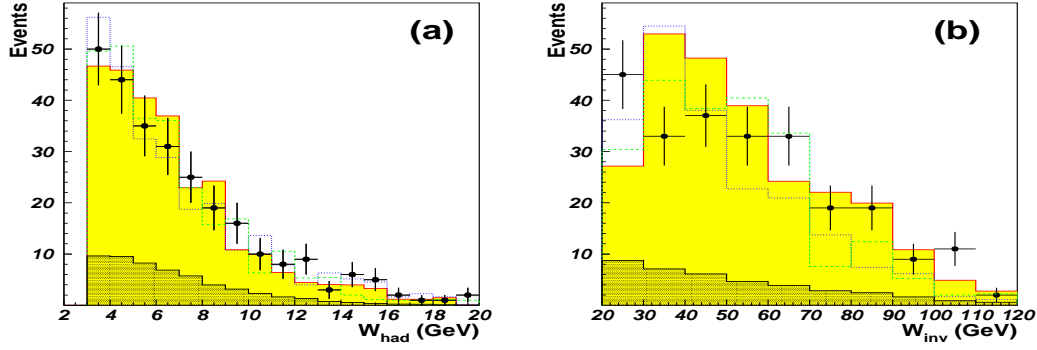
10

Figure 9: Comparison of data and normalized Monte Carlo for double tag events: a) The invariant mass of the hadronic system, b) Reconstructed invariant mass. Points are data, the hatched area is the background, lines show Monte Carlo: solid line and shaded area is TWOGAM, the dashed line is PHOJET, and the dotted line is PYTHIA.

It seems that all generators work better when both particles have a scattering angle far from zero in contrast to the events with very low Q^2 (which is impossible to reach if both leptons are tagged). For such events there is an indication that the simulation disagree increasingly with a decreasing Q^2. Therefore the differences between data and simulated samples are larger in the single tag case.
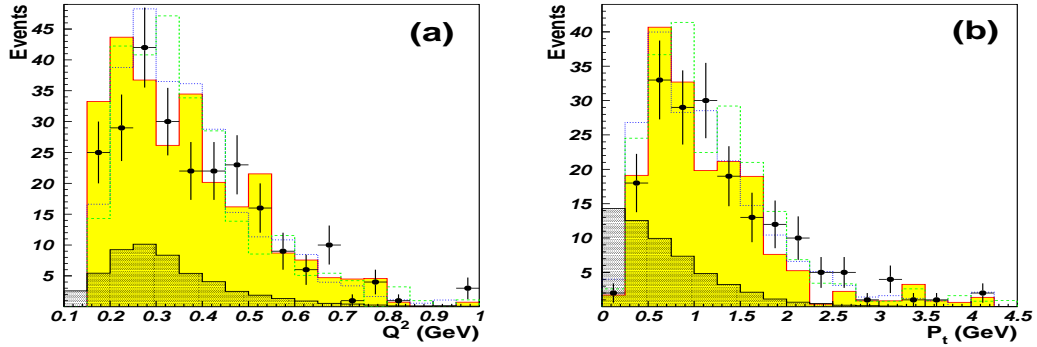

Figure 10: Comparison of data and normalized Monte Carlo for double tag events: a) The distribution of Q^2, b) The transversal momentum of hadronic system. Points are data, the hatched area is the background, lines show Monte Carlo: solid line and shaded area is TWOGAM, the dashed line is PHOJET, and the dotted line is PYTHIA.

11

5 Cross-section calculation

In order to extract the total $\gamma\gamma$ cross-section it is necessary to calculate the luminosity function of the photon flux. A considerable improvement to the equivalent photon approximation [17] for two-photon production was recently made in a work by Schuler [18], in which the previously used forms of the equivalent photon approximation were critically examined. The improved calculation of the two-photon luminosity function which includes beyond-leading-logarithm effects is implemented into the GALUGA program [19], used to calculate the photon flux for both the single tag and double tag topologies. An example of such a calculation for the single tag case is shown in Fig. 11. These luminosity functions (and similar ones for double tag events) were used in the extraction of the total $\gamma\gamma$ cross-section.
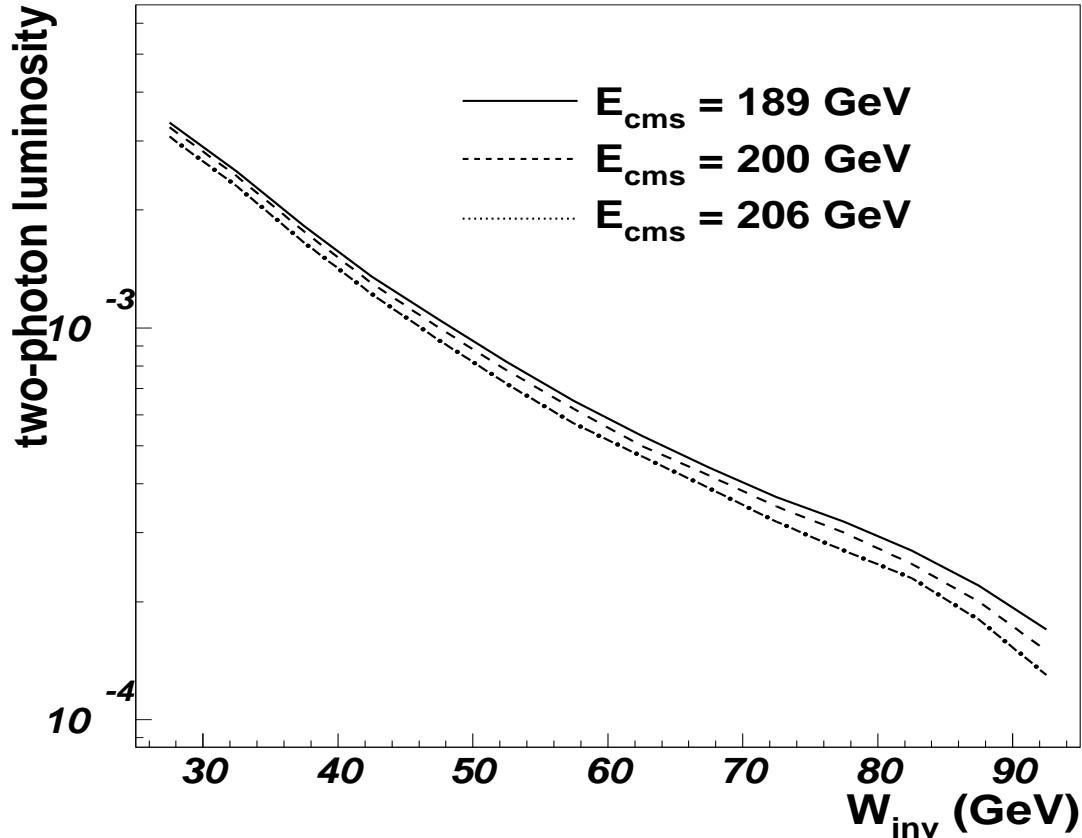

Figure 11: The two-photon luminosity function versus W_{inv} for different beam energies (189 GeV is shown as a dash-dotted line, 200 GeV as a dashed line and 206 GeV as a solid line). The so-called "two-photon luminosity" is the probability to have a $\gamma\gamma$ interaction.

Another very important task, in order to get the total $\gamma\gamma$ cross-section extracted correctly, is the transformation from the effective cross-section $e^+e^- \to hadrons$ measured in the experiment to the real cross-section of this physics process.

The level of complexity of this problem is clearly shown in Fig. 12 and 13 where the generated invariant mass distributions are shown for all generated events and those that passed all the selection criteria. Both the single and double tag distributions can be seen in comparison with the initial distribution of the generated W_{inv} in Fig. 12 and then after selection in Fig. 13. Due to the small acceptance of the VSAT detector (including the cut-maps in the background subtraction procedure) the selection of events introduces a drastic change in the shape of the distribution of the reconstructed W_{inv}.
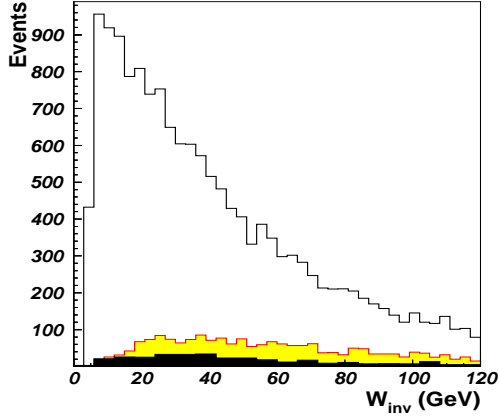

Figure 12: The simulated W_{inv} distribution (module 2) of year 2000 data. The solid line is W_{inv} before selection. After single tag selection is shown as a shaded area. The dark area is the selected double tag events in all modules.
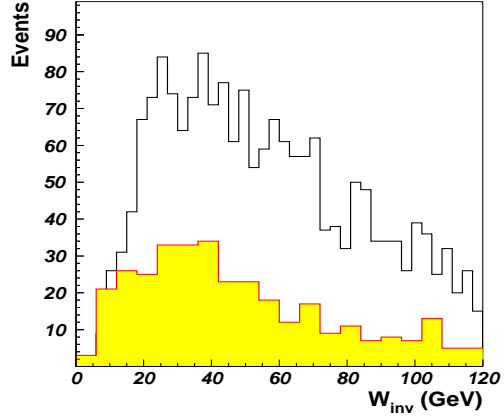
Figure 13: The simulated W_{inv} distribution after the selection of single tag events (module 2) and of double tag events (all modules) for year 2000. The solid line is for single tag data while double tag is shown as a shaded area.

Since the simulated samples agree well with data (after renormalization of TWOGAM, PYTHIA and PHOJET) all of them have been used to calculate the detection efficiency at different invariant masses of the hadronic states and with all effects of the event selection included. An efficiency averaged over all simulated samples was finally used in the total $\gamma\gamma$ cross-section calculations. Specially generated samples with TWOGAM for no-tag conditions were used to transform the cross-section in single and double tag topologies to the total effective $\gamma\gamma$ cross-section of the process $\gamma\gamma \to hadrons$. This was done for the same W_{inv} intervals that were used in the extraction.

13

As the inner VSAT modules were considerably less affected by the background conditions, only events tagged by those modules have been used for the cross-section extraction in the single tag case in the 6 intervals of invariant mass. Final results are given in Table 3.

W_{inv}, GeV	30-36	36-42	42-50	50-60	60-75	75-100
Data	1071	815	901	803	672	267
TWOGAM	1514	1222	1227	1228	1222	510
PHOJET	2472	1851	1883	1621	1203	473
PYTHIA	2769	2055	1800	1575	1184	531
Statistical error, %	3.1	3.5	3.3	3.5	3.9	6.1
Systematical error, %	2.6	2.7	2.7	2.8	2.9	3.3
Total error, %	4.0	4.4	4.3	4.5	4.9	7.0
σ_{tot}, nb	370	406	437	474	513	604
Statistical error, nb	11	15	15	17	20	37
Systematical error, nb	10	11	12	13	15	20
Total error, nb	15	18	19	21	25	42

Table 3: The numbers of real events in different samples and the effective $\gamma\gamma$ hadronic cross-section for single tag events. The total error was calculated as the quadratic sum of the statistical and systematical error.

The average contributions to the systematic errors from different sources were estimated as follows:

- the background rejection procedure: $\sim 2.0\%$;

- the event selection procedure: $\sim 0.9\%$;

- the generation of no-tag samples: $\leq 0.7\%$;

- the calculation of the photon luminosity function: $\leq 0.2\%$.

The uncertainties due to the limited Monte-Carlo statistics used in the determination of the detection efficiency in different invariant mass intervals are also included in the systematic errors. The systematic error (calculated as the quadratic sum of the individual systematic errors) is therefore different for different W_{inv} intervals. The total errors shown in Table 3 are also calculated as the sums in quadrature of the statistical and systematical errors.

The total effective $\gamma\gamma$ cross-section was extracted in the same fashion from the double tag events. Due to the lower statistics, the event sample was only split into 4 intervals of invariant mass. All four VSAT modules were used as tagging devices. Thus both the diagonal (inner and outer modules) and the parallel (inner-inner or outer-outer) combinations contributed to the final data sample. Final results for the double tag case are shown in Table 4.

W_{inv}, GeV	20-34	34-50	50-72	72-100
Data	89	76	77	81
TWOGAM	310	238	208	266
PHOJET	256	208	176	92
PYTHIA	574	302	238	148
Statistical error, %	10.6	11.5	11.4	11.1
Systematical error,%	5.4	6.0	6.4	7.2
Total error, %	11.9	13.0	13.1	13.2
σ_{tot}, nb	344	412	478	624
Statistical error	36.5	47.4	54.5	69.3
Systematical error	18.6	24.7	30.6	44.9
Total error, nb	41	54	63	83

Table 4: The numbers of real events in different samples and the effective $\gamma\gamma$ hadronic cross-section for double tag events. The total error was calculated as the quadratic sum of the statistical and systematical error.

The systematic errors were estimated in the same manner as in the single tag analysis. For each W_{inv} interval the averaged uncertainties were as follows:

- the background rejection procedure: $\sim 4.0\%$;

- the event selection procedure: $\sim 1.0\%$;

- the generation of no-tag samples: $\leq 0.7\%$;

- the calculation of the photon luminosity function: $\leq 0.2\%$.

Analogously to the single tag case, these systematic errors are different for each W_{inv} interval, since the Monte Carlo statistics used in the determination of the detection efficiency varied between W_{inv} intervals.

The total $\gamma\gamma$ cross-section for both the single and double tag case is shown in Fig. 14 together with a compilation of measurements from L3 and OPAL. The total $\gamma\gamma$ cross-section predicted by the TWOGAM generator is also shown.

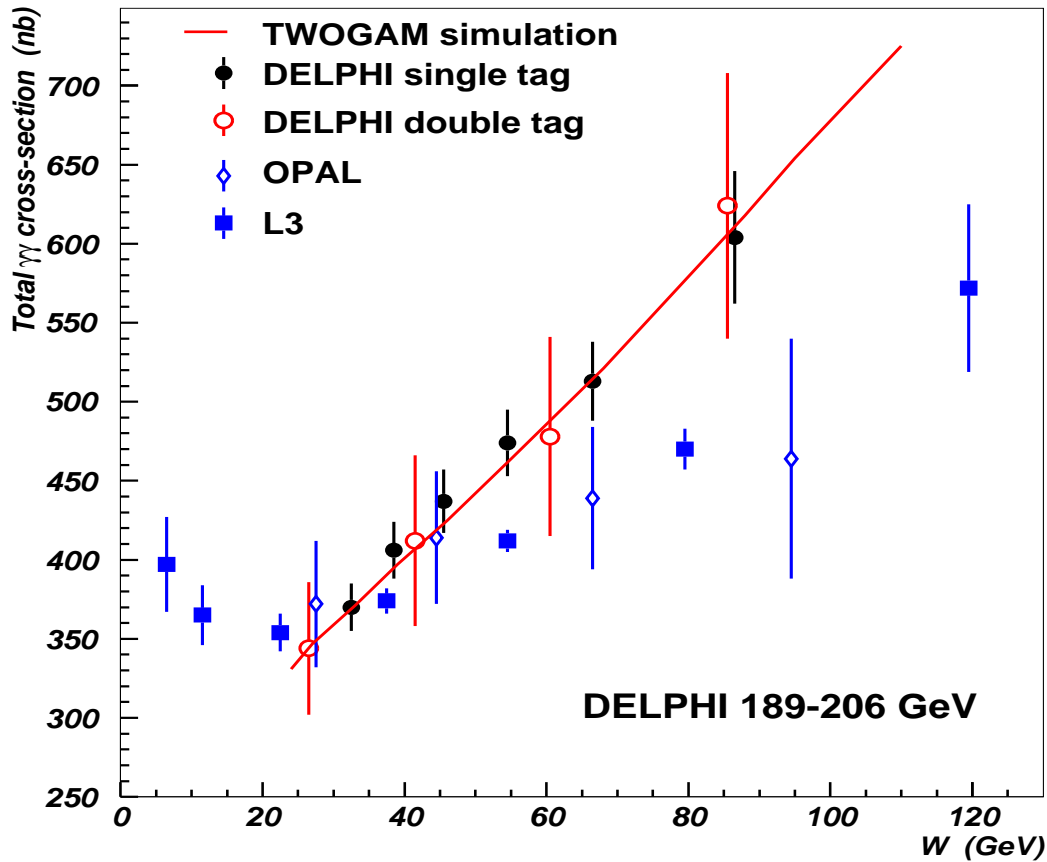The DELPHI measurements seem to be somewhat higher than what has been observed by L3 [4] and OPAL [5].

Figure 14: The total hadronic $\gamma\gamma$ cross-section measured by VSAT for single tag events (filled circles), double tag (open circles), TWOGAM simulation results (line), results from OPAL (open rombs) and L3 (filled rectangles). The error bars represents the total error.

The statistical uncertainty in the new VSAT double tag measurement is considerably smaller than in a previous work [20] based on a small sample of VSAT double tag events but it is consistent with it. The errors from the VSAT single tag events are of course noticeably smaller than those of the double tag events due to the better statistics. Results from all experiments indicate an approximately linear rise of the cross-section as a function of the invariant mass of the hadronic system. This can be explained by the predicted rise of the RPC process.

6 Conclusions

Hadronic events produced in two-photon collisions in single and double tag mode at centre-of-mass energies $\sqrt{s} \simeq 189$ - 206 GeV have been studied. Different experimental distributions can be reproduced by the simulation with reasonable accuracy. An effective total $\gamma\gamma$ cross-section have been measured in a $\gamma\gamma$ centre-of-mass energy range up to 100 GeV and for events with very low Q^2 (much closer to Q^2=0 than what has been studied by other LEP experiments). The rise of the $\gamma\gamma$ cross-section with W seen in this study is somewhat steeper than in previous measurements by the L3 [4] and OPAL [5] collaborations.

References

[1] TPC/2γ Coll., D. Bintinger et al., *Phys. Rev. Lett.* **54** (1985) 763.

[2] DELPHI Coll., P. Abreu et al., *Phys. Lett.* **B342** (1995) 402.

[3] N. Zimin, Proceedings of the Photon '97: the XIth International Workshop on Gamma-Gamma Collisions: Egmond aan Zee, The Netherlands, 10-15 May, 1997.

[4] M. Acciarri et al. (The L3 Collaboration),
Total Cross Section measurement in $\gamma\gamma$ Collisions at LEP 2.
CERN-EP/2001-012, January 30, 2001

[5] OPAL Coll., K. Ackerstaff et al., Eur. Phys. J. **C 14** (2000) 199.

[6] S.Almehed et al., Nucl.Inst. and Meth. **A305**(1991) 320.

[7] Ch. Berger et al., *Phys. Lett.* **B99** (1981) 287.
TPC/2γ Coll., *Phys. Rev.* **D41** (1990) 2661.

[8] DELPHI Coll., P. Abreu et al., *Phys. Lett.* **B342**(1995) 402. TPC/2γ (1985) 763.

[9] Physics at LEP2, Editors: G.Altarelli, T. Sjöstrand, F. Zwinger
CERN 96-1, Geneva, 1996, Vol.2, p. 224.
S. Nova, A. Olshevski and T. Todorov, DELPHI Note 90-35(1990).

[10] R. Engel, Z. Phys. **C66** (1993) 1657;
R. Engel and J. Ranft, Hadronic photon-photon interactions at high energies, ENSLAPP-A-540/95, September 1995.

[11] T. Sjöstrand, Comput. Phys. Comm. **82** (1994) 74;
PYTHIA 5.7 and JETSET 7.4: Physics and manual,
preprint CERN-TH 7112/93-REV.

[12] DELPHI Coll., P. Abreu et al., *Z. Phys. C - Particles and Fields* **62** (1994) 357.

[13] DELPHI Coll., P. Abreu et al., *Nucl. Instrum. Methods* **A378** (1996) 57.

[14] E. Bravin, B. Dehning, G.P. Ferri, A. Forsstrom, M. Merkel,
Luminosity measurements at LEP., CERN-SL-97-72 (BI)

[15] V. Blobel, In Proceedings of the CERN School of Computing,
Aiguablava, Spain, (1984), CERN 85-09.

[16] I. Tyapkin. Study of the hadronic photon structure function with the DELPHI detector
at LEP. PHOTON 2001 Conf. Proc., Ascona, Switzerland.

[17] V.M. Budnev, I.F. Ginzburg, G.V. Meledin and V.G. Serbo,
Physics Reports (Section C of Physics Letters) 15, no. 4 (1975)181-282.

[18] G.A. Schuler, CERN-TH/96-297 (1996).
Improving the equivalent-photon approximation in electron-positron collisions.

[19] Gerhard A. Schuler. Two-photon physics with GALUGA 2.0.
Computer Physics Communications 108 (1998) 279-303.

[20] Andreas Nygren. Hadronic Structure Measurements of the Photon by DELPHI at
LEP II. Lund University doctoral dissertation: LUNFD6(NFFL-7199)2001.
ISBN 91-628-4932-8